ІНСТИТУТ ЯДЕРНИХ ДОСЛІДЖЕНЬ
НАЦІОНАЛЬНОЇ АКАДЕМІЇ НАУК УКРАЇНИ

INSTITUTE FOR NUCLEAR RESEARCH
NATIONAL ACADEMY OF SCIENCES OF UKRAINE

ЩОРІЧНИК - 2013

ANNUAL REPORT - 2013

Київ 2014

У Щорічнику подається інформація про фундаментальні, науково-технічні та прикладні роботи, що виконувались в Інституті ядерних досліджень НАН України в 2013 р. До Щорічника увійшли анотації робіт за напрямками: ядерна фізика, атомна енергетика, радіаційна фізика та радіаційне матеріалознавство, фізика плазми, радіоекологія та радіобіологія; наводиться перелік структурних підрозділів інституту, список публікацій у реферованих журналах, перелік доповідей співробітників інституту на міжнародних конференціях, надається інформація про конференції, наради, проведені інститутом у 2013 р., дані про міжнародне співробітництво інституту.

Annual report contains information on the fundamental, scientific and applied investigations carried out in the Institute for Nuclear Research of the National Academy of Sciences of Ukraine in 2013. The report contains abstracts of research works in the fields of nuclear physics, atomic energy, radiation physics and radiation material science, plasma physics, radiation ecology and biology. Besides, the characteristics of the institute departments and experimental installations, the list of publications in peer-reviewed journals, the talks at International conferences, the information on the conferences and workshops, held by the institute in 2013, and international co-operation are presented.

Друкується за постановою вченої ради інституту

Директор ІЯД НАН України
І.М. Вишневський

Director of the Institute for Nuclear Research
I. M. Vyshnevskyi

Інститут ядерних досліджень НАН України
Проспект Науки, 47, м. Київ, 03680
Тел.: (380-44) 525-23-49;
Факс: (380-44) 525-44-63;
E-mail: kinr@kinr.kiev.ua

Institute for Nuclear Research
National Academy of Sciences of Ukraine
Prospekt Nauky, 47, Kyiv, 03680, Ukraine
Tel.:(380-44) 525-23-49
Fax: (380-44) 525-4463
E-mail: kinr@kinr.kiev.ua

Introduction

Within the year 2013 the Institute for Nuclear Research continued scientific investigations on the fundamental and applied aspects of nuclear physics, atomic energy, radiation physics and radiation material science, plasma physics, radiation ecology and biology.

The works on nuclear physics were concerned with the problems of nuclear structure and nuclear reactions. In particular, the formal definition of the scission point – the elongation, at which the fissioning nucleus splits into two parts – was formulated; the single γ-spectra and the coincidence spectra of γ- and K_X-rays in the decay of ^{120}Sb were measured; the inelastic process with the yield of protons and deuterons *dd*-collisions at the deuterons energy E_d= 36,9 MeV were investigated on the U-240 cyclotron; the angular distributions of elastic and inelastic scattering of ions ^{14}N та ^{15}N and the transfer reactions on the light nuclei ^{6}Li, ^{7}Li, ^{9}Be, ^{10}B, ^{11}B, ^{12}C, ^{13}C at energy 81 - 88 MeV were measured; from the analysis of the data on proton-proton collisions in LHCb experiment at the proton energy 7 and 8 TeV the frequencies of B-mesons with different quark structure were found; the new restrictions of the order of 10^{15}–10^{21} years on the decay half-lives of ^{96}Ru, ^{104}Ru, ^{106}Cd, ^{184}Os, ^{192}Os relatively to double beta decay were established.

The safe exploitation of the research reactor WWR-M up to 2024 was validated. The influence of reciprocal effects on the properties and stability of the nuclear fission traveling wave was investigated.

In the field of radiation physics and radiation material science the problem of evolution of the momentum formed by indirect excitons in condensed phase in semiconducting quantum well under the gap in metallic electrode was solved. The role of electron screening in the excitation of nuclei by electrons in hot plasma was examined. The duration of safe exploitation of the hull of unit No 1 of Zaporozhe NPP was estimated to be 59 years.

In the field of controlled fusion and plasma physics new equations describing the geodesic acoustic mode in plasmas with injected energetic ions and high pressure were derived and analyzed; it was found that the horizontal polarization of plasma during electro-cyclotron resonance heating can suppress the so-called “Alfven cascades”; the temperature of the base heated by the plasma of high frequency discharges with regulated magnetic fields in some gases and their mixtures was investigated; the new type of high-frequency discharge excited by the linear inductive aerial constructed in the form of two-conducted line perpendicular to magnetic field was examined.

In the field of radioecology and biology **a** method to determine the irradiation dose of blood cells by measuring the amount of radionuclides in blood circulation with account of the geometric and kinetic properties of the separate blood cells was developed. The model for the investigations of cytogenic effects in lymphocytes of peripheral human blood induced by radio nuclides *in vitro* was developed.

In 2013 the institute has gotten the mobile laboratory for the expertise of nuclear and other radioactive materials. The laboratory is equipped with modern radio-metric, dose-metric, alpha- and gamma- dosimetric equipment, automatic system of the air pumping for the determination of the contamination of the air by radioactive aerosols, systems of analysis of water and soil.

In 2013 the scientists of the institute have defended one candidate dissertation on the specialty physics of atomic nuclei and elementary particles. Another candidate dissertation was approved for defense. One monograph was prepared and published.

During the year the institute held the annual scientific conference of the institute, the 11th Ukrainian Conference on Control and Accounting of Nuclear Material (MPC&A), September 10 – 12, Neteshin (Khmelnytska NPP) and the 3rd International workshop on Radiopure Scintillators, Kyiv, September 17 – 20, the Ukrainian Conference on Plasma Physics and Controlled Fusion, Kyiv, September 24-25.

More details on the most important results obtained in the institute during 2013 are given in the Annual report below. I believe that the readers will find there the interesting and useful information.

Director of the Institute for Nuclear Research,
member of the National Academy of Sciences of Ukraine  I. M. Vishnevsky

Зміст

Contents

Ядерно-фізичні установки / Experimental installations

Циклотрон У-120
Завідувач – канд. фіз.-мат. наук,
А.Є. Борзаковський

Дослідницький реактор ВВР-М
Головний інженер В.М. Макаровський

Ізохронний циклотрон У-240
Завідувач – канд. фіз.-мат. наук,
О.Є. Вальков

Електростатичний перезарядний прискорювач (тандем) ЕГП-10К
Завідувач – доктор фіз.-мат. наук, В.В. Осташко

Cyclotron U-120
Head - Candidate of Phys.-math. Sciences
A.E. Borsakovsky

Research Reactor WWR-M
Chief engineer - V.M. Makarovsky

Isochronous Cyclotron U-240
Head - Candidate of Phys.-math. Sciences
O.E. Valkov

10 MV Electrostatic Tandem Accelerator
Head - Doctor of Phys.-math. Sciences
V.V. Ostashko

Відділи та лабораторії / Departments and laboratories

Секція ядерної фізики / Nuclear physics section

Відділ теорії ядра
Завідувач – доктор фіз.-мат. наук, член-кор. НАН України, професор В.М. Коломієць

Відділ ядерної фізики
Завідувач – кандидат техн. наук,
с. н. с. М.Ф. Коломієць

Відділ ядерної спектроскопії
Завідувач - доктор фіз.- мат.наук,
с.н. с. В.Т. Купряшкін

Відділ структури ядра
Завідувач – доктор фіз.-мат. наук, академік НАН України, професор І.М. Вишневський

Відділ ядерних реакцій
Завідувач – доктор фіз.-мат. наук,
с. н. с. Ю.М. Павленко

Відділ фізики лептонів
Завідувач – доктор фіз.-мат. наук,
с. н. с. Ф.А. Даневич

Відділ фізики важких іонів
Завідувач – доктор фіз.-мат. наук,
професор А.Т. Рудчик

Відділ ядерно-атомних процесів
Завідувач –доктор фіз.-мат. наук,
професор О.І. Левон

Відділ фізики високих енергій
Завідувач – доктор фіз.-мат. наук,
професор В.М. Пугач

Відділ ядерної електроніки та засобів автоматизації. Завідувач – доктор техн. наук,
с. н. с. А.П. Войтер

Відділ часового аналізу ядерних процесів. Завідувач – доктор фіз.-мат. наук,
професор В.С. Ольховський

Лабораторія теорії ядерних взаємодій та процесів. Завідувач – доктор фіз.-мат. наук,
с. н. с. В.Ю. Денисов

Nuclear Theory Department
Head – Corresponding Member of National Academy of Sciences of Ukraine, Prof. V.M. Kolomietz

Department of Nuclear Physics
Head – Camdidate of Techn. Sciences
M. F. Kolomietz

Nuclear Spectroscopy Department
Head - Doctor of Phys.-math. Sciences
V.T.Kupryashkin

Nuclear Structure Department
Head – Member of National Academy of Sciences of Ukraine, Prof. I.M. Vishnevsky

Department of Nuclear Reactions
Head – Doctor of Phys.-math. Sciences
Yu.M. Pavlenko

Lepton Physics Department
Head – Doctor of Phys.-math. Sciences
F.A. Danevich

Department of Heavy-Ion Physics
Head – Doctor of Phys.-math. Sciences,
Prof. A.T. Rudchik

Department of Nuclear-Atomic Processes
Head – Doctor of Phys.-math. Sciences,
Prof. A.I. Levon

High Energy Physics Department
Head – Doctor of Phys.-math. Sciences,
Prof. V.M. Pugatch

Nuclear Electronics and Automatic Means Department. Head - Doctor of Techn. Sciences
A.P. Voiter

The Time Analysis of Nuclear Processes Department. Head - Doctor of Phys.-math. Sciences,
Prof. V.S. Olkhovsky

Laboratory of Theory of the Nuclear Interactions and Processes. Head - Doctor of Phys.-math. Sciences, V. Yu. Denisov

Секція атомної енергетики / Atomic energy section

Відділ теорії ядерних реакторів
Завідувач – доктор фіз.-мат. наук,
професор В.М. Павлович

Відділ дослідницького ядерного реактора
Завідувач – доктор фіз.-мат.наук,
член-кор. НАН України В.І. Слісенко

Відділ нейтронної фізики
Завідувач – канд фіз.-мат. наук,
с. н. с. О.О. Грицай

Відділ проблем дозиметрії ядерних реакторів
Завідувач – кандидат фіз.-мат. наук
В.М. Буканов

Відділ радіаційної і загальної безпеки
Завідувач – доктор техн. наук,
с. н. с. С.І. Азаров

Навчальний центр з фізичного захисту, обліку та контролю ядерного матеріалу
Завідувач – канд. фіз.-мат. наук
В.І. Гаврилюк

Department of the Nuclear Reactor Theory
Head - Doctor of Phys.-math. Sciences,
Prof. V.M. Pavlovych

Department for Nuclear Research Reactor
Head – Corresponding Member of National Academy of Sciences of Ukraine V.I. Slisenko

Neutron Physics Department
Head – Candidate of Phys.-math. Sciences
O.O. Gritzay

Department of the Nuclear Reactor Dosimetry Problems
Head – Candidate of Phys.-math. Sciences
V.M.Bukanov

Radiation and General Protection Department
Head – Doctor of Techn. Sciences S.I.Azarov

George Kuzmycz Training Center for Physical Protection, Control and Accounting of Nuclear Material
Head – Candidate of Phys.-math. Sciences
V.I.Gavryliuk

Секція радіаційної фізики та радіаційного матеріалознавства / Radiation physics and radiation material science section

Відділ теоретичної фізики
Завідувач – доктор фіз.-мат. наук, член-кор. НАН України, професор В.Й. Сугаков

Відділ радіаційної фізики
Завідувач – доктор фіз.-мат. наук,
професор П.Г. Литовченко

Відділ радіаційного матеріалознавства
Завідувач – кандидат фіз.-мат. наук
Л.І. Чирко

Department of Theoretical Physics
Head - Corresponding Member of National Academy of Sciences of Ukraine, Prof. V.I. Sugakov

Department of Radiation Physics
Head - Doctor of Phys.-math. Sciences,
Prof. P.G. Litovchenko

Department for Radiation Material Science
Head - Candidate of Phys.-math. Sciences
L.I. Chyrko

Секція фізики плазми / Plasma physics section

Відділ теорії ядерного синтезу
Завідувач – доктор фіз.-мат. наук,
професор Я.І. Колесниченко

Відділ фізики плазми
Завідувач – канд. фіз.-мат. наук
А.Г. Борисенко

Відділ фізики плазмових технологій
Завідувач – канд. фіз.-мат. наук,
с.н.с. О.А. Федорович

Fusion Theory Department
Head – Doctor of Phys.-math. Sciences,
Prof. Ya.I. Kolesnichenko

Plasma Physics Department
Head - Candidate of Phys.-math. Sciences
A.G. Borisenko

Department of physics of plasma technologies
Head - Candidate of Phys.-math. Sciences
O.A. Fedorovich

Секція радіоекології та радіобіології / Radioecology and radiobiology section

Центр екологічних проблем атомної енергетики
Завідувач – канд. фіз.-мат. наук,
с.н.с. В.В.Тришин

Відділ радіобіології і радіоекології
Завідувач – докт.біол. наук,
с. н. с. А.І. Липська

Center for Ecological Problems of Atomic Energy
Head – Candidate of Phys.-math. Sciences,
V.V. Tryshyn

Radiobiology and Radioecology Department
Head – Doctor of Biol. Sciences,
A.I. Lypska

Abstracts of works on nuclear physics

GAMMA-RADIATION IN HOT NUCLEI

V. M. Kolomietz[1], S. V. Radionov[1], B. V. Reznichenko[2]

[1] *Institute for Nuclear Research, National Academy of Sciences of Ukraine, Kyiv*
[2] *Taras Shevchenko National University, Kyiv*

In the present work, we have studied the spectrum of fluctuations in nuclear shape variables. The precise form of such spectra can be expected to depend on the memory effects. Here, we study this dependency using the fluctuational γ-quanta emission. The spectral distribution of such kind of fluctuational radiation depends on the relaxation (dissipation) properties of the collective motion, in particular, on the dynamical distortion of the Fermi surface. We therefore guess that a study of the shape of the radiation spectrum emitted from the heated nucleus provides an opportunity to obtain information on the dissipative properties and on the transition from the low-temperature (quantum) to the high-temperature (classical) regime in a finite many body system like a nucleus.

We suggest a proof of the Langevin equation for the macroscopic collective variables starting from the collisional Landau - Vlasov kinetic equation, including the memory effects in the collisional integral. We derive then the macroscopic equations of motion for the collective variables $\alpha_{LM,\omega}$ of nuclear shape variations of multipolarity L in the following form

$$-\omega^2 m_L \alpha_{LM,\omega} + \left[C_L^{(LDM)} + C'_L(\omega)\right]\alpha_{LM,\omega} -$$

$$-i\omega\gamma_L(\omega) = \xi_{LM,\omega}, \qquad (1)$$

where m_L is the collective mass, $C_L^{(LDM)}$ is the static stiffness coefficient of nuclear liquid drop model (*LDM*), $C'_L(\omega)$ is the additional contribution to the stiffness due to the Fermi-surface distortion effects, $\gamma_L(\omega)$ is the fiction coefficient which depends on the relaxation-time parameter β and $\xi_{LM,\omega}$ is the random force.

Using Eq. (1), we have performed the analysis of the temperature dependence and the relaxation-time dependence of the energy E_{GQR} and the width Γ_{GQR} of the giant quadrupole resonance (GQR). The result for the A-dependency of the eigenenergy E_{GQR} in cold nuclei is shown in Fig. 1.

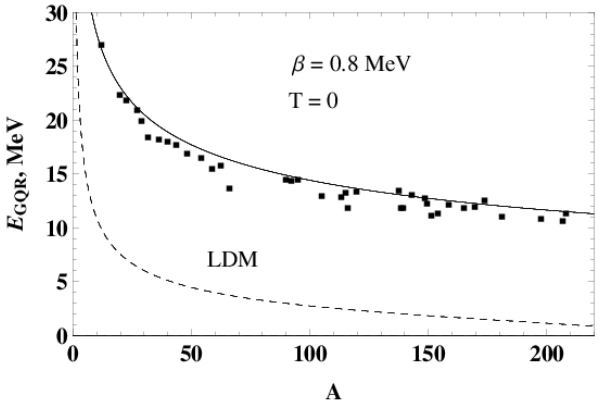

Fig. 1. The eigenenergies of the isoscalar GQR versus the nuclear mass number A. The results are obtained with the relaxation parameter β = 0.8 MeV. The dashed line is for the traditional liquid drop model with $C'_L(\omega) = 0$.

We have established that the nucleus is Coulomb unstable at some temperature $T_{\lim}$ which is strongly A-dependent. Using Eq. (1), we have also evaluated the spectral density $J_L(\omega)$ of the fluctuational γ-radiation for hot nuclei. The result for $A = 208$ is shown in Fig. 2.

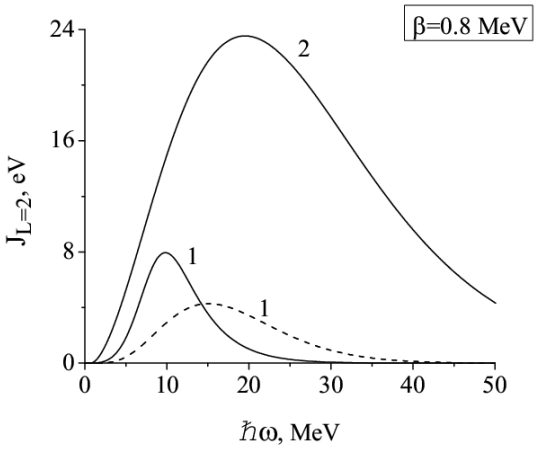

Fig. 2. The spectral density of the quadrupole gamma-quanta emission for temperatures $T = 3$ MeV $< T_{\lim}$ (curves *1*) and $T = 8$ MeV $> T_{\lim}$ (curve *2*). The dashed line 1 is for the statistical γ-quanta emission.

SYMMETRY ENERGY: FROM NUCLEAR MATTER TO FINITE NUCLEI

V. M. Kolomietz, A. I. Sanzhur

Institute for Nuclear Research, National Academy of Sciences of Ukraine, Kyiv

The Gibbs concept of dividing surface does not imply any specific energy density functional and relies on the value of the binding energy and the chemical potentials which are measurable quantities. It is possible to apply this concept to the phenomenological droplet model as well. We consider the relation of the nuclear macroscopic characteristics (surface and symmetry energies, Tolman length, incompressibility, etc.) to the bulk properties of nuclear matter.

Assuming a small deviations from the equilibrium, the equation of state (EOS) for an asymmetric nuclear matter can be written in the form of expansion around the saturation point. One has for the energy per particle (at zero temperature)

$$\mathcal{E}(\varepsilon, x) = \mu_\infty + K_\infty \varepsilon^2/18 + b_\infty x^2 + L_\infty \varepsilon x^2/3 + \ldots \quad (1)$$

where $\varepsilon = (\rho - \rho_\infty)/\rho_\infty$, $x = \rho_-/\rho$, ρ and ρ_- are the isoscalar and isovector particle densities, ρ_∞ is the matter saturation (equilibrium) density μ_∞ is the chemical potential, K_∞ is the nuclear matter incompressibility, b_∞ is the symmetry energy coefficient, L_∞ is the symmetry energy slope parameter (all values are taken for the saturation point $\varepsilon = 0$ and $x = 0$). Using $\mathcal{E}(\varepsilon, x)$, one can also evaluate isoscalar and isovector chemical potentials, μ, μ_- of nuclear matter beyond the saturation point. Similar to (1), in a finite uncharged system having the mass number A and the asymmetry parameter $X = (N - Z)/A$, the energy per particle E/A is usually presented as $(A^{-1/3}, X)$-expansion around infinite matter using the leptodermous approximation

$$E/A = a_V + X^2 b_V + A^{-1/3}\left(a_S + X^2 b_S\right) + \ldots \quad (2)$$

where a_V and a_S are, respectively, the volume and surface energy coefficients, b_V and b_S are, respectively, the volume and surface symmetry coefficients. The nuclear chemical potentials λ, λ_- are determined from (2). Following Gibbs-Tolman method, one can derive the actual nuclear matter densities ρ and ρ_- from the conditions

$$\mu(\varepsilon, x) = \lambda(A^{-1/3}, X),\ \mu_-(\varepsilon, x) = \lambda_-(A^{-1/3}, X). \quad (3)$$

Using (3), one can establish the relation of the macroscopic energy coefficients in the mass formula expansion (1) to the nuclear matter parameters in EOS (1).

The surface tension σ_∞ for the planar surface (semi-infinite matter) reads

$$\sigma_\infty = \sigma_0 + \sigma_- X^2, \quad (4)$$

where σ_0 and σ_- stand for the isoscalar and isovector surface tension coefficients, respectively. The values of σ_0 and σ_- at the equimolar dividing surface for different Skyrme parameterizations have been determined [1]. Taking the advantage of the large mass limit $\mathcal{E} = E/A\big|_{X=\text{const},\ A\to\infty}$ and Eqs. (1) – (4) one has $a_V = \mu_\infty$, $b_V = b_\infty$ and

$$a_S = 4\pi r_0^2 \sigma_0, \quad b_S = 4\pi r_0^2 \left(\sigma_- + \frac{2L_\infty}{K_\infty}\sigma_0\right). \quad (5)$$

Here $r_0 = (4\pi\rho_\infty/3)^{-1/3}$. To describe separately the neutron and proton density distributions we introduce the neutron radius, R_n, and proton radius, R_p, as the dividing radii with zero value for the corresponding surface densities (see [1]). The isovector shift of the neutron-proton radii, $R_n - R_p$, is then written as

$$R_n - R_p = X\left(-\frac{2\sigma_-}{b_\infty \rho_\infty} + O(A^{-1/3})\right) + O(X^3). \quad (6)$$

From (6) the value of neutron skin $\sqrt{\langle r_n^2\rangle} - \sqrt{\langle r_p^2\rangle}$ is given within the main order as

$$\sqrt{\langle r_n^2\rangle} - \sqrt{\langle r_p^2\rangle} \approx \alpha X,\ \alpha = -\sqrt{\frac{3}{5}}\frac{2\sigma_-}{b_\infty \rho_\infty}. \quad (7)$$

Here α is the neutron skin parameter which value correlates with the surface-to-volume symmetry energy ratio $r_{S/V} = |b_S/b_V|$ due to Eq. (5), see Table.

The neutron skin parameter α and the surface-to-volume symmetry energy ratio for different Skyrme forces

Force	SkM	SkM*	Sly230b	T6	SIII
α (fm)	0.980	0.996	0.950	0.775	0.586
$r_{S/V}$	1.44	1.47	1.40	1.17	0.930

1. V.M. Kolomietz and A.I. Sanzhur, Phys. Rev. C **88**, 044316 (2013).

DIFFUSION APPROXIMATION TO RELAXATION ON DISTORTED FERMI SURFACE

V. M. Kolomietz, S. V. Lukyanov

Institute for Nuclear Research, National Academy of Sciences of Ukraine, Kyiv

In present work, we have used the diffusion approximation [1] to the relaxation on deformed Fermi surface. Such kind of approximation gives a simple result for the dependence of the relaxation time $\tau_{r,l}$ on the Fermi-surface distortin multipolarity l in the following form

$$1/\tau_{r,l} = D_p(p_F)/p_F^2 l(l+1), \qquad l \geq 2, \qquad (1)$$

where $D_p(p_F)$ is the diffusion coefficient taken on the Fermi surface and p_F is the Fermi momentum.

The relation (1) can be used to adjust the diffusion coefficient $D_p(p_F)$ to the nuclear data. Within the fluid dynamic approach (FLDA) the relaxation time $\tau_{r,l=2}$ derives the width Γ_{GQR} of the isoscalar Giant Quadrupole Resonance (GQR) as

$$\Gamma_{GQR} = \frac{4\varepsilon_F \hbar}{m r_0^2} \frac{\tau}{1+(\omega_R \tau)^2} A^{-2/3}, \qquad (2)$$

where ε_F is the Fermi energy, r_0 is the nuclear mean nucleon-nucleon distance, $\tau = \tau_{r,l=2}$ and ω_R is the GQR eigenfrequency.

In Figure we show the results of calculations and the comparison with experimental data for the GQR widths for the nuclei through the periodic table of elements. We have here adopted ε_F = 40 MeV, r_0 = 1.2 fm and the experimental value of the GQR energy $\hbar\omega_R = 63 \cdot A^{-1/3}$ MeV. The relaxation time τ in Eq. (2) was taken from Eq. (1) with $D_p = 2.5 \times \times 10^{-21}$ MeV^2·fm^{-2}·s. As can be seen from Fig. 1, the FLDA provides a quite satisfactory description of the widths Γ_{GQR} if the quadrupole distortions of the Fermi surface are taken into consideration and the above mentioned diffuse coefficient is used.

Another possibility for the distortion of Fermi surface is the initial non-equilibrium particle-hole excitations. We will restrict ourselves by a nuclear matter which is homogeneous in ***r***-space and assume a spherical Fermi surface of radius p_F. The diffusion equation has been solved numericaly under the initial condition for the Wigner distribution function $f_{in}(p,t=0)$ assuming the particle-hole excitation. We have calculated the momentum dependence of the Wigner distribution function $f(p,t)$ for the different time intervals. We have assumed the initial excitation energy E_{ex} = 30 MeV. The momentum distribution $f(p,t)$ evolves to the Fermi-type equilibrium limit $f_{eq}(p)$. The corresponding equilibrium temperature can be estimated as $T = -D_p/K_p = 4$ MeV.

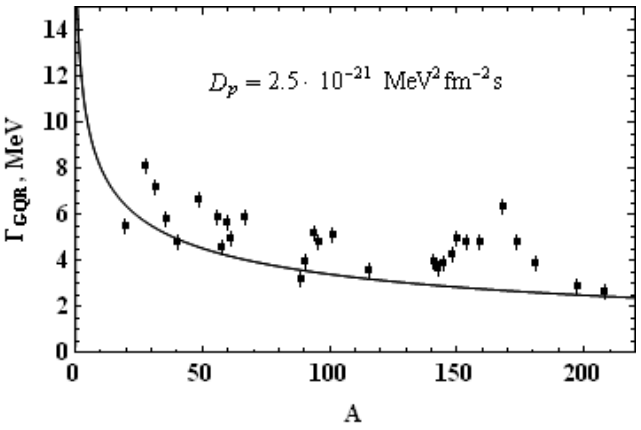

Fig. 1. The width of the isoscalar Γ_{GQR} versus the nuclear mass number A. The results are obtained from Eqs. (1) and (2) with $D_p(p_F) = 2.5 \cdot 10^{-21}$ MeV·^{2}fm^{-2}·s. The experimental data are taken from Ref. [2].

The excitation energy E_{ex} is related to the equilibrium temperature T of the compound nucleus as $E_{ex} = aT^2$, where a is the statistical level density parameter. For the considered case, we find $a \approx A/8.5$ MeV^{-1}. The obtained value of the level density parameter a agrees with the experimental one $a_{exp} \approx A/8$ MeV^{-1} quite well.

1. E.M. Lifshitz and L.P. Pitaevskii, *Physical Kinetics*, Pergamon Press, Oxford, 1981, Ch. 2.
2. F.E. Bertrand, Nucl. Phys. **A354**, 129 (1981).

BUBBLE BOILING OF LIQUID HELIUM-3

V. M. Kolomietz

Institute for Nuclear Research, National Academy of Sciences of Ukraine, Kyiv

The boiling of a liquid means the generation and the growth of the vapor bubbles inside the liquid. In a classical boiling liquid, both the equilibrium conditions and the dynamics of the vapor bubble of radius R are mainly derived by the thermodynamic potential $\Phi(R)$. The thermodynamic equilibrium between the vapor bubble and the surrounding metastable liquid is reached at the critical radius $R = R^*$. An essential feature of the bubble dynamics occurs in the case of a Fermi liquid where the dynamic distortion of the Fermi surface produces an additional pressure tensor. The purpose of this work is to study the features of the dynamic evolution of the bubble in a Fermi-liquid He-3 taking into consideration the influence of the Fermi motion in the liquid on the bubble dynamics. The main attention is paid to the dynamic effects related to the properties of the Fermi liquid.

Evaluating the variation of the thermodynamic potential $\Delta\Phi(R)$, its dependence on the overheating temperature δT was established. The final result is shown in Fig. 1.

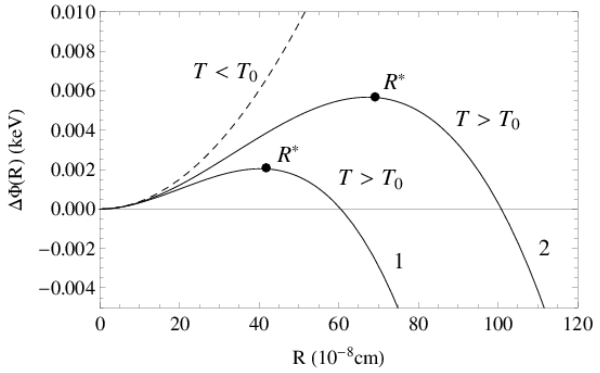

Fig. 1. Dependence of the thermodynamic potential $\Delta\Phi$ of metastable liquid He-3 on the radius of the bubble. The solid lines *1* and *2* are for the overheated temperatures δT = 0.05 K and δT = 0 .03 K, respectively. The dashed line is for $T < T_0$, where T_0 is the boiling temperature.

Considering the boiling regime, the following result for the critical radius was obtained

$$R^* = \frac{2\sigma(R^*, T_0)\, k_B T_0}{P_0 L_1} \cdot \frac{T_0}{\delta T},$$

where $\sigma(R^*, T_0)$ is the surface tension coefficient, k_B is the Boltzman constant, P_0 is the external pressure and L_1 is the latent heat of evaporation attributed to one particle. It was studied the dependence of $\sigma(R^*, T_0)$ on the curvature of the bubble surface (Tolman effect) and on the boiling temperature T_0. It was established

$$\sigma(R^*, T) = \sigma(R^*)\left(\frac{T_{crit}^2 - T^2}{T_{crit}^2 + T^2}\right)^{\nu},$$

where $T_{crit} = 3.35\,°\mathrm{K}$ is the critical temperature and $\nu \approx 1$ is the critical exponent.

It was shown that the development of instability of the bubble near the barrier point $R = R^*$ is strongly influenced by the memory effects, if the relaxation time $\tau = \hbar\beta / T^2$ is large enough. In this case, a growth of the bubble is accompanied by characteristic shape oscillations of the bubble radius. The corresponding results for $R(t)$ are shown in Fig. 2.

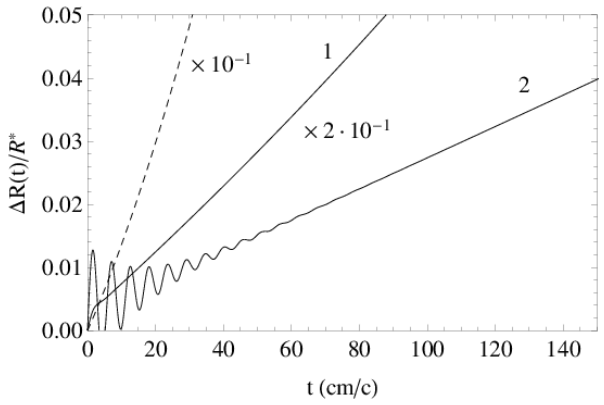

Fig. 2. Time variation of the bubble shape parameter R near the barrier point $R = R^*$ for various values of the relaxation parameter β. The solid curves *1* and *2* correspond to the values of $\beta = 2.6 \cdot 10^{-3}$eV (frequent collision regime) and $\beta = 2.6 \cdot 10^{-2}$eV (rare collision regime), respectively. The dashed is for an usual Markovian motion with a friction.

AVERAGE DESCRIPTION OF E1 GAMMA-TRANSITIONS IN HOT ATOMIC NUCLEI

V. A. Plujko[1,2], O. M. Gorbachenko[1], B. M. Bondar[1], E. P. Rovenskykh[1,2], V. A.Zheltonozhskii[2]

[1] Taras Shevchenko National University, Kyiv
[2] Institute for Nuclear Research, National Academy of Sciences of Ukraine, Kyiv

The average probabilities of gamma-transitions at γ-ray emission and photoabsorption can be described using the radiative (photon) strength functions (RSF) [1, 2]. These functions are involved in calculations of the observed characteristics of most nuclear reactions. They are also used for investigation of nuclear structure (nuclear deformations, energies and widths of the giant dipole resonances, contribution of velocity-dependent force, shape-transitions, etc.) as well as in studies of nuclear reaction mechanisms.

Isovector dipole electric γ-transitions (E1) are usually dominant in comparison with transitions of other multipolarities and types. Therefore reliable model of dipole RSF description is needed and simple expressions for RSF are preferable to decrease computation time.

The practical semiphenomenological methods of the RSF calculations based on excitation of the isovector giant dipole resonance (GDR) [1 - 3] are overviewed. New variant of modified Lorentzian approach (MLO4) for calculation of electric dipole RSF is proposed and tested [4, 5]. In this approach, RSF shape parameter ("energy-dependent width") is given as a function of the first quadrupole state energy in order to more properly take into account nuclear structure peculiarities. Recent data-base and systematics for the GDR parameters [3, 6, 7] were used for the calculations of the energy-dependent widths.

Figure shows an example of the comparison of the calculations of the dipole RSF of different forms with the experimental data for ^{168}Er ($U = S_n$) obtained at the JINR (Dubna) [8].

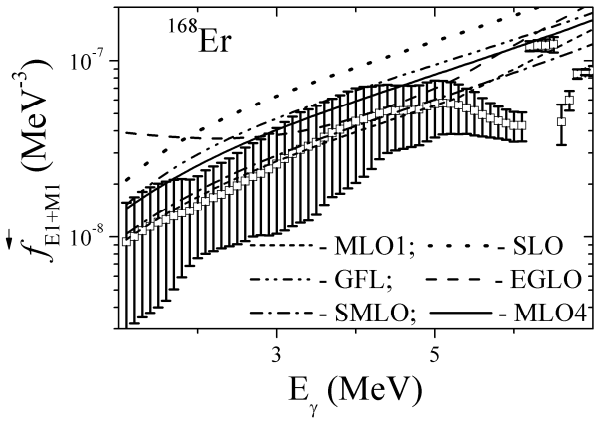

The calculations were performed within the framework of the approaches (see [1, 4, 5] for details): Standard Lorentzian (SLO), Enhanced Generalized Lorentzian (EGLO), Generalized Fermi Liquid (GFL), Modified Lorentzian (MLO1), Simplified Modified Lorentzian (SMLO) and MLO4.

The excitation functions and gamma-ray spectrum from (*n, xγ*) reactions on middle-weight and heavy atomic nuclei are also calculated with RSF of different shapes to choice optimal expression for the RSF [5, 9].

The overall comparison of the calculations within different simple models and experimental data shows that the EGLO and MLO (SMLO) approaches with vanishing values of strength function at zero gamma-ray energy provide rather reliable simple methods for estimation of the dipole RSF over a relatively wide energy interval ranging from zero to slightly above the GDR peak. In general, the new version of the MLO model (MLO4) leads to better description of the experimental data than previous ones as for gamma-decay and for photoexcitation functions.

1. R. Capote *et al.*, Nucl. Data Sheets **110**, 3107 (2009).
2. V.Yu. Denisov and V.A. Plujko, *Problems of atomic nucleus physics and nuclear reactions* (in Russian), (Kyiv University, Kyiv, 2013), 430 p.
3. V.A. Plujko, R. Capote, and O.M. Gorbachenko, At. Data Nucl. Data Tables **97**, 567 (2011).
4. V.A. Plujko, O.M. Gorbachenko, E.P. Rovenskykh, and V.O. Zheltonozhskii, Nucl. Phys. At. Energy **13**, 340 (2012).
5. V.A. Plujko, O.M. Gorbachenko, E.P. Rovenskykh, and V.A. Zheltonozhskii, Nucl. Data Sheets (to be published) (2014).
6. V.A. Plujko, O.M. Gorbachenko, V.M. Bondar, and R. Capote, J. Kor. Phys. Soc. **59** 1514 (2011).
7. V.A. Plujko, O.M. Gorbachenko, V.M. Bondar, and R. Capote, in *Proc. 3-rd Int. Conf. "Current Problems in Nuclear Physics and Atomic Energy", Kyiv, Ukraine, 2010* (Kyiv, 2011) Part 1, p. 342.
8. A.M. Sukhovoj, W.I. Furman, and V.A. Khitrov, in *Proc. XV Int. Sem. on Interaction of Neutrons with Nuclei, Dubna, 2007* (JINR, Dubna, 2008), p. 92.
9. V.A. Plujko, O.M. Gorbachenko, B.M. Bondar, and E.P. Rovenskykh, Nucl. Data Sheets (to be published) (2014).

KINETIC COEFFICIENTS FOR LOW-ENERGY PAIRING VIBRATIONS IN SUPERFLUID NUCLEI

V. I. Abrosimov

Institute for Nuclear Research, National Academy of Sciences of Ukraine, Kyiv

We study the effects of pairing on the kinetic properties of the low-energy collective nuclear motion by using the semiclassical anomalous density response function. The analytical expression of the anomalous density response function associated with the monopole pairing fluctuations has been obtained in a simple model, in which nuclei are represented as a system of A nucleons enclosed in a spherical cavity characterized by parameters (size, density, pairing gap Δ) typical of superfluid heavy nuclei [1]. It reads

$$\delta\kappa_r(r,\omega) = \frac{\alpha\, R_r^0(\omega)}{\alpha + R_r^0(\omega)}\delta U^{ext}(r,\omega) \qquad (1)$$

with

$$R_r^0(\omega) = I_1(\omega) - \frac{[I_2(\omega)]^2}{I_3(\omega)}\ , \quad \alpha = \int_0^\infty d\epsilon\, g(\epsilon)\frac{1}{E(\epsilon)}\ ,$$

$$I_i(\omega) = \int_0^\infty d\epsilon\, g(\epsilon)\frac{f_i(\epsilon)}{E^2(\epsilon)}\left[\frac{1}{\hbar\omega - 2E(\epsilon) + \imath\eta} - \frac{1}{\hbar\omega + 2E(\epsilon) + \imath\eta}\right],$$

$$f_1(\epsilon) = (\epsilon-\mu)^2\ ,\ f_2(\epsilon) = \epsilon-\mu\ ,\ f_3(\epsilon) = 1\,,$$

where $E(\epsilon) = \sqrt{(\epsilon-\mu)^2 + \Delta^2}$ is the quasiparticle energy and $g(\epsilon)$ is the energy density of states per unit volume in the equilibrium mean field, which is approximated in our model by a spherical square-well potential of radius R (and infinite depth), so that $g(\epsilon) \propto \epsilon^{1/2}$. The chemical potential μ is determined by the number of nucleons. The external field $\delta U^{ext}(r,\omega)$ causes the extra fluctuations of the real part of the pairing-field. The poles of the response function (1) correspond to pairing modes of the system.

We consider the low-frequency expansion (harmonic approximation) for the denominator of the response function (1). We have

$$\chi(\hbar\omega) \approx \chi(0) + i\left[\frac{\partial\chi}{\partial(\hbar\omega)}\right]_{\omega=0}\hbar\omega + \frac{1}{2}\left[\frac{\partial^2\chi}{\partial(\hbar\omega)^2}\right]_{\omega=0}(\hbar\omega)^2, \qquad (2)$$

where $\chi(\hbar\omega) \equiv \alpha + R_r^0(\hbar\omega)$. The three coefficients given by the expansion (2) define explicitly the kinetic parameters related to the low-frequency pairing vibrations.

The restoring force parameter $C = \chi(0)$ can be written as

$$C = \left[\Delta^2 + \left(\overline{(\epsilon-\mu)}\right)^2\right]\int_0^\infty d\epsilon\, g(\epsilon)\frac{1}{E^3(\epsilon)}, \qquad (3)$$

with

$$\overline{(\epsilon-\mu)} = \int_0^\infty d\epsilon\, g(\epsilon)\frac{1}{E^3(\epsilon)}(\epsilon-\mu)\Big/\int_0^\infty d\epsilon\, g(\epsilon)\frac{1}{E^3(\epsilon)}.$$

It is clear from Eq. (3) that the restoring force parameter is non-vanishing in superfluid nuclei.

The low-frequency (adiabatic) friction coefficient $\gamma = [\partial\chi/\partial(\hbar\omega)]_{\omega=0}$ is vanishing. This result is rather expected taking into account the fact of existence of double pairing gap in the single-particle energy spectrum. So that the Landau damping, which is the unique source of friction in our model, is absent.

From the expansion (2) we can obtain an explicit expression for the mass parameter that is defined as $B = -(1/2)[\partial^2\chi/\partial(\hbar\omega)^2]_{\omega=0}$. It can be written as

$$B = \frac{1}{4}\int_0^\infty d\epsilon\, g(\epsilon)\frac{1}{E^5(\epsilon)}\left[(\epsilon-\mu) - \overline{(\epsilon-\mu)}\right]^2. \qquad (4)$$

There is the coherent contribution to the mass parameter in superfluid nuclei.

By using the restoring force parameter (3) and the mass parameter (4) we can find the approximate analytical expression for the frequency of the monopole pairing mode. We can get

$$\hbar\omega_{pv} \approx 2\Delta\sqrt{\int_0^\infty d\epsilon\, g(\epsilon)\frac{1}{E^3(\epsilon)}\Big/\left(\int_0^\infty d\epsilon\, g(\epsilon)\frac{1}{E^3(\epsilon)} - \Delta^2\int_0^\infty d\epsilon\, g(\epsilon)\frac{1}{E^5(\epsilon)}\right)}.$$

The energy of the monopole pairing vibrations is greater than double pairing gap.

We have derived semiclassical analytical expressions for the restoring force and mass parameters associated with monopole pairing vibrations in the low-frequency limit. According to our semiclassical results, the pairing correlations give rise to a coherent contribution to the kinetic properties of slow collective nuclear motion.

1. V.I. Abrosimov, D.M. Brink, and F. Matera, in *Book of Abstracts. 63 Int. Conf. "Nucleus 2013"*. (Saint-Petersburg, 2013), p. 161.

SURFACE SYMMETRY ENERGY AND ISOVECTOR DIPOLE-RESONANCE STRUCTURE IN NUCLEI

J. P. Blocki[1], A. G. Magner[2], P. Ring[3]

[1] *National Center for Nuclear Research, Otwock, Poland*
[2] *Institute for Nuclear Research, National Academy of Sciences of Ukraine, Kyiv*
[3] *Technical University of Munich, Garching, Germany*

The collective excitations of exotic nuclei with a large neutron excess can be studied analytically by using the effective surface approximation (ES) within the extended Thomas - Fermi (ETF) approach and the semi-classical Fermi-liquid droplet model (FLDM) [1, 2]. The isovector dipole-resonance (IVDR) strength function $S(\omega)$ as a function of the excitation energy $\hbar\omega$ can be calculated using the macroscopic boundary conditions to the kinetic Landau - Vlasov equations with an isovector dipole external force [3]. The FLDM transition density was calculated as the dynamical part of the particle density. In the FLDM, the boundary condition of the equivalence of normal forces acting on the ES depends on the surface symmetry energy (SSE) constant k_S through the isovector capillary pressure $\delta P_S \propto k_S I^2 A^{1/3} \cos\theta$ for the IVDR radius vibrations $\delta R \propto R\cos\theta$ of the ES, where $I = (N-Z)/A$ is the asymmetry parameter, N is the neutron and Z is the proton number in a nucleus, $A = N + Z$.

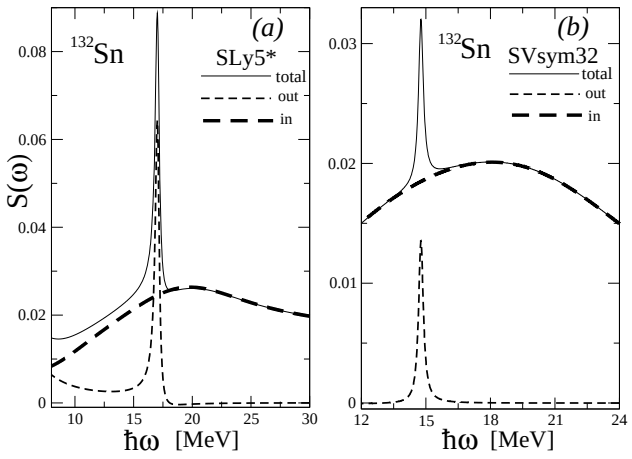

The IVDR two-peak strength functions $S_n(\omega)$, "out-of-phase" (n = 1) and "in-phase" (n = 2), as a function of the excitation energy $\hbar\omega$ for the Skyrme forces SLy5* (a) and SVsym32 (b), as example; $\tau = 4.4\cdot 10^{-21}$ s is the relaxation time of the collisional term in the Landau - Vlasov equations.

Figure shows the two-peak IVDR strength structure in ^{132}Sn for several Skyrme forces. The main n = 1 peak related to the "out-of-phase" vibration of the particle density inside of the nucleus for the Skyrme interaction SLy5* (a) appears at the energy $E_1 = 17.0$ MeV with the energy weighted sum rule $\mathrm{EWSR}_1 = 68$ %, $E_n = \hbar\omega_n$. The satellite n = 2 IVDR peak corresponding to the "in-phase" vibrations with $E_2 = 19.8$ MeV and $\mathrm{EWSR}_2 = 32$ % (a) is found on the right hand side of the main peak. For SVsym32 (b), one arrives at the opposite situation, $E_1 = 18.1$ MeV with $\mathrm{EWSR}_1 = 64$ % and $E_2 = 14.8$ MeV with $\mathrm{EWSR}_2 = 36$ % on the left side. The mean IVGDR energies and EWSRs are in fair agreement with the experimental data.

We found the satellite (pygmy) IVDR energies and EWSR to depend in a more sensitive way on the SSE value, k_S = -3.9 MeV for SLy5*, and 3.4 MeV for SVsym32, calculated all analytically through the Skyrme force parameters, as compared to the average characteristics of the main peaks. The corresponding isovector neutron skin stiffnesses are given respectively by Q = 107 MeV (stable vibration mode) and -118 MeV (unstable one), which differ e lot, even in sign.

The neutron transition densities are always significantly larger than the proton ones near the nuclear edge, such that one has a neutron skin around a symmetrical core. The characteristics of the pygmy IVDRs in several neutron-reach double-magic isotopes like ^{208}Pb, ^{132}Sn and ^{68}Ni are obtained in a qualitative agreement with the experimental data and other semi-microscopical calculations.

As perspectives, it would be worth to apply our results to the systematic IVDR calculations of the pygmy IVDRs within the FLDM and the isovector low-lying collective states by using the periodic orbit theory.

1. J.P. Blocki, A.G. Magner, P. Ring, and A.A. Vlasenko, Phys. Rev. C **87**, 044304 (2013).
2. V.M. Kolomietz, A.G. Magner, and S. Shlomo, Phys. Rev. C **73**, 024312 (2006).
3. J.P. Blocki, A.G. Magner, and P. Ring, arXiv:1312.6051 [nucl-th] (2013), Phys. Scr. T, in print, 2014.

SEMICLASSICAL SHELL-STRUCTURE MOMENT OF INERTIA IN THE PHASE-SPACE VARIABLES

D. V. Gorpinchenko[1,2], A. G. Magner[1], J. Bartel[3],

[1] *Institute for Nuclear Research, National Academy of Sciences of Ukraine, Kyiv*
[2] *National Technical University of Ukraine "Kyiv Polytechnic Institute", Kyiv*
[3] *Institut Pluridisciplinaire Hubert Curien, Strasbourg University, Strasbourg, France*

Many significant phenomena deduced from the experimental data on nuclear rotations were explained within theoretical approaches based mainly on the cranking model, and the Strutinsky shell correction method [1]. The moment of inertia (MI) for collective adiabatic (statistical-equilibrium) rotations can be simply described through a decomposition in terms of the Extended Thomas - Fermi (ETF) MI and shell corrections [1, 2]. The MI shell components are obtained analytically in the adiabatic approximation as a sum over periodic orbits (POs) in a mean potential well of the cranking model. In the present work, we obtain a semiclassical phase-space trace formula for the MI in terms of the free-energy shell corrections.

Such a local approach is based on the approximate semiclassical representation in terms of the particle density $\rho(\mathbf{r}) = \rho_{ETF}(\mathbf{r}) + \delta\rho(\mathbf{r})$ through the rigid body MI. For a statistically equilibrium rotation around the x axis, perpendicular to the symmetry z axis

$$\Theta_x \approx \Theta_x^{rig} = \int d\mathbf{r}\, r_x^2 \rho(\mathbf{r}) = \Theta_x^{ETF} + \delta\Theta_x$$

with $r_x^2 = y^2 + z^2$, where Θ_x^{ETF} is the smooth ETF component related to the local ETF particle density $\rho_{ETF}(\mathbf{r})$. The MI shell correction $\delta\Theta_x = \int d\mathbf{r}\, r_x^2 \delta\rho(\mathbf{r})$ is determined by the non-homogeneity of the energy spectrum near the Fermi surface. The shell correction to the particle density is given by $\delta\rho(\mathbf{r}) = -\mathrm{Im}\sum_{CT}\int d\varepsilon\, G_{CT}(\mathbf{r}_1, \mathbf{r}_2, \varepsilon)/\pi$ for $\mathbf{r}_1 \to \mathbf{r}_2 \to \mathbf{r}$. The integration is performed over the energies ε. The sum runs over the closed classical trajectories (CT), connecting two spatial points $\mathbf{r}_1$ and $\mathbf{r}_2$ in the volume of the rotating system with a non-zero action. The component of the single-particle Green's function G_{CT} for the isolated CT is given by the extended Gutzwiller periodic orbit theory.

By using the stationary phase method for the calculation of the MI, one obtains after simple transformations the phase-space trace formula:

$$\Theta_x \approx \mathrm{Re}\sum_{CT}\int d\varepsilon \int \frac{d\mathbf{r}''\, d\mathbf{p}'}{(2\pi\hbar)^3} r_x''^2\, |J_{CT}(\mathbf{p}_\perp', \mathbf{p}_\perp'')|^{1/2} \times$$

$$\times \delta(\varepsilon - H(\mathbf{r}', \mathbf{p}')) \exp\left\{\frac{i}{\hbar}\left[S_{CT}(\mathbf{r}', \mathbf{r}'', \varepsilon) + \mathbf{p}'(\mathbf{r}' - \mathbf{r}'')\right]\right\} \times$$

$$\times \exp(-i\pi\, \mu_{CT}/2), \qquad (1)$$

where $S_{CT}(\mathbf{r}', \mathbf{r}'', \varepsilon)$ is the action along the CT, J_{CT} is the Jacobian transformation from the initial $\mathbf{p}_\perp'$ to the final $\mathbf{p}_\perp''$ particle momenta perpendicular to the CT, and μ_{CT} is the Maslov phase. The sum runs over all isolated CTs.

Accounting for the phase-space trace formula for the semiclassical level density $g_{sc}(\varepsilon)$ [3] (see Eq. (1) but without an energy integration and the r_x^2 factor), one obtains an approximate relation between the MI Θ_x and the free energy F as a sum of smooth-ETF and oscillating (shell) components, $\Theta_x \approx \Theta_x^{ETF} + \left\langle r_x^2/\varepsilon \right\rangle \delta F$. Here, one applies $\left\langle r_x^2/\varepsilon \right\rangle = \int d\varepsilon\, r_x^2 g_{sc}(\varepsilon) / \int d\varepsilon\, \varepsilon\, g_{sc}(\varepsilon) = \left\langle r_x^2/\varepsilon \right\rangle_{ETF} + \delta\left\langle r_x^2/\varepsilon \right\rangle$, [with $g_{sc}(\varepsilon) = g_{ETF}(\varepsilon) + \delta g_{sc}(\varepsilon)$], and $F = F_{ETF} + \delta F$. The semiclassical (free-) energy shell corrections [1], $\delta F = \sum_{PO}[\pi t_{PO} T/\sinh(\pi t_{PO} T/\hbar)]\delta E_{PO}/\hbar$ and $\delta E = \sum_{PO}\delta E_{PO}$ are the sums over POs (or their isolated families), $\delta E_{PO} = (\hbar/t_{PO})^2 \delta g_{PO}(\varepsilon)$, $\delta g_{sc}(\varepsilon) = \sum_{PO}\delta g_{PO}(\varepsilon)$, $t_{PO} = \partial S_{PO}(\varepsilon)/\partial\varepsilon$ is the time period for a motion of the particle along the PO, $S_{PO}(\varepsilon)$ the action along the PO, and T the temperature. As a final result, the leading MI shell correction is given by $\delta\Theta_x \approx \left\langle r_x^2/\varepsilon \right\rangle \delta F$.

We shall use these phase-space trace formulas for calculating the MI shell corrections in the case of a spheroidal cavity potential like in [1], and then, compare them with the quantum-mechanical results.

1. A.G. Magner, A.S. Sitdikov, A.A. Khamzin, and J. Bartel, Phys. Rev. C 81, 064302 (2010).
2. A.G. Magner, D.V. Gorpinchenko, and J. Bartel, arXiv, 2013, Phys. At Nucl., in print 2014.
3. A.G. Magner, K. Arita, and S.N. Fedotkin, Prog. Theor. Phys. **115**, 523 (2006).

TRACE FORMULA FOR BIFURCATIONS NEAR THE SADDLE OF THE NON-INTEGRABLE HÉNON-HEILES POTENTIAL BARRIER

M. V. Koliesnik[1,2], A. G. Magner[1], Ya. D. Krivenko-Emetov[1,2], K. Arita[3], M. Brack[4]

[1] *Institute for Nuclear Research, National Academy of Sciences of Ukraine, Kyiv*
[2] *National Technical University of Ukraine "Kyiv Polytechnic Institute", Kyiv*
[3] *Department of Physics, Nagoya Institute of Technology, Nagoya, Japan*
[4] *Institute for Theoretical Physics, University of Regensburg, Regensburg, Germany*

The transition probability for the Fermi particle motion through the non-integrable Hénon-Heiles (HH) potential barrier in two and three dimensions is an exciting subject of nuclear and astronomic physics. A semi-analytical trace formula for the level density $g(E)$ within the periodic orbit (PO) theory [1] for the famous HH Hamiltonian was derived in [2] using uniform approximations based on the normal-form theory of pitchfork bifurcations [3]. The trace formula for the oscillating component $\delta g(E)$ of the level density $g(E)$ accounting for a dense cascade of such bifurcations near the saddle was considered also in [4] for an integrable HH-potential using the improved stationary phase method (ISPM) [5], based on extensions of the semiclassical Gutzwiller path integral approach [1]. In the present work, we obtain analytically the trace formula for $\delta g(E)$ for the standard non-integrable HH Hamiltonian within the ISPM [4, 5] valid for an arbitrarily dense sequence of bifurcations.

Within the generalized ISPM [5], the generating function $\hat{S}(Q,p,E)$ can be derived as an extension of the normal form theory [3] for suitable Poincaré variables Q and p. Using a 4th-order expansion of the action phase (and, relatively, the pre-exponential amplitudes) in the phase-space trace formula [4] near the stationary points x^*, p_x^* in the x, p_x coordinates perpendicular to y, p_y along the parent orbit A in a pitchfork bifurcation scenario [1 - 6], one has $\hat{S}_{CT}(Q,p,E) = S_{PO}(E) + pQ + \varepsilon_{PO}^{(Q)}Q^2 + a_{PO}^{(Q)}Q^4 + \varepsilon_{PO}^{(p)}p^2 + a_{PO}^{(p)}p^4$. Here, $Q = x(T_{PO}) - x^*$ for the finite spatial coordinate $x(T_{PO})$ at the PO time period T_{PO} and $p = p_x(0) - p_x^*$ with the initial momentum $p_x(0)$ for the classical trajectory (CT), $S_{PO}(E) = \oint_{PO} \mathbf{p}d\mathbf{r}$ is the action along the PO. The coefficients correspond obviously to the derivatives of $\hat{S}_{CT}(Q,p,E)$. The stationary points Q^* and p^* are related to the parent A_σ, rotational R_σ and librating L_σ POs, respectively, specified by the Maslov index σ in the pitchfork bifurcation scenarios. Performing more exact integrations over Q and p, one then obtains for the oscillating level density

$$\delta g_{scl}(E) = \frac{1}{(2\pi\hbar)^2}\,\mathrm{Re}\sum_{PO} T_{PPO} A\left(\frac{\varepsilon_{PO}^{(Q)}}{\hbar}, \frac{a_{PO}^{(Q)}}{\hbar}\right) A\left(\frac{\varepsilon_{PO}^{(p)}}{\hbar}, \frac{a_{PO}^{(p)}}{\hbar}\right) \times$$

$$\times \exp\left[\frac{i}{\hbar}S_{PO}(E) - \frac{i\pi}{2}\sigma_{PO} - i\phi\right], \qquad (1)$$

where T_{PPO} is the period for a primitive PO,

$$A(\varepsilon, a) = \frac{\pi}{2}\sqrt{\frac{\xi}{|\varepsilon|}}\exp\left[-i\left(\xi - \frac{\pi}{8}\right)\right] \times$$

$$\times\left\{J_{-1/4}(\xi) - \frac{\varepsilon}{|\varepsilon|}\exp\left[-i\frac{\pi}{4}\right]J_{1/4}(\xi)\right\},$$

is the amplitude, $\xi = \varepsilon^2/8a$, $a > 0$ (complex conjugate for $a < 0$), ϕ is another constant phase [5]. In (1), the sum runs over POs like A_σ, R_σ and L_σ near the saddle. $J_{\pm 1/4}(\xi)$ are the Bessel functions of fractional order $\pm 1/4$. (Bessel function components of order $\pm 3/4$ and etc. can be derived by taking into account higher-order terms in the pre-exponent amplitude expansion.) The trace formula (1) has the correct limit to the standard Gutzwiller formula for isolated POs asymptotically far away from the bifurcations, and continuously crosses all symmetry-breaking (bifurcation) points where an enhancement of the amplitudes occurs [4,5]. In particular, one gets also the results obtained in [3] locally near the bifurcation points. We expect to obtain good agreement between the semiclassical and quantum averaged level densities for the gross- and fine-shell structures, and for the exact energy shell corrections in the case of the infinitely dense cascade of bifurcations, which is in progress. For the (coarse-grained) gross-shell-structure, the trace formula (1) should agree with the uniform approximation found in [2].

1. M. Brack and R.K. Bhaduri, *Semiclassical Physics,* 2nd ed. (Westview, Boulder, CO, 2003).
2. M. Brack and J. Kaidel, Phys. Rev. E **70,** 016206 (2004).
3. H. Schomerus and M. Sieber, J. Phys. A **30** 4537 (1997).
4. A.G. Magner, K. Arita, and S.N. Fedotkin, Prog. Theor. Phys. **115**, 523 (2006).
5. A.G. Magner, I.S. Yatsyshyn, A. Arita, and K. Brack, Phys. At. Nucl. **74**, 1445 (2011).
6. S.N. Fedotkin, A.G. Magner, and M. Brack, Phys. Rev. E **77**, 066219 (2008).

SHELL EFFECT IN THE SCISSION-POINT CONFIGURATION OF FISSIONING NUCLEI

F. A. Ivanyuk

Institute for Nuclear Research, National Academy of Sciences of Ukraine, Kyiv

In the theory of nuclear fission quasistatic quantities like the potential energy surface, the ground state energy and deformation, the fission barrier height, etc., are commonly calculated within the macroscopic-microscopic method. In this method the total energy of the fissioning nucleus consists of the two parts, macroscopic and microscopic. Both parts are calculated at the fixed shape of nuclear surface. In the past a lot of shape parameterizations were proposed and used. A good choice of the shape parameterization is often a key to the success of the theory. Usually, one relies on physical intuition for the choice of the shape parameterization.

A method to define the shape of the nuclear surface which does not rely on any shape parameterization was proposed by V. Strutinsky in [1]. In this approach the shape of an axial, left-right symmetric nucleus was defined by looking for the minimum of the liquid-drop energy under the additional restrictions that fix the volume and elongation of the drop.

Recently the method was further developed [2, 3] by incorporating the axial [4, 5] and left-right asymmetry [6] of the nuclear shape.

The important result of the Strutinsky procedure [1] is the possibility to definite in a formal way the scission point as the maximal elongation at which the nucleus splits into two fragments.

In the present work the attention is focused on the scission point configuration. The shape at the scission point and the corresponding deformation energy are examined in detail and an approximation is suggested for the evaluation of the fission observables: the mass, total kinetic energy and total excitation energy distribution of the fission fragments.

Three minima in the scission point deformation energy are found corresponding to the "standard", "supershort" and "superlong" fission modes. The contribution of each fission mode to the mass distribution of the fission fragments and total kinetic energy is discussed and compared with the experimental results.

In the example of the fission process of U-235 by thermal neutrons it is shown that the present approach reproduces correctly the position of the peaks of the mass distribution of the fission fragments, the value and the fine details of the total kinetic energy distribution (see Figure) and the magnitude of the total excitation energy of the fission fragments.

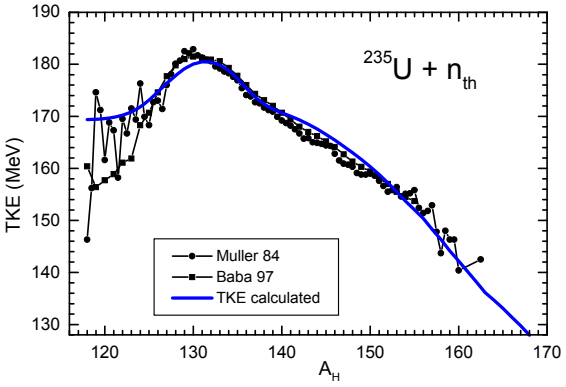

The calculated (solid line) and the measured (circles [7], squares [8]) total kinetic energy of fission fragments.

The results of this work will be published in [9].

1. V.M. Strutinsky, N.Ya. Lyashchenko, and N.A. Popov, Nucl. Phys. **46**, 659 (1963).
2. F. Ivanyuk, Int. J. Mod. Phys. E **18**, 130 (2009).
3. F. Ivanyuk and K. Pomorski, Phys. Rev. C **79**, 054327 (2009).
4. F.A. Ivanyuk, K. Pomorski, and J. Bartel, Int. J. Mod. Phys. E **21**, 1250032 (2012).
5. F.A. Ivanyuk and K. Pomorski, Phys. Scr. **154**, 014021 (2013).
6. F.A. Ivanyuk, Physics Procedia **47**, 17 (2013).
7. R. Muller *et al.*, Phys. Rev. C **29**, 885 (1984).
8. H. Baba *et al.*, J. Nucl. Sc. Techn. **34**, 871 (1997).
9. F.A. Ivanyuk, Physica Scripta, in print.

THE EFFECT OF THE NUCLEAR COULOMB FIELD ON ATOMIC IONIZATION AT POSITRON ELECTRON ANNIHILATION AT β^+-DECAY

S. N. Fedotkin

Institute for Nuclear Research, National Academy of Sciences of Ukraine, Kyiv

It is considered the process of annihilation of positron emitted at β^+-decay and K-electron of daughter's atom. A part of energy during this process is passed to other K-electron or to s-electrons from different n-shells (n = 2, 3, 4). As result this electron leaves atom.

At calculation of probability of this process for the atomic electron is used hydrogen like wave functions. Nuclear charge screening is essential for the electrons of external shells. Here this screening is taken in to account by use the Slater approach [1].

The parameter $Z\alpha c/\upsilon$ can be much bigger 1 at very small velocity of the ejected electron υ and Born approximation becomes in this case incorrect (here Z is a nuclear charge, α is the fine structure constant, c is a light velocity). Because of this in contrast to paper [2] the electron which leaves atom is described by the wave function of continuum spectra in Coulomb field. On this reason instead of free particle Green function is used Green function for electron in a Coulomb field. Since we consider the allowed β^+-decay and following positron annihilation with K-electron the Green function is proportional to the Whittaker function $W_{\eta_0,1/2}(2br)$ where

$$\eta_0 = Z\alpha\frac{E_1}{b} \qquad b = \sqrt{m^2 - E_1^2} \qquad E_1 = 2E_{1S} - \varepsilon \ .$$

Here m is a electron mass, ε is the energy of electron ejected from the atomic shell in point r, E_{1S} is K-electron energy.

General expression for probabilities of this processes are received for the atom with arbitrary Z.

It is shown that use of Sommerfeld factor for the correction of Born approximation at the calculation of this process probability is not enough [2]. The probability of this process calculated with exact wave functions is much smaller. In a case of β^+-decay of ^{45}Ti use of wave function of continuum spectra in Coulomb field reduces probability in several time. But use of Green function for electron in a Coulomb field gives opposite effect – probability of ionization of atom increases.

The ratio of probabilities of K-electron positron annihilation and following other K-electron knock-out with Coulomb field accounting $W^{coul}_{\beta^+K,K}$ and disregarding it $W_{\beta^+K,K}$ is approximately $W^{coul}_{\beta^+K,K}/W_{\beta^+K,K} \approx 1.7$ for this nucleus. The analogous ratio of probabilities for usual β^+-decay is $W^{coul}_{\beta^+}/W_{\beta^+} \approx 0.56$. Hereby there are the following estimates for the ratio of probabilities of considered processes

$$W^{coul}_{\beta^+K,K}/W^{coul}_{\beta^+} \approx 3\, W_{\beta^+K,K}/W_{\beta^+} \approx 1.8\cdot 10^{-5} .$$

For the ratio of probabilities of processes with participation of electrons from external shells the screening factor is more essential. The ratio of probabilities in this case is changed slightly.

Thereby taking into account the Coulomb field influence is important as for calculations of probability of β^+-decay and following atomic ionization at positron annihilation so for the ratios of these probabilities.

1. S.E. Frisch, *The optical spectra of the atoms* (Fiz.-Mat., Moscow, 1963), p. 197.
2. S.N. Fedotkin, Nucl. Phys. At. Energy **13**, 223 (2012).

THE MULTI-DIMENSIONAL MODEL OF CLUSTER DECAY

V. Yu. Denisov

Institute for Nuclear Research, National Academy of Sciences of Ukraine, Kyiv

The cluster decays ^{228}Th→^{208}Pb + ^{20}O, ^{232}U→ ^{208}Pb + ^{24}Ne, ^{236}Pu→ ^{208}Pb + ^{28}Mg and ^{242}Cm→ ^{208}Pb + ^{34}Si are considered in the framework of the multi-dimensional cluster preformation model [1].

The macroscopic potential energy surface related to interaction between the cluster and the residue nucleus is evaluated in the framework of the non-local $\hbar^4$ extended Thomas - Fermi approach with Skyrme and Coulomb forces.

The shell-corrections to the macroscopic potential energy are also taken into account.

The dynamical surface deformations of both the cluster and the residue nucleus are taken into consideration at the barrier penetration path. The heights of saddle points related to deformed nuclear shapes are lower than the barrier height between the spherical cluster and residue nuclei; therefore the dynamical deformations of nuclei increase the barrier penetrability and reduce the half-life of cluster decay.

The trajectories of cluster decay at hydrodynamic values of the collective mass parameters are related to very deformed shapes at small distances between cluster and daughter nuclei. In contrast to this, the trajectories of cluster decay at realistic values of the collective mass parameters pass through the slightly deformed shapes. The shape of residue nucleus is prolate along the cluster decay path.

Note that nuclei ^{20}O and ^{34}Si have spherical ground-state shape, while nuclei ^{24}Ne and ^{28}Mg have oblate and prolate ground-state shape, respectively. The dynamical deformation of the cluster nucleus depends on the ground-state deformation of the cluster strongly. So, the trajectory of cluster decay is different for spherical, prolate and oblate nuclei at large distances between the cluster and residue nucleus.

It is shown that the dynamical deformation of the residue nucleus effects the decay half-life much stronger than the dynamical deformation of the cluster.

The values of half-life evaluated with dynamical deformation are much smaller than the one without dynamical deformation.

The shell-correction contribution to total interaction potential between the cluster and the residue nucleus is very important for the potential energy landscape as well as for the half-life evaluation. The large negative value of shell-correction in the ground-state of ^{208}Pb drastically changes both the potential energy landscape and the cluster-decay half-life.

The heights of the barrier between prolate nuclei are lower than the height of the barrier between spherical nuclei. Therefore the dynamical deformations of nuclei increase the barrier penetrability and reduce the half-life value. The influence of dynamical deformations of nuclear shape around the barrier is very important for an accurate description of cluster emission half-life.

The experimental values of cluster decay half-lives are well reproduced in the model.

1. V.Yu. Denisov, Phys. Rev. C **88**, 044608 (2013).

RELAXED-DENSITY NUCLEUS-NUCLEUS POTENTIAL WITH SHELL-CORRECTION CONTRIBUTION AND EMPIRICAL NUCLEUS-NUCLEUS

V. Yu. Denisov

Institute for Nuclear Research, National Academy of Sciences of Ukraine, Kyiv

The nucleus-nucleus potential is a key ingredient for description of nuclear reactions. Microscopic evaluation of potential between nuclei is based on both the effective nucleon-nucleon force and the nucleon density distributions of interacting nuclei. There are also simple parametrization for the nucleus-nucleus potential, which are often used for description various heavy-ion reactions due to simplicity.

The goal of this study is to find the simple analytical parametrization of nucleus-nucleus potential, which nicely describes semi-microscopic nucleus-nucleus potentials around barrier for various heavy-ion systems and the empirical barriers.

According to the Strutinsky shell-correction prescription [1] the total energy of nucleus consists of macroscopic and microscopic contributions. The Strutinsky shell corrections [1] are important ingredient of atomic mass description, which strongly improve the accuracy of atomic mass prediction. Therefore we take into account the shell-corrections contribute into the nucleus-nucleus interaction.

The semi-microscopic nucleus-nucleus potential is a macroscopic part of a total potential. We evaluate the semi-microscopic potential by using the semiclassical approximation for realistic energy density functional and realistic relaxed-density parametrization of nucleon density dynamics during fusion reaction.

The interaction energy of two nuclei evaluated by using the non-local $\hbar^2$ and $\hbar^4$ terms of extended Thomas-Fermi energy density functional with Skyrme and Coulomb contributions are the macroscopic part of the total interaction energy. 1485 macroscopic potentials between all possible combinations of 54 spherical nuclei from ^{16}O to ^{216}Po are evaluated at 12 distances around the touching point. By fitting these values we obtain the macroscopic part of the nucleus-nucleus potential.

When the nuclei are approaching to each other the shell structures of both nuclei are changed due to interaction of nucleons belonging to different nuclei. The variation of the single-particle shell energies in both nuclei induced by nucleon-nucleus interaction should contribute into the full potential. Therefore the microscopic shell-correction energies of both nuclei are changed at small distances between nuclei. Such variation of the microscopic shell-correction energies should be added to the macroscopic contribution for correct evaluation the total interaction energy of two nuclei. We propose simple approximation for evaluation of the shell-correction contribution into the nucleus-nucleus potential.

As the result, we introduce the new semi-empirical relaxed-density nucleus-nucleus potential with shell correction contribution. This potential can reproduce both semi-microscopic nucleus-nucleus potentials for various heavy-ion systems and the empirical barrier heights with small value of the root mean square error.

We show that the shell correction contribution is important ingredient on the nucleus-nucleus interaction and propose a simple approach for evaluation of it. The shell correction contribution shows how the total potential for specific nucleus-nucleus system deviates from the global macroscopic potential, which smoothly depends on numbers of protons and neutrons in interaction nuclei. The shell correction contribution into potential relates to inner structure of nuclei, which is disturbed by mutual influence of colliding nuclei.

The comparative study of fusion barrier heights for spherical colliding nuclei evaluated for various empirical potentials show that the relaxed-density potential with shell correction contribution describes better the empirical barrier heights than other potentials.

1. V.M. Strutinsky, Sov. J. Nucl. Phys. **3**, 449 (1966); Nucl. Phys. A **95**, 420 (1967); **122**, 1 (1968); M. Brack, J. Damgaard, A.S. Jensen, *et al.*, Rev. Mod. Phys. **44**, 320 (1972).

BARRIER BETWEEN DEFORMED NUCLEI

V. Yu. Denisov, T. O. Margitych

Institute for Nuclear Research, National Academy of Sciences of Ukraine, Kyiv

Nuclei can deform at small distances between them due to interaction between nucleons in interacting nuclei. Therefore a barrier height of nucleus-nucleus potential depends on the deformations of the nuclei and the mutual orientation of them. We search the minimal barrier height between nuclei with spherical ground-states. The minimal value of barrier height is related to the nose-to-nose orientation of prolate nuclei [1].

The full nucleus-nucleus potential energy consists of Coulomb, nuclear parts and energy related to deformation of each nucleus. The ground-state shape of interacting nuclei are spherical, therefore the addition energy should be added to deform these nuclei.

The nuclear and Coulomb contributions into potential energy are evaluated using Eqs. in Refs. [1, 2]. Energy related to deformation is obtained in the framework of liquid-drop model. The quadrupole deformation of interacting nuclei is considered.

The total potential energy is evaluated at different distances between nuclei and various deformations of each nucleus. The barrier heights are obtained for various values of deformations of interacting nuclei; see, for example, Figs. 1 and 2.

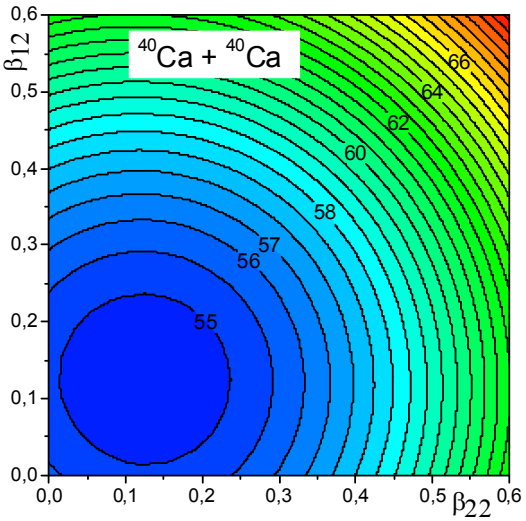

Fig. 1. The dependence of barrier height on the quadrupole deformation parameter for system nuclei ^{40}Ca + ^{40}Ca.

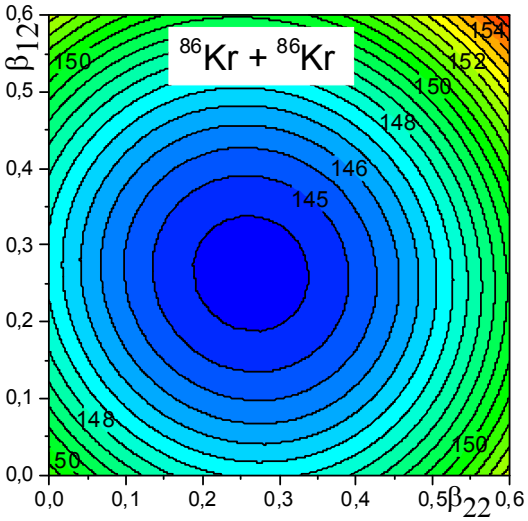

Fig. 2. The dependence of barrier height on the quadrupole deformation parameter for system nuclei ^{86}Kr + ^{86}Kr.

It is found that the lowest barrier height is taken place for both deformed nuclei, see Figs. 1 and 2. The values of deformation parameters are obtained.

The difference between the barrier height of spherical nuclei and the lowest barrier height rises with mass and charge of interacting nuclei.

The values of deformation parameter related to the lowest barrier increases with mass and charge of interacting nuclei too, compare Figs. 1 and 2.

1. V.Yu. Denisov and N.A. Pilipenko, Phys. Rev. C **76**, 014602 (2007).
2. V.Yu. Denisov, Phys. Lett. B **526**, 315 (2002).

ISOTOPIC AND NEUTRON EXCESS EFFECTS OF BOTH THE NUCLEUS-NUCLEUS INTERACTION AND THE FUSION CROSS SECTIONS

V. Yu. Denisov, V. A. Nesterov

Institute for Nuclear Research, National Academy of Sciences of Ukraine, Kyiv

The nucleus-nucleus interactionc potentials and the fusion cross-sections around barrier for heavy nuclei along and far the beta-stability are studied in details.

The nucleus-nucleus potentials are evaluated in the framework of semi-microscopic approximation [1 - 3]. The proton and neutron densities of nuclei are obtained in the Hartree-Fock-BCS approximation with Skyrme force. The nucleus-nucleus potentials are determined as

$$V(R) = E_{12}(R) - E_1 - E_2,$$

where E_1 and E_2 are the energy of corresponding nuclei at infinite distance between mass centers and $E_{12}(R)$ is the energy of nuclear system at finite distance between mass centers of nuclei. Energies E_1, E_2 and $E_{12}(R)$ are evaluated in the framework of energy-density approximation with Skyrme force [1 - 3]. The kinetic energy density is considered in the framework of semiclassical approximation with $\hbar^2$ gradient corrections [1 - 3].

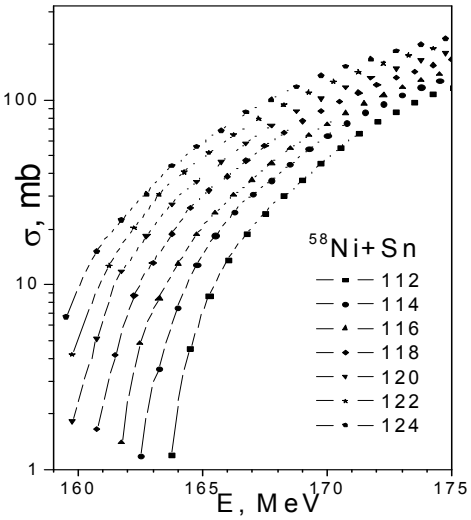

Fig. 1. Isotopic dependence in fusion cross sections for ^{58}Ni and different Sn isotopes.

The tails of semi-microscopic nucleus-nucleus potentials are approximated by the Woods-Saxon potential. The Woods-Saxon potential with obtained parameters is used at calculation the fusion cross sections around barrier. The fusion cross sections are found in the framework simplified coupled-channel model CCFULL [4] (see Figs. 1 and 2).

The nucleus-nucleus interaction potentials and the fusion cross-sections around barrier for systems ^{58}Ni+^{112}Sn, ^{58}Ni+^{114}Sn, ^{58}Ni+^{116}Sn, ^{58}Ni+^{118}Sn, ^{58}Ni+^{120}Sn, ^{58}Ni+^{122}Sn, ^{58}Ni+^{124}Sn, ^{58}Ni+^{126}Sn, ^{58}Ni+^{128}Sn, ^{58}Ni+^{130}Sn, ^{58}Ni+^{132}Sn, ^{64}Ni+^{112}Sn, ^{64}Ni+^{114}Sn, ^{64}Ni+^{116}Sn, ^{64}Ni+^{118}Sn, ^{64}Ni+^{120}Sn, ^{64}Ni+^{122}Sn, ^{64}Ni+^{124}Sn, ^{64}Ni+^{126}Sn, ^{64}Ni+^{128}Sn, ^{64}Ni+^{130}Sn and ^{64}Ni+^{132}Sn are studied. The isotopic and neutron excess effects are discussed in details.

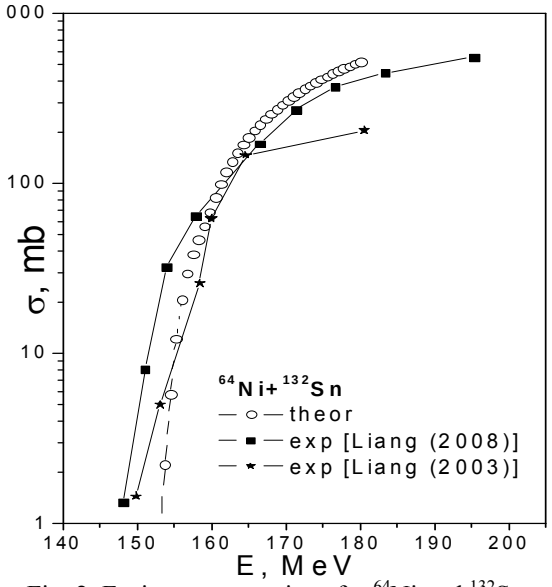

Fig. 2. Fusion cross sections for ^{64}Ni and ^{132}Sn.

1. V.Yu. Denisov and W. Norenberg, Eur. Phys. J. A **15**, 375 (2002).
2. V.Yu. Denisov and V.A. Nesterov, Phys .At. Nucl. **69**, 1472 (2006).
3. V.Yu. Denisov and V.A. Nesterov, Phys. At. Nucl. **73**, 1142 (2010).
4. K. Hagino, N. Rowley, and A.T. Kruppa, Comp. Phys. Comm. **123**, 143 (1999).

RIGID-PROJECTILE MODEL FOR THE ELASTIC DEUTERON SCATTERING FROM α-CLUSTER NUCLEI

Yu. A. Berezhnoy[1], D. V. Fedorchenko[2], V. P. Mikhailyuk[3], V. V. Pilipenko[2]

[1] V. N. Karazin Kharkiv National University, Kharkiv
[2] National Science Center "Kharkov Institute of Physics and Technology", Kharkiv
[3] Institute for Nuclear Research, National Academy of Sciences of Ukraine, Kyiv

Theoretical description of light-nuclei scattering from various nuclei was a subject of numerous publications. In the intermediate energy region the proper description of such processes requires both accounting of the incident nucleus internal structure and the structural features of the target nuclei. Moreover, in the consideration of the nucleus-nucleus scattering the influence of the environment, in which nuclear nucleons are placed, play an important role. In this case solution of the many-body scattering problem is highly complicated as the nucleons or clusters of the incident nuclei interact both with each other and with target nuclei structural components. This interaction distorts the standard "elementary free" scattering amplitudes and leads to introduction of effective amplitudes.

From this point of view deuteron, being the simplest light nucleus is unique object for theoretical treatment by itself and also as a test-nucleus for validation of different theoretical models. So, on one hand its complex structure implies usage of the "effective" amplitudes to describe deuteron-nucleus interaction. From the other hand given deuteron small binding energy and taken into account founding similarities between the measured values of some observables for polarized deuteron and those for the polarized proton in the intermediate energy region scattering one can expect the sufficient accuracy from the model using "free" nucleon-nucleon (cluster) amplitudes for calculation of deuteron scattering.

The main purpose of this report is to develop for the case of deuteron-nucleus scattering the multiple diffraction scattering theory conventional approach that uses the nucleon-nucleon scattering amplitudes by including in the consideration cluster degree of freedom of the target-nuclei. So, here to calculate the elastic d-^{12}C and d-^{16}O scattering observables we use the α-cluster model with dispersion for the target-nuclei [1] and the rigid-projectile approximation with "effective" full form spin-dependent d-α scattering amplitude in the form

$$f_{d\alpha}(\mathbf{q}) = f_1(q) + f_2(q)(\boldsymbol{Sn}) + \\ + f_3(q)(\boldsymbol{Sn})^2 + f_2(q)(\boldsymbol{S}\hat{\boldsymbol{q}})^2, \qquad (1)$$

$$f_i(q) = k_d \sum_{j=1}^{2} G_j^{(i)} \exp(-\beta_j^{(i)} q^2), \qquad (2)$$

The results of such calculations are given in the figure by solid curves. The dashed curves in this figure were calculated in [3] with allowing only for the first two terms in (1).

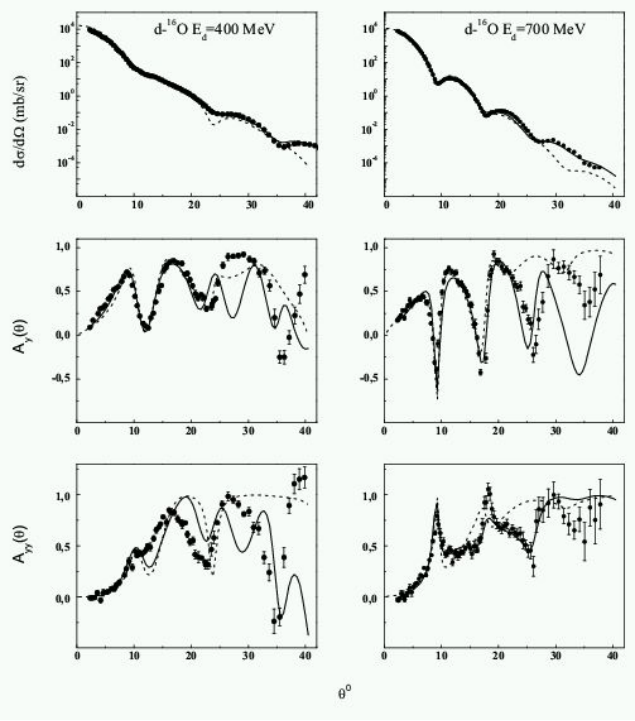

The differential cross-sections $d\sigma/d\Omega$ (mb/sr) and analyzing powers A_y, A_{yy} for the elastic deuteron scattering from ^{12}C and ^{16}O nuclei at 400 and 700 MeV. The experimental data are taken from [2].

As can be seen from Figure, the calculated observables are in sufficient agreement with the existing experimental data.

1 Yu.A. Berezhnoy, D.V. Fedorchenko, V.P. Mikhailyuk, and V.V. Pilipenko, Eur. Phys. J. A **48**:4 (2012).
2 Nguyen Van Sen, Ye Yanlin, J. Arvieux *et al.*, Nucl. Phys. A **464**, 717 (1987).
3 Yu.A. Berezhnoy, D.V. Fedorchenko, V.P. Mikhailyuk, and V.V. Pilipenko, Phys. Atom. Nucl. **76**, 862 (2013).

REACTION ^{40}Ca(d, pn) ^{40}Ca AT 56 MeV IN THE DIFFRACTION APPROXIMATION

V. V. Davydovskyy, A. D. Foursat

Institute for Nuclear Research, National Academy of Sciences of Ukraine, Kyiv

Investigation of the deuteron breakup reaction on nuclei gives information on the mechanism of the reaction as well as the nature of the interaction of complex particles with nuclei. Theoretical studies of the reaction developed in two ways: using the method of distorted waves and in the diffraction model. Taking the Coulomb interaction into account is essential.

The diffraction theory of the interaction of complex particles with nuclei suggests that each nucleon, which forms the deuteron, being scattered by a force center, leads to a phase shift associated only with the transfer of transverse momentum. This assumption is valid for deuteron elastic scattering at small angles. In the inelastic breakup process, the longitudinal momentum is transferred to the deuteron's nucleon as well. This fact leads to the incoherence of the breakup process and as a consequence it cannot be described by a profile function corresponding to the elastic scattering [1]. Therefore, it is interesting to consider the process of the deuteron breakup in the diffraction approximation taking into account both the longitudinal Q_z and transverse $\mathbf{Q}_\perp$ components of the transferred momentum, which is the main purpose of the work.

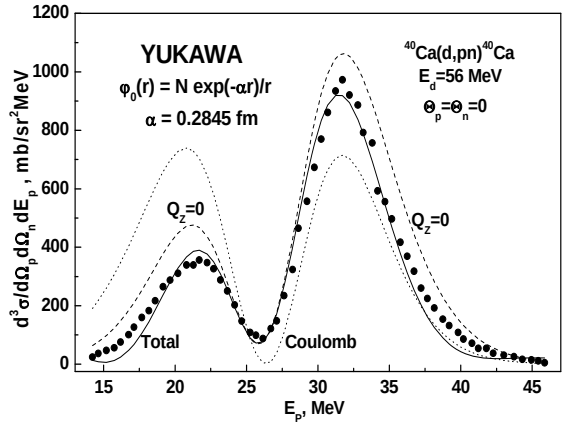

Energy spectrum of protons in ^{40}Ca(d, pn)^{40}Ca reaction at 56 MeV. Filled circles represent the experiment [2]; dotted line shows contribution of the Coulomb amplitude (2) only; solid line is our full calculation; dashed line is full calculation with longitudinal momentum transfer effects neglected.

The available experimental data [2] on the deuteron breakup by nuclei, when the deuteron breakup products are emitted at zero angle relatively to the momentum of the deuteron, allow a detailed comparison between theory and experiment. Numerical calculations are carried out for the calcium nucleus at 56 MeV.

Following the technique described in [1], we get the amplitude of (d, np) reaction as a sum of two terms, responsible for the Coulomb and nuclear-Coulomb breakups:

$$F(\mathbf{Q},\mathbf{p}) = \frac{ik_d}{2\pi}\int d^2B \exp\left(i\mathbf{Q}_\perp\mathbf{B}\right)\times$$

$$\times\int d^3r\varphi^*_{\mathbf{p}}(\mathbf{r})\Omega(\mathbf{B},\mathbf{r})\varphi_0(\mathbf{r}) = F_c + F_{Nc}\,. \qquad (1)$$

After some considerations, it is possible to represent the Coulomb breakup amplitude, introduced in (1), as a product of three terms:

$$F_c(\mathbf{Q},\mathbf{p}) = 2f_c(Q,\frac{k_d}{2})F(Q)G(\mathbf{Q},\mathbf{p})\,. \qquad (2)$$

For the amplitude of the nuclear-Coulomb breakup, we take three first terms of its expansion into series in the small parameter, which in this case is a ratio of the deuteron and target nucleus radii:

$$F_{Nc}(\mathbf{Q},\mathbf{p}) = \sum_{\lambda=0}^{2} F_{Nc}^{(\lambda)}(\mathbf{Q},\mathbf{p})\,. \qquad (3)$$

The integration in the amplitudes is carried out numerically with the profile function chosen in the Fermi form with the real volume and the imaginary surface parts.

The Figure shows the results of our calculations of the energy spectrum of protons. The effect of Q_Z is noticeable, although small. In the region of the spectrum $E_p \sim E_n$, the curves coincide and the effect disappears, which is clearly explained by the specifics of the experiment kinematics. At the wings of the spectrum, the energies of the nucleons are significantly different and the effect is considerable. At higher energies, the role of the effects related to the Q_z transfer, especially in the asymmetric geometry, should increase.

1. Е.В. Левшин, А.Д. Фурса, ЯФ **24**, 1115 (1976).
2. H. Okamura, S. Hatori, and N. Matsuoka *et al.*, Phys. Lett. B **325**, 308 (1994).

ON SOME MATHEMATIC METHODS IN THE BASE OF QUANTUM COLLISIONS AND NUCLEAR REACTIONS AND THEIR ORIGINATING OF CERTAIN PHYSICAL PHENOMENA

V. S. Olkhovsky

Institute for Nuclear Research, National Academy of Sciences of Ukraine, Kyiv

In part I of this review paper the analytical structure of the non-relativistic unitary and non-unitary *S*-matrix are investigated for the cases of any interactions with any motion equations inside a sphere of radius a, enclosed by the centrifugal and rapidly decreasing (exponentially or by the Yukawian law or by the more rapidly decreasing) potentials. Some kinds of the symmetry conditions are imposed. The Schroedinger equation for $r > a$ for the particle motion and the condition of the completeness of the correspondent wave functions are assumed. The connection of the obtained results with the causality is examined. Partially some analytical properties for the multi-channel *S*-matrix are investigated and the sum rules for mean compound-nucleus time delays and the density of compound-nucleus levels. *Sometimes* (*as physical revelations of profound general methodic and in very good consistent accordance with the experiment*) *observable physical effects, such as parity violation enhancement and time resonances or explosions, are manifested.*

In part II it is known the appearance of time advance (due to distortion by the non-resonant background) instead of the expected time delay in the region of a compound-nucleus resonance in the center-of-mass C-system. Here at the same conditions we study cross sections and durations of the neutron-nucleus scattering in the laboratory L-system. Here a review of papers where it is shown that such time advance is a virtual paradox and in the L-system the time-advance phenomenon does not occur and only the trivial time delay is observed. At the same time the transformations from C-system into the L-system appeared to be different from the standard kinematical transformations because in the C-system the motion of a compound nucleus is absent but it is present in the L-system. Here we analyze the initial wave-packet motion (after the collision origin) and the cross section in the laboratory L-system. Also *here* (*as physical revelations of profound general methodic and in very good consistent accordance with the experiment*) *several results of the calculated cross sections for the neutron-nucleus in comparison with the experimental data in the L-system at the range of one or two overlappedcompound resonances are presented. It is shown in the space-time approach that the standard comparison with the experimental data in the L-system at the range of one or two overlapped, using the only cinematic transformations of cross sections from the C-system to the L-system are not valid because it is necessary to consider the center-of-mass motion in the L-system.*

L.D. Landau has said [1] that the main useful thing in the theoretical and mathematical physics is a new good method because the good method can bring us to many new effects which can in a new way explain the experimental data. And namely there is a reincarnation of this idea in my paper. There are new physical effects which had followed almost directly from my methods in both parts of my review paper.

In I part they are the new effect of the time resonances (or explosions), which had followed from the analytical structure of the *S*-matrix, and the parity-violation-enhancement effect, which had followed from the analytical structure of the *S*-matrix for the interactions with the violated parity. In the part II they are the new transformations between the C- and L-system for cross sections for two and more interaction mechanisms, which generalize the well-known standard cinematic transformations between the C- and L-systems for cross sections for one direct (or prompt) mechanism, and also the virtual delay-advance effect in the C-system and absence of it in L-system (both revealed firstly by me); these both results or effects, which had resulted in the very good coincidence with the experimental data, had followed from the space-time analysis (or method) of neutron-nucleus scattering, which has also firstly was elaborated by me.

1 L.D. Landau, private communication.

TO A NON SIMPLE AND STILL FAR FROM BEING COMPLETED HISTORY OF QUANTUM MECHANICS

V. S. Olkhovsky

Institute for Nuclear Research, National Academy of Sciences of Ukraine, Kyiv

In this review paper it is analyzed the *really far from being completed history of quantum mechanics – quantum theory of measurements*. The last interpretation of quantum mechanics, after the long discussion between A. Einstein and N. Bohr was finished, is the interpretation of many worlds (IMW). There is assumed the existence of parallel universes in this interpretation of quantum mechanics (and quantum cosmology). In every from them the same nature laws and the same physical constants act, but all of them are found in various states. *IMW does not contain the undetermined collapse of wave function which is connected with the measurement in the Copenhagen interpretation.*

There are two main statements in various IMW versions: The fist statement is the existence of wave function of the whole Universe which is described by the Schrödinger equation but without any undetermined collapse. The second statement is the following: every state of the Universe the quantum superposition of many (or, may be, of infinite number of) states of equal parallel universes which do not interact one with each other.

The main argument for the acceptance of IMW is the absence in it of the collapse of wave function. Besides that, also the experimental testimonies in the favor of collapse and against IMW are absent. IMW is the deterministic theory of physical Universe and it explains why the world seems to be undeterministic for the human observer.

IMW is not the most popular interpretation of quantum theory between physicists but its popularity apparently increases. And also starting from the elegant conception of the de-coherence proposed in 1970 by D. Zeh, it is possible to explain that the various branches of the unique wave function, describing these worlds, are oscillating in time with phase shift and therefore each for other as if do not exist [1].

Furthermore there is the relatively recently finished chapter of quantum mechanics which for a long time had not been resolved. For the non-relativistic quantum mechanics it was finally finished in [2]. For the quantum electrodynamics it was finished in [2]. For the Klein Gordon theory and for the Dirac theory it was finished in [2]. *Finally in* [2] *there are presented many remained unresolved problems in time analysis of quantum processes.*

1. H.D. Zeh, Foundations of Physics **1**, 69 (1970); H.D. Zeh, Foundations of Physics **3**, 109 (1973).
2. V.S. Olkhovsky, Advances in Mathem. Phys., 2009, article ID 859710, 83 pages (2009), doi:10.1155/2009/859710;
3. V.S. Olkhovsky, *Time as a quantum observable canonically conjugate to energy. Time analysis of quantum processes of tunneling and collisions* (*nuclear reactions*), LAP LAMBERT (Academic Publishing, Germany, 2012), 177 p.

THE TOP QUARK MASS MEASUREMENT IN THE DILEPTON CHANNEL WITH MATRIX ELEMENT METHOD

M. S. Borysova (on behalf of the DØ collaboration)

Institute for Nuclear Research, National Academy of Sciences of Ukraine, Kyiv

The precise measurement of the top quark mass is the legacy of the Tevatron (Fermilab). The measurement of the top-quark mass in the tt-bar dilepton channel using the matrix element method (MEM) is presented. The MEM was developed by DØ to measure the top quark mass in the l + jets channel in Run I [1]. The analysis presented here follows the ones described in [2] but using a full dataset which has been collected between April 2002 and September 2011. The full dataset corresponds to an integrated luminosity of ≈10 fb^{-1}. The dilepton event selection follows the cuts developed for the measurement of the angular asymmetry in in dilepton channel in the Run II [3].

The signal Monte Carlo (MC) samples used to derive the calibration curves have been produced using Alpgen followed by Pythia generators. The generated top quark masses are: 165, 170, 172.5, 175 and 180 GeV. Background processes are generated with Alpgen followed by Pythia for Z → ee, Z → μμ and Z → ττ and Pythia - to simulate diboson events (WW, WZ, ZZ).

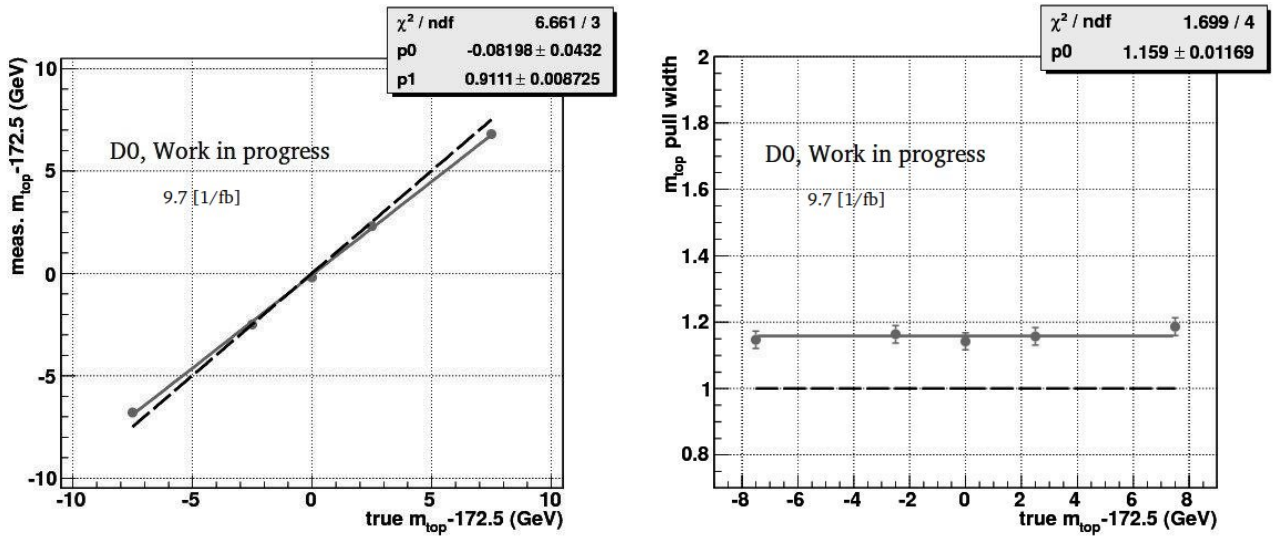

Fig. 1. Comparison of the reconstructed and generated top-quark mass m_{top} (*a*) and correction to the estimated uncertainty - pull width (*b*) in the eμ channel. Only signal tt-bar events are taken into accout.

Before the MEM is applied to the selected data sample, the method needs to be calibrated using MC events. The total number of tt-bar events in the pool used for the calibration is around 60000 for each generated mass which allows to generate 1,000 independent ensembles. We expect about 300 tt-bar events in the Run II for eμ channel. MC events which have been run through the full simulation of the DØ detector are used to derive the final calibration of the fitting procedure. The calibration curves show the mean values of top-quark mass measured in 1,000 pseudo-experiments as a function of the generated ones. To improve the precision and top-mass calibration it was chosen in three jets events to use lepton jets with highest b-tag output. The results for this ensemble testing are presented in the Figure. In Figure, *b* the pull width which is defined as the mean deviation of m_{top} in single pseudo-experiment from the mean for all 1,000 values at a given input m_{top}, in units of the measured uncertainty per pseudo-experiment is plotted. The signal only calibration curves demonstrate that the method doesn't suffer from any bias as calibration straight line offset very close to zero and a slope very close to unity.

In the future there should be added background and instrumental background, chosen the optimal treatment of 3 jet events and performed analyses for diem and dimu channels.

1. V.M. Abazov *et al.*, Nature **429**, 638 (2004).
2. V.M. Abazov *et al.*, Phys. Rev. Lett. **107,** 08 (2011).
3. V.M. Abazov *et al.*, arXiv:1308.6690 [hep-ex], submitted to Phys. Rev. D.

MSSM NEUTRAL HIGGS PRODUCTION CROSS SECTION VIA GLUON FUSION AND BOTTOM QUARK FUSION AT NNLO IN QCD

T. V. Obikhod

Institute for Nuclear Research, National Academy of Sciences of Ukraine, Kyiv

Understanding the mechanism that leads to the breaking of the electroweak symmetry and that is responsible for the generation of the mass of the elementary particles is one of the major challenges of high energy physics. As the Higgs mass have already been set it requires an accurate control of all the Higgs production and decay mechanisms, including the effects due to radiative corrections [1].

The next-to-leading order of QCD corrections to the production cross sections of scalar Higgs bosons have been calculated in [2]. They are significant for the theoretical prediction of the cross sections leading to the increase up to the factor of two compared to the lowest order results. In this paper the program HIGLU for the calculation of the Higgs production cross sections including next-to-next-to-leading order of QCD corrections will be presented. Possible options are minimal supersymmetric extension of Standard Model with various relevant input parameters. Within Standard Model as well as in most of the parameter space of MSSM the contribution of the top and bottom quarks in the loops provides the excellent approximation for all cases in practice.

The program HIGLU calculates five terms in formula contributing to the total cross section separately, as well as their sum for all kinds of neutral Higgs bosons. Resulting cross sections for the light scalar MSSM Higgs boson h for energies $\sqrt{s} = 7, 8, 14$ TeV are shown in Fig. 1.

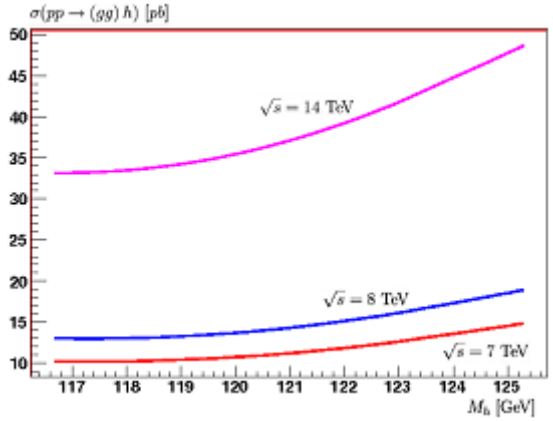

Fig. 1. Total gluon-fusion cross sections of the light scalar MSSM Higgs boson h for $\sqrt{s} = 7,\ 8,\ 14$ TeV.

Despite the fact that the dominant production mode for Higgs boson is gluon fusion, next-to-leading order (NLO) corrections have been also evaluated for Higgs boson production in association with top quarks [3]. MSSM contains after spontaneous symmetry breaking five physical Higgs bosons, where mass eigenstates are denoted by $h, H, H^{\pm}, A$. One interesting consequence of this more complicated Higgs sector is that compared to Standard Model, the bottom quark Yukawa coupling can be enhanced with respect to the top quark Yukawa coupling. In Standard Model, the ratio of the $t\bar{t}H$ and $b\bar{b}H$ couplings is given at the tree-level like

$$\lambda_t^{SM} / \lambda_b^{SM} = m_t / m_b = 35.$$

On the contrary, in MSSM, its depends on the value $\lambda_t^{MSSM} / \lambda_b^{MSSM}$.

The consequence is that for Higgs boson production in association with bottom quarks can become an important channel: $pp \to b\bar{b}\varphi$, $\varphi \in h, H, A$. For the calculation one evaluates virtual and real corrections to Higgs production in $b\bar{b}, gb, gg, bb, qb, q\bar{q}$ scattering and then performs ultraviolet renormalization and mass factorization. The resulting cross section is shown in Fig. 2.

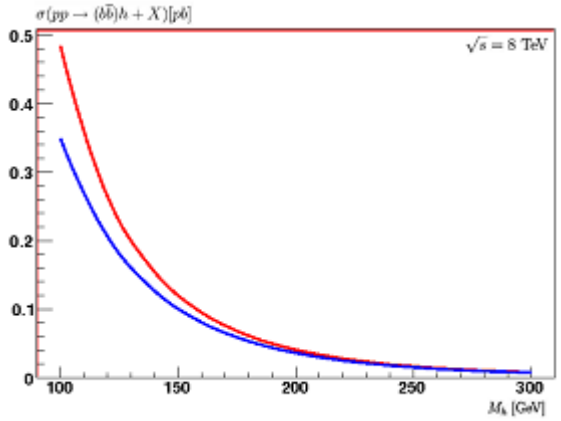

Fig. 2. Cross section for Higgs boson production in bottom quark annihilation at the LHC at NNLO. The upper (lower) line corresponds to a choice of the factorization scale of $\mu_F = 0.7 M_k$ $(\mu_F = 0.1 M_k)$. The renormalization scale is set to $\mu_R = M_h$.

1. S. Dittmaier *et al.*, arXiv:1101.0593 [hep-ph].
2. A. Djouadi, M. Spira, and P.M. Zerwas, Phys. Lett. B **264**, 440 (1991).
3. L. Reina and S. Dawson, Phys. Rev. Lett. **87**, 201804 (2001).

SEARCHES FOR SUPERPARTICLES AT THE LHC BY APPLICATION OF COMPUTER SIMULATION

T. V. Obikhod

Institute for Nuclear Research, National Academy of Sciences of Ukraine, Kyiv

The searches for new physics at the LHC motivated the necessary tools for building Grand Unification Theory (GUT) models in F-theory [1]. It is known that Minimal Supersymmetric Standard Model (MSSM) [2] through its connection to string theory improves the Standard Model (SM). There are several problems of SM, connected with our experimental knowledge and with some theoretical aspects:

1) there is the neutrino mass problem - the SM predicts neutrinos having zero mass, whereas we have experimental evidence for massive neutrinos;

2) SM field theory which include gravity ends up being non-renormalizable without predictions below the Planck scale;

3) SM has 19 free parameters to be determined experimentally;

4) the hierarchy problem;

5) the unification problem.

These problems can be decided with the help of MSSM model. The construction of MSSM model from superstring theory is connected with the notion of derived category of D-branes. There are several aspects that are necessary for construction the category of D-branes [3]:

D-brane is associated to the locally-free sheaf;

an open string from one D-brane (sheaf *E*) to another D-brane (sheaf *F*) is given by an element of the group *Ext* (*E, F*);

the category of D-branes is the derived category of coherent sheaves *D(X)* ;

if *X* and *Y* are mirror Calabi-Yau threefolds then the category *D*(*X*) is equivalent to the triangulated category Tr*F*(*Y*);

MSSM model is connected with more than 100 parameters. The analysis, based on observational hints and theoretical considerations, allows to restrict the parameter space to five free parameters:

$$M_0 = 450 \text{ GeV}, M_{1/2} = 425 \text{ GeV},$$

$$A_0 = 0,\ \tan\beta = 10,\ \operatorname{sgn}(\mu) = +1. \qquad (1)$$

Using the restricted parameter set it is possible to calculate the mass spectrum, partial widths of superpartners by application of the computer programs SOFTSUSY and SDECAY.

By application of computer program PYTHIA it is possible to calculate production cross sections at center-of-mass energy $\sqrt{s} = 14$ TeV. These cross sections are shown in the Table.

Cross sections of superpartners

channel	cross-section, pb
$gg \to \tilde{g}\tilde{g}$	$\sigma_{\tilde{g}\tilde{g}} = 0.323$
$qg \to \tilde{d}_R\tilde{g}$	$\sigma_{\tilde{d}_R\tilde{g}} = 0.260$
$qg \to \tilde{u}_R\tilde{g}$	$\sigma_{\tilde{u}_R\tilde{g}} = 0.489$
$qq' \to \tilde{u}_R\tilde{d}_R$	$\sigma_{\tilde{u}_R\tilde{d}_R} = 0.132$

To construct histograms describing mass distributions for superpartners $\tilde{q}_R$ and $\tilde{g}$ we choose the set of parameters (1). Using this parameter set it is possible to construct histograms of mass distributions for superpartners by application of the computer program PYTHIA. Histogram of mass distribution for $\tilde{g}$ is shown in the Figure.

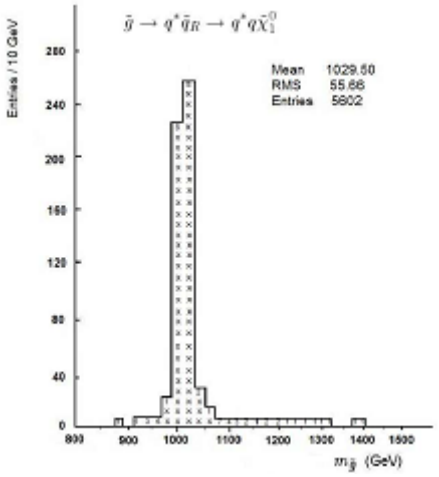

Histogram of mass distribution for $\tilde{g}$.

1. C. Beasley, J.J. Heckman, and C. Vafa, arXiv: 0802.3391 [hep-th].
2. H.E. Haber, arXiv: hep-ph/9306207.
3. P.S. Aspinwall, arXiv: hep-th/0403166.

MATTER FROM TORIC GEOMETRY AND ITS SEARCH AT THE LHC

T. V. Obikhod

Institute for Nuclear Research, National Academy of Sciences of Ukraine, Kyiv

At high energy, the three gauge interactions which define the electromagnetic, weak, and strong interactions, are merged into one single interaction characterized by one larger gauge symmetry Grand Unified Theory (GUT) [1] and thus one unified coupling constant. This gauge coupling unification works quite well in the Minimal Supersymmetric Standard Model (MSSM) motivating not only grand unification (or some superstring theories with similar properties) but also that supersymmetry emerges. One of the branches of string theory is F-theory which allows string theorists to construct new realistic vacua - in the form of F-theory compactified on elliptically fibered Calabi-Yau fourfolds.

It is natural to consider F-theory compactifications on a Calabi-Yau threefold which admits an elliptic fibration [2]. We will study elliptic Calabi-Yau manifolds which in addition admit a K3 fibration; in other words we consider the case where the K3 fiber itself is elliptically fibered. This would be useful for dualities with heterotic strings. Then the proposed Calabi-Yau must have a singularity. Our purpose is to describe a general method for constructing of Calabi-Yau hypersurfaces in toric varieties. From the toric description of the Calabi-Yau manifold used for compactification can be read off the Newton polyhedron that provides nonabelian gauge groups occurring in type IIA and F-theory. There is a natural sequence of group embeddings which gives the MSSM gauge group and matter structure that can be detected at the LHC [3]

A great many Calabi-Yau manifolds are known in terms of toric data [4] and there is the correspondence, pointed out by Batyrev, between Calabi-Yau manifolds and reflexive polyhedra Δ. This reflexive polyhedron is Newton and we may define the dual or polar polyhedron which we denote by ∇. By means of a computer program we have computed the dual polyhedra for the fourfolds $X_{18k+18}\left(1,\,1,\,1,\,3k,\,6k+6,9k+9\right)\left(k=1,\ldots,6\right)$.

The following observations summarize the structure of the polyhedron ∇:

1. Omitting the first two points and the last point of ∇ leaves us with the dual polyhedron ${}^3\nabla$ of the K3 surface $X_{12}\left(1,\,1,\,4,\,6\right)$;
2. Omitting the first three points and the last two points of ∇ leaves us with the dual polyhedron ${}^2\nabla$ of the torus $X_6\left(1,\,2,\,3\right)$;
3. The polyhedron ${}^3\nabla$ is divided into a 'top' and a 'bottom' by the polyhedron ${}^2\nabla$ and we may write

$$ {}^3\nabla = \nabla_{bot}^{H} \cup \nabla_{top}^{k=1}, $$

where $\nabla_{top}^{k=1}$ depends only on $k=1$ while ∇_{bot}^{H} depends only on the enhanced gauge group H.

Applying this consideration to tops we obtain the following gauge content for fourfolds:

$$\begin{aligned} &H\times SU(1) \quad for\ k=1,\\ &H\times SO(8) \quad for\, k=2,\\ &H\times E_6 \quad\ for\, k=3,\\ &H\times E_7 \quad for\, k=4,\\ &H\times E_8 \quad for\ k=5,\\ &H\times E_8 \quad for\ k=6. \end{aligned}$$

We consider now the possibility of adding combinations of the points in all possible ways such that the bottom corresponds to a reflexive polyhedron. All the groups do appear and, as a matter of consistency, we see the inclusions

$$\begin{aligned} E_7 \supset E_6 \supset SO(10) \supset SU(5) \supset SU(4),\\ \supset SU(3) \supset SU(2) \supset SU(1). \end{aligned}$$

This phase transition can be interpreted as a group chain of spontaneous symmetry breaking

$$SO(10) \to SU(5) \to SU(3)\times SU(2)\times U(1).$$

This transition can be realized with the help of partial widths of super partners calculations. Using the restricted parameter set of MSSM model

$$\begin{aligned} M_0 = 800\ \text{GeV},\ M_{1/2} = 650\ \text{GeV},\\ A_0 = 0,\ \tan\beta = 10,\ \ \operatorname{sgn}\left(\mu\right) = +1. \end{aligned}$$

it is possible to calculate partial widths of superpartners by application of the computer program SDECAY.

Thus we see the duality between the compactifications of the $E_8\times E_8$ heterotic string and the type IIA string compactification on a Calabi-Yau manifold provides an economical way to break the exceptional gauge group to gauge symmetries closer to the MSSM.

1. A.J. Buras *et al.*, Nucl. Phys. B **135**, 66 (1978).
2. C. Vafa, arXiv: hep-th/9602022.
3. C. Beasley, J.J. Heckman, and C. Vafa, arXiv:0802.3391 [hep-th].
4. M. Kreuzer and H. Skarke, Nucl. Phys. B **388,** 113 (1992).

ENERGY SPECTRA OF ODD NUCLEI IN THE MODEL OF NUCLEON-PHONON INTERACTION

I. O. Korzh, A. D. Foursat

Institute for Nuclear Research, National Academy of Sciences of Ukraine, Kyiv

In this article, according to the generalized atomic nucleus model, which is synthesized on the basis of the shell-type nuclear model and liquid-drop nuclear model, the energy spectra of such elements as ^{25}Mg, ^{41}K, and ^{65}Cu are determined, and the structure of wave functions for these elements in the excited state and in the ground state is studied.

To describe the structure of odd nuclei a simple model is used, in which the nucleus is considered as a even-even core with a single odd particle outside of the core. It is assumed, that the core is presented as a liquid drop with constant density and a distinct boundary, which is characterized by the well-known formula describing the multiple expansion for the nucleus surface radius.

The change in the average nucleus potential caused by fluctuations of the multiplicity λ results in the appearance of relationship between the degrees of freedom for vibrations and the degrees of freedom for the odd particle. The Hamiltonian function of the system consisting of the even-even core and the nucleon is defined as follows:

$$H = H_c + H_p + H_{int}, \qquad (1)$$

where H_c is the collective Hamiltonian function of a harmonic oscillator, H_p is the one-particle Nilsson Hamiltonian function, and H_{int} is the Hamiltonian function of nucleon-phonon interaction.

In this article, the energy levels for odd nuclei in the excited state and in the ground state are determined by the diagonalization of the energy matrix:

$$\| \left(\varepsilon_{NR} + \varepsilon_j \right) \delta_{NRj}^{N'R'j'} + \left\langle N'R'j'; JM \mid H_{\text{int}} \mid NRj \right\rangle \| . \qquad (2)$$

As an example of calculating the energy spectra of odd nuclei, we performed detailed numerical calculations for determining the energy spectrum of the ^{65}Cu nucleus. For the first time, the model of a core in the exited state designed for determining this nucleus spectrum was successfully used in publications [1, 2]. The principal defect of those and further calculations of the energy spectra of cuprum nuclei is insufficient accuracy in determining the radial matrix elements of the nucleon-phonon interaction operator. The assumption that these elements are constant is not justified, as, according to our calculations, the element values can significantly differ. If these elements are assumed to be variable, the calculated spectra can be in much better agreement with the experimental spectra. The comparison of the calculated spectrum with the experimental spectrum of the ^{65}Cu nucleus has shown that the sequence of energy levels is in agreement with their arrangement.

According to the proposed calculation method, the multicomponent wave functions for nucleus energy levels are determined as the linear transformation coefficients which diagonalize the energy matrix (2). The values of the coefficients for the ground states |NRj; J>, with the absolute spin J calculated for the lowest energy states of the ^{65}Cu nucleus, indicate that the main component of the wave function of the ^{65}Cu nucleus is a component defined by the quadrupole 2^+ phonon of the core and $2p_{3/2}$ proton state. This result allows the formula for the model of an exited core to be used in calculations for determining inelastic nucleon scattering [3].

1. R.D. Lawson and J.L. Uretsky, Phys. Rev. **108**, 1300 (1957).
2. A. De-Shalit, Phys. Rev. **122**, 1530 (1961).
3. P.E. Hodgson, *Nuclear reaction and nuclear structure* (London, Clarendon Press, 1971).

^{8}Be* RESONANCE DECAY PROPERTIES IN THE ^{11}B(p, αα)α REACTION AT E_p = 3.75 MeV

Yu. N. Pavlenko[1], V. M. Pugatch[1], V. L. Shablov[2], O. K. Gorpinich[1], A. V. Stepanyuk[1], T. O. Korzyna[1], Yu. Ya. Karlyshev[1], V. P. Verbytsky[1], O. V. Babak[1], V. V. Ostashko[1], I. P. Dryapachenko[1], E. M. Mozhzhukhin[1], V. O. Kyva[1], D. V. Kasperovych[1,3], L. L. Dulger[1,3]

[1] Institute for Nuclear Research, National Academy of Sciences of Ukraine, Kyiv
[2] Obninsk Institute for Nuclear Power Engineering, Obninsk, Russia
[3] Taras Shevchenko National University, Kyiv, Ukraine

The measurements of spatial and energy correlations of α-particles in the exit channel of reaction ^{11}B(p, αα)α have been performed at the Tandem Generator EGP-10K of the Institute for Nuclear Research (Kyiv) in order to further research the properties of decay of the first excited state of ^{8}Be nucleus in this reaction at low energies. Some unusual peculiarities of this process, such as a strong change in the shape of resonance curves in correlation spectra, were observed earlier at the proton energy E_p = 2.65 MeV [1, 2] and qualitatively explained by the interference of the resonant interaction of two pairs of α-particles simultaneously. A full explanation of this phenomenon has not been received to date.

To our knowledge, this reaction has not been investigated so far in kinematically complete experiments at the energy E_p = 3.75 MeV, which corresponds to the excitation of the compound nucleus ^{12}C*($J^{\pi} = 2^{+}$, E_x = 19.39 MeV).

Correlation measurements using the simple Si-detectors and position-sensitive detector have been performed at the kinematic conditions corresponding to the resonant interaction of two pairs of α-particles at the energies around $E_x(^{8}\text{Be}) \sim 3$ MeV. Measured spectra are shown in Figure.

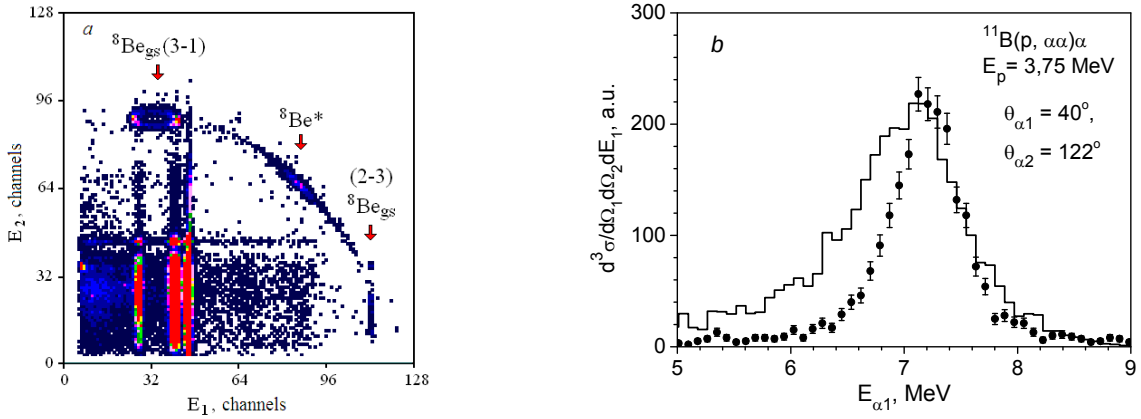

a – two-dimensional plot of coincidence spectrum of p + ^{11}B(Ni) reaction products, which was measured at E_p = = 3.75 MeV and the angles $\theta_1 = 40°$, $\theta_2 = 122°$, $\varphi_1 - \varphi_2 = 180°$. Arrows indicate the location of events from the three-particle reaction p + ^{11}B → $\alpha_1 + \alpha_2 + \alpha_3$. *b* – the projection of measured αα-coincidence spectrum (*a)* in the range of the contributions of the first excited state of ^{8}Be (E_x = 3.03 MeV, Γ = 1.513 MeV [3]) on the energy axis E_1. The histogram corresponds to the Monte Carlo calculations of the expected contribution of formation and decay of ^{8}Be* resonance in a pair of particles (2-3). The calculation has been performed with taking into account real experimental conditions as well as the penetrability of the Coulomb and centrifugal barrier. It was assumed that the resonance width Γ is independent on the relative energy $E_{α\text{-}α}$ (Γ = const = 1.5 MeV).

In contrast to the results of previous measurements at the energy E_p = 2.65 MeV [1], which corresponds to the formation of the compound nucleus ^{12}C*($J^{\pi} = 2^{+}$, E_x = 18.39 MeV), the effect of destructive interference is not observed (see Figure). At the same time, there is a significant narrowing of the resonance curve (Γ ~ 1 MeV) in comparison with the data for the binary process of αα-scattering (Γ = 1.5 MeV [3]).

The difference between the results obtained at E_p = 2.65 MeV and 3.75 MeV may be caused by different mechanisms of formation of ^{8}Be* resonance at these proton energies, as well as by the influence of the Coulomb field of accompanying α-particle on the decay of this short-lived resonance.

1. Yu.N. Pavlenko *et al.*, in *Book of Abstracts "XX Annual Conf. of Inst. for Nucl. Research of NAS of Ukraine, January 28 - February 01, 2013* (Kyiv, 2013). - P. 54.
2. V.I. Grantsev *et al.*, Izv. AN SSSR, Ser. Fiz. **41**, 147 (1977).
3. D.R. Tilley *et al.*, Nucl. Phys. A **745**, 155 (2004).

SUB-BARRIER INTERACTION OF DEUTERONS WITH ^{124}Sn NUCLEI

Yu. N. Pavlenko, V. P. Verbytsky, O. V. Babak, O. I. Rundel, O. K. Gorpinich, O. D. Grygorenko, A. V. Stepanyuk

Institute for Nuclear Research, National Academy of Sciences of Ukraine, Kyiv

Investigation of deuteron interaction with heavy atomic nuclei at sub-barrier energies showed a significant effect of polarizability and the breakup processes on the elastic scattering cross sections. While the elimination of the incident particle from the elastic channel for the forward scattering angles ($\theta \le 90°$) is adequately described by taking into account polarization and breakup in the Coulomb field of the target nucleus, at the angles over 90° the deviation from the Rutherford cross section is substantially larger and is not described by the theory.

It has been suggested that due to the deuteron finite size and the asymmetric distribution of its charge and mass, the external field can polarize the deuteron, stretching it along the field direction and thus allows to penetrate into the region of the nuclear interaction in spite of the fact that the energy of the incoming particles is essentially sub-barrier and classical Coulomb turning points is far away from the nucleus.

General three-particle equation using the adiabatic approximation [1] and the results of [2 - 4] can be reduced to the form

$$[E_d - \hat{K}_{\vec{R}} - \overline{V}_N(R) - \delta V(R) + V_c(R)]\chi_d(\vec{R}) = 0\,,$$

where E_d is the kinetic energy of deuteron; $\hat{K}_{\vec{R}}$ is the deuteron center of mass kinetic energy operator; $\delta V(R)$ is the complex potential takes into account the polarizability and the breakup of the deuteron; V_C is the Coulomb potential; $\chi_d(\vec{R})$ is the deuteron relative motion wave function; $\overline{V}_N(R)$ is the single folded potential of deuteron nuclear interaction with the target nucleus [2]:

$$\overline{V}_N(R) = \left\langle \phi_{\vec{R}}(\vec{r}) \middle| V_n(\vec{r}_n) + V_p(\vec{r}_p) \middle| \phi_{\vec{R}}(\vec{r}) \right\rangle;$$

$\phi_{\vec{R}}(\vec{r})$ is the distorted internal deuteron wave function in the external Coulomb field; V_n and V_p denote the neutron and proton nuclear interaction potentials, respectively.

It was shown that the folding procedure leads to a significant strengthening of nuclear potentials in the peripheral region of interaction. Measured and calculated angular distributions of differential cross sections for ^{124}Sn(d, d) elastic scattering at the energies of 4.0, 5.0 and 5.5 MeV are shown in Figure.

Calculations were performed without any variations of the nuclear potential parameters.

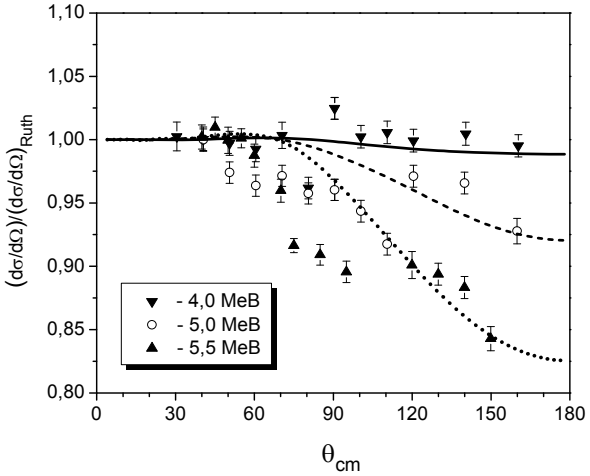

The differential cross sections of ^{124}Sn(d, d) elastic scattering. The experimental values [5] are denoted by triangles and open circles. The results of theoretical calculations in the framework of the model above are represented by lines: solid – 4.0 MeV; dashed – 5.0 MeV and dotted – 5.5 MeV.

It is shown that taking into account the finite size of incident particles leads to a significant increase the potentials in the peripheral region, what enabled to significantly improve the agreement of calculated differential elastic scattering cross sections with experimental data.

1. K.O. Terenetsky, Sov. J. Nucl. Phys., **37**, 698 (1983).
2. Y. Nishida, Progr. Theor. Phys, **19**, 389 (1958).
3. V.P. Verbitsky, L.Ya. Zhukalyuk and K.O. Terenetsky, Sci. Papers of the Inst. for Nucl. Research, **3**, 24 (2001).
4. O.V. Babak, V.P. Verbytsky and O.D. Grygorenko, Nucl. Phys. At. Energy, **14**, 247 (2013).
5. Yu.N. Pavlenko, K.O. Terenetsky, V.P. Verbitsky *et al*., in *Book of Abstracts. 2-nd Int. Conf. "Current Probl. in Nucl. Phys. At. Energy", June 09-15, 2008, Kyiv, Ukraine*. - P. 179.

PROTON GENERATION IN SPLITTING REACTIONS IN DD-COLLISIONS (Experimental part)

O. O. Belyuskina, V. I. Grantsev, K. K. Kisurin, S. E. Omelchuk, Yu. S. Roznyuk, B. A. Rudenko, L. I. Slusarenko, B. G. Struzhko

Institute for Nuclear Research, National Academy of Sciences of Ukraine, Kyiv

Study of processes of interaction of deuterons with deuterons is an important source of information about the processes that take place in few-nucleon systems. Along with elastic scattering of deuterons on deuterons, fission processes, quasi-free scattering of deuterons on nucleons, generation of two singlet deuterons, etc. play an important role. Information about the above-mentioned processes may be obtained both from analysis of the exclusive experiments of D(d, pn)D, D(d, nd)p, D(d, pd)n, D(d, 2p)2n type and inclusive experiments that supplement each other.

At the accelerator U-240 of the Institute for Nuclear Research of NAS of Ukraine, at energy of deuterons $E_d = 36{,}9$ MeV, there were studied inclusive spectra of protons in D(d, p) reaction in energy range $5 \le E_p \le 40$ MeV. Measurements were carried out on targets CD_2 and ^{12}C. Proton spectra, obtained on targets CD_2 and C at angles of 15 and 30° is shown in Fig. 1.

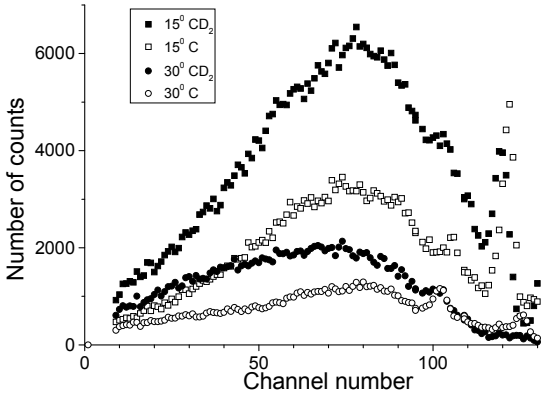

Fig. 1. Proton spectra on targets CD_2 and C at angles of 15 and 30° at energy of deuterons of $E_d = 36{,}9$ MeV.

Energy and angular distributions of protons are obtained within the range of $15° \le \theta_p \le 55°$. Absolute values of reaction cross-sections are determined with accuracy of ~15 %. Energy spectra are shown in Fig. 2. Spectra form broad, almost symmetric maximums and, by their shape, are similar to energy spectra of protons and neutrons from D(d, n) reactions that is mentioned in literature at $E_d = 10$ - 60 MeV.

In Fig. 3, there is shown comparison of cross-sections in maximums of energy distributions of protons for $E_d = 36{,}9$ MeV and 59,9 MeV [1].

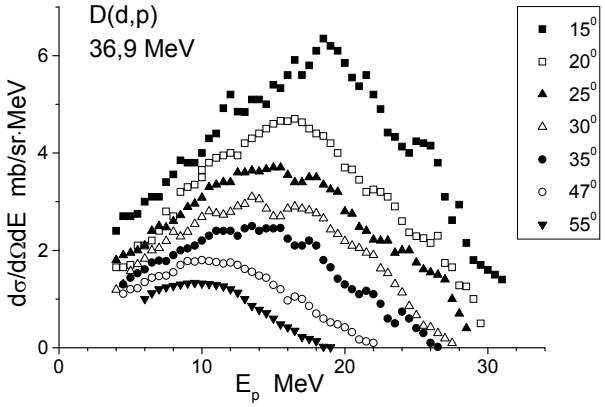

Fig. 2. Energy spectra of protons from D(d, p) reaction at energy of $E_d = 36{,}9$ MeV.

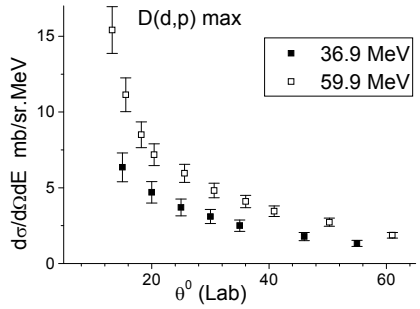

Fig. 3. Angular dependence of cross-sections in maximums of energy distributions of protons at $E_d = 36{,}9$ MeV and 59,9 MeV.

Proton cross-sections sharply increase under small angles. In fig.4, there are given angular distributions of protons from D(d, p) reaction.

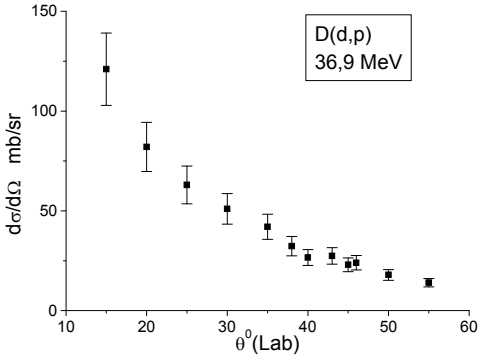

Fig. 4. Angular dependence of differential cross-sections of protons from D(d, p) reaction at $E_d = 36{,}9$ Me**V**.

1. K. Fukunaga, T. Ohsawa, S. Kakigi *et al.*, Nucl. Phys. **A390**, 19 (1982).

PROTON GENERATION IN SPLITTING REACTIONS IN DD-COLLISIONS (Theoretical analysis)

O. O. Belyuskina, V. I. Grantsev, K. K. Kisurin, S. E. Omelchuk, Yu. S. Roznyuk, B. A. Rudenko, L. I. Slusarenko, B. G. Struzhko

Institute for Nuclear Research, National Academy of Sciences of Ukraine, Kyiv

There were considered three-particle and four-particle reactions that lead to appearance of protons in exit channel of the reaction D(d, p). Analysis of energy and angular distributions of protons in three-particle splitting reactions was carried out according to the diffraction theory, developed by V. K. Tartakovsky. Two cases were considered: 1) fission of incident deuteron and 2) fission of target deuteron.

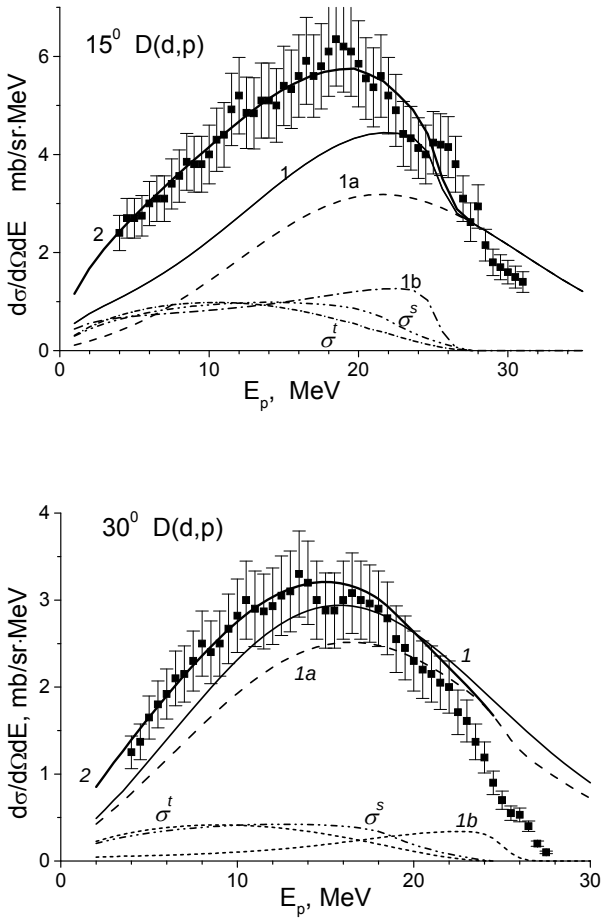

Fig. 1. Comparison of theoretical calculations with experimental cross-sections of protons under the angles of θ_p = 15° and θ_p = 30° at E_d = 36,9 MeV: *1* – energy distributions of protons according to microscopic diffraction model; *1a* – contribution of proton cross-sections from fission of incident deuteron; *1b* – contribution of proton cross-sections from fission of target deuteron. *2* – energy distributions of protons from the reaction D(d, p) taking into account *np* couples in singlet σ^s and triplet σ^t spin states.

Results of calculations according to the diffraction model of inclusive spectra of protons are given in Fig. 1, and the results for angular distributions – in Fig. 2.

The analysis performed has shown that three-particle fission reactions give essential contribution into cross-sections for proton generation at small angles θ_p <25°, and at angles θ_p >25° they are determinative.

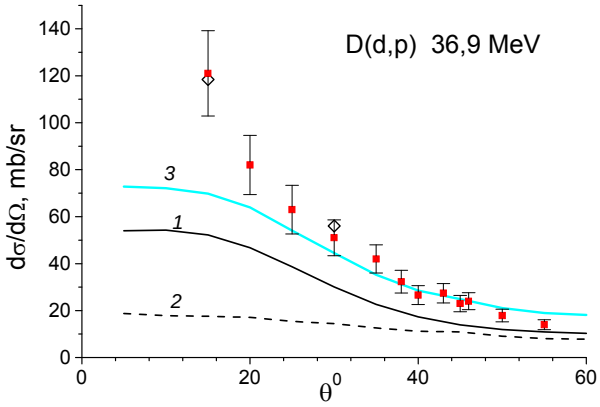

Fig. 2. Comparison of theoretical angular distributions of protons from D(d, p) reaction with experimental ones at E_d = 36,9 MeV. Points – experiment, *1* – angular distributions of protons from fission of incident deuteron; *2* – angular distributions of protons from fission of target deuteron; *3* – total cross-section from both processes. Circles – angular distributions taking into account np interaction in final state.

Analysis of four-particle reactions has shown that only cross-sections of generation of *np* couples in singlet and triplet spin state are essential. Satisfactory correspondence of theoretical and experimental distributions of protons both by form and by value was achieved due to taking into account of quasi-free processes from analysis of three-particle fission reactions by microscopic diffraction model and cross-sections for generation of *np* couples in singlet and triplet spin states. It is shown that, for the angle of θ_p = 15°, total contribution of cross-sections for generation of *np* couples in singlet and triplet spin states reaches 40 %, and for the angle θ_p = 30° it decreases to 20 - 25 %.

CROSS SECTIONS OF THE ^{3}H(d, t)np REACTION AT A DEUTERON BEAM ENERGY OF 37 MeV

O. O. Belyuskina, V. I. Grantsev, K. K. Kisurin, S. E. Omelchuk, Yu. S. Roznjuk, B. A. Rudenko, L. I. Slyusarenko, B. G. Struzhko

Institute for Nuclear Researches, National Academy of Sciences of Ukraine, Kyiv

Inclusive ^{3}H particle spectra and differential cross sections $\frac{d\sigma(E,\theta)}{dEd\Omega}$ of the ^{3}H$(d, t)pn$ reaction were obtained at E_d = 36.9 MeV. Experiments were performed with deuteron beam of the variable energy cyclotron at the Institute for Nuclear Researches (INR, Kyiv). Tritium–titanium (^{3}HTi) and titanium (Ti) targets and charge particle ΔE–E telescopes were used in the experiment. Other details of the experimental technique are given in [1, 2].

Experimental spectra of the ^{3}H ions are shown in the Figure along with simulated ones (curves 1–5) calculated by the Monte Carlo method taking into account the nonmonochromaticity of the accelerated deuteron beam, the target thickness, spectrometer energy resolution, the beam spot size on the target, detector aperture, and the target–detector distance. Differential cross sections were calculated as a noncoherent contributions of the proton-neutron Final State Interactions (FSI) in the singlet ^{1}S$_0$ state (singlet deuteron) and in the triplet ^{3}S$_1$ one, sequential decay via the ^{4}H* resonance and the proton (neutron) - triton Quasifree Scattering (QFS) processes.

Appropriate amplitudes $F_S(k_{23})$, $F_T(k_{23})$, $F_R(k_{13})$ and $F_{QF}(k)$ were calculated as

$$F_{S(T)}(k)\infty\frac{r(k^2+\alpha^2)}{2(rk^2/2-1/a-ik)},\ \alpha=\frac{1+\sqrt{1-2r/\alpha}}{r},$$

with a = -23.748 Fm, r = 2.75Fm for the ^{1}S$_0$ np state and a = –5.424 Fm, r = 1.75 Fm [3] for the ^{3}S$_1$ one

$$F_R(k)\infty\frac{\Gamma/2}{\frac{k^2}{2\mu}-E_R+i\Gamma/2},$$

where μ, E_R = 2.2 MeV and Γ= 3.4 MeV are the reduced mass, a resonance energy of the neutron-triton subsystem and the resonance width respectively [4],

$$\left|F_{QF}\right|^2=\left|\phi(k)\right|^2\frac{d\sigma(\vartheta)}{d\Omega},$$

where $d\sigma(\vartheta)/d\Omega$ is a cross sections of the elastic scattering proton (neutron) – triton,

$$\phi(k)=(2\pi)^{-3/2}\int_R\phi(\vec{r})e^{-ik\vec{r}}d\vec{r}$$

is a Fourier transform of the deuteron wave function of the Hülthen type in the space representation [5]

$$\phi(r)=\sqrt{\frac{\alpha\beta(\alpha+\beta)}{2\pi(\beta-\alpha)^2}}\frac{\exp(-\alpha r)-\exp(-\beta r)}{r},$$

R = 5.0 Fm, $\alpha^2 = mE_\alpha$, E_α = 2.2245 MeV, $\beta^2 = mE_\beta$, E_β = 59.8 MeV and $\frac{d\sigma(\vartheta)}{d\Omega}$ was taken as a constant.

Simulated distributions are in a qualitative agreement with the experimental ones. Differential cross sections of a singlet deuteron formation were found to be about half of those for dineutron in the ^{3}H(d, ^{3}He)nn reaction [2]. Such a ratio was foreseen in the Supermultiplet Potential Model of scattering of the lightest clusters and was confirmed in experiment at deuteron beam energy of 13.8 MeV [3].

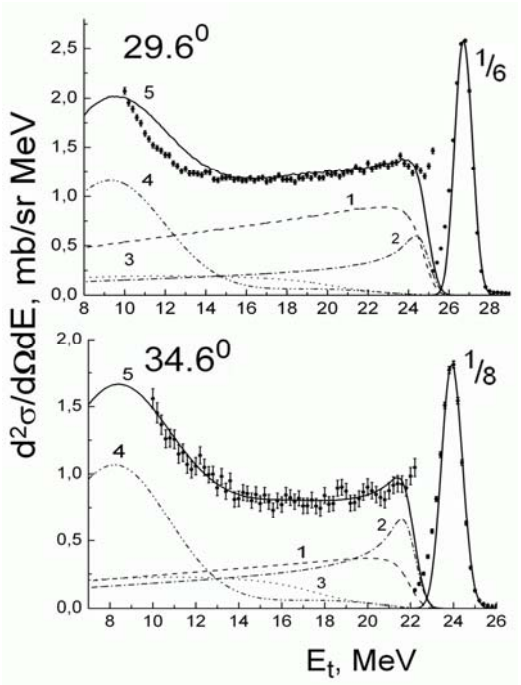

Experimental ^{3}H spectra and simulated contributions of the proton-neutron FSI in the ^{3}S$_1$ state (*1*); ^{1}S$_0$ one (*2*); sequential decay via the ^{4}H* resonance (*3*); proton (neutron) - triton QFS (*4*) and a total simulated spectrum (5).

1. O.O. Belyuskina, S.V. Berdnichenko, V.I. Grantsev, *et al.*, Yad. Fiz. Energet. **21**, 54 (2007).
2. O.O. Belyuskina, S.V. Berdnichenko, V.I. Grantsev, *et al.*, Yad. Fiz. Energet. **25**, 466(2008).
3. B.G. Struzhko, Izv. Akad. Nauk, Ser. Fiz. **64**, 3 (2000).
4. V.I. Konfederatenko, B.G. Struzhko, O.M. Povoroznik, Ukr. Fiz. Zh. **39,** 393 (1994).
5. G. Paic, J.C. Koung and O.J. Margaziotis, Phys. Lett. B**32,** 437 (1970).

ELASTIC AND INELASTIC SCATTERING OF ^{12}C IONS BY ^{7}Li AT 115 MeV

A. T. Rudchik[1], V. Yu. Kanishchev[1], A. A. Rudchik[1], O. A. Ponkratenko[1], E. I. Koshchy[2], S. Kliczewski[3], K. Rusek[4,5], V. A. Plujko[6], S. Yu. Mezhevych[1], Val. M. Pirnak[1], A. P. Ilyin[1], V. V. Uleshchenko[1], R. Siudak[3], J. Choiński[5], B. Czech[3], A. Szczurek[3]

[1] Institute for Nuclear Researches, National Academy of Sciences of Ukraine, Kyiv
[2] V. N. Karazin Kharkiv National University, Kharkiv
[3] H. Niewodniczański Institute of Nuclear Physics, Polish Academy of Sciences, Cracow, Poland
[4] National Centre for Nuclear Research, Warsaw, Poland
[5] Heavy Ion Laboratory of Warsaw University, Warsaw, Poland
[6] Taras Shevchenko National University, Kyiv

Angular distributions of the ^{7}Li + ^{12}C elastic and inelastic scattering as well as the ^{7}Li(^{14}N, X) reactions with exit stable and unstable nuclei (Z = 3 - 6) were measured at E_{lab}(^{12}C) = 115 MeV using ^{12}C beam of Warsaw cyclotron U-200P [1].

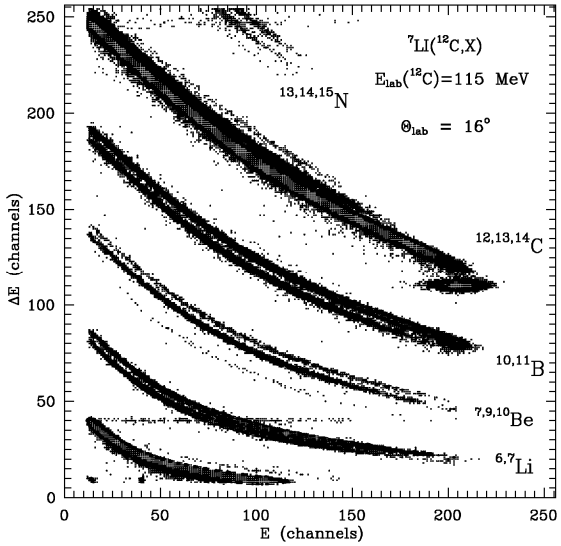

Fig. 1. Typical $\Delta E(E)$-spectrum of the ^{7}Li(^{12}C, X) reaction products.

The data were analyzed within t coupled-reaction-channels (CRC) method using nuclear potential of Woods - Saxon type and Coulomb potential of a uniform charge sphere. The elastic and inelastic scattering, reorientations of ^{7}Li in ground and excited states, spin reorientation of ^{7}Li and more important one and two-step transfer reactions were included in a channels-coupling-scheme.

In Fig. 2, the curves <x> and <xy> show the CRC calculations for transfers clusters x and $x + y$, $y + x$ as well as potential scattering (<pot>) and ^{7}Li spin reorientation (<reor>).

The ^{7}Li + ^{12}C potential parameters for ground and excited states of ^{7}Li and ^{12}C as well as deformation parameters of these nuclei were deduced. The real part of the deduced Li + ^{12}C potential is in a good agreement with the double-folding potential (Fig. 3).

Typical $\Delta E(E)$-spectrum of the ^{7}Li(^{12}C, X) reaction products is shown in Fig. 1. Measured new angular distribution of the ^{7}Li + ^{12}C elastic scattering is shown in Fig. 2.

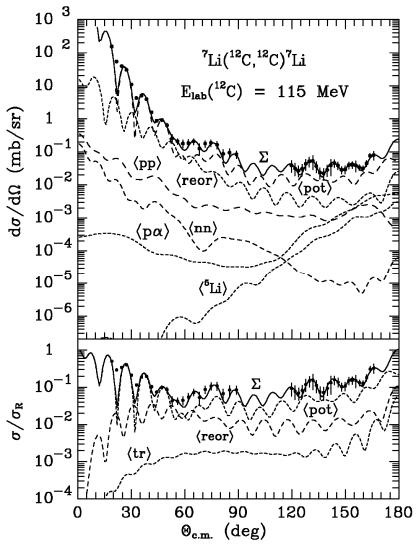

Fig. 2. Angular distribution of the ^{7}Li + ^{12}C elastic scattering at E_{lab}(^{12}C) = 115 MeV.

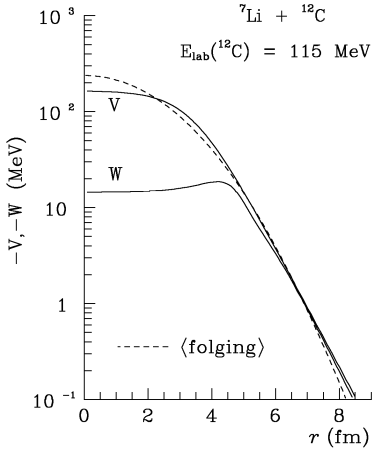

Fig. 3. The ^{7}Li + ^{12}C potential.

It was found that the potential scattering predominates over others mechanisms.

1. A.T. Rudchik *et al.*, Nucl. Phys. At. Energy **14**, 25 (2013).

^{14}C(^{11}B, ^{9}Be)^{16}N REACTION MECHANISMS AND POTENTIAL OF THE ^{9}Be + ^{16}N INTERACTION

S. Yu. Mezhevych[1], A. T. Rudchik[1], K. Rusek[2,3], E. I. Koshchy[4], S. Kliczewski[5], A. V. Mokhnach[1], A. A. Rudchik[1], S. B. Sakuta[6], R. Siudak[5], B. Czech[5], J. Choinski[3], A. Szczurek[5]

[1] Institute for Nuclear Research, Ukrainian National Academy of Sciences, Kyiv
[2] National Centre for Nuclear Research, Warsaw, Poland
[3] Heavy Ion Laboratory of Warsaw University, Warsaw, Poland
[4] V. N. Karazin Kharkiv National University, Kharkiv
[5] H. Niewodniczański Institute of Nuclear Physics, Cracow, Poland
[6] National Research Centre "Kurchatov Institute" Moscow, Russia

Angular distributions of the ^{14}C(^{11}B, ^{9}Be)^{16}N reaction for ground and excited states of ^{9}Be and ^{16}N were measured simultaneously with the ^{14}C + ^{11}B elastic and inelastic scattering at the energy $E_{lab.}$(^{11}B) = 45 MeV using ^{11}B beam of the Warsaw cyclotron U-200P [1].

Fig. 1 shows the sum of the ^{14}C(^{11}B, ^{9}Be)^{16}N reaction data for ground and lowest excited states of ^{16}N unresolved in the experiment.

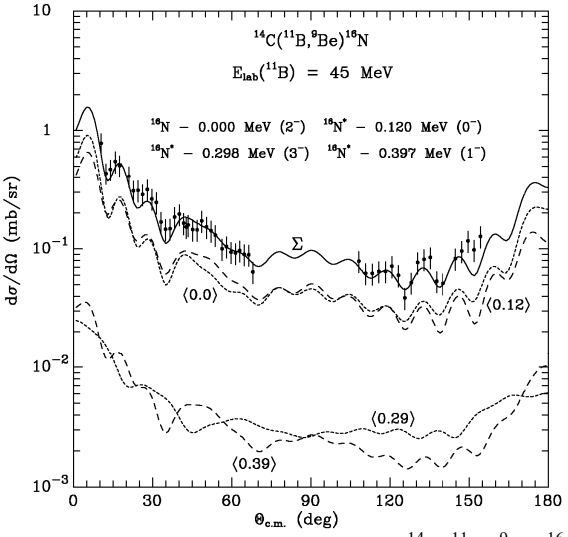

Fig. 1. Angular distributions of the ^{14}C(^{11}B, ^{9}Be)^{16}N reaction at the energy $E_{lab.}$(^{11}B) = 45 MeV for the ground and lowest excited states E^* of ^{16}N. Curves <E^*> show the corresponding CRC-calculations for deuteron transfers. Curve Σ presents incoherent sum of these CRC calculations.

The ^{14}C(^{11}B, ^{9}Be)^{16}N reaction data were analyzed within the coupled-reaction-channels (CRC) method for one- and two-step transfers of nucleons and clusters. In the CRC calculations, the ^{11}B + ^{14}C potential of Wood - Saxon type deduced from the CRC analysis of the ^{11}B + ^{14}C elastic scattering data was used for the entrance reaction channel. Spectroscopic amplitudes of nucleons and clusters needed in the reaction CRC calculations were obtained within nuclear shell-model using code DESNA. The ^{9}Be + ^{16}N potential parameters were fitted to describe ^{14}C(^{11}B, ^{9}Be)^{16}N reaction data. The ^{11}B + ^{14}C and ^{9}Be + ^{16}N potential parameters are given in the Table, while the deduced ^{9}Be + ^{16}N potential is shown in Fig. 2.

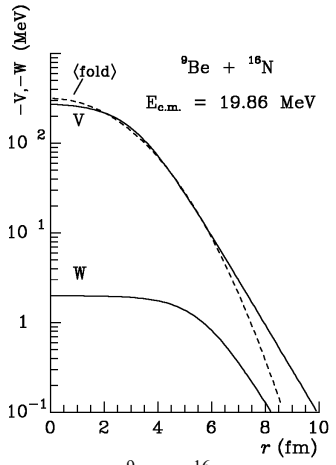

Fig. 2. The ^{9}Be + ^{16}N potential.

It was found that the deuteron transfer dominates in this re-action. The corresponding CRC calculations are shown in Fig. 1.

Parameters of the nucleus-nucleus potentials

Nuclear system	$E_{c.m.}$, MeV	V_0, MeV	r_V, fm	a_V, fm	W_S, MeV	r_W, fm	a_W, fm	Ref.
^{9}Be + ^{16}N	19.86	164.5	0.800	0.900	3.0	1.250	0.900	[1]
^{9}Be + ^{16}N	29.02	174.5	0.800	0.900	5.0	1.250	0.900	[2]
^{11}B + ^{14}C	25.20	266.6	0.750	0.740	7.5	1.345	0.740	[3]

1 S.Yu. Mezhevych *et al.,* Nucl. Phys. At. En. **14**, 18 (2013).
2 A.T. Rudchik, Yu.M. Stepanenko, K.W. Kemper *et al.,* Nucl. Phys. **A860**, 8 (2011).
3 S.Yu. Mezhevych e*t al.,* Nucl. Phys. At. Energy **13**, 123 (2012)

ЕНЕРГЕТИЧНА ЗАЛЕЖНІСТЬ ПОТЕНЦІАЛУ ВЗАЄМОДІЇ ЯДЕР $^{16}O + ^{12}C$

О. А. Понкратенко, В. В. Улещенко, Ю. О. Ширма

Інститут ядерних досліджень НАН України, Київ

У той час як проблема визначення енергетичної залежності параметрів потенціалу взаємодії легких частинок (p, n, α) з ядрами достатньо досліджена в широкому діапазоні енергій [1], у випадку взаємодії важких іонів вона залишається актуальною. Важливо побудувати енергетичну залежність параметрів у широкому діапазоні енергій ($1 \div 100$ МеВ/нуклон). Це сприятиме звуженню неоднозначностей у визначенні параметрів потенціалу, а також допоможе прогнозувати диференціальні перерізи пружного, непружного розсіяння та перерізи злиття і реакцій при тих енергіях, для яких не існує експериментальних даних.

Нами виконано систематичний аналіз кутових розподілів пружного розсіяння ядер $^{16}O + ^{12}C$ при 42 енергіях іона ^{16}O з урахуванням перерізів злиття цих ядер у рамках оптичної моделі (ОМ) (рисунок).

Отримано набори параметрів оптичного потенціалу для кожної з 42 енергій окремо.

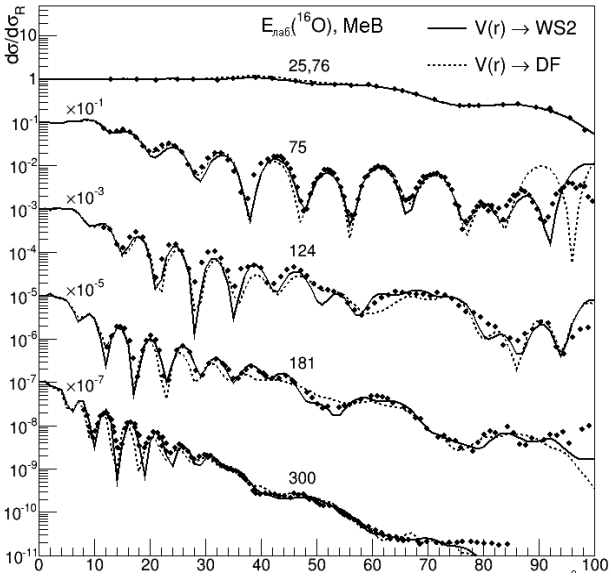

Порівняння експериментальних диференціальних перерізів (у відношенні до кулонівського розсіяння) пружного розсіяння $^{16}O + ^{12}C$ з ОМ-перерізами.

Використовуючи параметризацію:

$$p_i(E) = \begin{cases} p_i(+\infty)(1-\exp[(E_{0i}-E)/\Delta_i]), & E > E_{0i} \\ 0, & E < E_{0i} \end{cases} \quad p_i = W_S, W_D$$

$$p_i(E) = p_i(+\infty) + [p_i(0) - p_i(+\infty)]\exp(-E/\Delta_i) \quad p_i = R_{WS}, a_{WS}, R_{WD}, a_{WD}$$

шляхом підгонки розрахунків за ОМ до експериментальних кутових розподілів пружного розсіяння та перерізів злиття в діапазоні енергій від 1 до 100 МеВ/нуклон, було знайдено енергетичну залежність уявної частини оптичного потенціалу. Енергетична залежність дійсної частини потенціалу визначалась залежністю фолдінг-потенціалу від енергії та дисперсійним співвідношенням між дійсною та уявною частинами потенціалу. Розрахунки з енергетично залежним потенціалом описують експериментальні перерізи задовільно, але все ж таки гірше, ніж із потенціалами, що знайдені для кожної енергії окремо. Можливими причинами такого результату, на наш погляд, є:

неврахування залежності ядерного потенціалу від орбітального моменту відносного руху ядер;

вибір форми енергетичної залежності параметрів саме у вигляді вищенаведеної параметризації;

урахування енергетичної залежності дійсної частини потенціалу лише через залежність від енергії фолдінг-моделі та поправки відповідно до дисперсійного співвідношення; насправді, ця залежність може бути складнішою;

вплив на розсіяння при низьких енергіях ($< 5 \div 10$ МеВ/нуклон) резонансних процесів час, що призводить до порушення гладкої енергетичної залежності параметрів ОМ-потенціалу.

У ході дослідження енергетичної залежності параметрів уявної частини оптичного потенціалу встановлено:

ріст з енергією глибин як об'ємної, так і поверхневої частин потенціалу, що спостерігалось також в інших роботах [2], і пояснюється збільшенням кількості непружних каналів з ростом енергії;

зменшення з енергією параметрів радіуса як об'ємної, так і поверхневої частин потенціалу; характерно, що радіус об'ємної частини (відповідає за злиття ядер) є меншим за радіус поверхневої (відповідає за прямі процеси);

ріст з енергією параметрів дифузності як об'ємної, так і поверхневої частин потенціалу.

1. F.D. Becchetti *et al.*, Phys. Rev. **182**, 1190 (1969).
2. S. Szilner *et al.*, Phys. Rev. C **64**, 064614 (2001).

IDENTIFICATION OF 0^+ STATES IN ^{228}Th THROUGH B1/B2 RATIOS

A. I. Levon[1], S. Pascu[2]

[1] *Institute for Nuclear Research, National Academy of Sciences of Ukraine, Kyiv*
[2] *Horia Hulubei National Institute for Physics and Nuclear Engineering, Bucharest-Magurele, Romania*

The aim of the presented IBM-calculations is to describe simultaneously both the hadronic (transfer strength to 0^+ states) and the existing electromagnetic data. The first ones are discussed in previous annotation. Here we discuss the B1/B2 ratios at decay of 0^+ states. The quadrupole electromagnetic transition operator is:

$$\hat{T}(E2) = e_2 \hat{Q}_{spdf}\,, \qquad (1)$$

where e_2 represents the boson effective charge. To ensure novanishing $E2$ transitions between the states containing no pf bosons and those having $(pf)^2$ components we follow the approach described in Refs. [1], where the mixing of different positive parity-states with different pf components is achieved by introducing in the Hamiltonian a dipole-dipole interaction term of the form:

$$\hat{H}_{int} = \alpha \hat{D}^{\dagger}_{spdf} \cdot \hat{D}_{spdf} + H.c. \qquad (2)$$

where

$$\hat{D}_{spdf} = -2\sqrt{2}[p^{\dagger}\tilde{d} + d^{\dagger}\tilde{p}]^{(1)} + \sqrt{5}[s^{\dagger}\tilde{p} + p^{\dagger}\tilde{s}]^{(1)} + \\ + \sqrt{7}[d^{\dagger}\tilde{f} + f^{\dagger}\tilde{d}]^{(1)} \qquad (3)$$

is the dipole operator arising from the O(4) dynamical symmetry limit, which does not conserve separately the number of positive and negative parity bosons [2]. The interaction strength is given by the a parameter and is chosen to have a very small value, α = 0.0005 MeV, similar to Refs. [1].

For the $E1$ transitions, a linear combination of the three allowed one-body interactions was taken:

$$\hat{T}(E1) = e_1[\chi^{(1)}_{sp}(s^{\dagger}\tilde{p} + p^{\dagger}\tilde{s})^{(1)} + (p^{\dagger}\tilde{d} + d^{\dagger}\tilde{p})^{(1)} + \\ + \chi^{(1)}_{df}(d^{\dagger}\tilde{f} + f^{\dagger}\tilde{d})^{(1)}]\,, \qquad (4)$$

where e_1 is the effective charge for the $E1$ transitions and $\chi^{(1)}_{sp}$ and $\chi^{(1)}_{df}$ are model parameters. In ^{228}Th there are no lifetimes measured for the negative-parity states, hence no absolute transition probabilities could be extracted. Therefore we would restrict the present discussion to reproducing the B(E1)/B(E2) ratios. A detailed comparison between the experimental data and the present calculations is presented in the Table. The agreement is obtained by using e_1 = 0.005 efm and e_2 = 0.19 eb as the effective charges in Eq. (4) and (1), respectively. The remaining $E1$ parameters are χ_{sp} = 0.4 and χ_{df} = -1.4.

K^{π}	E_i (keV)	J_i	J_{f1}	J_{f2}	Exp. (10^{-4} b^{-1})	IBM (10^{-4} b^{-1})
0^+_1	832	0^+	1^-_1	2^+_1	5.1(4)	6.1
	874	2^+	3^-_1	4^+_1	7.1(15)	7.6
		2^+	3^-_1	2^+_1	24.5(31)	15.2
		2^+	3^-_1	0^+_1	14.7(24)	23.6
		2^+	1^-_1	4^+_1	4.2(9)	4.4
		2^+	1^-_1	2^+_1	14.5(19)	8.9
		2^+	1^-_1	0^+_1	8.7(14)	13.7
	968	4^+	5^-_1	6^+_1	22.8(80)	9.2
		4^+	5^-_1	4^+_1	10.8(27)	18.2
		4^+	5^-_1	2^+_1	6.7(13)	20.7
		4^+	3^-_1	6^+_1	19.1(67)	5.9
		4^+	3^-_1	4^+_1	9.0(23)	11.8
		4^+	3^-_1	2^+_1	5.6(11)	13.4
0^+_3	1176	2^+	1^-_1	4^+_1	0.060(25)	0.08
		2^+	1^-_1	2^+_1	0.25(10)	0.27
		2^+	1^-_1	0^+_1	0.62(28)	0.38
		2^+	3^-_1	4^+_1	0.09(5)	0.16
		2^+	3^-_1	2^+_1	0.39(20)	0.52
		2^+	3^-_1	0^+_1	0.95(51)	0.72

The B(E1)/B(E2) ratios discussed in Table belong to the $K^{\pi} = 0^+_1$ (the predicted double-octupole phonon band) and $K^{\pi} = 0^+_3$ (β-vibrational) bands. The comparison between them is important, because it can be used as a tool for providing additional information about the nature of the $K^{\pi} = 0^+_1$ band. All the states belonging to this band are having $2pf$ bosons in their structure and are supposed to have a double-octupole phonon character. Further information confirming this hypothesis comes from the analysis of the $E1$ and $E2$ branching ratios. If the picture proposed by the IBM is correct, the states belonging to the $K^{\pi} = 0^+_1$ band will show strong transitions into the negative-parity states (if they have a double-octupole character), while the levels stemming from the $K^{\pi} = 0^+_3$ (β-band) will show very weak $E1$ transitions to these states. The experimental values in Table I fully confirm this hypothesis, showing that the B(E1)/B(E2) ratios are at least one order of magnitude larger for the $K^{\pi} = 0^+_1$ band.

1. N.V. Zamfir and D. Kusnezov, Phys. Rev. C **63**, 054306 (2001); Phys. Rev. C **67**, 014305 (2003).
2. D. Kusnezov, J. Phys. A **23**, 5673 (1990); J. Phys. A **22**, 4271 (1989).

DESCRIPTION OF THE (p, t) TRANSFER STRENGTHS TO 0^+ STATES IN ^{228}Th IN THE IBM MODEL

O. I. Levon[1], S. Pascu[2]

[1] *Institute for Nuclear Research, National Academy of Sciences of Ukraine, Kyiv*
[2] *Horia Hulubei National Institute for Physics and Nuclear Engineering, Bucharest-Magurele, Romania*

All previous calculations in the *IBM-spdf* framework with a simplified Hamiltonian [1] indicated that IBM fails completely to reproduce the (p,t) spectroscopic factors. The calculated first excited states were found with a transfer strength of ~1% of that of the ground state and the higher states were even weaker, whereas experimentally the first excited state is seen with ~30 % of the ground-state intensity. Therefore the method [2] was used, where the addition of the second-order O(5) Casimir operator in the Hamiltonian can account for the observed (p, t) spectroscopic factors. The Hamiltonian employed is:

$$\hat{H}_{spdf} = e_d\hat{n}_d + e_p\hat{n}_p + e_f\hat{n}_f + k(\hat{Q}_{spdf}\cdot\hat{Q}_{spdf})^{(0)} +$$

$$+a_3[(\hat{d}^{\dagger}\tilde{d})^{(3)}\times(\hat{d}^{\dagger}\tilde{d})^{(3)}]^{(0)}, \qquad (1)$$

where e_d, e_p, and e_f are the boson energies and n_p, n_d, and n_f are the boson number operators, k is the quadrupole-quadrupole interaction strength and a_3 is the strength of the O(5) second order Casimir operator. The L = 0 transfer operator has the form:

$$\hat{P}_{\nu}^{(0)} = (\alpha_p\hat{n}_p + \alpha_f\hat{n}_f)\hat{s} +$$

$$+a_{\nu}\left(\Omega_{\nu} - N_{\nu} - \frac{N_{\nu}}{N}\hat{n}_d\right)^{\frac{1}{2}}\left(\frac{N_{\nu}+1}{N+1}\right)^{\frac{1}{2}}\hat{s}, \qquad (2)$$

where $i\backslash_V$ is the pair degeneracy of neutron shell, N_V is the number of neutron pairs, N is the total number of bosons, and a_p, af, and a_V are constant parameters. The L=0 transfer operator contains two additional terms beside the leading order term [3].
The Hamiltonian is diagonalized in a Hilbert space with a number of bosons $N_B = n_s + n_d + n_p + n_f$. We used an extended basis allowing up to three negative parity bosons ($n_p + n_f = 3$). The vibrational strengths used in the calculations are $e_d = 0.2$ MeV, $e_p = 1.0$ MeV, and $e_f = 1.1$ MeV, while the quadrupole-quadrupole interaction strength has a value of $k = -21$ keV. The strength of the O(5) second order Casimir operator is set to $a_3 = 0.053$ MeV, while the quadrupole operator parameters are ($\chi_{sd}^{(2)} = -1.09$, $\chi_{pf}^{(2)} = -1$).

In Figure we display the calculated two-neutron intensities for ^{228}Th in comparison to the integrated

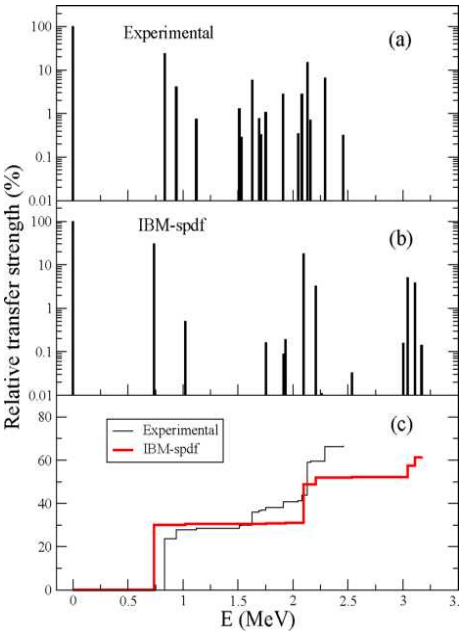

experimental cross sections normalized to that of the ground state. The calculations reproduce the strong excitation of the first 0^+ state at 832 keV in good agreement with the experiment. The experimental spectrum of 0^+ states is dominated also by a single state located at 2.1 MeV, showing a high cross section of about 15 % of that of the ground state. In the IBM, there is predicted a state located at 2.1 MeV, which have the transfer intensities of about 18 %. This state has a double-octupole phonon structure. Another state at 2.29 MeV with a relative cross section of about 7% can be put in correspondence to the in the IBM state at 2.2 MeV also with a double-octupole phonon structure. The running sum is taken up to 3.25 MeV, where group of states with significant transfer strength is predicted by the IBM. The parameters from Eq. (2) were estimated from the fit of the known two-neutron transfer intensities. The values employed in the present paper are $\alpha_p = 1.3$ mb/sr, $a_f = -0.4$ mb/sr, and $a_v = 0.03$ mb/sr. The location and transfer intensity of the strongest states is well reproduced by the calculations.

1. A.I. Levon *et al.,* Phys. Rev. C **79**, 014318 (2009).
2. S. Pascu, N.V. Zamfir, Gh. Cata-Danil, and N. Marginean, Phys. Rev. C **81**, 054321 (2010).
3. F. Iachello, A. Arima, *The Interacting Boson Model* (Camb. Univ. Pres., Cambridge, England, 1987).

METROLOGY MEASUREMENTS AT THE KINR OF NASU TANDEM ACCELERATOR

V. I. Soroka, V. A. Onischuk, E. M. Mozhzhukhin,
M. V. Artsimovich, I. V. Posmitiukh, A. F. Sharov

Institute for Nuclear Research, National Academy of Sciences of Ukraine, Kyiv

The renovate approach of the resonance proton scattering use for the beam parameters check of the electrostatic accelerators has been suggested in the paper. Its expediency has been confirmed by experiment. Silicon and oxygen were used as targets. The silicon targets were of two types of thickness: 1) the target of complete absorption, 2) the target with the thickness in which the loss of protons energy exceeded the width of the selected resonance. The elastic and non elastic proton scattering from silicon were used in region of the 3100 ± 2 keV proton energy resonance (Γ = 12,5 ± 0,2 кеV, Γ_p/Γ = = 0,2, $j^{\pi} = 7/2^-$). The resulting calibration curve for non elastic proton resonance scattering is shown in fig. 1 (a). The energy, which existed up to the accelerator modernization, is put on the X-axis. The midpoint of the relative yield rise corresponds to the ~ 3114 keV resonance energy. Thus, the difference from the real resonance energy equals to ~ 14 keV.

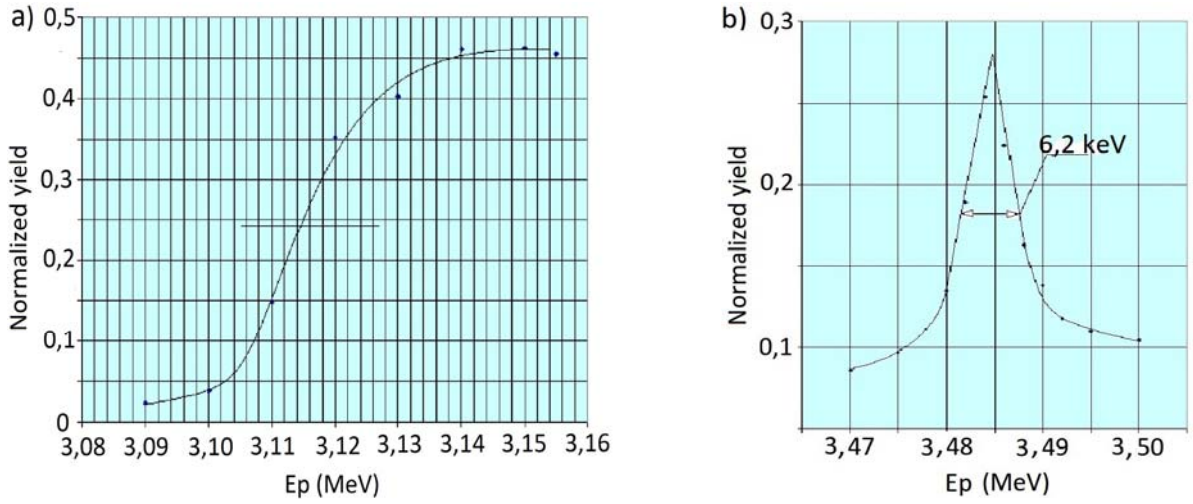

Energy dependences of the normalized yield: *a*) of nonelastic scattered protons on silicon in the 3100 keV resonance region; b) of elastic scattered protons on oxygen in the 3470 keV resonance region.

The oxygen target as component of the surface oxidizing layer on beryllium had the thickness which in terms of the loss of proton energy (0,460 keV) was less than the width of the selected elastic narrow resonance at the 3470 keV proton energy (Γ = 1.53 ± ± 0,2 keV, $j^{\pi} = 5/2^-$). The form of this resonance for the scattering angle of 165° is practically symmetrical. The scattering cross-section increases in maximum approximately twenty times. The resulting calibration curve for $^{16}O(p, p)^{16}O$ elastic proton resonance scattering is shown in Figure, *b*. The yield peak for the thin target is observed near the 3484 keV. Thus, the difference from the real resonance energy equals to ~ 14 keV too. FWHM of the experimental yield is ~ 6,2 keV. Calculation of the beam proton energy scattering gives the value of ± 3 keV.

The silicon and oxygen target may be recommended as template for the calibration purposes. Variable thickness self-supporting silicon targets can be manufactured by known methods. The thin oxygen targets of the surface oxidizing layer on the polished beryllium surface are accessible too.

The paper also proposes the modified nuclear-analytical method of thickness measurement of nanometer self-supporting films and surface layers. The method was successfully tested for the purpose of thickness measurement of the carbon stripper target for the tandem accelerator. Average thickness of the trial batch of targets was 20 μg/cm^2.

CORRELATION PROPERTIES OF MOTION THE ACCOMPANYING PARTICLE RELATE MOTION THE MAIN PARTICLE IN THE RADIOACTIVE DECAY PROCESSES AND INTERNAL CONVERSION

N. F. Mitrokhovich, V. T. Kupryashkin, L. P. Sidorenko

Institute for Nuclear Research National Academy of Sciences of Ukraine, Kyiv

On motion accompanying particles (electrons "shake-off", Auger electrons) strong correlating motion it with the main (primary) particles (beta particle, conversion electron) are observed [1 - 4] and $\Upsilon(\Omega) = 4\pi DP/D\Omega P >> 1$. Accept to attention that $\Upsilon(\Omega = 0) \sim \sqrt{E_{Sh}}$, it point to mechanism as magnetic interaction currents from moving charged particles.

To confirm (or refute) this mechanism, the spatial correlation of $\Upsilon(\Omega)$ "shake-off" electrons with relation to beta-particle in the direction of it motion $\Upsilon(0)$, and in opposite direction from it $\Upsilon(2\pi)$, has been investigated. A similar correlation in the motion of associated particle ("shake-off" electron and Auger-electron) relate to the conversion electron has been investigated also. The experimental implementation observation of these correlations accompanying particles relate beta- particles and conversion electrons transitions 122 E2 and 344 E2 in ^{152}Eu decay is adduced in Figure.

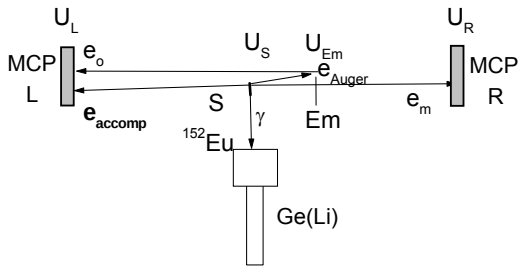

Technique of definition correlating the motion of accompanying particle (e_{accomp}) with main particle (e_m) at measurement γe_{accomp} or γe_o – and $\gamma e_m e_{accomp}$ or $\gamma e_m e_o$ - coincidences from a source S ^{152}Eu at registration of e_{accomp} electrons on e_o -electrons of the secondary electron emission at $\Omega = 0$ or directly at $\Omega = 2\pi$. At potentials $U_S > U_L$, $U_{Em} = 0$ it occurs for $\Omega = 0$ only from emitter Em and only by lelt MCP-detector of electron. At potentials $U_S = U_{Em} > U_L$, it occurs for $\Omega = 2\pi$. MCP- detectors (L and R) are on basis micro-channel plates. Ge(Li) – γ- detector. At $\Omega = 2\pi$ activity faces to detector L.

In measurements it is necessary to receive correlation $\Upsilon(\Omega = 0)$ as relation the yield accompanying electron per one unit decay in direction forward with main electron to the yield accompanying electron per one unit decay in arbitrary direction it relate main particle electron. It was determined as $\Upsilon(\Omega = 0) = \text{Yield}(\Omega = 0)/\text{Yield}(\Omega = 4\pi) = (N\gamma e_a e_o/N\gamma e_a)/(N\gamma e_o/N\gamma)$, because in treble coincidences e_{accomp} can moves only in direction main electron (see Figure) for registering by e_o-electron from emitter Em. Similar - for $\Upsilon(\Omega = 2\pi) = \text{Yield}(\Omega = 2\pi)/\text{Yield}(\Omega = 4\pi) = (N\gamma e_m e_{acc}/N\gamma e_m)/(N\gamma e_{acc}/N\gamma)$, but detector L are registering accompanying particle directly.

The obtained data for $\Upsilon(\Omega)$ are listed in the Table.

Correlations properties $\Upsilon(\Omega)$ in motion accompanying particle relate main particle in the forward direction ($\Omega = 0$) and in opposite direction from her ($\Omega = 2\pi$) in beta-decay and internal conversion

Process, accompanying	$\Upsilon(0)$	$\Upsilon(2\pi)$
β^-, "shake-off"	4.3(5)	< 0.3
IC 122 E2, "shake-off"	5.6(11)	
IC 122, "shake-off"+ Auger	7.5(3)	< 0.5
IC 344, "shake-off"+ Auger	10(4)	
IC 122 E2, M-Auger	10(3)	

The data indicate that the correlation properties of accompanying particles in motion relate the main particles in the processes radioactive decay and internal conversion are connected to mechanisms, which are put in their appearance, as interaction current components from movement charged particles in the final state.

1. N.F. Mitrokhovich, in *Proc. Int. Conf. "Current Problems in Nuclear Physics and Atomic Energy"* (K., 2006), p. 412.
2. N.F. Mitrokhovich, V.T. Kupryashkin, Nucl. Phys. At. Energy **19**, 61 (2007).
3. N.F. Mitrokhovich, Nucl. Phys. At. Energy **11**, 136 (2010).
4. N.F. Mitrokhovich, V.T. Kupryashkin, L.P. Sidorenko, Nucl. Phys. At. Energy **14(2),** 129 (2013).

YIELDS OF e_0-ELECTRONS FROM THE TARGET SURFACE AT LOW ENERGIES OF α-PARTICLES

V. T. Kupryashkin, L. P. Sidorenko, A. I. Feoktistov, V. A. Lashko

Institute for Nuclear Research National Academy of Sciences of Ukraine, Kyiv

This work is a continuation of our researches of the dependence on the yields of near-zero energy electrons (e_0- electrons) coursed by α-particles bombardment of target in the radioactive decay of ^{226}Ra (energy range from 4.8 to 7.6 MeV) [1] and on the cyclotron U-120 (9.7 - 24.3 MeV) [2]. In present work we measured the yields of e_0-electrons (e_0) and fast electrons (e_{ef}) in the low-energy range (0.9 - 5.5 MeV) under bombardment by α-particles of aluminum and titanium targets. Yield dependences of e_0-electrons on the energy of α- particles were measured by the time (eα) – coincidence method.

Al-foils of different thicknesses are used for changing the energy of the α-particles from the source of ^{238}Pu ($E\alpha$ = 5.5 MeV). Two measurements were carried out for aluminum target and one measurement for the titanium target. Yields of electrons is proportional to the detection probabilities R_{e0}, R_{ef} and $Ye_0 = Re_0/\varepsilon\Omega$, where ε-detection efficiency, and Ω-solid angle. Measurement results are shown in the table in terms of R (10^{-3}) per one α-particle passed through Al- or Ti- target.

Energy	Target							
	Aluminum						Titanium	
E_α, MeV	1		2		Average		3	
	R_{e0}	R_{ef}	R_{e0}	R_{ef}	R_{e0}	R_{ef}	R_{e0}	R_{ef}
5,5	7,21(14)	5,02(7)	6,8(13)	5,08(7)	6,99(10)	5,05(5)	10,51(17)	7,16(9)
4,5	7,89(15)	5,73(8)	8,08(14)	5,64(8)	7,99(10)	5,69(6)	10,84(19)	8,44(10)
3,8	8,86(17)	6,23(9)	8,83(15)	6,21(8)	8,84(11)	6,22(6)	13,1(26)	9,36(13)
3,4	9,11(17)	6,24(9)	9,25(16)	6,43(8)	9,18(12)	6,35(6)	13,52(19)	9,53(13)
2,5	9,75(17)	6,75(9)	10,32(17)	7,13(9)	10,04(12)	6,94(6)	15,04(19)	9,95(10)
2	11,3(18)	7,52(9)	11,14(17)	7,24(9)	11,22(12)	7,38(6)	17,21(22)	10,42(10)
1,5	12,13(20)	7,83(10)	11,16(17)	7,53(10)	11,57(13)	7,68(7)	19,75(33)	11,51(15)
0,9							24,39(31)	12,08(17)

Yields of e_0-electrons for α-particles of different energies E_α are well described by the relation $Y(E\alpha) \sim Re_0 \sim E\alpha^{-1/2} \sim v^{-1}$ as previously observed in our works [1, 2] and they are consistent with our view of them as a result of the shake-off effect: the passage of alpha particles near the surface of target suddenly formed a charge that brings the system to a perturbation and to shaking of weakly bound electrons from the surface of target.

1. V.T. Kupryashkin, L.P. Sidorenko *et al.*, Ukr. J. Phys. **51**, 5 (2006).
2. A.O. Valchuk, V.T. Kupryashkin *et al.*, Ukr. J. Phys. **53**, 853 (2008).

LOG *ft* VALUES FOR BETA-TRANSITIONS AT ^{175}Hf DECAY

A. P. Lashko[1], T. N. Lashko[1], V. A. Martinishin[2]

[1] *Institute for Nuclear Research, National Academy of Sciences of Ukraine, Kyiv*
[2] *Department of Nuclear Physics, Taras Shevchenko National University, Kyiv*

According to the newest experimental data, ^{175}Hf decays ($T_{1/2}$ = 70 days) by means of electron capture onto the excited ^{175}Lu states with energies of 514.6, 432.8, 353.3, and 343.4 keV (see Figure). By measuring the intensity and multipolarity of γ-rays one can determine capture probabilities to different levels of ^{175}Lu and then calculate corresponding log *ft* values for β-transitions. Since the probabilities of β-transitions differ by several orders of magnitude depending on their type, the intensities of transitions between the levels of daughter nucleus also differ considerably. This circumstance complicates the measurements significantly and requires using spectrometers with high resolution.

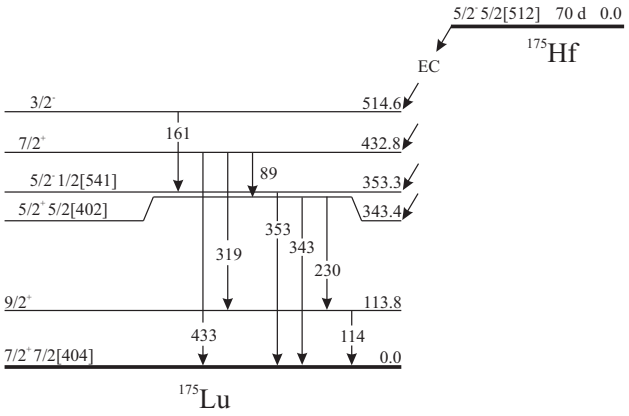

The decay scheme of ^{175}Hf.

The relative intensities of γ-rays following the decay of ^{175}Hf were measured with a gamma-spectrometer that comprises two horizontal coaxial HPGe-detectors: GMX-30190 and GEM-40195, having the resolution of 1.89 and 1.73 keV for the γ1332-line of ^{60}Co and efficiency of 33 and 43 % respectively.

The radioactive ^{175}Hf sources were obtained in the (n, γ) reaction at a research nuclear reactor WWR-M. Natural hafnium targets were used for the purpose.

The standard ^{60}Co, ^{133}Ba, ^{137}Cs, ^{152}Eu, ^{228}Th, and ^{241}Am γ-sources were used for accurate calibration of detectors for the energy range of 26 to 1620 keV. The shape of the efficiency curve is well described by the Campbell function [1]. The uncertainty in the efficiency curve of both detectors does not exceed 2 % throughout the energy range.

To minimize possible systematic errors a series of measurements were performed – using different types of detectors, at different geometries, at different gains and channel widths of an amplitude-to-digital converter (8192 and 16384 quantization levels of the input signal) – 38 series of measurements in all.

The results of these measurements are listed in Table 1. The data from compilation [2] is also shown. The γ-ray energies were taken from Ref. [3].

Table 1. **The relative intensities of γ-rays from the ^{175}Hf decay**

Energies, keV	Intensities, relative units	
	Present work	[2]
89.362	34.5 ± 1.5	28.6 ± 2.2
113.801	3.46 ± 0.20	3.5 ± 0.3
161.20	0.45 ± 0.14	0.27 ± 0.10
229.609	8.29 ± 0.19	8.13 ± 0.20
318.971	1.57 ± 0.23	2.0 ± 0.5
343.410	1000	1000
353.3	2.66 ± 0.18	2.72 ± 0.20
432.771	17.5 ± 0.4	17.1 ± 0.3

On the basis of data quoted in Table 1 and internal conversion coefficients from Ref. [2], the values for the population of levels in ^{175}Lu at the ^{175}Hf decay were determined.

These values were used to calculate log *ft* of β-transitions. The results of calculations are presented in Table 2. The β-ray branching ratios (%) is also shown.

Table 2. **The electron capture branching ratios and log *ft* values of ^{175}Hf**

E(level), keV	Iε, %	Log *ft*
514.6	0.076 ± 0.024	9.24 ± 0.14
432.8	20.1 ± 0.8	7.27 ± 0.02
353.3	0.155 ± 0.028	9.66 ± 0.09
343.4	79.6 ± 1.2	6.99 ± 0.02

The obtained values of log *ft* for β-transitions do not contradict the corresponding systematization in this nuclear range [4].

1. L.A. McNelles and J.L. Campbell, Nucl. Instrum. Methods **109**, 241 (1973).
2. M. Shamsuzzoha Basunia, Nucl. Data Sheets **102**, 719 (2004).
3. A.P. Lashko and T.N. Lashko, Nucl. Phys. At. Energy **13**, 7 (2012).
4. B. Singh, J.L. Rodriguez, S.S.M. Wong, and J.K. Tuli, Nucl. Data Sheets **84**, 487 (1998).

K X-RAYS FROM ^{177m}Lu DECAY

A. P. Lashko, T. N. Lashko, A. N. Savrasov, V. A. Zheltonozhsky

Institute for Nuclear Research, National Academy of Sciences of Ukraine, Kyiv

Over 50 γ-transitions in the energy range from 14 to 465 keV are excited by the decay of ^{177m}Lu ($T_{1/2}$ = 160.44 days).While the intensities of γ-rays for energies above 100 keV are well known (not without our participation), the region below 100 keV is poorly understood. It is not better regarding the ^{177m}Lu X-ray spectrum measurements. Our current research was to clarify all controversial questions in this area.

Low Energy Photon Spectrometers (LEPS) were used for the energy range below 100 keV: SLP-04160 (12.5 mm^2, Si(Li), planar) and GLP-10180 (80 mm^2 × 7 mm, HPGe, planar) with FWHM (full width at half maximum) 160 and 180 eV at 5.9 keV of ^{55}Fe respectively.

The radioactive ^{177m}Lu sources were obtained in the (n, γ) reaction as a result of enriched to 27.1 % in 176 mass number lutetium target irradiation with neutrons at the research nuclear reactor WWR-M. The measurements of gamma-ray spectra started two months after the end of irradiation so that ^{177}Lu ($T_{1/2}$ = 6.647 days), having much larger activation cross-section, must have decayed en masse.

The γ-ray spectra were analysed using WinSpectrum, a computer program which allows determining with high precision the energy and intensity of components that have an asymmetric line shape and the ones that are overlapping.

It should be noted that the γ55 keV cannot be resolved in a spectrum with the K X-rays of hafnium. When decomposing this part of γ-spectrum we exercised the fact that the energy of γ55 is known with high accuracy as well as the energy of X-rays. The position of γ55 keV in the spectrum was tethered to the Hf Kα$_1$ line, and during the fitting process distance between these peaks remained constant. Besides that, the intensities of X-rays, which are also known with high accuracy - better than 2% [1], were controlled.

The result of fitting part of γ-spectrum of ^{177m}Lu near the γ55 keV line is shown in Figure for illustration purposes. The experimental values of relative intensities of Kα$_2$ and Kα$_1$ lines of hafnium $(\text{Hf K}\alpha_2/\text{Hf K}\alpha_1)_{exp} = 0.569 \pm 0.002$ are also in a very good agreement with adjusted experimental values from the tables of Salem *et. al.* [1] $(\text{Hf K}\alpha_2/\text{Hf K}\alpha_1)_{Salem} = 0.572 \pm 0.011$. These facts directly confirm that the systematic errors are insignificant, and our estimates on the intensity of the γ55 keV line are correct.

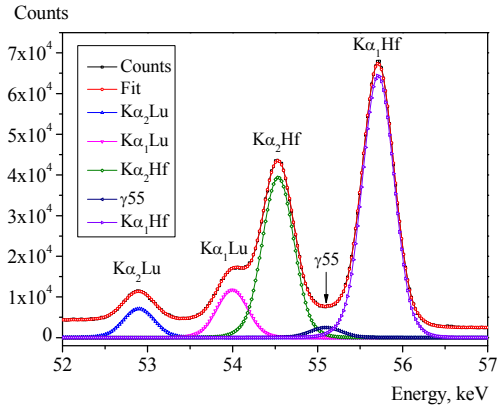

Partial γ-spectrum of ^{177m}Lu in 52 to 57 keV energy range obtained by means of planar Si(Li)-detector SLP-04160.

The results of these measurements are listed in Table. The data from Ref. [2] is also shown. The K X- and γ-transition energies are taken from Ref. [3] and Ref. [4].

The relative intensities of K X- and γ-rays from the ^{177m}Lu decay

Energies, keV	Comments	Intensities, relative units	
		Present work	[2]
52.965	Lu Kα$_2$	34.0 ± 1.7	67 ± 5
54.070	Lu Kα$_1$	61.0 ± 3.7	350 ± 20
54.611	Hf Kα$_2$	209 ± 9	
55.168	γ	13.5 ± 1.0	508 ± 29
55.790	Hf Kα$_1$	367 ± 15	
61.219	Lu Kβ$_1'$	19.1 ± 1.3	30.6 ± 2.1
63.166	Hf Kβ$_1'$	126 ± 6	172 ± 10
63.200	Lu Kβ$_2'$		
65.211	Hf Kβ$_2'$	35.4 ± 1.9	44 ± 3
71.642	γ	6.64 ± 0.32	7.7 ± 0.3
105.3589	γ	100	100

Intensities of ^{177m}Lu K X-rays measured by authors of Ref. [2] using a 1 cm^3 planar Ge(Li)-detector with the resolution of 0.8 keV at 122 keV line are (1.2 ÷ 2.0) times greater than our values. Relative K X-ray emission rates for lutetium and hafnium calculated based on our data are in good agreement with the values from the tables [1], while the data from Ref. [2] are not.

1. S.I. Salem, S.L. Panossian, and R.A. Krause, At. Data and Nucl. Data Tables **14**, 91 (1974).
2. V. Hnatowicz, Czech. J. Phys. **B31**, 260 (1981).
3. J.A. Bearden, Rev. Mod. Phys. **39**, 78 (1967).
4. F.G. Kondev, Nucl. Data Sheets **98**, 801 (2003).

INVESTIGATION OF 12^- HIGH SPINS ISOMERIC STATES IN ^{196,198}Au NUCLEI IN (p,n)- REACTIONS

I. N. Vishnevsky, V. A. Zheltonozhsky, A. M. Savrasov, E. P. Rovenskykh

Institute for Nuclear Research, National Academy of Sciences of Ukraine, Kyiv

Investigation of isomeric ratios is a common type obtaining information both concerning structure of excited levels of atomic nuclei and concerning nuclear reactions mechanism. Choice of (p,n)-reaction in nearthreshhold energy region of projectiles and at great spins difference of ground and isomeric states of residual nucleus allows to evaluate the contribution both of nonstatistical channel and the structure of excited levels of residual nucleus in nuclear reaction mechanism. It can be done by comparison of the experimental and theoretical values of isomeric cross-sections ratios. It should be noted that for low energy protons this evaluation can make more uniquely. Earlier we studied the population of isomeric states with 12^- high spins in ^{196,198}Au nuclei in reactions with deuterons and gamma-rays [1]. So, considering all above mentioned points, there is scientific interest to continue investigation of these levels population in (p,n)-reaction.

Targets were made of metallic foils of Pt (natural isotopic composition or ^{196}Pt enriched to 99%) with thickness of 20-30 μm. They were irradiated by protons with 6.8 MeV energy value on U-120 accelerator. Gamma-spectra of the reaction products were measured on the HPGe-spectrometers with energy resolution 1.8-2 keV for the 1332-keV γ-line of ^{60}Co and detection efficiency of 15-40% in comparison with a $3' \times 3'$ NaI(Tl)-detector.

Gamma-spectra fragments were showed on figure 1. Evidently, the ^{196,198m,g}Au activities have been reliably observed. Using obtained experimental data and tabular quantities such values of the isomeric cross-sections ratios have been measured: for ^{196}Pt(p,n)^{196m,g}Au - $\sigma_m/\sigma_g = (2{,}3\pm0{,}4)\cdot10^{-4}$; for ^{198}Pt(p,n)^{198m,g}Au - $\sigma_m/\sigma_g = (7{,}8\pm1{,}5)\cdot10^{-4}$.

The calculation of the cross - sections ratios was done using TALYS-1.4 code [2]. There are statistical and preequilibrium mechanisms of the nuclear reactions in this code. In the process of calculation, using default parameters given in TALYS-1.4, 12^- isomeric levels are not populated. With regard to all above – stated we can do conclusion that there are perhaps high-spins excited levels, which populate isomeric states or possible significant contribution of direct mechanism in the population of these 12^- levels.

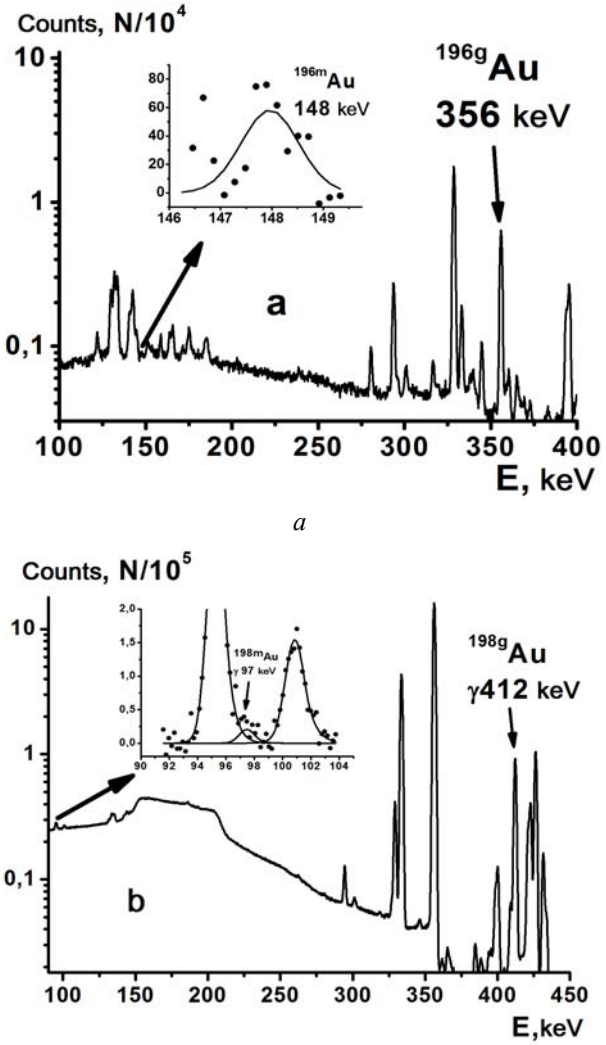

a

b

The γ-spectra fragments of irradiated platinum targets measured by GX4019 (*a*) and GR1519 (*b*) HPGe-detectors.

1. I.N. Vishnevsky, V.O. Zheltonozhsky, E.V. Kulich *et al.*, Bull. Rus. Acad. Sci. Phys. **72**, 1577 (2008).
2. A.J. Koning, S. Hilaire, and M.C. Duijvestijn, in *Proc. of the Int. Conf. on Nuclear Data for Science and Technology*, 2004, p.1154.

^{120}Sb DECAY

I. N. Vishnevsky, S. S. Drapey, V. A. Zheltonozhsky, A. N. Savrasov, V. P. Khomenkov

Institute for Nuclear Research, National Academy of Sciences of Ukraine, Kyiv

^{120}Sb decay provides a rare opportunity to investigate penetration effects in $E1$- and $E2$-transitions, since the excited states of ^{120}Sn which are populated in this decay, then depopulate via inhibited $E1$- and $E2$-transitions.

In this paper, ^{120}Sb decay to ^{120}Sn excited states is studied. Measurement of single γ-spectra and γγ- and K_Xγ-coincindence were performed. From these data, internal conversion coefficients (ICC) on K-shell and total ICC for the inhibited $E1$-and $E2$-transitions were determined.

For such measurements precise calibration of the spectrometer in the low and high energy range becomes a critical factor. The spectrum of ^{182}Ta decay is almost perfect for our calibration purpose. γ-spectra of both ^{182}Ta and ^{120}Sb decay, consist of two similar fragments, and the errors of needed ^{182}Ta γ-transitions is about (0.3 - 0.6) %.

Following abovementioned, we prepared ^{120}Sb source obtained in (p, n)-reaction (E_p = 6.8 MeV) on tin target enriched up to 98 % of ^{120}Sn. Irradiation was carried out in U-120 accelerator of KINR. The activity of ^{182}Ta was accumulated in (n, γ)-reaction at KINR WWR reactor. The thickness of targets was about 25 - 30 mg·cm^{-2}. The measurements were performed using HPGe-spectrometer with beryllium input window. The spectra were processed with WinSpectrum software, the fitting errors were of order of (0.1 - 0.2) %. The resulting intensity of γ-lines with the energy of 89 keV and 197 keV accompanying ^{120}Sb decay, total ICC with their relative deviations from the tabulated data are given below in the Table.

Gamma intensity, ICC, relative ICC deviation and nuclear penetration parameters

E_γ, keV	I_γ, %	α_K	$\delta\alpha_K$, %	α_{tot}	$\delta\alpha_{tot}$, %	F_W	λ_1	λ_2
89	78.1 (5)	0.232 (9)	8.9 (42)	0.268 (8)	8.5 (32)	18000	3.6 ± 1.6	~ 100
197	86.2 (5)	0.136 (7)	13.8 (58)	0.161 (7)	9.9 (48)	260	6 ± 2	~ (100 - 200)

To determine ICC on K-shell the relative intensity of γ- and K_X-transitions was compared. The spectra of γγ- and K_Xγ-coincidence were measured using Compton suppression spectrometer with Ge-detector having an input beryllium window to allow the registration of γ-rays above 5 keV energy. For this decay scheme the measurement of relative intensities of certain γ-transitions and the corresponding X-ray photons allows to determine α_K for both $E2$- and $E1$-transitions using the expression $\alpha_K = I_{Kx} / (\omega_K \cdot I_\gamma)$, where I_γ and I_{Kx} are the relative intensities of γ-transition and X-rays, and ω_K is fluorescence yield.

The following table summarizes our findings about the ICC and their relative deviation from the tabulated values of $\delta\alpha = |\alpha_{exp} - \alpha_{tab}| / \alpha_{tab}$. One can see that significant anomalies are observed in ICC of $E1$- and $E2$-transitions. To assess the role of penetration effects in electrical transitions one should have two or more experimental values of ICC, as the expression for the ICC has two nuclear penetration parameters: $\alpha_{exp}(EL) = \alpha_{tab} \cdot (1 + \lambda_1 A_1 + \lambda_1^2 A_2 + \lambda_2 A_3 + \lambda_2^2 A_4 + \lambda_1 \lambda_2 A_5)$, where A_i are electronic parameters. Parameter λ_1 corresponds mainly to the spin current and, consequently, to the transient toroidal momentum, while λ_2 is due to convection current.

Obtained values for nuclear penetration parameters are shown in the Table. Also the contribution of spin current to the matrix element of γ-radiation of $E1$ transition was determined: K_γ = - (0.5 ± 0.2)%.

SEARCH FOR 2β DECAYS OF ^{96}Ru AND ^{104}Ru BY ULTRA-LOW BACKGROUND HPGe γ SPECTROMETRY AT LNGS: FINAL RESULTS

P. Belli[1], R. Bernabei[1,2], F. Cappella[3,4], R. Cerulli[5], F. A. Danevich[6], S. d'Angelo[1,2], A. Incicchitti[3,4], G. P. Kovtun[7], N. G. Kovtun[7], M. Laubenstein[5], D. V. Poda[6], O. G. Polischuk[3,6], A. P. Scherban[7], D. A. Solopikhin[7], J. Suhonen[8], V. I. Tretyak[6]

[1] Istituto Nazionale di Fisica Nucleare, Sezione di Roma "Tor Vergata", Rome, Italy
[2] Dipartimento di Fisica, Università di Roma "Tor Vergata", Rome, Italy
[3] Istituto Nazionale di Fisica Nucleare, Sezione di Roma "La Sapienza", Rome, Italy
[4] Dipartimento di Fisica, Università di Roma "La Sapienza", Rome, Italy
[5] Laboratorio Nazionali del Gran Sasso, Istituto Nazionale di Fisica Nucleare, Assergi (AQ), Italy
[6] Institute for Nuclear Research, National Academy of Sciences of Ukraine, Kyiv
[7] National Science Center "Kharkov Institute of Physics and Technology", Kharkiv
[8] Department of Physics, University of Jyväskylä, Jyväskylä, Finland

Double-beta (2β) decay is a process of transformation of a nucleus (A, Z) either to (A, Z + 2) with simultaneous emission of two electrons ($2\beta^-$ decay) or to (A,Z-2) through one of the following ways: emission of two positrons ($2\beta^+$), capture of electron and emission of positron ($\varepsilon\beta^+$), or double-electron capture (2ε) [1]. The two-neutrino (2ν) double β decay, in which two (anti)neutrinos are also emitted, is allowed in the standard model (SM) and registered for 13 nuclei; however, being a second-order process in the weak interactions, it is characterized by very long half-lives in the range of 10^{18}-10^{24} yr. Neutrinoless (0ν) double β decay is predicted by many SM extensions but not registered yet, however, with positive claim for ^{76}Ge [2] which is not confirmed by other experiments.

^{96}Ru is one of the only six isotopes where decay with emission of two positrons is allowed thanks to the high energy release of 2714.51 keV. It also has a quite large natural abundance of 5.54 %. Moreover, in the case of the capture of two electrons from the K and L shells or both from the L shell, the decay energies are close to the energy of the excited levels of ^{96}Mo that could give rise to a resonant enhancement of the process by few orders of magnitude [3].

An experiment to search for double β decay processes in ^{96}Ru and ^{104}Ru, which are accompanied by γ rays, has been realized in the underground Gran Sasso National Laboratories of the INFN (Italy). Ruthenium samples with masses of ≈ 0.5 - 0.7 kg were measured with the help of ultralow-background high-purity Ge γ ray spectrometry. After 2162 h of data taking, the samples were deeply purified to reduce the internal contamination by ^{40}K. The last part of the data has been accumulated over 5479 h with the Ru sample of 719.5 g in the GeMulti set-up with 4 HPGe detectors 225 cm^3 each. Comparison of the spectra measured with the initial Ru, purified Ru and background is given in Figure. New improved half-life limits on $2\beta^+/\varepsilon\beta^+/2\varepsilon$ processes in ^{96}Ru have been established on the level of 10^{20} yr, few times better than in our previous measurements [4] and in a recent experiment by other group in the HADES underground laboratory [5]. Various 2β2ν and 2β0ν half-lives of ^{96}Ru have been estimated in the QRPA framework. In addition, the $T_{1/2}$ limit for $2\beta^-$ transitions of ^{104}Ru to the first excited state of ^{104}Pd has been set as 6.5×10^{20} yr. The results are published in [6].

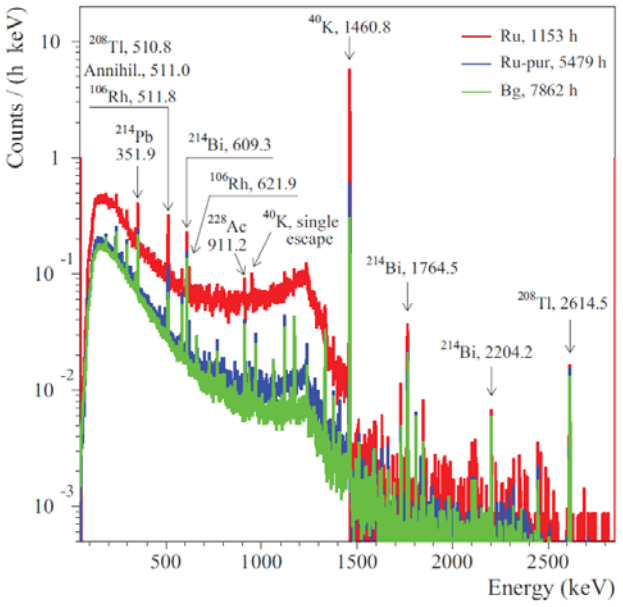

The energy spectra accumulated with the initial Ru sample over 1153 h (Ru) and with the purified Ru over 5479 h (Ru-pur) in comparison with the background (Bg) of the GeMulti ultra-low background HPGe γ spectrometer measured over 7862 h. The energies of γ lines are in keV.

1. J.D. Vergados *et al.*, Rep. Prog. Phys. **75**, 106301 (2012).
2. H.V. Klapdor-Kleingrothaus *et al.*, Mod. Phys. Lett. A **21**, 1547 (2006).
3. M.I. Krivoruchenko *et al.*, Nucl. Phys. A **859**, 140 (2011).
4. P. Belli *et al.*, Eur. Phys. J. A **42**, 171 (2009).
5. E. Andreotti *et al.*, Appl. Radiat. Isot. **70**, 1985 (2012).
6. P. Belli *et al.*, Phys. Rev. C **87**, 034607 (2013).

FIRST SEARCH FOR DOUBLE-β DECAY OF ^{184}Os AND ^{192}Os

P. Belli[1], R. Bernabei[1,2], F. Cappella[3,4], R. Cerulli[5], F. A. Danevich[6], S. d'Angelo[1,2], A. Di Marco[2], A. Incicchitti[3], G. P. Kovtun[7], N. G. Kovtun[7], M. Laubenstein[5], D. V. Poda[6], O. G. Polischuk[3,6], A. P. Shcherban[7], V. I. Tretyak[6]

[1] *Istituto Nazionale di Fisica Nucleare, Sezione di Roma "Tor Vergata", Rome, Italy*
[2] *Dipartimento di Fisica, Università di Roma "Tor Vergata", Rome, Italy*
[3] *Istituto Nazionale di Fisica Nucleare, Sezione di Roma "La Sapienza", Rome, Italy*
[4] *Dipartimento di Fisica, Università di Roma "La Sapienza", Rome, Italy*
[5] *Laboratorio Nazionali del Gran Sasso, Istituto Nazionale di Fisica Nucleare, Assergi (AQ), Italy*
[6] *Institute for Nuclear Research, National Academy of Sciences of Ukraine, Kyiv*
[7] *National Science Center "Kharkov Institute of Physics and Technology", Kharkiv*

Osmium contains two potentially double β active isotopes: ^{184}Os (decay energy $Q_{2\beta} = 1453.7(0.6)$ keV [1]; isotopic abundance $\delta = 0.02(1)$ % [2]; 2ε and $\varepsilon\beta^+$) and ^{192}Os ($Q_{2\beta} = 412.4(2.9)$ keV [3]; $\delta = 40.78(19)$ % [2]; $2\beta^-$). There is also a possibility of a resonant enhancement of the 0ν double-electron capture in ^{184}Os to a few excited levels of ^{184}W. The most promising of them is the level $(0)^+$ 1322.2 keV [4].

An experiment to search for double β decay of osmium has been realized for the first time with the help of an ultra-low background HPGe γ detector GeCris (with a volume of 465 cm^3) at the underground Gran Sasso National Laboratories of the INFN (Italy). After 2741 h of data taking with a 173 g ultra-pure (more than 99.999 % purity grade [5]) osmium sample, limits on double β processes in ^{184}Os have been established at the level of $T_{1/2} \sim 10^{14}$- 10^{17} y (see Table). Possible resonant double-electron captures in ^{184}Os were searched for with a sensitivity of $T_{1/2} \sim 10^{16}$ y. A half-life limit $T_{1/2} \geq 5.3 \cdot 10^{19}$ y was set for the double β decay of ^{192}Os to the first excited level of ^{192}Pt.

Half-life limits on 2β processes in ^{184}Os and ^{192}Os

Decay channel ^{184}Os→^{184}W	Level of daughter nucleus (keV)	Exp. limit, $T_{1/2}$ (yr), 90 % C.L.
$(2\nu + 0\nu)\ \varepsilon\beta^+$	g.s.	$\geq 2.5 \cdot 10^{16}$
$(2\nu + 0\nu)\ \varepsilon\beta^+$	2^+ (111.2)	$\geq 2.5 \cdot 10^{16}$
$2\nu 2K$	2^+ (903.3)	$\geq 3.2 \cdot 10^{16}$
	0^+ (1002.5)	$\geq 3.8 \cdot 10^{17}$
$0\nu 2K$	g.s.	$\geq 2.0 \cdot 10^{17}$
$0\nu 2\varepsilon$	2^+ (903.3)	$\geq 2.8 \cdot 10^{16}$
	0^+ (1002.5)	$\geq 3.5 \cdot 10^{17}$
Resonant $0\nu KL$	$(0)^+$ (1322.2)	$\geq 2.8 \cdot 10^{16}$
^{192}Os→^{192}Pt $(2\nu + 0\nu)\ 2\beta^-$	2^+ (316.5)	$\geq 5.3 \cdot 10^{19}$

The radiopurity of the osmium sample has been investigated and radionuclides ^{137}Cs, ^{185}Os and ^{207}Bi were detected in the sample, while activities of ^{40}K, ^{60}Co, ^{226}Ra and ^{232}Th were limited at the ≈ mBq/kg level. The energy spectra of accumulated data are presented in Figure.

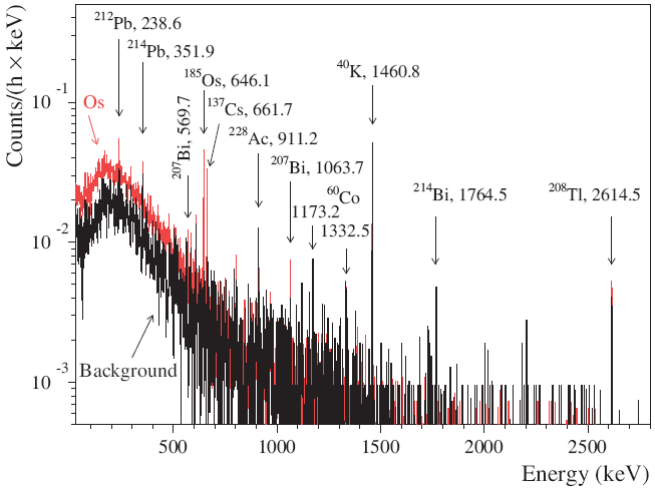

Energy spectra measured with the ultra-low background HPGe γ spectrometer with the osmium sample over 2741 h (Os) and without the sample over 1046 h (Background). The energies of the γ lines are in keV.

The results of this work are published in [6].

1. C. Smorra *et al.*, Phys. Rev. C **86**, 044604 (2012).
2. M. Berglund and M.E. Wieser, Pure Appl. Chem. **83**, 397 (2011).
3. G. Audi, A.H. Wapstra, and C. Thibault, Nucl. Phys. A **729**, 337 (2003).
4. M.I. Krivoruchenko *et al.*, Nucl. Phys. A **859**, 140 (2011).
5. V.M. Azhazha, G.P. Kovtun, and G.F. Tihinsky, Metallofiz. Noveishie Tekhnol. **22,** 21 (2000) (in Russian).
6. P. Belli *et al.*, Eur. Phys. J. A **49**, 24 (2013).

NEW SEARCH FOR CORRELATED e^+e^- PAIRS IN THE α DECAY OF ^{241}Am

R. Bernabei[1,2], P. Belli[1,2], F. Cappella[3,4], V. Caracciolo[5], S. Castellano[5], R. Cerulli[5], C. J. Dai[6], A. D'Angelo[3,4], A. Di Marco[1,2], H. L. He[6], A. Incicchitti[3,4], M. Laubenstein[5], X. H. Ma[6], F. Montecchia[1,7], X. D. Sheng[6], V. I. Tretyak[8], R. G. Wang[6], Z. P. Ye[6,9]

[1] Istituto Nazionale di Fisica Nucleare, Sezione di Roma "Tor Vergata", Rome, Italy
[2] Dipartimento di Fisica, Università di Roma "Tor Vergata", Rome, Italy
[3] Istituto Nazionale di Fisica Nucleare, Sezione di Roma "La Sapienza", Rome, Italy
[4] Dipartimento di Fisica, Università di Roma "La Sapienza", Rome, Italy
[5] Laboratorio Nazionali del Gran Sasso, Istituto Nazionale di Fisica Nucleare, Assergi (AQ), Italy
[6] Institute of High Energy Physics, Chinese Academy of Sciences, Beijing, China
[7] Dipartimento di Ingegneria Civile e Ingegneria Informatica, Università di Roma "Tor Vergata", Rome, Italy
[8] Institute for Nuclear Research, National Academy of Sciences of Ukraine, Kyiv
[9] University of Jing Gangshan, Jiangxi, China

It has long been experimentally known that emission of β particles in β decay sometimes is accompanied by γ quanta (this phenomenon is called internal bremsstrahlung, IB) or by e^+e^- pairs (internal pair production, IPP) [1]. For α decay, the IB process is also known (see e.g. [2] and refs. therein) while the IPP phenomenon was observed previously in 1973 - 1990 only in 3 works due to its extremely low probability of ~10^{-9} (see Table).

Intensities of e^+e^- emission in α decay of heavy nuclei (in 10^{-9} units)

Source	Experiment	Theory
^{210}Po	5.3 ± 1.7 [3]	4.4 [6]
^{239}Pu	7 ± 9 [3]	2.2 [6]
^{241}Am	3.1 ± 0.6 [4]	1.2 [4]
	2.15 ± 0.25 [3]	2.3 [6]
	1.8 ± 0.7 [5]	
	4.70 ± 0.63 [7]*	

* This work

In the present work, a new search for production of correlated e^+e^- pairs in the α decay of ^{241}Am has been carried out deep underground (3600 m w.e.) at the Gran Sasso National Laboratory of the INFN (Italy). It is worth noting that this is the first result on IPP obtained in an underground experiment that allows to suppress background from e^+e^- production by cosmic rays.

Some detectors of the DAMA/LIBRA set-up, built from 25 NaI(Tl) crystal scintillators with mass of 9.70 kg each, were used in pairs to detect double coincidences of events with energy around 511 keV in faced pairs of detectors (other NaI(Tl)'s served as anticoincidence shield). Six pairs of the detectors were used in the 1st run (1.29 d) and three pairs in the 2nd (2.63 d). Background was measured during 24.6 d. Activities of ^{241}Am sources were around 30 kBq. The results are shown in Figure.

Many side reactions were analyzed which could imitate the observed effect, but they cannot explain the measured excess (see details in [7]). A relative activity is $A(\alpha e^+e^-)/A(\alpha) = (4.70 \pm 0.63) \cdot 10^{-9}$ for the IPP with respect to the alpha decay of ^{241}Am. This value is of the same order of magnitude as previous determinations. In a conservative approach the upper limit $< 5.5 \cdot 10^{-9}$ (90 % C.L.) can be derived.

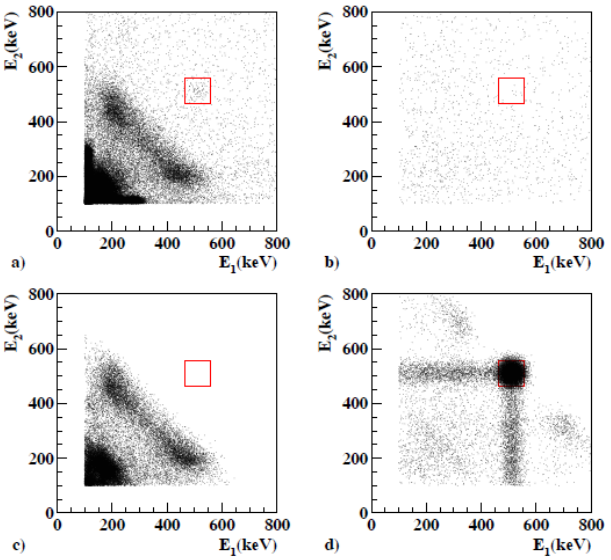

a) Experimental coincidence scatter plot of the faced NaI(Tl) detectors for 3.92 d; b) background data accumulated during 24.6 d (normalized to 3.92 d); c) simulation of ^{241}Am α decay in accordance with [8]; d) simulation of e^+ annihilation within the ^{241}Am sources.

The results are published in [7]. Further investigations are foreseen in the future.

1. K. Siegbahn (ed.), *Alpha-, Beta- and Gamma-Ray Spectroscopy*, North-Holland Publ. Comp., 1965, ch. 25(C) and 25(D).
2. S.P. Maydanyuk *et al.*, Nucl. Phys. A **823**, 38 (2009).
3. J. Stanicek *et al.*, Nucl. Instrum. Meth. B **17**, 462 (1986).
4. A. Ljubicic and B.A. Logan, Phys. Rev. C**7**, 1541 (1973).
5. T. Asanuma *et al.*, Phys. Lett. B **237**, 588 (1990).
6. K. Pisk *et al.*, Phys. Rev. C **17**, 739 (1983).
7. R. Bernabei *et al.*, Eur. Phys. J. A **49**, 64 (2013).
8. M.S. Basunia, Nucl. Data Sheets **107**, 2323 (2006).

DEVELOPMENT OF A Li_2MoO_4 SCINTILLATING BOLOMETER FOR LOW BACKGROUND PHYSICS

L. Cardani[1,2], N. Casali[3,4], S. Nagorny[3], L. Pattavina[3], G. Piperno[1,2], O. P. Barinova[5], J. W. Beeman[6], F. Bellini[1,2], F. A. Danevich[7], S. Di Domizio[8,9], L. Gironi[10,11], S. V. Kirsanova[5], F. Orio[2], G. Pessina[10,11], S. Pirro[3], C. Rusconi[11], C. Tomei[2], V. I. Tretyak[7], M. Vignati[2]

[1] *Dipartimento di Fisica, Università di Roma "La Sapienza", Rome, Italy*
[2] *Istituto Nazionale di Fisica Nucleare, Sezione di Roma, Rome, Italy*
[3] *Laboratorio Nazionali del Gran Sasso, Istituto Nazionale di Fisica Nucleare, Assergi (AQ), Italy*
[4] *Dipartimento di Scienze Fisiche e Chimiche, Universita degli studi dell'Aquila, Coppito (AQ), Italy*
[5] *D. I. Mendeleev University of Chemical Technology of Russia, Moscow, Russia*
[6] *Lawrence Berkeley National Laboratory, Berkeley, CA, USA*
[7] *Institute for Nuclear Research, National Academy of Sciences of Ukraine, Kyiv*
[8] *Dipartimento di Fisica, Universita di Genova, Genova, Italy*
[9] *Istituto Nazionale di Fisica Nucleare, Sezione di Genova, Genova, Italy*
[10] *Dipartimento di Fisica, Universita di Milano Bicocca, Milano, Italy*
[11] *Istituto Nazionale di Fisica Nucleare, Sezione di Milano Bicocca, Milano, Italy*

Lithium molybdate crystal was proposed and studied as scintillating bolometer to search for neutrinoless double beta ($0\nu2\beta$) decay of ^{100}Mo in [1]. Radioactive contamination of the material was estimated in [2] with the help of low background HPGe gamma spectrometry. ^{100}Mo is one of the favorite isotopes in searches for $0\nu2\beta$ decay because of very promising theoretical estimations of the decay probability (see [3] and references therein), high energy release $Q_{\beta\beta}$ = 3.034 MeV and quite big natural abundance δ = 9.82 % which can be relatively cheaply increased by centrifugal method.

A 33 g Li_2MoO_4 crystal was tested as scintillating bolometer for more than 400 h in a dilution refrigerator installed at the underground laboratory of Laboratori Nazionali del Gran Sasso (Italy). Low temperature scintillating properties were investigated by means of different alpha, beta (gamma) and neutron sources, and for the first time the light yield for different types of interacting particle is estimated. The detector shows great ability of tagging fast neutron interactions. We demonstrated the detector ability to identify neutrons from beta (gamma) and from alpha events. This feature is important for direct dark matter searches, where high energy neutrons may induce an unavoidable background in the region of interest.

Radioactive contamination of the crystal was tested in the low background run. The light versus heat signals scatter plot for the 344 h low background measurement with the Li_2MoO_4 crystal is presented in Figure. The radiopurity of the detector was estimated to be on the level < 0.09 mBq/kg for ^{238}U and < 0.11 mBq/kg for ^{232}Th. Contamination of the crystal by ^{210}Po is 0.729 ± 0.016 mBq/kg.

The radiopurity level and the scintillation properties make the studied compound a good candidate for the search of $0\nu2\beta$ decay in ^{100}Mo, also because of the large fraction of molybdenum with respect to the total mass of the molecule (55 %).

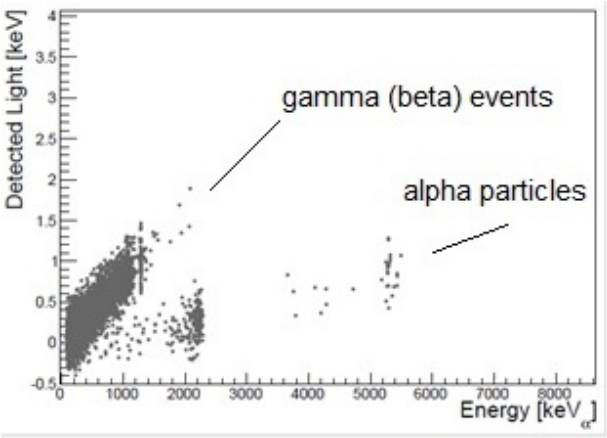

Light versus heat signals scatter plot for the 344 h low background measurement with 33 g Li_2MoO_4 scintillating bolometer. Gamma (beta) events are clearly separated from alpha particles. The alpha events with the energy up to 2.3 MeV are due to the samarium source used for calibration, while the alpha events at ≈ 5.4 MeV are due to contamination of the crystal by ^{210}Po.

The results of this work are published in [4].

1. O.P. Barinova *et al*., Nucl. Instrum. Meth. A **613**, 54 (2010).
2. O.P. Barinova *et al*., Nucl. Instrum. Meth. A **607**, 573 (2009).
3. J.D. Vergados, H. Ejiri and F. Šimkovic, Rep. Prog. Phys. **75**, 106301 (2012).
4. L. Cardani *et al*., JINST **8**, P10002 (2013).

OPTICAL, LUMINESCENCE AND THERMAL PROPERTIES OF RADIOPURE $ZnMoO_4$ CRYSTALS USED IN SCINTILLATING BOLOMETERS FOR DOUBLE BETA DECAY SEARCH

D.M. Chernyak [1,2], F.A. Danevich [1], V.Ya.Degoda [3], I.M.Dmitruk [3], F.Ferri [4], E.N.Galashov [5], A.Giuliani [2,4,6], I.M.Ivanov [5], V.V.Kobychev [1], M.Mancuso [2,4], S.Marnieros [2,4], V.M. Mokina [1], C.Nones [7], E.Olivieri [2], G.Pessina [6], C.Rusconi [4,6], V.N.Shlegel [5], O.P.Stanovyi [3], M.Tenconi [2], V.I.Tretyak [1], I.A.Tupitsyna [8]

[1] Institute for Nuclear Research, National Academy of Sciences of Ukraine, Kyiv
[2] Centre de Sciences Nucléaires et de Sciences de la Matière, Orsay, France
[3] Kyiv National Taras Shevchenko University, Kyiv, Ukraine
[4] Dipartimento di Scienza e Alta Tecnologia dell'Università dell'Insubria, Como, Italy
[5] Nikolaev Institute of Inorganic Chemistry, Novosibirsk, Russia
[6] Sezione INFN di Milano-Bicocca, Italy
[7] Service de Physiquedes Particules, CEA-Saclay, Gif sur Yvette, France
[8] Institute of Scintillation Materials, National Academy of Sciences of Ukraine, Kharkiv

Zinc molybdate ($ZnMoO_4$) crystals are an excellent candidate material to fabricate scintillating bolometers for the study of neutrinoless double beta decay of ^{100}Mo [1-3], provided that the crystal quality meets strict optical, thermal and radiopurity requirements. We have performed characterization of improved crystalline samples grown by the low-thermal-gradient Czochralski technique.

Transmittance measurements confirm significant improvement of the material with respect to previously developed samples (see Figure).

Luminescence properties (emission spectra, dependence of intensity on temperature, thermally stimulated luminescence and phosphorescence) have been studied under X ray excitation from liquid-helium to room temperature. The studied sample shows intensive thermo stimulated luminescence at ≈ 75 K and intensive phosphorescence after irradiation of the sample at a temperature of 8 K. Both the phenomena indicate the presence of defects and impurities in the crystal. This shows that there are still margins of improvement of the material quality.

The index of refraction was measured in the wavelength interval 406-655 nm. The crystal was found to be biaxial with refractive indexes in the range of 1.87–2.01.

Samples of $ZnMoO_4$ crystals with masses of 5.07 g and 23.8 g were operated as scintillating bolometers at temperatures below 30 mK, with simultaneous detection of scintillation and heat signals, confirming an excellent alpha/beta rejection power. Radioactive contamination of the $ZnMoO_4$ crystal was estimated by using data of cryogenic measurements. It confirms the improvement of $ZnMoO_4$ crystal radiopurity as a result of purification performed with the aim to enhance the optical quality of the material.

The light collection from $ZnMoO_4$ scintillators was Monte Carlo simulated, analysing different crystal size, shape and surface properties and different photodetector sizes. The simulations show the advantages of hexagonal (or at least octahedral) crystal shape in comparison to cylindrical. Scintillators surfaces should be diffused to provide better light collection and uniformity.

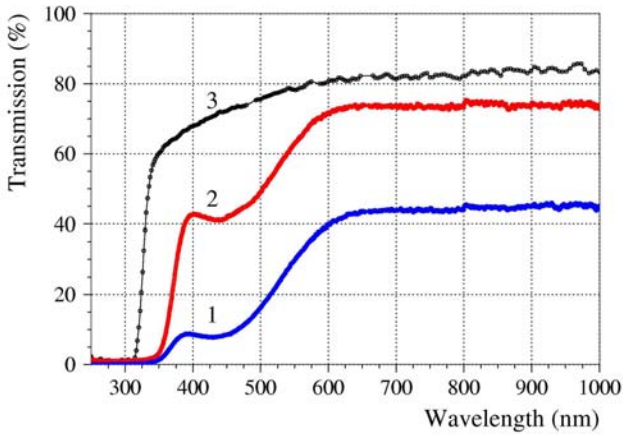

Optical transmission curve of the improved $ZnMoO_4$ crystal of thickness 5 mm developed in the present work (3). Data for $ZnMoO_4$ samples produced in [4] (1) and in [5] (2) are given for comparison.

A paper describing the results of this work is published in [6].

1. L. Gironi *et al*., J. of Instrumentation **5**, P11007, 12 p. (2010).
2. J.W.Beeman et al.,Physics Letters B 710, 318 (2012).
3. J.W.Beeman et al.,Astroparticle Physics **35**, 813 (2012).
4. L.I. Ivleva *et al*., Crystallog. Rep. **53**, 1087 (2008).
5. L.L. Nagornaya *et al*., IEEE Trans. Nucl. Sci. **56**, 2513 (2009).
1. D.M. Chernyak *et al*., Nucl. Instr. Meth. A **729**, 856 (2013).

ON THE POTENTIALITY OF THE $ZnWO_4$ ANISOTROPIC DETECTORS TO MEASURE THE DIRECTIONALITY OF DARK MATTER

F. Cappella[1], R. Bernabei[2,3], P. Belli[3], V. Caracciolo[4], R. Cerulli[4], F. A. Danevich[5], A. d'Angelo[1,6], A. Di Marco[2,3], A. Incicchitti[6], D. V. Poda[5], V. I. Tretyak[5]

[1] Dipartimento di Fisica, Universita di Roma "La Sapienza", Rome, Italy
[2] Dipartimento di Fisica, Universita di Roma "Tor Vergata", Rome, Italy
[3] Istituto Nazionale di Fisica Nucleare, Sezione di Roma "Tor Vergata", Rome, Italy
[4] Laboratorio Nazionali del Gran Sasso, Istituto Nazionale di Fisica Nucleare, Assergi (AQ), Italy
[5] Institute for Nuclear Research, National Academy of Sciences of Ukraine, Kyiv
[6] Istituto Nazionale di Fisica Nucleare, Sezione di Roma "Tor Vergata", Rome, Italy

Astrophysical observations have given evidence for the presence of Dark Matter (DM) on all astrophysical scales and many arguments have also suggested that a large fraction of the DM should be in form of relic particles. There is a range of experiments aimed to detect nuclear recoils produced by dark matter interaction with matter. In the direct search for DM, a positive model independent result has been obtained at about 9σ C.L. for the presence of DM particles in the galactic halo by the DAMA/NaI and DAMA/LIBRA experiments [1 - 3] exploiting the DM annual modulation signature [4, 5] in highly radio-pure NaI(Tl) target over 13 annual cycles.

A different possible approach is the directionality [6], in principle effective just for those DM candidate particles able to induce nuclear recoils. In the anisotropic scintillators the light output and the pulse shape for heavy particles (p, α, nuclear recoils) depend on the direction with respect to the crystal axes; the response to γ/β radiation is isotropic instead. This feature offers the possibility to study the directionality approach, which is applicable in the particular case of those DM candidate particles inducing just nuclear recoils.

Among the anisotropic scintillators, the $ZnWO_4$ has unique features, which make it an excellent candidate for this type of research. A possibility to use the dependence of $ZnWO_4$ scintillation pulse shape on direction of irradiation by high ionizing particles to search for diurnal modulation of DM particles inducing recoils was pointed out for the first time in [7]. If an experiment performed at a latitude similar to, e.g., the latitude of the Gran Sasso National Laboratory (42°27′ N latitude) at a certain time of the day the DM particles come mainly from the top, while 12 h later they come near the horizon and from North (see Figure). Thus, if a scintillator with an anisotropic light yield is considered (it should be noted $ZnWO_4$ is a strongly anisotropic scintillator), a suitable arrangement for such an experiment is to install the setup with the detectors' axis having the largest quenching factor value in the vertical direction, and with the axis having the smallest quenching factor value towards the North. In this way, the behaviour of the energy spectrum of the DM induced nuclear recoils diurnally varies and, therefore, also the counting rate. A similar approach can be repeated also when considering the anisotropic response of the scintillation decay kinetics (again it is the case of $ZnWO_4$).

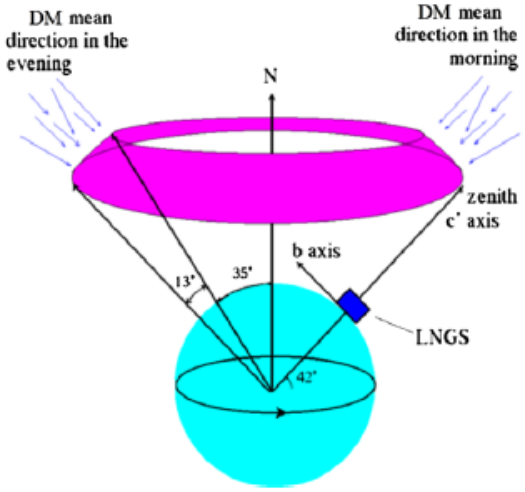

Schematic representation of the experimental approach to detect direction of recoils after interaction of dark matter particles. The detector is considered here as placed at the Gran Sasso laboratory (LNGS) with the axis in the vertical direction and another axis pointing to the North. The area in the sky from which the dark matter particles are preferentially expected is highlighted [8].

To conclude, an experiment with $ZnWO_4$ scintillators could represent a first realistic attempt to investigate the directionality of dark matter. The results of this work are published in [9].

1. R. Bernabei *et al.*, Riv. Nuovo Cimento **26**, 1 (2003).
2. R. Bernabei *et al.*, Eur. Phys. J. C **56**, 333 (2008).
3. R. Bernabei *et al.*, Eur. Phys. J. C **67**, 39 (2010).
4. K.A. Drukier *et al.*, Phys. Rev. D **33**, 3495 (1986).
5. K. Freese *et al.*, Rev. Mod. Phys. **85**, 1561 (2013).
6. D.N. Spergel, Phys. Rev. D **37**, 1353 (1988).
7. F.A. Danevich *et al.*, Nucl. Instr. Meth. A **544**, 553 (2005).
8. R. Bernabei *et al.*, Eur. Phys. J. C **28**, 203 (2003).
9. F. Capella *et al.*, Eur. Phys. J. C **73**, 2276 (2013).

RADIOACTIVE CONTAMINATION OF ^{7}LiI(Eu) CRYSTAL SCINTILLATORS

P. Belli[1], R. Bernabei[1,2], S. V. Budakovsky[3], F. Capella[4,5], R. Cerulli[6], F. A. Danevich[7], S. d'Angelo[1,2], A. Incicchitti[4,5], M. Laubenstein[6], D. V. Poda[7], O. G. Polischuk[4,7], V. I. Tretyak[7]

[1] Istituto Nazionale di Fisica Nucleare, Sezione di Roma "Tor Vergata", Rome, Italy
[2] Dipartimento di Fisica, Università di Roma "Tor Vergata", Rome, Italy
[3] Institute for Scintillation Materials, National Academy of Sciences of Ukraine, Kharkiv
[4] Istituto Nazionale di Fisica Nucleare, Sezione di Roma "La Sapienza", Rome, Italy
[5] Dipartimento di Fisica, Università di Roma "La Sapienza", Rome, Italy
[6] Laboratorio Nazionali del Gran Sasso, Istituto Nazionale di Fisica Nucleare, Assergi (AQ), Italy
[7] Institute for Nuclear Research, National Academy of Sciences of Ukraine, Kyiv

The europium doped lithium iodide (LiI(Eu)) scintillator is known since about 70 years [1]. Single LiI(Eu) crystals, in particular enriched in ^{6}Li, are used for a long time for efficient neutron detection (see e.g. Refs. [2 - 5]).

Recently, LiI(Eu) scintillators were proposed to search for the resonant capture of axions possibly emitted in the solar pp-cycle by excited ^{7}Li [6]. Taking into account the high natural isotopic abundance of ^{7}Li (92.41 %), different Li-containing targets have been already used in several solar axions experiments (see Ref. [7] and references therein). In order to search for solar axions, one of the main requirements for the targets is the achievement of a level of radioactive contamination as low as possible. The radiopurity plays an important role also in other applications of scintillation detectors, including neutron detection.

Two ^{7}LiI(Eu) single crystals (∅20 × 20 mm, with masses of 26 g each one) grown by the Bridgman–Stockbarger method in the Institute of Scintillation Materials (Kharkiv, Ukraine) were used in the present study. The enrichment of the lithium used for the crystals growth in ^{7}Li was 99.9 %. The radioactive contamination of the samples was tested by using two different low background techniques: (1) as a scintillator in a low background set-up at sea level; (2) with the help of ultra-low background HPGe gamma spectrometry deep underground.

The energy spectrum measured with the ^{7}LiI(Eu) scintillation detector in the low background set-up at the sea level in the Institute for Nuclear Research (Kyiv, Ukraine) is presented in Figure. There are no peculiarities in the spectrum which could be interpreted as internal contamination of the scintillator. Therefore, we have estimated only limits on radioactive contamination of the detector. Besides, the scintillators were measured with the help of ultra-low background γ spectrometry deep underground in the Gran Sasso National Laboratories of the INFN (Italy). Finally, no radioactivity was detected in the detectors on the level of sensitivity 1 mBq/kg for ^{226}Ra, ^{228}Th, ^{210}Po, 10 mBq/kg for ^{60}Co, ^{137}Cs and ^{152,154}Eu, 0.1 – 1 Bq/kg for ^{40}K, ^{90}Sr and ^{210}Pb. This makes the detector promising for low counting applications, including solar ^{7}Li axions search.

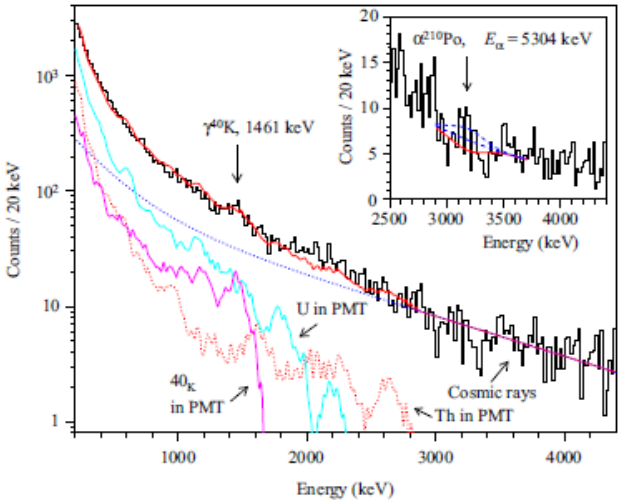

The energy spectrum measured with the ^{7}LiI(Eu) scintillation detector over 126 h in the low background set-up at the sea level. The fit of the spectrum in the range (220 - 4400) keV is shown together with the main components of the background. (Inset) High energy part of the spectrum where α peak of ^{210}Po is expected. Fit of the data is shown by the solid line, while the exponential background model and α peak of ^{210}Po excluded at 90% confidence level are shown by the dashed lines.

The results of this work are published in [8].

1. J. Schenck, Nature **171**, 518 (1953).
2. R.B. Murray, Nucl. Instr. Meth. **2**, 237 (1958).
3. D.R. Johnson, J.H. Thorngate, and P.T. Perdue, Nucl. Instr. Meth. **75**, 61 (1969).
4. N.E. Hertel and J.W. Davidson, Nucl. Instr. Meth. A **238**, 509 (1985).
5. A. Syntfeld *et al.*, IEEE Trans. Nucl. Sci. **NS-52**, 3151 (2005).
6. P. Belli *et al.*, Nucl. Phys. A **806**, 388 (2008).
7. P. Belli *et al.*, Phys. Lett. B **711**, 41 (2012).
8. P. Belli *et al.*, Nucl. Instr. Meth. A **704**, 40 (2013).

NEW LIMITS ON HEAVY STERILE NEUTRINO MIXING IN ^{8}B DECAY OBTAINED WITH THE BOREXINO DETECTOR

V. V. Kobychev
(on behalf of the Borexino Collaboration)

Institute for Nuclear Research, National Academy of Sciences of Ukraine, Kyiv

If heavy sterile neutrinos with mass $m_{\nu_H} \geq 2m_e$ are produced in the Sun via the decay $^8\mathrm{B} \rightarrow {}^8\mathrm{Be} + e^+ + \nu_H$ in a side branch of the pp chain, they would undergo the observable decay into an electron, a positron and a light neutrino $\nu_H \rightarrow \nu_L + e^+ + e^-$. In the present work Borexino data were used to set a bound on the existence of such decays. Thanks to the uniquely low radioactive background and large target mass of the Borexino detector [1], new limits on the mixing parameter $|U_{eH}|^2$ of a hypothetical massive neutrino to the electron neutrino have been set. We constrain the mixing of a heavy neutrino with mass between 1.5 and 14 MeV to be $|U_{eH}|^2 \leq (10^{-3} - 4 \cdot 10^{-6})$, respectively. These limits are ten- to 1000-fold stronger than those obtained by experiments searching for $\nu_H \rightarrow \nu_L + e^+ + e^-$ decays at nuclear reactors and 1.5 - 4 times stronger than those inferred from decays of $\pi^{\pm} \rightarrow \nu_H + e^{\pm}$ in accelerators (see Figure).

The work has been published in [2].

1. G. Alimonti *et al.* (Borexino Collaboration), Nucl. Instrum. Methods Phys. Res. A **600**, 568 (2009).
2. G. Bellini *et al.* (Borexino Collaboration), Phys. Rev. D **88**, 072010 (2013).
3. C. Hagner, M. Altmann, F. Feilitzsch *et al.*, Phys. Rev. D **52**, 1343 (1995).
4. D.I. Britton *et al.*, Phys. Rev. D **46**, R885 (1992).

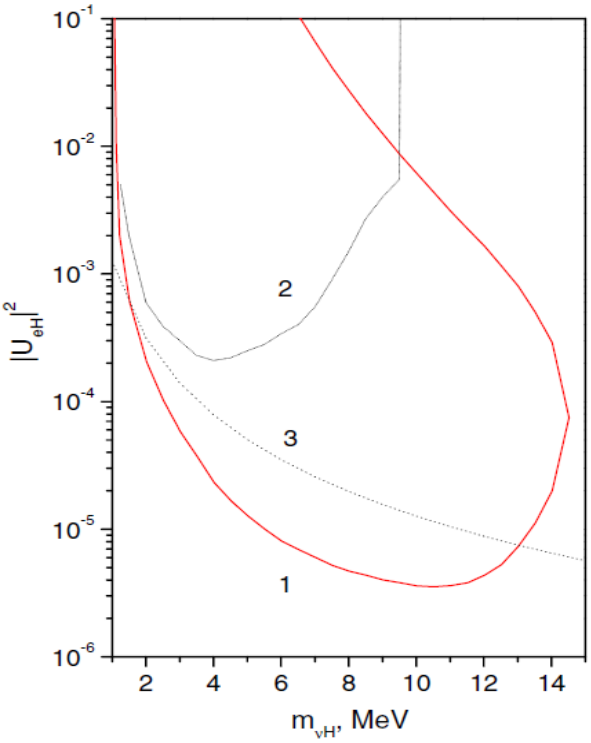

Limits on the mixing parameter $|U_{eH}|^2$ as a function of neutrino mass m_ν (90 % C.L.): *1* - present work excludes values of $|U_{eH}|^2$ and m_ν inside region 1; *2* - upper limits from reactor experiments on the search for the decay of $\nu_H \rightarrow \nu_L + e^+ + e^-$ due to W-exchange mode [3]; 3 - upper limits from $\pi^{\pm} \rightarrow \nu_H + e^{\pm}$ decay [4].

LIFETIME MEASUREMENTS OF ^{214}Po AND ^{212}Po WITH THE CTF LIQUID SCINTILLATOR DETECTOR AT LNGS

V. V. Kobychev
(on behalf of the Borexino Collaboration)

Institute for Nuclear Research, National Academy of Sciences of Ukraine, Kyiv

In the present work, we have studied the alpha decays of ^{214}Po into ^{210}Pb and of ^{212}Po into ^{208}Pb. The decays are tagged by the coincidence with the preceding β-decays from ^{214}Bi and ^{212}Bi, respectively. The ^{222}Rn, ^{232}Th, and ^{220}Rn sources used were sealed inside quartz vials and inserted in the Counting Test Facility (CTF) [1] of Borexino [2]. The CTF is a ≈ 1 ton liquid scintillator detector installed at the underground Gran Sasso National Laboratory in Italy. Thanks to extreme radio-purity of the CTF detector and to a long expertise in source preparation and insertion systems, new accurate measurements of the ^{214}Po and ^{212}Po lifetimes have been provided. We have found the following mean lifetimes:

^{214}Po: (236.00 ± 0.42(stat) ± 0.15(syst)) μs;

^{212}Po: (425.1 ± 0.9(stat) ± 1.2(syst)) ns.

Our results, obtained from data with signal-to-background ratio larger than 1000, reduce the overall uncertainties and are compatible with previous measurements (Figure).

The work has been published in [3].

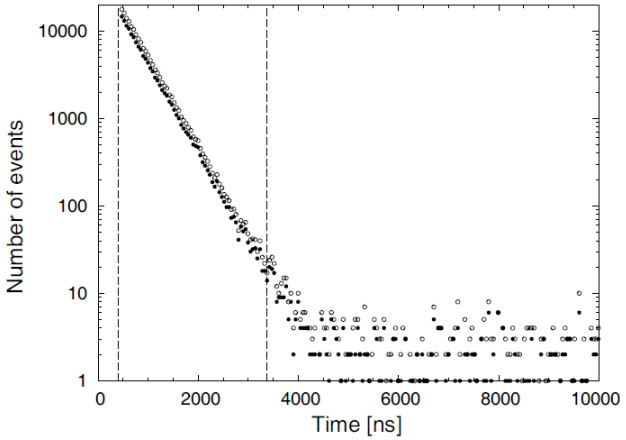

Data from one of the ^{212}Po sources with 1000 bins between 400 and 48000 ns are shown up to 10000 ns. Number of totally contained events as a function of the time difference t between the first (^{212}Bi) and the second (^{212}Po) decay. Filled (open) dots show data with (without) the energy cuts. Vertical lines delimit a seven-lifetime window.

1. G. Alimonti *et al.*, Nucl. Instrum. Methods A **406**, 411 (1998).
2. G. Alimonti *et al.* (Borexino Collaboration), Nucl. Instrum. Methods Phys. Res. A **600**, 568 (2009).
3. G. Bellini *et al.* (Borexino Collaboration), Eur. Phys. J. A **49**, 92 (2013).

COSMOGENIC BACKGROUNDS IN BOREXINO AT 3800 M WATER-EQUIVALENT DEPTH

V. V. Kobychev
(on behalf of the Borexino Collaboration)

Institute for Nuclear Research, National Academy of Sciences of Ukraine, Kyiv

The solar neutrino experiment Borexino [1], located in the Gran Sasso underground laboratories (see Figure), is in a unique position to study muon-induced backgrounds in an organic liquid scintillator. In this study, a large sample of cosmic muons is identified and tracked by a muon veto detector external to the liquid scintillator, and by the specific light patterns observed when muons cross the scintillator volume. Based on thermal neutron captures in the scintillator target of Borexino, a spallation neutron yield of muon-induced neutrons is found to be $Y_n = (3.10 \pm 0.11)\cdot 10^{-4}$ $n/(\mu\cdot(\mathrm{g/cm^2}))$. The distance profile between the reconstructed parent muon track and the neutron capture point has the average value $\lambda = (81.5 \pm 2.7)$ cm.

Additionally the yields of a number of cosmogenic radioisotopes are measured for ^{12}N, ^{12}B, ^{8}He, ^{9}C, ^{9}Li, ^{8}B, ^{6}He, ^{8}Li, ^{11}Be, ^{10}C and ^{11}C based on a simultaneous fit to energy and decay time distributions. Results of a corresponding analysis performed by the KamLAND collaboration for the Kamioka underground laboratory [2] are similar to our findings. All results are compared with Monte Carlo simulation predictions using the Fluka and Geant4 packages. General agreement between data and simulation is observed for the cosmogenic production yields with a few exceptions (^{12}B, ^{11}C, ^{8}Li for both codes and ^{8}B, ^{9}Li for Geant4 only) which show a significant deviation between data and Monte Carlo simulation predictions (the most prominent case being ^{11}C yield for which both codes return about 50 % lower values). The predicted μ-n distance profile and the neutron multiplicity distribution are found to be overall consistent with data. The simulated neutron yield of Fluka shows a deficit of ~20 %, while the result of the Geant4 simulation is in good agreement with the measured value.

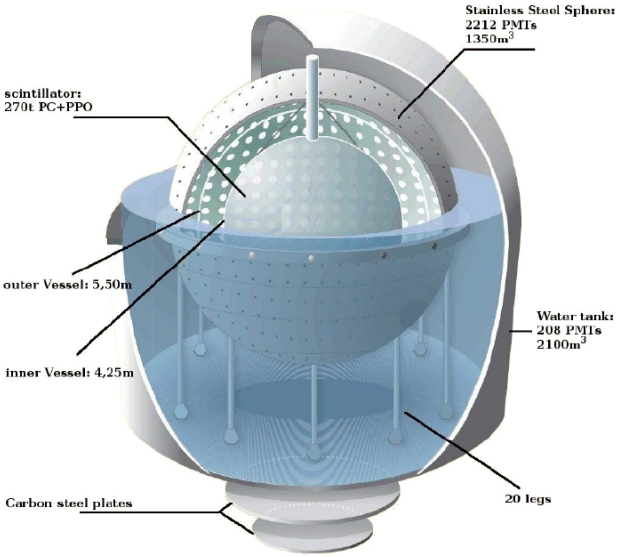

Sketch of the Borexino detector.

The results are not only essential to low-energy neutrino analyses, but are also of substantial interest for direct dark matter and 0ν2β searches at underground facilities.

The work has been published in [3].

1. G. Alimonti *et al.* (Borexino Collaboration), Nucl. Instrum. Methods Phys. Res. A **600**, 568 (2009).
2. S. Abe *et al.* (KamLAND collaboration), Phys. Rev. C **81**, 025807 (2010).
3. G. Bellini *et al.* (Borexino Collaboration), JCAP **08**, 049 (2013).

SIMULATION OF SECONDARY ELECTRON TRANSPORT IN THIN METAL AND FULLERITE FILMS

E. O. Petrenko[1], M. V. Makarets[2], V. M. Mikoushkin[3], V. M. Pugach[1]

[1] Institute for Nuclear Research, National Academy of Sciences of Ukraine, Kyiv
[2] Taras Shevchenko National University, Kyiv
[3] Ioffe Physical-Technical Institute, Russian Academy of Sciences, St. Petersburg, Russia

Studying primary and secondary electron transport in metal films and in fullerites is important both for improving the efficiency of strip detectors [1] and for better understanding the mechanisms of fullerite modification and pixel formation Figure.

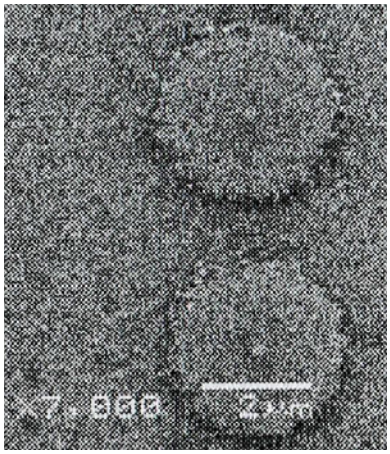

Carbon clusters formed in the 300 nm fullerite film on the Si-substrate by a nanoprobe with energy 15 keV [4]. Cluster radius is about 1.5 μ.

Program package to simulate the motion of secondary electrons in solids under electron irradiation was developed [2, 3]. At the beginning, the model was tested in the photoionization of nickel film thickness of 50 μ [5], where the calculations qualitatively coincide with the experimental. The minimum yield of the photoelectrons in the energy range 8 - 10 keV is due to the presence of nickel atomic levels with energy 8.3 keV. Further, debugged model is applied to simulate the experiment on the formation of polymerized fullerite clusters by 15 keV electron beam. Fullerite layer 200 ÷ 400 nm was deposited on a silicon substrate. It was obtained that simulated cluster radius in two and a half times less than the experimental (1.5 mm) [4], where changes in the internal structure of fullerite affects on the secondary electrons transport. In the polymerization field of fullerene molecules, electrons with higher atomic shells are not involved in collective oscillations, i.e. no plasmons formation. The gradual reduction of the cross-sections of collective processes at the three times allows obtaining experimental cluster radius. Also, secondary electrons tracks analysis shows that the indicated fullerite thickness is transparent to high-energy electrons, and the clusters forms by electrons diffusion which are reflected from silicon back to fullerite.

It is shown a new mechanism for secondary electrons distribution due to gradual changes in the medium properties, through a decrease influence of inelastic collisions.

1. M.V. Makarets, E.O. Petrenko, and V.M. Pugatch, Journal of Nuclear Physics and Atomic Energy. **13,** 146 (2012).
2. N.V. Makarets, Yu.I. Prylutskyy, O.V. Zaloyilo *et al.*, Mol. Cryst. & Liquid Cryst. **426**, 171 (2005).
3. E.O. Petrenko, N.V. Makarets, and V.M. Mikoushkin, Fullerenes, Nanotubes and Carbon Nanostructures. **20(04-07)**, 378 (2012).
4. V.N. Nevedomsky, V.M. Mikoushkin, A.V. Nashekin *et al.*, Nanotubes and Carbon nanostructures. **16(5-6)**, 682 (2008).
5. C. Thomas and G. Rehm, Short *Report on New XBPM tested on B16*. Doc No: TDI-DIA-OPT-0011, July 1, 2011.

OBSERVATION OF THE DECAY $B^+_c \to J/\psi K^+ K^- \pi^+$ IN LHCb EXPERIMENT

V. M. Iakovenko[1,2]

[1] *for LHCb Collaboration*
[2] *Institute for Nuclear Research, National Academy of Sciences of Ukraine, Kyiv*

The B^+_c meson is of special interest, as it is the only meson consisting of two heavy quarks of different flavours. It is the heaviest meson that decays through weak interactions, with either the c or anti-b quark decaying or through their weak annihilation [1]. Although the B^+_c meson was discovered in 1998 by the CDF collaboration [2], relatively few decay channels were observed prior to LHCb measurements [3].

In the factorisation approximation, the $B^+_c \to J/\psi K^+ K^- \pi^+$ decay is characterised by the form factors of the $B^+_c \to J/\psi W^+$ transition and the spectral functions for the subsequent hadronisation of the virtual W^+ boson into light hadrons. A measurement of the branching fractions of exclusive B^+_c meson decays into final states consisting of charmonium and light hadrons allows the validity of the factorisation theorem to be tested. The predictions for the ratio of branching fractions B ($B^+_c \to J/\psi K^+ K^- \pi^+$)/B ($B^+_c \to J/\psi \pi^+$) are 0.49 and 0.47 [4].

The first observation of the decay $B^+_c \to J/\psi K^+ K^- \pi^+$ and a measurement of B ($B^+_c \to J/\psi K^+ K^- \pi^+$)/B ($B^+_c \to J/\psi \pi^+$) are presented. The analysis is based on proton-proton (pp) collision data, corresponding to an integrated luminosity of 1 fb^{-1} at a centre-of-mass energy of 7 TeV and 2 fb^{-1} at 8TeV, collected with the LHCb detector.

Invariant mass distribution of $B^+_c \to J/\psi K^+ K^- \pi^+$ and $B^+_c \to J/\psi \pi^+$ are shown in Figure (*a*) and (*b*) respectively.

The decay $B^+_c \to J/\psi K^+ K^- \pi^+$ is observed for the first time, and a signal yield of 78 ± 14 is reported.

The significance, taking into account the systematic uncertainties due to the fit function, peak position and mass resolution in the default fit, is estimated to be 6.2 standard deviations.

Using the $B^+_c \to J/\psi \pi^+$ mode as a normalisation channel, the ratio of branching fractions is calculated as:

$$\frac{B(B_C^+ \to J/\psi K^+ K^- \pi^+)}{B(B_C^+ \to J/\psi \pi^+)} = \frac{N(B_C^+ \to J/\psi K^+ K^- \pi^+)}{N(B_C^+ \to J/\psi \pi^+)} \times \frac{\varepsilon(B_C^+ \to J/\psi \pi^+)}{\varepsilon(B_C^+ \to J/\psi K^+ K^- \pi^+)},$$

where N is the number of reconstructed decays obtained from the fit from Fig. 1. The ratio of branching fractions is measured to be

$$\frac{B(B_C^+ \to J/\psi K^+ K^- \pi^+)}{B(B_C^+ \to J/\psi \pi^+)} = 0.53 \pm 0.10 \pm 0.05,$$

where the first uncertainty is statistical and the second is systematic.

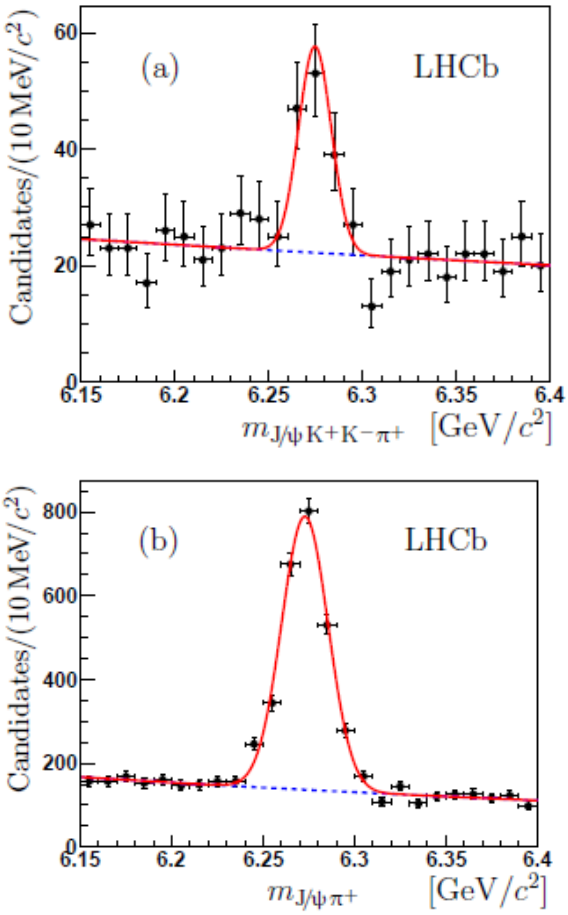

Mass distribution for selected (*a*) $B^+_c \to J/\psi K^+ K^- \pi^+$ and (*b*) $B^+_c \to J/\psi \pi^+$ candidates. The results of the fit is in solid line, background component – dashed.

The theoretical predictions for the branching fraction ratio of 0.49 and 0.47 [4] are found to be in good agreement with this measurement.

1. C.-H. Chang, and Y.-Q. Chen, Phys. Rev. **D49**, 3399 (1994).
2. CDF collaboration, F. Abe *et al.*, Phys. Rev. Lett. **81**, 2432 (1998).
3. LHCb collaboration, R. Aaij *et al.*, Phys. Rev. Lett. **108**, 251802 (2012).
4. A.V. Luchinsky, Production of K mesons in exclusive Bc decays, arXiv:1307.0953.

STUDY OF $B^0_s \to \mu^+\mu^-$ AND $B^0 \to \mu^+\mu^-$ DECAYS IN LHCb EXPERIMENT

V. M. Iakovenko[1,2]

[1] *for LHCb Collaboration*
[2] *Institute for Nuclear Research, National Academy of Sciences of Ukraine, Kyiv*

Studies of rare effects in B-physics provide a possibility to precision tests of the Standard Model (SM) and discover the evidences of New Physics (NP). Precise measurements of rare B decays are performed with the LHCb experiment at Large Hadron Collider. The LHCb detector [1] is a single-arm forward spectrometer at the Large Hadron Collider covering the pseudo-rapidity range $2 < \eta < 5$, designed for the study of particles containing *b* or *c* quarks.

One of the most promising channels for detecting signals of NP is the rare decay $B^0_s \to \mu^+\mu^-$, which originates in the SM from penguin and box topologies. Branching fraction measurements of these decays can test models with an extended Higgs sector.

Rare decays $B^0_s \to \mu^+\mu^-$ and $B^0 \to \mu^+\mu^-$ are highly suppressed in the SM, as they can occur only via helicity suppressed loop diagrams. Precise predictions of their branching fractions are provided in [2]:

$$\mathrm{B}(B^0_s \to \mu^+\mu^-) = (3.23 \pm 0.27) \cdot 10^{-9},$$

$$\mathrm{B}(B^0 \to \mu^+\mu^-) = (1.07 \pm 0.10) \cdot 10^{-10},$$

which make these modes powerful probes in the search for deviations from the SM, especially in models with a non-standard Higgs sector, which can give rise to higher branching fractions.

A search for the rare decays $B^0_s \to \mu^+\mu^-$ and $B^0 \to \mu^+\mu^-$ is performed using data collected in 2011 and 2012 with the LHCb. The data samples comprise 1.1 fb^{-1} of proton-proton collisions at $\sqrt{s}$ = 8 TeV and 1.0 fb^{-1} at $\sqrt{s}$ = 7 TeV. We observe an excess of $B^0_s \to \mu^+\mu^-$ candidates with respect to the background expectation. The probability that the background processes can produce the observed number of $B^0_s \to \mu^+\mu^-$ candidates or more is $5 \cdot 10^{-4}$ and corresponds to a statistical significance of 3.5 standard deviations. The value of the $B^0_s \to \mu^+\mu^-$ branching fraction obtained from the fit is

$$\mathrm{B}(B^0_s \to \mu^+\mu^-) = (3.2\ ^{+1.4}_{-1.2}\ (\mathrm{stat})^{+0.5}_{-0.3}\ (\mathrm{syst})) \cdot 10^{-9}.$$

This result is in agreement with the SM expectation [3]. The invariant mass distribution of the $B^0_s \to \mu^+\mu^-$ candidates with boosted decision tree (BDT, high level trigger variable) multivariate discriminant on kinematics and topology variables > 0.7 is shown in Figure.

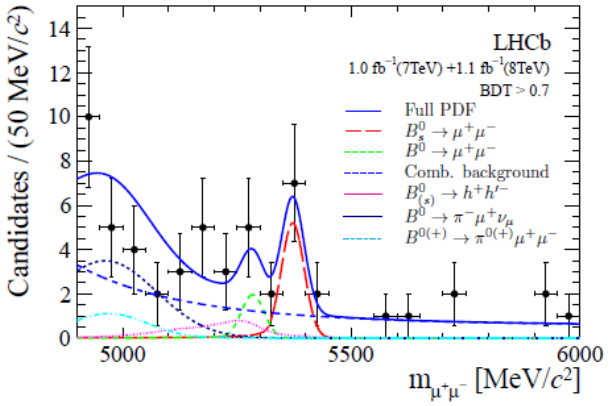

The invariant dimuon mass distribution for very signal-like $B^0_{(s)} \to \mu^+\mu^-$ candidates together with the signal and back-ground contributions included in the branching fraction fit.

The most powerful result on this decay comes from LHCb based on a combined analysis of 1.0 fb^{-1} of 2011 data and 1.0 fb^{-1} of 2012 data [4]. The measurement is based on a BDT and the invariant dimuon mass to separate signal and background and uses the decays $B \to J/\psi K^\pm$ and $B^0 \to K^\pm\pi^\pm$ to normalize the observed number of signal events.

In the case of $B^0 \to \mu^+\mu^-$ no significant excess over background has been seen by CDF, CMS and LHCb which have analyzed this decay. The most stringent upper limit has been observed by LHCb using 1.0 fb^{-1} of 2011 data and 1.1 fb^{-1} of 2012 data [33], resulting in

$$\mathrm{B}(B^0 \to \mu^+\mu^-) < 9.4 \cdot 10^{-10} @ 95\ \%\ \mathrm{C.L.}$$

1. A.A. Alves Jr. *et al.*, *LHCb collaboration,* JINST. 3 S08005 (2008).
2. J. Buras, J. Girrbach, D. Guadagnoli, and G. Isidori, Eur. Phys. J. **C72**, 14 (2012)., arXiv:1208.0934.
3. A.A. Alves Jr. *et al.*, *LHCb collaboration,* Phys. Rev. Lett. **108**, 231801 (2012).
4. R. Aaij *et al.* (LHCb collaboration), Phys. Rev. Lett. **110**, 021801 (2013), 1211.2674

MICRODETECTOR FOR BEAM MONITORING AND POSITIONING IN HADRON RADIOTHERAPY

A. O. Iliukhina[1,2], V. M. Pugatch[2], V. M. Iakovenko[2], O. S. Kovalchuk[2], D. I. Storozhyk[2]

[1] Taras Shevchenko National University, Kyiv
[2] Institute for Nuclear Research, National Academy of Sciences of Ukraine, Kyiv

Hadron radiotherapy is a hadron irradiation malignancies (protons, nuclei ^{12}C, ^{16}O etc.). The main advantage of this method is Bragg peak - the increase in energy loss immediately before the particles stop. To define the dose distribution, detector should have good precision of positioning and beam monitoring, as well as high radiation tolerance, since modern radiotherapy seek to reduce the beam size(thus increasing the intensity of the beam).

In 2014 High Energy Physics Department in KINR together with The National Center for Scientific Research (France) are planning the experiment «Towards in vivo dosimetry in ^{12}C therapy» in Heidelberg Ion Therapy center (Germany). The main aim of this project is measurement of depth-dose distribution when irradiated nuclei ^{12}C phantom with the energy of 150-300 MeV per nucleon. The metal strip detector is developed for this experiment (Figure).

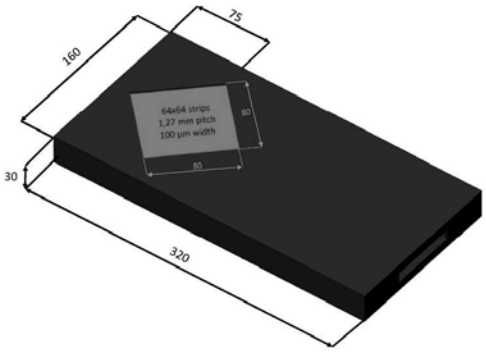

Metal-strip detector scheme
for hadron radiotherapy experiments.

The prototype of strip detector for monitoring the beam was made in HEP department (KINR). It consists of two perpendicular parts, each with 64 copper strips. Each strip diameter is 100 μm with 1.25 mm pitch. The principle of metal strip detector is secondary electron emission, which is initiated by incident particles. When this happens, a positive charge appears at the strip measured by the XDAS (X-ray data acquisition system).

Likewise experiment with ion ^{12}C at HIT, experiment with protons will take place in Nice in 2014 with 65 MeV proton beam energy. Using GEANT4 platform the simulation of strip detector and proton beam was made. Quark Gluon String model with Bertini-style cascade was used as physics model. The detector is located at the 10 cm distance from the source, which is 2 cm in diameter. Beam profile at the distance of 30 cm from the detector along beam direction was simulated. Thus, after passing strip detector, beam diameter is less than 4 cm, which is possible to use for online monitoring.

One part of the detector was tested with electron beam at KINR electron accelerator. The results are presented in the work. Intensity varied between 1 nA/cm^2 and 10 nA/cm^2. Because of signal dependence on intensity is linear, this detector is stable for intensity range per strip 0.8 - 8 nA/s.

Preliminary results:

precision of beam positioning is 1.25 mm, which is applicable in hadron radiotherapy;

high radiation tolerance (up to few MGy).

POSITION SENSITIVE DETECTOR SYSTEM FOR X-RAY DIFFRACTION STUDIES OF FLEETING PROCESSES

O. S. Kovalchuk[1], V. M. Pugatch[1], D. I. Storozhyk[1], V. M. Militsiya[1], V. O. Kyva[1], Y. V. Panasenko[1], V. V. Burdin[2]

[1] Institute for Nuclear Research, National Academy of Sciences of Ukraine, Kyiv
[2] Frantsevich Institute for Problems of Materials Science, National Academy of Science of Ukraine, Kyiv

This article presents status of the project on the development of a prototype of X-ray optical system based on position-sensitive detector and data acquisition system for X-ray diffraction studies of fleeting processes. The aim of the project is to improve spatial and time resolution of equipment to provide an opportunity for studies of changes in crystal structure of metals and their alloys during fleeting processes such as phase transitions under heating or cooling of the samples. Position-sensitive detector as a part of X-ray analytical equipment is needed to determine in real time a position of the diffraction peaks, their intensity and width as well as their evolution along the temperature of the sample. The requirements to the detector system are as follows:

operating area: (8 × 25) mm^2;
spatial resolution: 50 - 200 μm;
sensitivity: 200 photons per channel;
sampling frequency: 50 - 500 Hz.

Microstrip silicon detectors matching these requirements have been studied in combination with the commercial data acquisition system X-DAS (SENS-TECH, UK) [1] successfully explored earlier with microstrip metal detectors [2]. X-DAS allows creating large detector arrays with high speed readout in digital format. It consists out of Detector head boards with analog output modules and Signal processing boards with 16-bit digital output. Each detector head board acquires 128 channels of data, using a charge integrating ASIC and sends it via a local data bus to the signal processing board. The signal processing board converts the data into 14-bit format. On-board processing enables up to 4 data samples to be taken and added to produce a 16-bit output. This is transmitted via a data interface board to the host processor via USB2, data I/O, Ethernet or frame-grabber card. A system can handle more than 20000 channels with a scan time from 100μs to 100ms, depending on the number of channels.

The prototype of the position sensitive system has been built in the year 2013. Tests of the system have been performed at the X-ray installation for phase transition studies at the IPMS NASU. Silicon micro-strip detector was connected by ultrasonic bonding to the X-DAS system and mounted in the focal plane of the optical system of the X-Ray diffraction analysis setup.

Positioning strip-detector at the X-ray diffraction peak (X-ray energy 7.1 keV, sample of steel, T = = 24 °C) provided a clear proper response of the channels of the system corresponding to the strip position (see Figure).

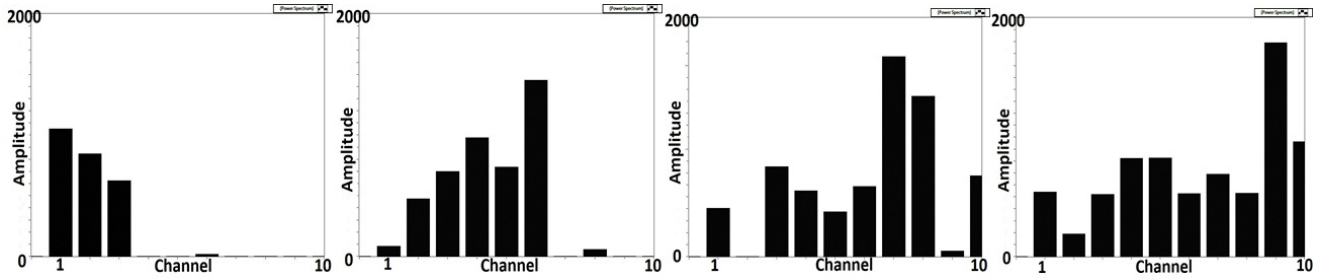

Response the position sensitive system with a strip-detector mechanically moved via X-ray diffraction peak.

Positive results of the tests allow us to start a production of three 128-channel detector modules for installation in the focal plane of the X-ray setup for studies of fleeting processes in metals and their alloys under heating/cooling in the year 2014.

1. http://www.sens-tech.com
2. O. Fedorovich, O. Kovalchuk, V. Pugatch *et al*., Problems of Atomic Science and Technology, Series "Plasma Physics" **6** (**82**), 196 (2012)

COMMISIONING OF THE TEST CO_2 COOLING SYSTEM FOR THE CBM SILICON TRACKING SYSTEM

E. Lavrik[1], A. O. Lymanets[1,2], H.-R. Schmidt[1]

[1] *University of Tuebingen, Tuebingen, Germany*
[2] *Institute for Nuclear Research, National Academy of Sciences of Ukraine, Kyiv*

The CBM Silicon Tracking System [1] is a compact detector that consists of double-sided silicon microstrip sensors that comprises the volume of about 2 m^3 defined by aperture of the dipole magnet. The sensors have to be kept at a temperature of -7 °C during the in-beam operation in order to avoid thermal runaway and slow down the reverse annealing of radiation defects. The heat sources include self-heating of sensors due to leakage current and heat dissipated by the front-end electronics. The sensors produce about 1 W power in the innermost region that can be removed using forced convection cooling, e.g., with dry N_2. The 2133k channels of the front-end electronics will dissipate up to 40 kW power localized at the periphery of the tracking stations. Particularly high heat density requires a cooling system with high volumetric heat transfer. Necessary cooling power can be achieved with bi-phase evaporative cooling [2].

A test system designed to dissipate about 200 W under realistic geometrical constraints has to verify the cooling efficiency. The heat generated by the resistive thermal load will be dissipated in the front-end board (FEB) box with 110 × 70 × 30 mm^3 size and removed by the integrated capillary with total length of about 2 m and about 2 mm diameter. For this test, an open-loop CO_2 cooling system has been assembled [3] and commissioned.

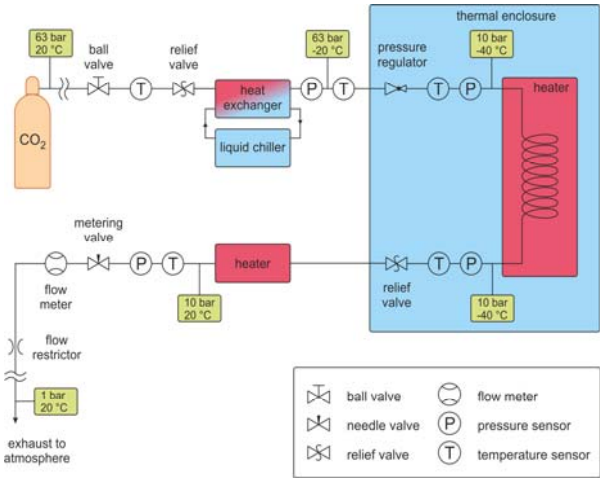

Fig. 1. Conceptual scheme of the open-loop test CO_2 cooling system.

The operation principle of the test system is sketched in Fig. 1. The liquid CO_2 is supplied from a gas bottle at room temperature and 63 bar pressure. By precooling the liquid down to -25 °C in the heat exchanger and expanding it behind the pressure regulator, the liquid is brought to the phase boundary at -40 °C and 10 bar from whereon the latent heat can be utilized for cooling. After passing the thermal load and leaving the thermal enclosure, the bi-phase mixture with about 50 % dryout is evaporated in the water-based heater and exhausted into the atmosphere. A metering needle valve with flow coefficient up to 0.004 controls the gas flow. A flow restrictor at the end of the transport line prevents the over-expenditure of CO_2. Pressure, temperature and flow are controlled along the line in order to ensure the proper operating conditions.

Temperature is controlled using miniature Pt100 sensors with nominal tolerance less than 0.15 °C at 0 °C. The sensors are read out with NI cDAQ-9188 system equipped with NI-9217 plugin modules. In order to verify the measurement precision, sensors have been characterized (see Fig. 2). The offsets of the calibration curves have been extracted in order to further improve the measurement precision.

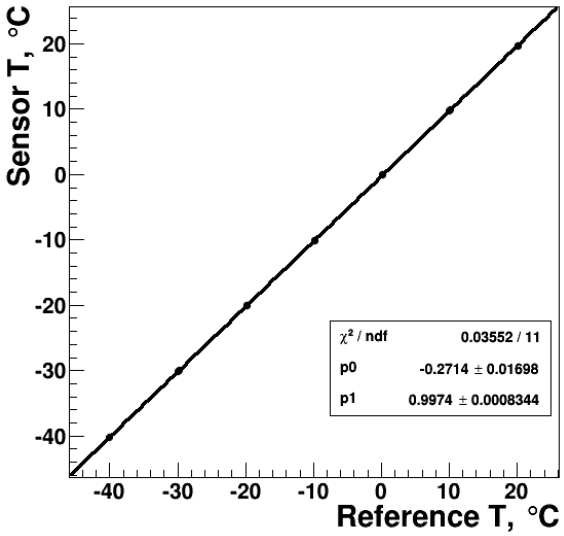

Fig. 2. Calibration curve for one of the temperature sensors. Offset is used to improve the measurement precision.

1. J.M. Heuser *et al.*, Nucl. Instr. Meth. A **568**, 258 (2006).
2. B. Verlaat *et al.*, Topical Workshop on Electronics for Particle Physics, Naxos, Greece, 15 - 19 Sep 2008, p. 328.
3. E. Lavrik *et al.*, *CBM Progress report 2012*, p. 20.

THE IMPROVED DETECTOR RESPONSE SIMULATION FOR THE SILICON TRACKING SYSTEM OF THE CBM EXPERIMENT

H. M. Malygina[1,2], V. Friese[3], J. Heuser[3], V. M. Pugatch[1]

[1] *Institute for Nuclear Research, National Academy of Sciences of Ukraine, Kyiv*
[2] *Goethe University Frankfurt, Frankfurt/Main, Germany*
[3] *GSI Helmholtzzentrum für Schwerionenforschung, Darmstadt, Germany*

The Compressed Baryonic Matter (CBM) is a future experiment designed to explore the QCD phase diagram in the region of high net-baryon densities. It will be built at the GSI (Darmstadt, Germany). The Silicon Tracking System (STS) of the CBM is based on double-sided micro-strip sensors [1]. It is necessary for the simulations and the experiment to know the sensor response as precise as possible. The Digitizer is a program, which simulates a complete chain of physical processes caused by a charged particle traversing the detector, from charge creation in silicon to a digital output signal. Current version of the Digitizer [2] doesn't include all the processes needed to get the sufficient results. It assumes a uniform energy loss distribution along the incident particle track and accounts for the Lorentz shift and the effects of the read-out electronics: threshold, random noise, charge collection inefficiency, channel dead time. We considered the following improvements to the Digitizer: non-uniform energy loss distribution, thermal diffusion, charge redistribution over the read-out channels due to interstrip capacitances (so-called "cross-talk").

There are several possibilities to model each process with a different level of detalization. We suggest the following procedure:

1) to divide the incident particle trajectory into thin layers (3 μm);

2) to calculate the deposited energy in each layer according to the Urban method [3];

3) to estimate the charge broadening due to thermal diffusion according to the Gaussian low for the charge in each layer [4];

4) to advance the register position due to the Lorentz force;

5) for each fired strip to calculate the charge sharing due to cross-talk, to add random noise distributed according to the Gaussian low with σ = ENC (Equivalent Noise Charge);

6) to convert the charge in each strip from number of electrons to ADC-value;

7) to apply a threshold and other effects of electronics.

To verify the new procedure we wrote a separate program. We chose 1 GeV-pions for incident particles, tracks with random impact and inclination from -45 to 45° (for other input parameters and details see [5]). We used the Center-Of-Gravity algorithm [6] to reconstruct clusters.

The obtained results lead us to the following conclusion: the most significant effect is the non-uniform energy loss along the incident particle track. Figure shows a comparison between experimental data from the LHCb and our simulation. The experimental data agrees better with the new simulation.

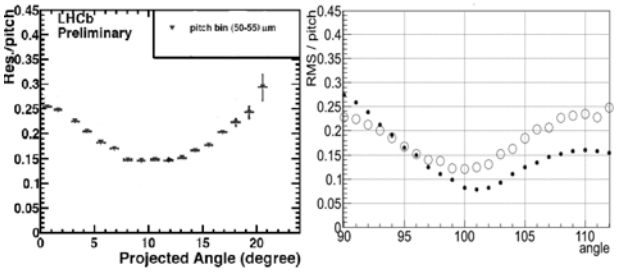

The RMS of the hit position residuals distribution VS track inclination: left panel – the LHCb Vertex Locator (0° - perpendicular tracks) [7]; right panel – our simulation (circles – the new Digitizer, dots – the current version of the Digitizer, 90° - perpendicular tracks).

In our simulation we put a threshold of 2 ADC, which corresponds to 6250 electrons = 4 ENC. Such a high value makes the spatial resolution worse. The fiducial value is 3.5 ENC, but we can put the threshold only in ADC units, so it can be either 2 ADC = = 4 ENC or 1 ADC = 2 ENC. The threshold is, thus, an issue to discuss.

Next step: to compare the results obtained with the new Digitizer to the experimental data, which we got in the beam test at COSY (Juelich, Germany) in December 2013.

1. P. Senger, CBM Progress Report 2012, Darmstadt 2013, p. 1.
2. A. Kotynia and J.M. Heuser, CBM Progress Report 2011, Darmstadt 2012, p. 14.
3. K. Lassila-Petini and L. Urban, Nucl. Instrum. Methods **A362**, 416 (1995).
4. M. Brigida *et al.*, Nucl. Instrum. Methods. **A533**, 322 (2004).
5. V. Friese and H. Malygina, STS-Note-07-2013.
6. R. Turchetta, Nucl. Instrum. Methods. **A335**, 44 (1993).
7. Rodrigues, Presentation at Vertex 2013.

COLLIMATOR FOR A PROTON MINIBEAM RADIATION THERAPY

I. L. Momot[1,2], V. M. Pugatch[2], Y. Prezado[3]

[1] Institute for Nuclear Research, National Academy of Sciences of Ukraine, Kyiv
[2] Taras Shevchenko National University, Kyiv
[3] CNRS, Paris 7 and Paris11 Universities, Orsay Cedex, France

One of the main difficulties in the design of an adequate collimator for proton minibeam radiation therapy (pMBRT) is to reduce at maximum the possible blurring of the dose profiles due to lateral proton penetration. In this work the study of collimators for pMBRT was done by simulation software package GATE v_6.2.

GATE – is a software environment designed for simulation in medical physics and based on Geant4 [1]. An ideal collimator was assumed. The input data for this simulation were as follows: energy of protons – 105 MeV; two field sizes – (20 × 0.7) mm^2 and (2 × 2) см^2, beam width – 0.7 mm; collimators from brass (6 plates, 2.8 mm thick, 5 cm long), cylindrical water phantom with radius 8 cm and height 16 cm. We consider the case when the beam is stationary and operates in a single direction. Sensitive areas where absorbed dose has to be measured are located at depths of 1, 2, 3, 4, 5, 6 and 7 cm of phantom. Spatially fractionated dose profile consists of peaks and valleys, that is a high-dose on the way of the beam and low-dose – between the beams [2]. Minimum dose in the central region between the two beams is called valley dose and the dose at the center of the beam – is the peak dose. The ratio of these values is called PVDR (peak-to-valley dose ratio) and plays an essential role in the biological response. The PVDR calculation for different collimators and sizes of the beam are presented in this work.

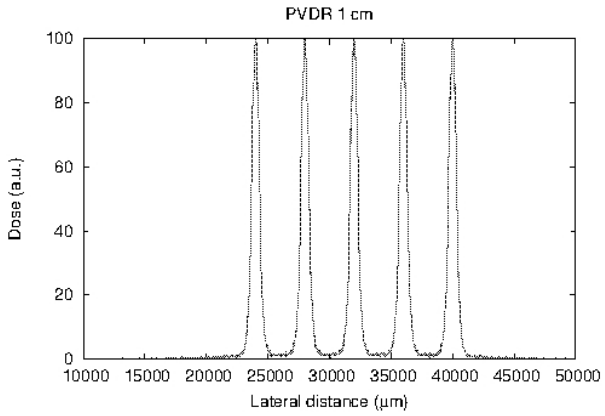

Fig. 1. Dose profile in phantom at the depth of 1 cm.

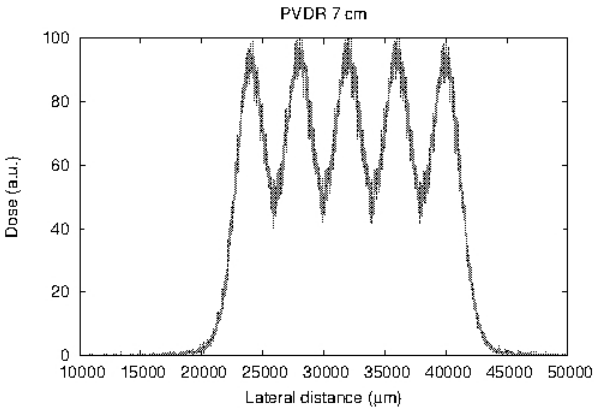

Fig. 2. Dose profile in phantom at the depth of 7 cm.

Submillimeter field sizes for the radiation therapy are expected to be efficient, exploring the so called dose-volume effect: the smaller the field size is, the higher tolerance of the healthy tissues is [3]. It is important to provide PVDR as large as possible, in order to ensure the safety and survival of normal tissues [4]. The results of simulation for the PVDR at 1 cm-depth and 7 cm-depth in phantom are shown in Figs. 1 and 2, respectively. The smearing of the beams is clearly visible at the depth of 7 cm.

The next step of this work will be taking into account the scattering of protons on the walls of the collimator.

1. B. Verla, S. Jan *et al.*, Phys. Med. Biol. **56**, 81 (2011).
2. Y. Prezado, I. Martınez-Rovira, S. Thengumpallil, and P. Deman, *Dosimetry protocol for the preclinical trials in MBRT*, (2011).
3. Y. Prezado, G. Fois, G. Le Duc, and A. Bravin, Med. Phys. **36**, 3568 (2009).
4. I. Martınez-Rovira, J. Sempau, J.M. Fernandez-Varea *et al.*, Phys. Med. Biol. **55**, 4375 (2010).

MEASUREMENT OF OSCILLATION FREQUENCIES OF B^0 AND B^0_S MESONS AT THE LHCB EXPERIMENT

O. Y. Okhrimenko, V. M. Iakovenko, V. M. Pugatch
(for LHCb Collaboration)

Institute for Nuclear Research, National Academy of Sciences of Ukraine, Kyiv

The LHCb experiment is the forward spectrometer and one of the four experiments located at the LHC [1]. The main aim of the LHCb is precise measurement of the CP violation (CPV) and search for the B-meson rare decays.

The LHCb detector consists of following parts: Vertex Locator, Inner and Trigger Trackers and Outer Tracker to reconstruct tracks of charged particles and their decay vertexes and to separate Primary (proton-proton collisions) and Secondary (B-mesons decay) Vertexes; Magnet to measure charge particle momentum; Cherenkov Detectors to separate kaons and pions; Hadronic and Electromagnet Calorimeters to measure the particles energy; Muon detector to detect the muons.

In the Standard Model (SM), transitions between quark families (flavours) are possible via the charged current weak interaction. Flavour changing neutral currents (FCNC) are forbidden at lowest order, but are allowed in higher order processes. Since new particles can contribute to these loop diagrams, such processes are highly sensitive to contributions from Beyond SM. An example FCNC transition is neutral meson mixing, where neutral mesons can transform into their antiparticles.

This article is devoted to precise measurement of the oscillation frequencies Δm_d and Δm_s of the B^0 and B^0_s mesons, respectively. The frequency of B^0_s meson oscillations is the highest. On average, a B^0_s meson changes its flavour nine times between production and decay. This poses a challenge to the detector for the measurement of the decay time. Another key ingredient of this measurement is the determination of the flavour of the B^0 and B^0_s meson at production, which relies heavily on good particle identification and the separation of tracks from the primary interaction point.

The observed particle and antiparticle states neutral B-mesons are linear combinations of the mass eigenstates B_H and B_L with masses m_H and m_L and decay widths Γ_H and Γ_L, respectively. The B^0 and B^0_s oscillation frequency is equivalent to the mass difference $\Delta m_{d(s)} = m_{d(s)H} - m_{d(s)L}$. Parameters Δm_d and Δm_s is an essential ingredient for all studies of time-dependent matter–antimatter asymmetries involving neutral B-mesons.

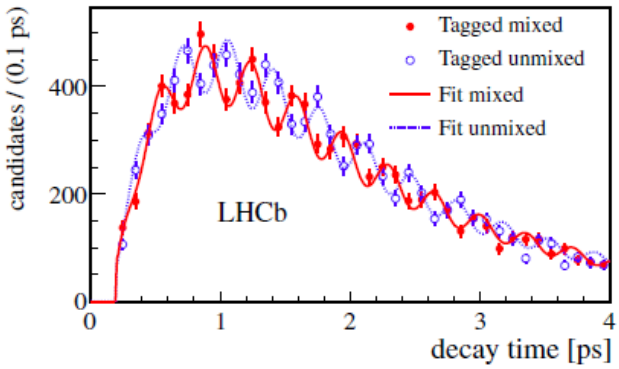

Decay time distribution for the sum of the five decay modes for candidates tagged as mixed (different flavour at decay and production; red, continuous line) or unmixed (same flavour at decay and production; blue, dotted line). The data and the fit projections are plotted in a signal window around the reconstructed B^0_s mass of 5.32 - 5.55 GeV/c^2.

From 1 fb^{-1} (out of 3 fb^{-1} accumulated) data a total of about 88000 and 39000 B^0 mesons are reconstructed, using its signal decays to $D^-(K^+\pi^-\pi^-)\pi^+$ and $J/\psi(\mu^+\mu^-)K^{*0}(K^+\pi^-)$ [2], respectively, with an average decay time resolution of 44 fs. About 34000 B^0_s mesons were reconstructed using $B^0_s \to D^-_s\pi^+$ decay [3].

The combined value for Δm_d is calculated as the weighted average of the individual results taking correlated systematic uncertainties into account $\Delta m_d = 0.5156 \pm 0.0051_{\text{stat}} \pm 0.0033_{\text{syst}}$ ps^{-1}. It is currently the most precise measurement of this parameter.

The result of B^0_s meson oscillation frequency is shown in Fig 1. The oscillation frequency is found to be $\Delta m_s = 17.768 \pm 0.023_{\text{stat}} \pm 0.006_{\text{syst}}$ ps^{-1}, in good agreement with the current world average, 17.69 ± 0.08 ps^{-1} (Particle Data Group). This is the most precise measurement of Δm_s to date, and will be a crucial ingredient in future searches for Beyond SM physics in B^0_s oscillations. Next year the whole dataset for integrated luminosity of 3 fb^{-1} is planned for analysis.

1. LHCb Collaboration, JINST **S08005** (2008).
2. LHCb Collaboration, Phys. Lett. **B 719**, 318 (2013).
3. LHCb Collaboration, New J. Phys. **15**, 053021 (2013).

SOFTWARE FOR THE DATA ANALYSIS OF THE INTERFERENCE PHENOMENON IN THE REACTION ^{11}B(p, 3α)

M.V. Pugach[1,4], M. Campbell[2], C. Grania[3], X. Llopart[2], S. Pospisil[3], O. S. Kovalchuk[1], V. O. Kyva[1], O. Y. Okhrimenko[1], E. O. Petrenko[1], Yu. M. Pavlenko[1], V. M. Pugatch[1], D. I. Storozhyk[1]

[1] *Institute for Nuclear Research, National Academy of Sciences of Ukraine, Kyiv*
[2] *European Organization for Nuclear Research (CERN), Geneva, Switzerland*
[3] *Institute of Experimental and Applied Physics, Czech Technical University, Prague, Czech Republic*
[4] *Taras Shevchenko National University, Kiev*

The new experimental set up for correlative studies of multiparticle nuclear reactions has been built at the Tandem generator of the Institute for Nuclear Research NASU. Hybrid micropixel detectors TimePix [1] (matrix of 256 × 256 silicon sensors with area 55 × 55 μm^2 and 300 μm thickness) were explored in the kinematics complete studies of the reaction ^{11}B(p, 3α) at low energies of protons. In particular, the results were obtained for the phase space where interference phenomenon occurs due to the identity of alpha-particles originated at the excitation and decay of the ^{8}Be*(2.9 MeV) nuclei. The software allows to find out the experiment conditions for observing interference of short living states of nuclei and to perform analysis of the energy spectra of final products taking into account constructive or destructive interference. A significant solid angle of the TimePix detector allows for studying of the interference phenomena in a wide range of polar and azimuthal angles during single exposition, minimizing systematical errors of the experiment. The micropixel detector provides simultaneous measurement of coincident particle senergies (E_1, E_2), polar (θ_1, θ_2) and azimuthal (φ_1, φ_2) angles as well as a time of arrival of the particles in the TimePix detectors. The software has been developed to identify alpha-particles by the events cluster size. Fig. 1 shows an example of the two-dimensional energy spectra measured in a coincidence mode by the TimePix detector (θ_2 = 120°, φ =180°) and a single diode silicon detector (θ_1 = 45°, φ = 0°). Clearly visible are contributions of the narrow ^{8}Be$_{g.s.}$ (4 event clusters at ~800 ADC) as well as of the wide ^{8}Be*(2.9 MeV, Γ = 1.46 MeV) along the kinematics locus for the reaction ^{11}B(p, 3α). Applying procedure of the alpha-particles identification the background contribution was suppressed a by factor of few thousands. Two-dimensional data projected to the energy axis of the TimePix detector will be approximated by the formula

$$d^5\sigma/(dE_2*d\theta_1*d\theta_1*d\theta_2*d\varphi_2)\sim k*|F_{\alpha\alpha\alpha}|^2*\rho(E_2),$$

where the three-particles final state amplitude $F_{ααα}$:

$$|F_{\alpha\alpha\alpha}|^2 \sim |f_{\alpha1\alpha2}|^2 + |f_{\alpha2\alpha3}|^2 + 2*f_{\alpha1\alpha2}*f_{\alpha2\alpha3}*\cos(\delta\psi)$$

includes interference term (phase shift δψ) while pair interactions between alpha-particles $f_{α1α2}$ and $f_{α2α3}$ are presented by the Breit-Wigner distribution for the first excited state of ^{8}Be*(2.9 MeV, Γ = = 1.46 MeV).

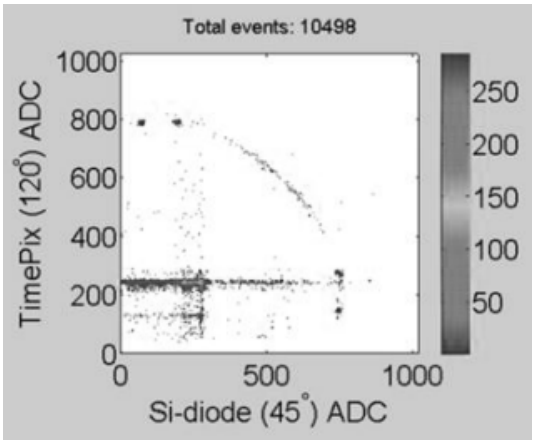

Fig. 1.Two-dimensional energy spectrum for coincident events in the silicon detector (θ_1 = 45°) and the TimePix detector (θ_2 = 120°). Incident proton energy – 2.65 MeV.

Fig. 2 illustrates these three components of the energy spectrum of alpha-particles from the reaction ^{11}B(p, 3α) together with final spectrum shown in the right bottom part of the Fig. 2. From fitting procedure phase shift parameter δψ will be derived as a function of polar and azimuthal angles for chosen angular combinations.

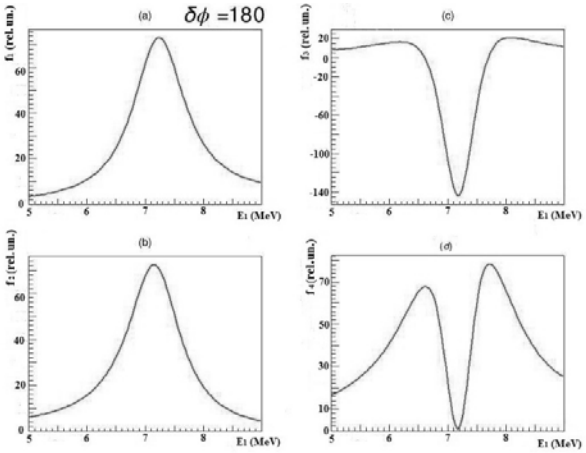

Fig. 2. Simulation of the components of the energy spectrum of alpha-particles from the reaction ^{11}B(p, 3α).

1. X. Llopart *et al.*, Nucl. Instr. Meth**. A 581**, 485 (2007).

MEASUREMENT OF THE COUPLING AND THE INTERSTRIP CAPACITANCES IN SILICON MICROSTRIP DETECTORS

I. E. Sorokin[1,2]

[1] *Goethe University Frankfurt, Frankfurt/Main, Germany*
[2] *Institute for Nuclear Research, National Academy of Sciences of Ukraine, Kyiv*

The main component of the future CBM experiment [1] at FAIR (Darmstadt, Germany) [2] is the Silicon Tracking System [3]. It is going to be based on double-sided silicon strip detectors. Among the important characteristics of silicon strip detectors are the coupling (C_c) and the interstrip capacitances (C_{iImp}, C_{iStrip}), because they affect the signal amplitude [4, 5]. Measurement of these capacitances is therefore important both in the stage of detector prototyping and in the stage of series production of the detectors for their quality assurance.

The coupling capacitance is the capacitance between a metal strip ("Metalisation" in Fig. 1) and the implant underneath. C_{iImp} – is the total capacitance of an implant to the neighboring metal strips, and C_{iStrip} – is the total capacitance of a metal strip to the neighboring metal strips.

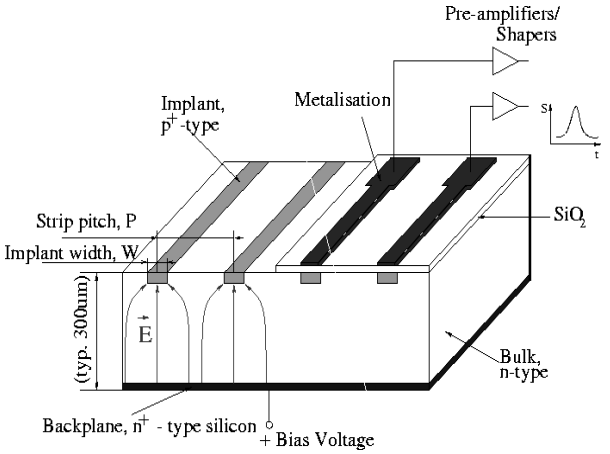

Fig. 1. Schematic view of one side of a silicon microstrip detector.

The capacitances were measured with a Quad-Tech 7600 precision LCR meter. To determine the coupling capacitance the test voltage (0.5 V) was applied to the selected implant, and the current, induced on the metal strip above, was measured. To measure C_{iImp}, the test voltage was applied to an implant, the metal strip above the implant was grounded, and the current was picked from the neighboring metal strips (three on each side). For C_{iStrip} measurement the test voltage was applied to a metal strip, and the current was picked up from the neighboring metal strips (three on each side).

In the measurements of C_c and C_{iImp} the observed value drops down at high frequencies (example in Fig. 2) because the impedance of the implant (order of 100 kΩ/cm) becomes larger than the impedance of the coupling capacitance, thus the test signal does not propagate along the whole implant length [5, 6]. True values for C_c and C_{iImp} are obtained only at low frequencies.

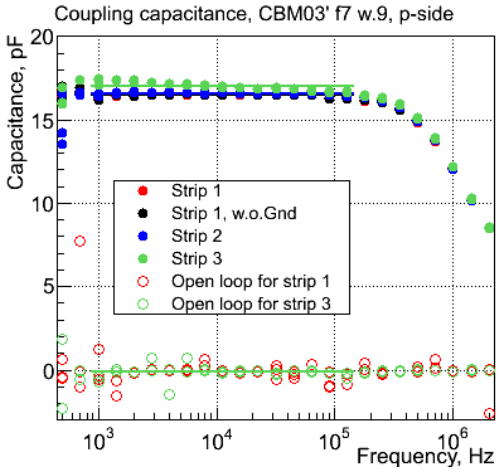

Fig. 2. Coupling capacitance as a function of frequency in the CBM03' detector.

The obtained values (Table below) were applied to estimate the expected signal amplitude [5]. The developed measurement techniques will be used for further characterization and quality assurance of the detectors.

Detector, side	C_c, pF/cm	C_{iImp}, pF/cm	C_{iStrip}, pF/cm
CBM02, p	37.8 ± 0.5	1.0 ± 0.5	1.4 ± 0.5
CBM02, n	34.7 ± 0.5	1.4 ± 0.5	2.2 ± 0.5
CBM03', p	17.2 ± 0.5	1.0 ± 0.5	1.5 ± 0.5

1. http://www.fair-center.eu/for-users/experiments/cbm.html
2. http://www.fair-center.eu/
3. Technical Design Report for the CBM Silicon Tracking System (STS), GSI, Darmstadt (2013)
4. C. Bozzi, Signal-to-Noise Evaluations for the CMS Silicon Microstrip Detectors, CMS Note 1997/ 026, 1997
5. I. Sorokin, Characterization of silicon micro-strip sensors, front-end electronics, and prototype tracking detectors for the CBM experiment at FAIR, submitted as dissertation thesis, Frankfurt am Main.
6. E. Barberis, Nucl. Instr. Meth. **A342**, 90 (1994).

POSITION SENSITIVE MICROPIXEL DETECTOR IN X-RAY STUIDES OF PHASE TRANSITIONS IN TITANIUM ALLOYS

V. M. Militsiya[1], V. V. Burdin[2], M. Campbell[3], S. O. Firstov[2], O. S. Kovalchuk[1], X. Llopart[3], B. Minakov[2], S. Pospisil[4], V. M. Pugatch[1], D. I. Storozhyk[1]

[1] Institute for Nuclear Research, National Academy of Sciences of Ukraine, Kyiv
[2]Institute for Problems of Material Science, National Academy of Sciences of Ukraine, Kyiv
[3] European Organization for Nuclear Research (CERN), Geneva, Switzerland
[4] Institute of Experimental and Applied Physics, Czech Technical University, Prague, Czech Republic

The X-ray diffraction is widely used for studies of phase transitions in material science. The knowledge of kinetics of the transformation mechanisms allows for a choice of rational thermal processing of materials. Nowadays thermal processing involves fleeting heating and cooling which provide fast arrival to a critical temperature point and reduce a time of phase coexistence. Physical properties like density and thermal expansion vary significantly from phase to phase, inducing change of the corresponding diffraction maximum position. This phenomenon is explored for characterization studies of a metal structure [1].

We report here on the application of the TimePix micropixel detector [2] for measuring and imaging in real time a dynamics of phase transitions in Ti alloys under heating and cooling at the experimental setup of the IPMS NASU (X-ray energy – 7.1 keV). The TimePix hybrid detector consists out of (256 × 256) array of 300 μm thick silicon sensors with a pixel size of (55 × 55) μm^2, bump-bonded to the read-out ASIC microchip designed in a commercial 0.25 μm 6-metal CMOS technology. It covers about 10° (2θ) in a focal plane of the X-ray experimental setup with angular resolution of 0.017° at the distance of 220 mm from the specimen. The TimePix detector providing two-dimensional measurement of the scattered X-rays may be treated as an 'electronic plate' imaging in real time a dynamics of phase transitions.

TimePix chip was readout by the PIXELMAN hardware/software via USB connection to PC. The fast framing rate of up to 100 Hz is provided by the USB interface FitPix [3]. This is a key feature for studies of fast phase transitions. The evolution of the diffraction pattern measured by the TimePix detector is illustrated in Figure. A sample of titanium alloy (BT-8)was sequentially heated from room temperature (Figure, *a*), via 900 (Figure, *b*) to 1200 Celsius degrees (Figure, *c*). Clearly visible is transition from different phase states in Ti to the case of creation of intermetallic structure demonstrating itself as a bright area at left bottom corner in the two-dimensional distribution in the Figure, *c* (or corresponding peak at the projected distribution (upper part in the Figure, *c*).

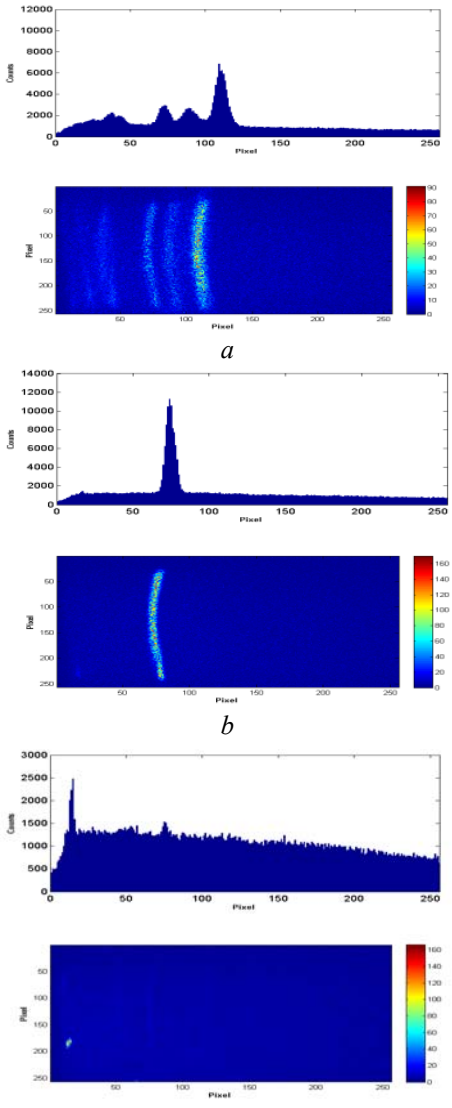

a

b

c

TimePix detector imaging two-dimensional and projected onto angle axis distribution of the X-rays scattered by Ti-alloy at different temperatures: 24 °C (*a*), 900 °C (*b*), 1200 °C (*c*).

We appreciate a support of the MEDIPIX Collaboration which allowed for these studies possible.

1. V.V. Burdin, Metal physics and new technologies. **31**, 1343 (2010).
2. X. Llopart, R. Ballabriga, M. Campbell *et al.*, Nucl. Instr. and Meth. **A581**, 485 (2007).
3. V. Kraus V. *et al.*, Journal of Instrumentation. **6,** Issue: 01, C01079 (2011).

DEVELOPMENT AND IMPLEMENTATION AT THE CYCLOTRON U- 240 OF INR NAS OF UKRAINE OF SYSTEMS AND DEVICES FOR PRODUCTION OF MEDICAL RADIOISOTOPES

O. E. Valkov, L. V. Mikhailov, M. V. Makowski, S. V. Timchenko, T. P. Rudenko, O. I. Kolosov, O. I. Shpachenko, D. C. Lyubovych, A. I. Ustinov, A. I. Piskarev, V. V. Yourievev, G. M. Pravednikov, L. G. Makarenko

Institute for Nuclear Research, National Academy of Sciences of Ukraine, Kyiv

More than 50 % of the annual production of radionuclides in the world is necessary for the nuclear medicine. Production of strontium-82 is carried out in the USA (Los Alamos and Brookhaven National Laboratories), Canada (TRIUMF – company "Nordion"), South Africa (laboratory Themba) and Russia (INR RAS IPPE) [1 - 6].

Strontium-82 used for the manufacture of generators short-lived rubidium-82, which is used for cardiac diagnosis using a positron emission tomography (PET), but operating accelerators, other than those listed, can turn out strontium-82 unavailable.

Given the characteristics of the cyclotron U-240 (large enough energy) and the conjuncture of radioisotopes in the world market has been developed target for s isotopes strontium-82 and germanium-68. Both isotopes are used in generators to highlight distinguish of positron emitters rubidium-82 and gallium-68, respectively. First isotope obtained proton irradiation salt RbCl, second – proton irradiation metal gallium.

The Isochronous cyclotron U-240 INR of NAS only active accelerator, which covers the desired range of energies and in what can be made strontium-82 and almost all cyclotron radionuclides, which are widely used in nuclear medicine [7].

For production of strontium-82 and other radionuclides cyclotron for high-intensity beams in the isochronous cyclotron U-240 was developed an installation which target is rotated, with the internal proton beam irradiation.

Were carried out further experimental and analytical studies internal targets for RbCl and Ga. Based on work irradiation selected metal for target capsules. Held engineering development comnents and systems (vacuum, water cooling, and diagnostic system management). Made thermal calculation modes this rotation target during irradiation [8, 9].

1. S. Kastleiner, S.M. Qaim *et al.*, Appl. Radiat. Isot. **56**, 685 (2002).
2. T. Ido, A. Hermanne *et al.*, NIM, **B 194**, 369 (2002).
3. E.Z. Buthelezi, F.M. Nortier, and I.W. Schroeder, Appl. Radiat. Isot. **64**, 915 (2006).
4. S.M. Qaim, G.F. Steyn *et al.*, Appl. Radiat. Isot. **65**, 247 (2007).
5. E.Z. Buthelezi, F.M. Nortier, and I.W. Schroeder, Appl. Radiat. Isot. **64**, 915 (2006).
6. M. Finlan *et al.*, in *Proc. of the 11th Int. Conf. on Cyclotrons and their Applications* (*1986*), p. 689.
7. A.E. Valkov, A.K. Zajshenko, M.V. Makovskiy *et al.*, *Development of technology and systems for the production stable and radioactive isotopes on the basis of complex isochronous cyclotron U-240, Report on the research work for* 2009 - 2010 y. y., DR No. 0109U005725.
8. J.M. Owen and R.Y. Rogers, Rotor - Stator Systems, Research Studies Press Itd., 278 (1996).
9. R. Boutarfa, S. Harmand *et al.*, Experiments in fluides **38**, 209 (2005).

PROGRAMMABLE PULSE GENERATOR

A. N. Kovalev, A. P. Voiter, M. I. Doronin, I. A. Mazny

Institute for Nuclear Research, National Academy of Sciences of Ukraine, Kyiv

The programmable pulse generator is designed for digital formation of various signals with high stability of time parameters and can be used for adjustment and calibration of devices and modules of nuclear electronics.

PC is used to control the operation modes of the generator through USB-connection. All manipulations on selection and setting of the required operation mode of generator are performed from the console of virtual adjustments, which is created in LabVIEW software.

Formers of input and output signals, reference generator, digital-to-analog converter (DAC), bandpass filter, buffer amplifier, algorithm unit, control unit and USB interface unit are the main elements of the developed pulse generator.

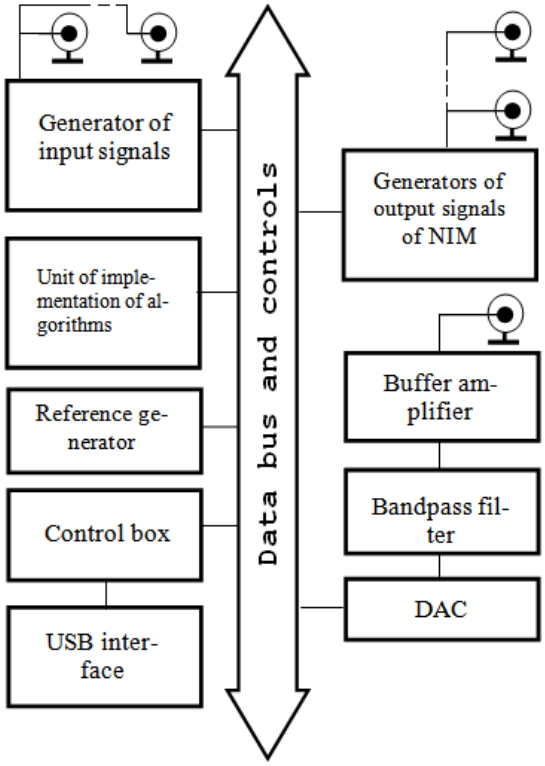

Structure diagram of the programmable pulse generator

The multifunctional generator provides:
– pulse frequency within the range 1 Hz – 100 (200) MHz at internal startup, stability of frequency ± 100 parts on one million, pulse duration and period in the range from 10 (5) ns to 1 s with the discreteness of frequency setting, which is equal to the period of the reference generator;
– rise and downturn times of output pulse 2 (1) ns (measured at the level 0.1 – 0.9 of pulse amplitude);
– the formation of the desired number of pulses (1 to 65535) after external starting pulse;
– generation of reference pulse and pulse delayed for some time relative to the first one. Discreteness of delay time is equal to one period of the reference generator;
– generation of nine synchronous pulses delayed relative to each other for some time. The delay is fixed and can be 10, 80, 160 or 320 ns;
– formation of random time intervals with minimum value of 10 (5) ns and maximum value, determined by digit capacity (from 8 to 16 bits) of time interval grid of the reference generator. Operation is possible in one of two modes, namely with uniform distribution of random intervals or Gauss distribution;
– generation of pulse amplitudes in the range from 0 to 9 V with fixed duty factor. Discreteness of amplitude change is determined by grid of 8 - 16 bits. The frequency of change of amplitudes and duration of their detention is determined by the type of applied DAC and by settings of the reference generator. Operation is possible in one of two modes (uniform distribution of amplitudes or Gauss distribution);
– formation of random amplitudes with chosen distribution and varying duty factor.

The scheme of the multifunctional generator is based on two programmable elements: programmable logic matrix FPGA Cyclone-I (block implementation of algorithms) and microcontroller HMEGA128 (control unit).

Technical parameters of FPGA Cyclone-I provide the operation of generator in nanosecond range. The control of operation mode, preliminary data processing and communication with PC are performed by microcontroller.

The parameters of signals, which are formed by generator, conform to the standard of nuclear electronics NIM. The generator is constructively implemented in the form of CAMAC module with 1M width.

PULSER FOR SPECTROSCOPY SYSTEMS

M. I. Doronin, A. P. Voiter, O. M. Kovalev

Institute for Nuclear Research, National Academy of Sciences of Ukraine, Kyiv

The pulser is designed to simulate the output from a solid-state or scintillation detector/preamplifier combination and the output from a pulse-shaping amplifier, thus providing a means of testing and calibrating the electronics in a nuclear counting system.

Typical applications of the pulser include: determining the proper timing of linear gates and coincidence units, threshold setting of discriminators, calibration of nuclear spectroscopy systems and multichannel analyzers, measurement of the integral nonlinearity and differential nonlinearity, and selection of delays in coincidence timing systems. The variable repetition rate is also useful in determining the system's count rate performance.

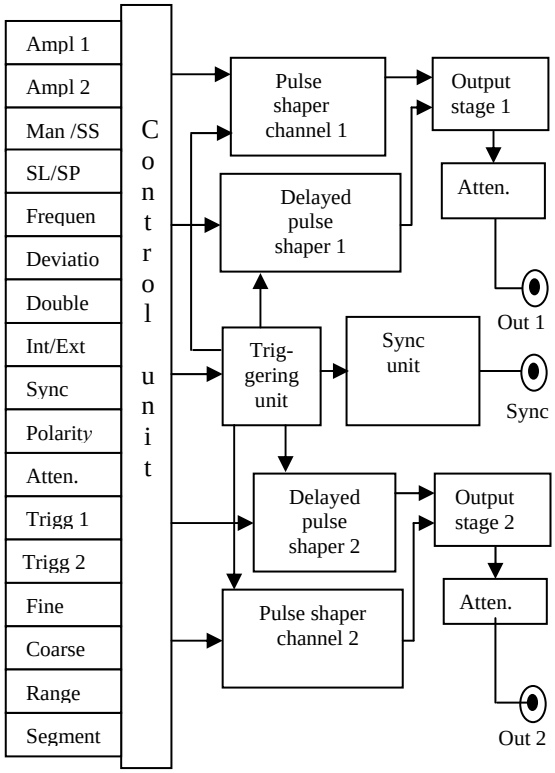

Block diagram of the pulser.

The pulser consists of two independent channels. Each channel has individual sync input and can be synchronized with either external trigger or internal pulse generator.

Channel 1 output provides single/double attenuated positive or negative tail pulse, pulse height from 0 to 10 V into high impedance and 0 to 5 V maximum pulse into 50 ohms. A pulse pair separation is varied by the delay controls.

Channel 2 output provides single/double attenuated positive or negative semi-gaussian pulse shape, pulse amplitude from 0 to 8 V open circuit (0 to 4 V when terminated into 50 ohms). A pulse pair separation is varied by the delay controls.

The pulser offers a fast rise time (typically 20 ns) tail signal and variable repetition rates of up to 2 kHz.

Pulse parameters are displayed on two numeric LEDs with three-digit resolution.

The pulser operates in several modes.

1. Ramp

The pulser provides linearly increasing amplitude signal with a short decay time. Rear panel switch selects full range of the signal with either 12-bit resolution or 16-bit resolution.

2. Tail pulse

The pulser provides a pulse train of linearly increasing tail pulses to simulate output of charge-sensitive preamplifier. Output tail pulse amplitude can also be controlled by front panel multi-turn potentiometer manually.

3. Semi-gaussian pulse

The pulser provides a pulse train of linearly increasing semi-gaussian shape pulses to simulate output of pulse-shaping amplifier. Output pulse amplitude can also be controlled by front panel multi-turn potentiometer manually.

4. Sliding semi-gaussian pulse

4.1. Semi-gaussian pulse shape amplitude varies with deviation equal to one-eighth of the full output amplitude range. Front panel potentiometer controls the location of the deviation within the full range.

4.2. Semi-gaussian pulse shape stepwise increasing amplitude with deviation equal to one-eighth of the full amplitude range at each step.

5. Double pulse

The pulser provides either double tail pulse or double semi-gaussian pulse shape. The amplitude of each pulse in the pair can be controlled by a separate potentiometer. Varying the pulse amplitude and the delay between them to simulate various kinds of pulse pile-up. Double pulse mode can be used to test pile-up rejection circuits. This mode also allows you to evaluate the dead time of analyzers.

APPROACH TO GAMMA SPECTRUM ANALYSIS WITHOUT ENERGY CALIBRATION PROCEDURE

A. M. Sokolov

Institute for Nuclear Research, National Academy of Sciences of Ukraine, Kyiv

If a gamma spectrometer is used to determine the quantity of gamma emitters present in the source the measured spectrum usually described as a sum of spectra of the gamma-emitting nuclides contained in the source [1]:

$$Sp_j = \sum_{i=0}^{N} c_i \cdot sp_j^{(i)} . \qquad (1)$$

where Sp_j – the spectrum, represented by the number of counts *Sp*(*j*) in the *j*-th channel of a spectrometer; c_i – the coefficients to determination; $sp_j^{(i)}$ - particular components (e.g. the spectra of specific nuclides); *j*-channel number; *i* – particular component number.

However usually at measuring components and spectrum a background is present. Therefore instead of components we have spectra of type $sp_j^{(i)} + Fon1_j$ and instead of spectrum measuring gives $Sp_j + Fon2_j$. To take that *Fon1* and *Fon2* into account, they are measured separately (*Fon1* in the same conditions as for components, and *Fon2* in one conditions with the first spectrum in the series of measuring). In addition, if the series of spectra are measured, then the conditions of these measuring can change, that is reflected in the change of energy calibration for the channels of spectrometer. Thus a spectrum is shifted and stretches or compresses in relation to the spectrums of radiation of components, measured at other energy calibration. For scintillation detectors such effect is related to sensibility of their characteristics on a temperature variation.

For correctness of equation (1) it is necessary to bring results of measuring of spectrum and separate components to one system of channels with identical calibration on energy. For this purpose usually energy calibration provides for a spectrum and for separate components. Procedure can require additional measuring with the use of gauge standard sources.

The worked out method [2] and program do not require knowing of calibrations on energy, and suppose only, that calibrations for components and for background Fon1 are identical, calibration at *Fon2* and first in the series of spectra is the same, and at subsequent spectra can differ. It is assumed also, that relationship between energy and channel number for spectrum and for components, which we denote as $E = Fs(k)$ and $E = Fc(k)$, satisfy the condition: $Fc(k) = Fs(a \cdot k + b)$. The program does not use the explicit form of functions $Fs(k)$ and $Fc(k)$ and finds itself the coefficients *a* and *b*. A task in a formula (1) will be transformed in a task for a minimum

$$\min_{a,b}\left(\min_{c_i}\left\|\sum_{i=0}^{N} c_i \cdot sp_j^{(i)} - Sp^*_{a\cdot j+b}\right\|^2\right), \qquad (2)$$

which resolves in two stages (linear for c_i and nonlinear for *a* and *b*). At that a spectrum is transformed by special procedure "of pouring" on the scale of channels for components. Later the activities of particular nuclides in the sample can be obtained on the found coefficients c_i, on known activity of gauge sources and taking into account time of measuring of separate components and spectrum.

During statistical analysis the estimation of accuracy of activities is performed. The program checks also are the set of components enough for description of spectrum and whether all components significantly deviate from zero.

1. P.H.G.M. Hendriks, J. Limburg, and R.J de Meijer, J. Environmental Radioactivity **53**, 365 (2001).
2. A.M. Sokolov, in *Proc. of the 4-th Int. Conf. "Current Problems in Nuclear Physics and Atomic Energy", Ukraine, Kyiv, Sept. 3 - 7, 2012.* (Kyiv, 2013). - p. 580.

BETWEEN PROTOCOL DEPENDENCE OF THE EFFECTIVE TRANSMISSION RATE FOR ADAPTIVE CONTROL IN MONOCHANNEL NETWORKS

A. P. Voiter, A. N. Kovalev

Institute for Nuclear Researchб National Academy of Sciences of Ukraine, Kyiv

An effective speed of transmission in monochannel computer networks is always below the physical speed due to an existence of interferences of various natures, a protocol redundancy of packet and protocol procedures of different levels. The interferences lead to unavoidable damage of packets on the physical level and necessity to repeat the transmission, or introduction of the code redundancy for error corrections in the packets. The channel level of network, which includes both the sublevel control of logical channel (LLC-Logical Link Control) and the sublevel control of access to monochannel (MAC- Medium Access Control), also decreases an effective speed transmission, due to both the redundant information of data packet formats of LLC-protocol and the conflicts, which appear in MAC-protocol at using the competitive access procedures.

The goal of the work is to build an analytic model for the evaluation of the efficiency of joint work of physical and channel levels of the monochannel networks with adaptive control length packets. Obviously, that the probability of successful transmission on the physical level depends on the error rate in monochannel and increases with decreasing of the packet length. On the other hand, LLC-protocol of channel level decrease (increase) of its effective transmission speed at shortening (increasing) of the packet length due to existence of fixed space of overhead information in the data packet formats.

We define the effective transmission speed C at fixed physical transmission speed V by taking into account the complex influence of the both physical and channel level. The physical level is defined by the probability of successful packet transmission. The channel level is determined by the joint influence of both the received frame format of LLC-protocol and the probability of successful transmission of the access to the monochannel to the protocol to control. The mathematical model is proposed for the analysis of the effective speed of transmission. This model takes into account the mutual influence of physical level, MAC and LLC protocols. The effective transmission speed is

$$C = \frac{V\lambda T}{1+2a\lambda+\lambda T+aT\lambda^2}\frac{[rn_o+(r-1)c](1-p)^{r(n_o+c)}}{r(n_o+c)},$$

where T – the transmission time of the packet; λ – the intensity of the incoming packets; a – the interval of sensitiveness of MAC protocol; n_0 – the optimal length of the information part of the packet; c – the fix length of the protocol part of the packet; r – the factor of the packet length variation at adaptive control; p – the intensity of interferences in the monochannel.

We present the dependence of C on λ for the optimal value of the length of informational part of packet in Fig. 1. This dependence is evaluated for different intensities of interferences: $p = 10^{-6}$ (curve *1*), $p = 10^{-5}$ (curve *2*) and $p = 10 – 4$ (curve *3*).

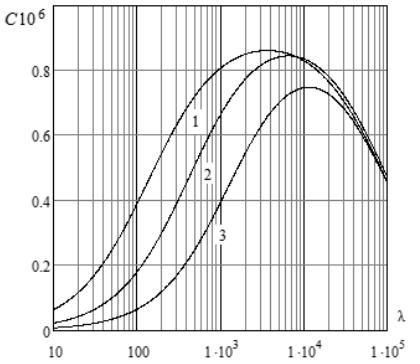

Fig. 1. Effective speed transmission with change *p.*

The dependence $C(\lambda)$ obtained at $p = 10^{-5}$ and various values of the length of the information part of packet is presented in Fig. 2. Curve *1* corresponds to the optimal length of information part of the packet and curve *2* (*3*) relates to increased (reduced) 10 times the length of information part of the packet.

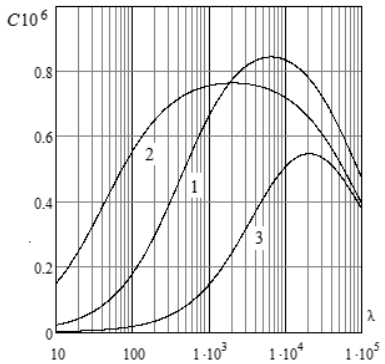

Fig. 2. Effective speed transmission with changing length packets.

It is shown, that the strategy of adaptive control on the MAC level should be based on the procedures of increasing length of packets relatively n_o only

Abstracts of works on atomic energy

DESIGN OF SYMPTOM-ORIENTED GUIDES FOR OUT-OF-PROJECT ACCIDENTS MANAGEMENT ON NUCLEAR POWER PLANTS

S. I. Azarov[1], A. V. Taranovski[2]

[1] *Institute for Nuclear Research, National Academy of Sciences of Ukraine, Kyiv*
[2] *Limited liability company "Energorisk", Kyiv*

Complex analyses of severe accidents on NPPs (Chornobyl and Fucushima-1) have found out a limitation of traditional regulatory and methodological support for out-of-project accidents management. This approach excludes effective management for radiation accident with relatively unlikely initial events and accident-related sequences. Also, it does not take into consideration that process and accident-related sequences depend on events preceding conditions of core damage.

Stages of origin and process of severe accident in vessel reactors are shown at Fig. 1.

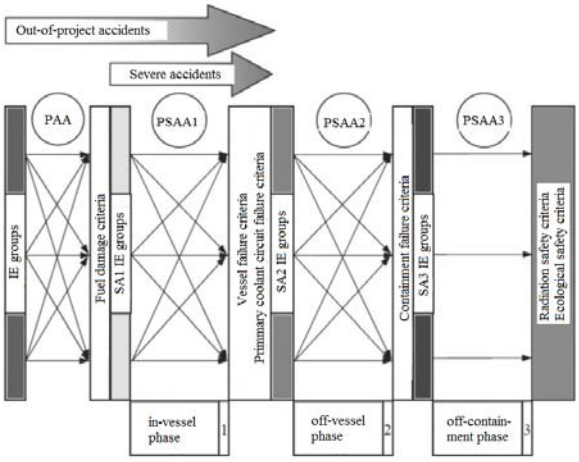

Fig. 1. Stages of origin and process of severe accident in vessel reactors. Here: IE – initial event; PAA – project accidents analysis; PSAA1 (2, 3) – severe accident analysis for different stages.

Severe radiation accident leads to loss of control on chain reaction in nuclear core. This leads to critical mass formation and heat removal failure. Radioactive products are emitted in quantity, that is more than NPP normal exploitation limit.

Authors are suggesting to use risk-informed decision making for planning and modeling of severe accidents on nuclear sites.

The structure of integrated risk-informed decision making process in extreme emergency is shown in Fig. 2.

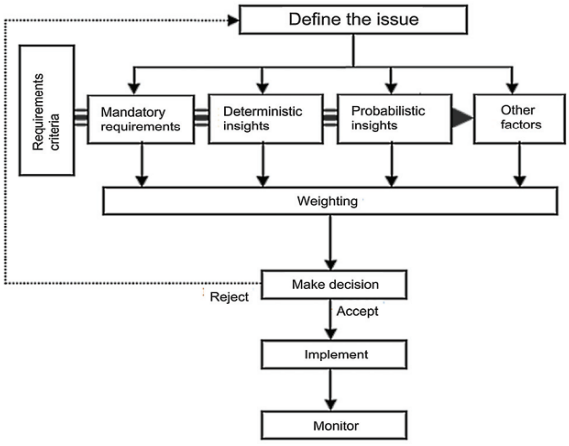

Fig. 2. Integrated risk-informed decision making process.

The process starts from identifying the problem and how it can be solved. Then, mandatory requirements, deterministic and probabilistic assumptions are considered as input data for decision of accident consequences localizing and elimination. Technical input data is weightened and combined to produce the best decision. Uncertainties of deterministic, probabilistic, and other factors also should be considered. Monitor program should be applied, after decision is accepted and implemented, to define the effectiveness of change, and whether review is required.

The goal of this structure is to provide balanced decision that takes into account all important factors.

1. IAEA-TECDOC-1590. Application of Reliability Centered Maintenance to Optimize Operation and Maintenance in Nuclear Power Plants. – Vienna: IAEA, 2007. - 87 p.
2. Review of Maintenance by Reliability Centered Maintenance (RCM) for SUK NPP: TACIS Contract No 98-0344. - FRAMATOM REALISATION NUCLEAIRES, 26/02/1998.

RESEARCH AND DEVELOPMENT OF THE WAYS OF THE IMPROVEMENT OF RADIATION TECHNOLOGIES IMPLEMENTATION IN THE MODERN INDUSTRIAL PRODUCTION

T. V. Kovalinska, I. A. Ostapenko, V. I. Sakhno, I. M. Vyshnevskyy

Institute for Nuclear Research, National Academy of Sciences of Ukraine, Kyiv

The beginning of the third millennium is characterized with the stagnation of the economy almost in all countries of the world. The search of the intensive methods of the production of goods and services and the creation of science-intensive and energy saving technologies of the industrial production on their basis is urgent now. Radiation technologies are among the most perspective technologies for many branches. Certain experience of their creation is accumulated in the radiation technologies sector. During the last ten years some high-efficient technologies for industry, food services, medicine, ecology etc. were developed. The last period is marked with the accent of research and development on the creation of the technologies with minimal energetic resources consumption. All the problems are solved in complex – the research, technological developments are accompanied with the creation of the appropriate technique for the practical implementation of new technologies. The developments are carried out in two directions – the industrial usage of ionizing irradiation and the usage of low-energy charged particles as an instrument of modern energy saving technologies. The most important developments of this year are as follows:

1. The technology with the usage of ionizing irradiation. The development of complex methods of functional radiation testing and the qualification of the equipment of nuclear power plants. New automated computer system of spatial control of the radiation field in the reactionary chamber of the experimental installation of the sector with electron accelerator of 4 MeV is created and tested under the beam of electrons. New data are obtained concerning the ways of the reproduction on the existing radiation installation of actual operating conditions of the equipment in pressurized zones, energetic reactors VVER-1000. The necessity of the research expansion towards the usage of electrons with energies below 4 - 3 MeV is defined and substantiated.

With this purpose the materials concerning the projection of necessary accelerating technique are researched and the project of electron accelerator with adjustable energy of 0,07 - 400 keV is worked out which is aimed at the achievement of the current up to 50 mA in the beam. Construction works started.

Technological researches continue in the direction of the usage of radiation technologies for the disinfection of ready food forms. The original technology of fish products' disinfection is created and tested on the edge of their normative storage through electron flows with wide energy spectrum. Experimental researches of new methodology are done and positive conclusions of food hygiene establishments are received. It was experimentally demonstrated that irradiation according to this methodology provides reliable suppression of pathogenic microflora, even when irradiation doses are below 1 kGy. The methodology is discussed and approved by the experts- technologists of the fishing industry on the conference in Kaliningrad.

2. Technologies with the usage of the interaction effects of charged particles of low and ultra-low energy with matter.

The occurrence and formation mechanisms of charged particle flows of low energy range and their interaction with a wide class of organic materials and composites which are intensively spread in nuclear energetic are researched and published.

The kinetics of the movement of low-energy charged particles in the atmosphere, bio-physical processes in intense flows of charged particles, the influence of air-ions on the chemical processes in materials are researched. New information about the absorption mechanisms and the transformation of charged particles energy with complex organic systems and living matter is received.

High efficiency of charged particles of this range in processes of the modification of complex organic systems is revealed. Energy saving technologies of raw materials modification in food production are developed and tested with their usage. The original methods of surface activation of chemically resistant materials and their combinations in structures of new composite materials for the industry are done. The original experimental technique is created and the research of technological effects started, with which the interaction of charged particles of ultra-low energy with living matter and organic systems is characterized. The research results are presented on scientific conferences and seminars, as well as at international meetings concerning the implementation of knowledge based processes in industry, and discussed with leading specialists of various branches of science and technique.

CONVERSION OF RESEARCH NUCLEAR REACTOR INTO FUEL WITH LOW ENRICHED URANIUM

I. M. Vyshnevskyi[1], V. I. Slisenko[1], V. Yu. Bodnar[1], I. Bolshinskiy[2], J. Dewes[2], N. I. Mazina[1], V. M. Makarovskyi[1]

[1] Institute for Nuclear Research, National Academy of Sciences of Ukraine, Kyiv
[2] National Nuclear Security Administration (NNSA) of US Department of Energy, USA

During implementation of the Highly Enriched Fuel Return Program to Russian Federation it has been envisaged: to perform conversion of research reactor into fuel with low enriched Uranium (LEU < 20 % U-235), receive pilot batch of LEU fuel, and if it is acceptable for the use to receive such fuel in equivalent to the removed highly enriched Uranium (HEU).

The work on conversion from HEU to LEU in Ukraine has started in 2005. Mutually with the specialists of Argonne National Laboratory of US DOE the possibility of the use of HEU for research reactor of Ukraine without design changes of reactor core was investigated. Besides, the flux density declining is not essential that allows performing needed scope of research work. Developed technical and economical substantiation and design decision on the use of LEU fuel (both together with HEU, and independently) were approved by Regulatory Authority in 2006.

In October 2008 PC TVEL (Russia) delivered 33 LEU fuel assemblies made at Novosibirsk Plant of Chemistry Concentrated Products (comparative characteristics are given in the table). In December 2009 these assemblies were loaded into the reactor core and were in operation together with HEU. 194 assemblies were delivered in December 2010, and 200 LEU assemblies were received in February 2012.

Comparative characteristics

Technical Characteristics	Number of sections in fuel assembly			
	1	3	1	3
Enrichment, %	19.7		36	
Number of fuel elements in assembly	3	9	3	9
Mass U^{235} in fuel assembly, g	41.7	125.1	37.5	112.5
Height of active part of assembly, mm	500			
Coating thickness, mm	<0.5 min			
Tubes thickness of fuel element, mm	2.5			

In accordance with the international commitments of Ukraine regarding removal of the whole scope of HEU from its territory: in December 2010 all the HEU assemblies were reloaded from reactor core. Received LEU assemblies we loaded to the reactor core; as a result total number of LEU fuel assemblies were 88 units in reactor core. Such number of fuel assemblies didn't allow to reach rated output of reactor (10 MWt), nevertheless, in the course of time, after deletion of beryllium reflectors from reactor core and filling this space with LEU assemblies we shall come to rated output of reactor.

In December 2010 KINR of NAS of Ukraine has loaded out about 10 kg of non-irradiated HEU fuel and special fissionable materials of Russian origin, and sent to Russian Federation (RF). It means plutonium disks, HEU (90% for U^{235}) in the form of pellets, rods and so on, as well as HEU fuel assemblies.

HEU and specific fissionable materials were packed into special casks, then loaded into special containers under control of the IAEA representatives and concerned RF enterprise, and in special column were transported to the airport and shipped to RF.

So taking into account the fact that simultaneously with HEU shipment from KINR the shipment of HEU was carried out from other institutions of Ukraine before Seoul Summit 2012. It can be stated that Ukraine met its international engagements and set its territory free of HEU.

SPENT NUCLEAR FUEL MANAGEMENT AT RESEARCH NUCLEAR REACTOR WWR-M, INSTITUTE FOR NUCLEAR RESEARCH, NATIONAL ACADEMY OF SCIENCES OF UKRAINE

I. M. Vyshnevskyi[1], V. I. Slisenko[1], V. Yu. Bodnar[1], I. Bolshinskiy[2], J. Dewes[2], N. I. Mazina[1], V. M. Makarovskyi[1]

[1] Institute for Nuclear Research, National Academy of Sciences of Ukraine, Kyiv
[2] National Nuclear Security Administration (NNSA) of US Department of Energy, USA

The last removal of SNF from INR, NAS of Ukraine to IE "Mayak" (Russian Federation) was conducted in 1988; therefore at the beginning of RRRFR program more than 700 pc of spent fuel assembles (SFA) were stored at the reactor, in recalculation to the single assembles. These are fuel assembles (FA) of WWR-M2 and WWR-M5 (M7) types with 36 and 90 % enrichment by Uranium-235, accordingly.

The decision was taken to use the casks of VPVR/M type («Skoda», Czechia) for SFA shipment (cask capacity - 36 triple or 108 single FA of the same type).

Taking into account the difference in dimensions, weight and considerable difference in loading technique of FA there was the necessity to change design documentation, in particular documentation of reservoir of SNF storage; design of upper biological protection (cover) of storage reservoir; hoisting machine; premises of CP-2; SFA transportation line for CP-1 (old SNR storage facility) in CP-2. Changes have been completed, agreed with regulatory authorities, and premises with CP-2 have been constructed and put into operation. Financial support was given by National Nuclear Security Administration (NNSA) of US Department of Energy. Thus, in the view of technical aspects INR, NAS of Ukraine, has been ready to perform SFAs shipment till December 2009.

In April 2010 at Washington Summit of Nuclear Security the President of Ukraine declared about Ukraine intention to become free of HEU till the next Summit that has been planned to conduct in Seoul, on March 26, 2012. This decision allowed to proceed to the next stage of RRRFR program, namely to obtaining of necessary permissions and then shipments of cargo.

For performing shipments of HEU SFA of Russian origin relevant permissions and licenses were received from regulatory authorities of Ukraine.

Loading of SFA to transport casks was carried out by WWR-M reactor personnel with the assistance of Czech Institute for Nuclear Research.

The first batch with 748 SFAs was shipped in May 2010 to IE "Mayak" (RF) for reprocessing, and in March 2012 the second batch with 218 SFAs was shipped (See Table).

Thus, as a result of six years activity within RRRFR program in the frames of Global Threat Reduction Initiative the modernization of systems important for safe operation of the reactor have been conducted and 17 kg of U^{235} was shipped consisted of HEU SNF; and about 10 kg of fuel and special fissionable materials.

Type of assemble	BBP-M2	BBP-M5(M7)	BBP-M2
	May 2010		March 2012
Output enrichment, %	36(20)	90	36
Assembles single triple	101 193(6)	15(5) (5)	38 60
Number of transport casks	7		4
Full activity in the cask, TBq	2053		2790
Full residual heat, W	209,8		217,1
Number of assembles (у перерахунку на одиничні)	748		218
Total load ^{235}U, kg	11. 864		5. 146
Total load U, kg	55. 780		19. 354

FRACTALITY AND PERCOLATION IN NUCLEAR REACTORS

V. V. Ryazanov

Institute for Nuclear Research, National Academy of Sciences of Ukraine, Kyiv

A fractal and multifractal are many physical systems. Some possibilities of description of motion of neutrons in a reactor are considered through approaches of percolation and multifractality. Especially expressly fractal properties show up in critical range. Stationary work of nuclear reactor (NR) passes exactly in a critical point, and fractal description is very important for description of behavior of neutrons in a reactor. Practical importance for the calculations of reactors can have a necessity of passing to neutron transport equation in fractional derivatives, although often there is not sharp distinction between percolation processes and diffusion.

The importance of the relations of percolation theory for neutron processes in the reactor is visible from the fact that they allow you to immediately interpreting the general relations of percolation theory, an equation of the neutron multiplication and the equation of the critical size of the reactor obtain. The value should be helpful for the propagation velocity of perturbations at the local supercritical. Percolation is a critical process with a threshold, a critical point. At the threshold of the flow occurs along a fractal set, which is determined by the geometry of criticality. Fractal geometric characteristics are independent of the microscopic properties of the environment. The kinetic processes below the critical point are limited of finite region of the phase space, scattering, absorption and other neutron processes. At the critical point becomes important fractal set, emerging at lower free energy of the statistical ensemble. Nonequilibrium steady states in fractal structures are chaotic, turbulent.

The evolution of hierarchical structures reduces to the process of anomalous diffusion in ultrametric space, resulting in a stationary distribution of the hierarchical levels, which reduces to a power Tsallis law inherent in non-additive systems. Tsallis distribution is a special case of superstatistics related with distribution containing lifetime [1], applied to the study of processes in a nuclear reactor [2, 3]. Kinetics and transport processes in reactor fractal structures requires of separate detailed study. In the area of critical points appear long-range correlation effects are manifested in the non-Gaussian behavior of the kinetic processes, determines the topological invariants of self-similar fractal sets. In transport processes at the percolation threshold is used the equation in fractional derivatives, taking into account the effects of memory, nonlocality and intermittency.

1. V. V. Ryazanov and S. G. Shpyrko, Condensed Matter Physics **9**, 1(45), 71 (2006).
2. В. В. Рязанов, Атомная энергия **99,** 348 (2005).
3. В. В. Рязанов, Атомная энергия **110,** 307 (2011).

NEUTRON SPECTROMETRY METHOD FOR DETERMINATION OF HYDROGEN CONTENT IN METAL HYDRIDES

P. M. Vorona, O. I. Kalchenko, V. G. Krivenko

Institute for Nuclear Research, National Academy of Sciences of Ukraine, Kyiv

Permanent attention to metal hydrides caused by escalation of field of hydrides application in technique, especially perspective use in energetics [1, 2]. Practical requirements stimulate the investigations and design the new methods of metal hydride development on an industrial scale. In this connection it is important to develop the new methods of analysis (especially nondestructive) for hydrogen content in metal hydride. This is the demand of escort control at development and selection of the most effective technologies of metal hydride synthesis. Among nondestructive methods of analysis the important position take nuclear physics methods [3].

Undestructive method for analysis of stoichiometric ratio in metal hydride MeH_n, where index n – the number of hydrogen atoms (H) per one atom of metal (Me). Method is founded on the measurement and analysis of the total neutron cross sections of metal hydride samples for slow neutrons.

For experimental verification of this method and its possibilities the measurements of total neutron cross sections σ_t^{obs} for samples of titanium hydride TiH_n with different hydrogen concentration were fulfilled. For evaluation of chemical purity of used titanium metal and possible impurity contribution to measured cross section of samples TiH_n, it was measured the total neutron cross section of such sample. In addition, for verification of this method the measurement of standard sample, where the stoichiometric ratio is well-known, was fulfilled. Polyethylene (CH_2) was used as a standard sample.

Neutron cross sections were researched with neutron beam transmission method using the investigated samples at horizontal channel of Research Reactor WWR-M. Neutron energy analysis has been done with neutron time of flight spectrometer [4]. Two types of spectrometer regime were used: energy resolution 0.9 mcs/m (energy range 0.0253 - 50 eV) and 0.055 mcs/m (energy range 2.5 - 18000 eV). The list of several investigated samples and the received results are placed in Table. As at titanium hydride example it is shown, that the measurement and analysis of total neutron cross sections for samples TiH_n allow to evaluate the value of ratio metal-hydrogen in hydride (n) with accuracy ~ 1 %.

Parameters of investigated samples, measurement regimes and analysis of results

Parameters of samples		Measurement regimes			Measured and calculated data	
Sample marking	Concentration, 10^{20} mol/cm^2	Neutron beam area, mm^2	Energy resolution, mcs/m	Energy range, eV	σ_t^{obs} (at E_n = 50 eV) barn	n - stoichiometric ratio
TiH_n - powder	166	1.5 × 11	0.9	0.0253 - 50	40.5 ± 0.30	1.87 ± 0.02
TiH_n- plate -1	235.1	1.5 × 11	0.9	0.0253 - 50	43.6 ± 0.50	2.03 ± 0.03
TiH_n- plate -2	234.9	1.5 × 11	0.9	0.0253 - 50	41.1 ± 0.40	1.90 ± 0.03
TiH_n- plate -1	235.1	45 × 20	0.055	2.5 - 18000	43.4 ± 0.24	2.02 ± 0.02
Standard sample (CH_2)						
Polyethylene -1	366	1.5 × 11	0.9	0.0253 - 50	45.8 ± 0.56	2.00 ± 0.03

1. T. P. Chernyaeva and A. V. Ostapov, Problems of Atomic Science and Technology. Ser. Physics of Radiation Effect and Radiation Material Science, (87) 5, 16 (2013).
2. V. F. Zelensky, Problems of Atomic Science and Technology. Ser. Nuclear Physics Investigations (85) 3, 76 (2013).
3. P. Khabibulayev and B. Skorodumov, *Nuclear Physics Methods for Determination of Hydrogen in Materials*, (Publishing House FAN, Tashkent, 1985), p. 96 (in Russian).
4. V. P. Vertebnyi, P. M. Vorona, A. I. Kalchenko *et al*., in *Neutron Physics, All Union Conference, Kyiv, 1971,* p. 24. Publishing House "Naukova Dumka", 1972. Part 2, p. 232 (in Russian).

EXCITON AUTOSOLITONS IN SEMICONDUCTOR QUANTUM WELLS UNDER THE SLOT IN METALLIC ELECTRODE

O. I. Dmytruk[1], V. I. Sugakov[2]

[1] *Taras Shevchenko National University, Kyiv*
[2] *Institute for Nuclear Research, National Academy of Sciences of Ukraine, Kyiv*

The paper presents a continuation of investigations of the indirect exciton condensation in double quantum well under the slot in the metalic electrode. An electron and a hole of the indirect exciton are separated in the space into different quantum wells that inhibits their mutual recombination, and as result the exciton has large value of a lifetime. The condensed phase has been considered phenomenologically taking into account the finite value of the exciton lifetime with the free energy in Landau - Ginzburg form [1, 2] .It was shown in the previous works, that at some values of the pumping G the uniform distribution of exciton density becomes unstable and a periodical distribution of the exciton condensed phase islands arises in the quantum well in the form of a chain oriented along the slot. The periodical structure exists at some interval of pumping $G_1 < G < G_2$. Outside of this interval the exciton density distribution is uniform along the slot. In this paper [2] we showed that in this region there are solutions in the form of localized islands of the condensed phase side by side the uniform solution. In the case of the dissipative system, which we investigate, these localized states may be called "static autosolitons". The autosolitons exist in some region of the pumping outside the regions where the periodical structure arises. At $G < G_1$ autosoliton has a shape of a peak (Fig. 1), and can be called "bright autosoliton" by analogy with the soliton's terminology. At $G > G_2$ the autosoliton manifestates itself in a form of a dip (Fig. 2, dark autosolitons). The autosoltons are situated in the quantum well under the center of the slot. With increasing the width of the slot the position of the soliton shifts to the one of the edges of the slot.

The autosolitons are excited by laser. They move in nonhomogeneous external fields and may be used in microscopic devices for the information transfer controlled by laser.

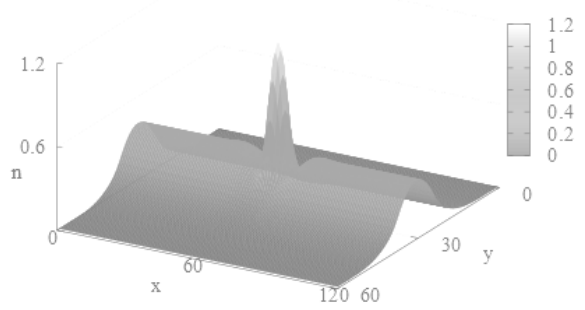

Fig. 1. Bright autosoliton.

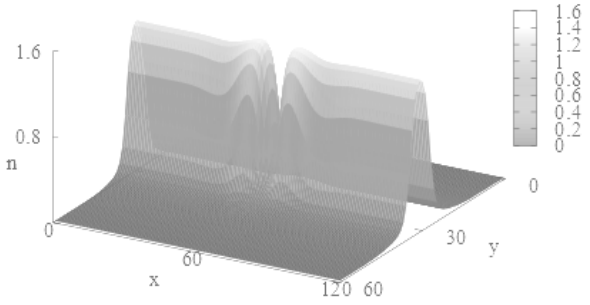

Fig. 2. Dark autosoliton.

1. V.I. Sugakov, J. Phys.: Condens. Matter **21**, 275803 (2009).
2. O.I. Dmytruk and V.I. Sugakov, Physica B: Condensed Matter **436**, 80 (2014).

EMISSION OF CONDUCTIVITY ELECTRONS FROM METALS, PRODUCED BY IONS

A. Ya. Dzyublik, V. Yu. Spivak

Institute for Nuclear Research, National Academy of Sciences of Ukraine, Kyiv

Lately the problem of secondary electron emission caused by the bombardment of solids by ions became acute due to construction of metal strip detectors [1]. Here we address the questions about ejection of the conductivity electrons from the conductivity band in metals, as well as the role of crystal environment. It is done in analogy with our treatment [2, 3] of the shake-off process of conductivity electrons, provided either by β decay of the nuclei or by electron capture and internal conversion, which lead to abrupt alteration of the Coulomb field governing electrons.

We treated conductivity electrons as an ideal gas confined in the potential well. We analyzed emission of the conductivity electrons from metals bombarded by ions, taking for the first time into account spreading of these electrons over the levels of the conductivity band, corresponding to different energies and momenta. We also took into account the attenuation of the electron wave excited by an ion inside the crystal, as well as its refraction at the crystal surface. The interaction between the ion and electrons was approximated by the screened Coulomb potential, with the screening length determined by the well known formula $r_0 = \left(\frac{E_F}{6\pi e^2 n_0} \right)^{1/2}$. It occurs to be equal 5.8 nm.

We performed numerical calculations of the electron yield produced by protons and deuterons incident on the golden film. For protons the results are presented in Fig. 1, when its energy ranges from 0 to 100 keV.

The protons with such energies have velocities of the same order of magnitude as the conductivity electrons on the Fermi level. Therefore the electrons are able to follow moving protons. In other words, a proton entering the crystal gives rise to polarization of electrons in the conductivity band, which then moves together with the proton inside the crystal. As a result, polarized cloud of electrons screens the Coulomb field of the projectile. However, this screening may be more weak than that in the case of a stationary charge embedded in a crystal. Respectively, the screening radius becomes larger than r_0 given above. Therefore in Figure we displayed also the curves for the screening lengths $2r_0$ and $3r_0$. We see that the yield of secondary electrons quickly falls down with decreasing screening length. Such behavior has simple explanation. With lowering screening radius the attractive Coulomb potential of the ion narrows, that is its effective attraction weakens. Then the conductivity electron, moving relative to the ion, spends less time in this potential well, that leads to lowering of the kinetic energy transfer probability from the ion to electron.

Notice that the emission curves for deuterons and protons, when plotted as a function of their velocities, completely coincide in correspondence with the observations [4].

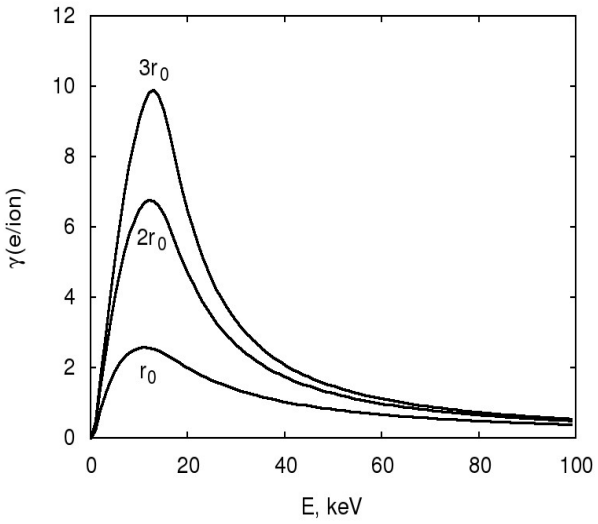

Dependence of the electron yield from Au on the energy of incident protons for different screening radii ($r_0 = 5.8$ nm).

1. V. Pugatch and O. Mykhailenko, Nucl. Instr. Meth. A**581**, 531 (2007).
2. A.Ya. Dzyublik and V.Yu. Spivak, Ukr. J. Phys., **53**, No. 2, 120 (2008).
3. A.Ya. Dzyublik and V.Yu. Spivak, Ukr. J. Phys., **55**, No. 4, 426 (2010).
4. B.A. Brusilovsky, Appl. Phys. A**50**, 111 (1990).

ROLE OF SCREENING IN COULOMB EXCITATION OF NUCLEI IN HOT PLASMA

A. Ya. Dzyublik[1], G. Gosselin[2], V. Méot[2], P. Morel[2]

[1] Institute for Nuclear Research, National Academy of Sciences of Ukraine, Kyiv
[2] CEA, Centre DAM-Ile de France, Arpajon, France

In hot plasma there are free electrons with energies sufficient for excitation of nuclei of ions. In papers [1, 2] it was analyzed the inelastic scattering of such electrons by nuclei, leading to their excitation. Analytic formulas for the excitation cross section of nuclei were derived using DWBA. However, the role of screening of the nuclear field both by bound atomic electrons and free electrons remained unclear. This point has been clarified in [3].

We have shown first that the electrons, surrounding the nucleus, influence only the central Coulomb field, which takes the form

$$V_c(r) = -\frac{Ze^2}{r} g(r), \qquad (1)$$

where $g(r)$ denotes the screening factor. At the same time, the residual Coulomb interaction providing the nuclear excitation remains unchanged. For numerical calculations we were choosing $g(r) = \exp(r / r_0)$, where r_0 is the screening radius, being calculated with the aid of the Debye - Hückel formula.

Now the incident and scattered electrons are described by the waves, distorted by the screened field (1). As usually, they are expanded in the partial waves, labeled by the orbital angular momentum l, and the Schrödinger equation for the radial wave functions $F_l(kr)$ is solved numerically. By using these wave functions, we calculated then the Coulomb excitation cross section $\sigma_{exc}(E)$ of nuclei by incident electrons with the energy E. When E approximates the threshold energy E_0 the cross section $\sigma_{exc}(E) \sim \mathrm{v}_f$, where v_f is the velocity of scattered electrons. We calculated $\sigma_{exc}(E)$ for the E2 transition in the nucleus ^{201}Hg from its ground state $3/2^-$ to the first excited state $1/2^-$ with the energy E_0 = 1.556 keV. The results are presented in Fig. 1 as a function of $\Delta E = E - E_0$ for a few values of the screening radii. The value $r_0 = 0.012$ nm corresponds to weakly ionized atoms, $r_0 = 0.3$ nm to highly ionized ions of hot plasma and $r_0 = 0.003$ nm with extremely dense plasma, which may be realized in dense stars. The line $r_0 = 0.3$ nm practically coincides with that, calculated for the unscreened Coulomb field [1]. A screening becomes essential only at $r_0 \sim 0.01$ nm, when ΔE varies in the interval from 0 to 6 keV. At subsequent decreasing of r_0 the cross section quickly falls down approaching the line calculated in simple Born approximation ignoring the central Coulomb field.

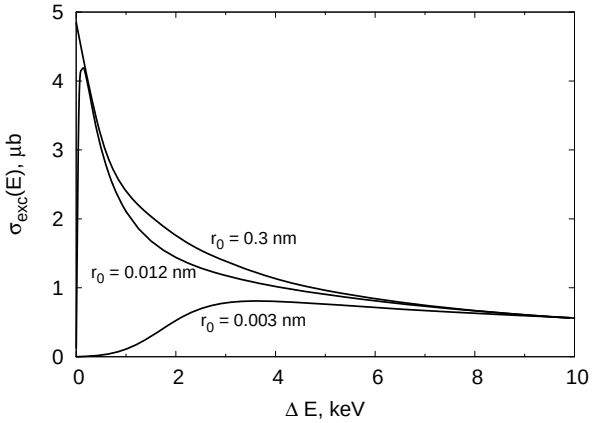

Fig. 1 Dependence of the Coulomb excitation cross section of ^{201}Hg on the energy of incident electrons.

We calculated also the Coulomb excitation rate of the nuclei Λ_{exc}, averaged over the distribution of electrons in energies. For the density of electrons $n_0 = 10^{20}$ cm^{-3} the results are displayed in Fig. 2.

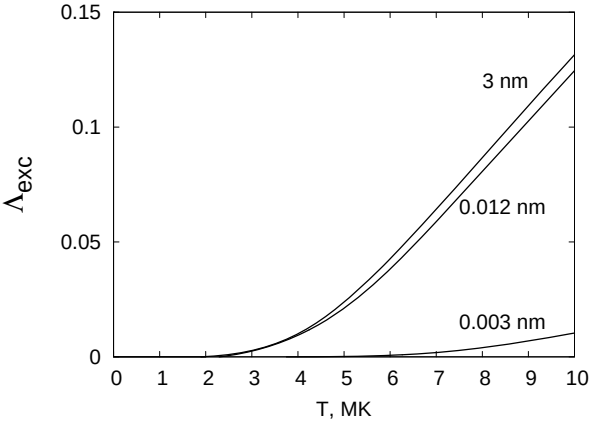

Fig. 2 Temperature dependence of the excitation rate of ^{201}Hg for the same screening radii.

1. G. Gosselin, N. Pilet, V. Méot *et al.*, Phys. Rev. C **79**, 014604 (2009).
2. E. Tkalya *et al.*, Phys. Rev. C **85**, 044612 (2012).
3. A.Ya. Dzyublik, G. Gosselin, V. Méot, and P. Morel, EPL **102**, 62001 (2013).

EXCITON STATES WITH PERMANENT DIPOLE MOMENTUM IN TYPE II $SI_{1-X}GE_X$ SEMICONDUCTOR QUANTUM WELLS

G. V. Vertsimakha

Institute for Nuclear Research, National Academy of Sciences of Ukraine, Kyiv

Semiconductor Si/SiGe type II quantum wells are extensively used to study collective effects of excitons [1] due to long lifetimes of dipolar excitons that can be created without external electric field application.

In $Si_{1-x}Ge_x/Si_{1-y}Ge_y/Si/Si_{1-x}Ge_x$ heterostructures with different Ge concentration in the neighbour layers the electron and the hole can be spatially separated in different quantum wells (see Figure, *a*). It leads to the creation of the exciton states with the permanent dipole momentum along the growth direction of the heterostructure.

To calculate the energy and the wave function of the lowest Wannier exciton state the variational method was used with the trial function

$$\Phi(\vec{r}, z_e, z_h) = f_e(z_e)\, f_h(z_h)\, \varphi(r),$$

where $\vec{r} = \vec{r}_e - \vec{r}_h$, $\vec{r}_{e(h)} = (\vec{\rho}_{e(h)}, z_{e(h)})$ are the electron (the hole) position, the axis z coincides with the growth direction, $\varphi(\vec{r}) = N\, e^{-r/\lambda}$, λ is the variational parameter, N is the normalization constant. To calculate the one-particle wave function for the heavy hole the numerical solution of the Schrodinger equation for the valence band edge profile the was obtained. The one particle wave function for the electron was calculated with the use of the variational method that was proposed in [2]. To calculate the band offsets on the interfaces of the heterostructure $Si_{1-z}Ge_z$ /$Si_{1-x}Ge_x$ the following expressions were used [3]:

$\Delta E_{hh}(x, z) = [0.74 - 0.07z][x - z]$ eV for the heavy hole subband of the valence band;

$\Delta E_e(x, z) = [0.67 - 0.093z][x - z]$ eV for Δ_2 - subband of the conduction band.

The following parameters were used for the calculations: the dielectric constant $\varepsilon = 12.7$, the effective masses of the heavy hole $m_{hh,z} = 0.27\, m_0$ and $m_{hh,\parallel} = 0.19\, m_0$, the effective masses of the electron for the Δ_2 - subband of the valence band $m_{e,z} = 0.92\, m_0$ and $m_{e,\parallel} = 0.19$ [4].

Obtained wave functions allow to calculate the dipole momentum of the state

$$\vec{P} = e\left(\langle z_h \rangle - \langle z_e \rangle\right)\vec{e}_z,$$

where e is the absolute value of the electron charge, $\vec{e}_z$ is the unit vector in the growth direction, $\langle z_{e(h)} \rangle$ is the average value of the electron (the hole) position in this direction. The dipole momentum exists even without applying an electric field and rises as the $Si_{1-y}Ge_y$ layer width rises due to the spatial separation of the carriers (see Figure, *b*). For the very thin $Si_{1-y}Ge_y$ layers the hole wave function penetrates to the left $Si_{1-x}Ge_x$ barrier layer and the asymmetrical shape of the wave function leads to the increasing of the dipole momentum.

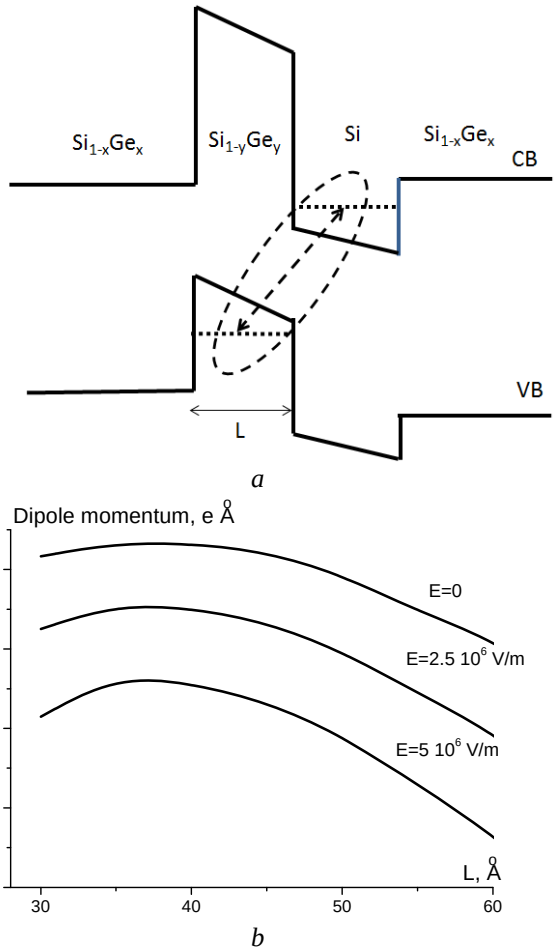

A schematic illustration of the system (*a*). Dependence of the dipole moment of the exciton state on the width of the $Si_{1-y}Ge_y$ layer for several values of the external electric field intensity (*b*).

1. T.M. Burbaev, V.S. Bagaev, E.A. Bobrik *et al.*, Thin Solid Films, **517**, 55 (2008).
2. A. Bellabchara, P. Lefebvre, P. Christol, and H. Mathieu, Phys. Rev. B **50**, 11840 (1994).
3. S. Galdin, P. Dollfus, V. Aubry-Fortuna *et al.*, Semicond. Sci. Technol. **15**, 565 (2000).
4. M.M. Rieger and P. Vogl, Phys. Rev. B **48**, 14 276 (1993).

ANALYTIC MODEL OF HOPPING TRANSPORT IN ORGANIC SEMICONDUCTORS INCLUDING BOTH ENERGETIC DISORDER AND POLARONIC CONTRIBUTIONS

I. I. Fishchuk,[1] A. K. Kadashchuk,[2] A. Köhler[3], H. Bässler[3]

[1] *Institute for Nuclear Research, National Academy of Sciences of Ukraine, Kyiv*
[2] *Institute of Physics, National Academy of Sciences of Ukraine, Kyiv*
[3] *Experimental Physics II and Bayreuth Institute of Macromolecular Research, Bayreuth, Germany*

We developed an analytical model to describe hopping conductivity and mobility in organic semiconductors including both energetic disorder and polaronic contributions due to geometric relaxation. The model is based on a Marcus jump rate in terms of the small-polaron concept with a Gaussian energetic disorder, and it is premised upon a generalized Effective Medium approach (EMA) yet avoids shortcoming involved in the effective transport energy or percolation concepts. In this approach the effective charge carrier conductivity σ_e can be calculated from the equation

$$\left\langle \frac{\sigma_{12}-\sigma_e}{\sigma_{12}+2\sigma_e} \right\rangle = 0 . \qquad (1)$$

Here σ_{12} is the conductivity in two-site cluster, and the angular brackets denote the configuration averaging. The effective charge carrier mobility μ_e can be calculated from the expression $\mu_e = \sigma_e / en$, where n is the charge carrier density.

It is superior to our previous treatment [1, 2] since it is applicable at arbitrary polaron activation energy E_a with respect to the energy Gaussisn disorder parameter σ. It can be adapted to describe both charge-carrier mobility and triplet exciton diffusion. The model is compared with results from Monte-Carlo simulations and is obtained very good coincides. In case of very low charge carrier density an expression for the effective mobility μ_e has the form

$$\mu_e \propto \exp\left[-\frac{E_a}{k_B T} - C\left(\frac{\sigma}{k_B T} \right)^2 \right]. \qquad (2)$$

If $E_a << \sigma$, we have Factor $C \cong 0.44$ and if $E_a >> \sigma$, we have $C \approx 0.1$. Factor C versus σ/E_a is presented in Figure.

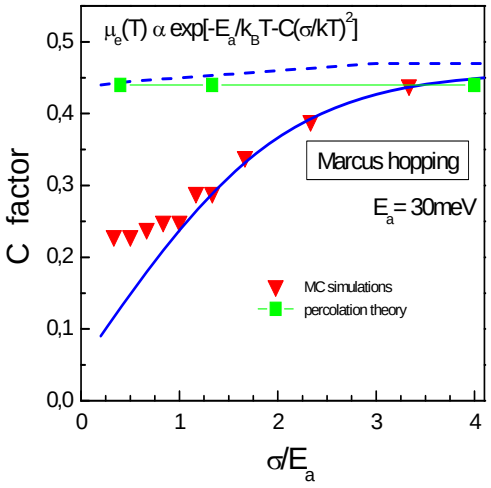

Factor C versus σ/E_a calculated by the present theory and theory of paper [3] (solid and dashed blue curves, respectively).

We show (i) that the activation energy of the thermally activated hopping transport can be decoupled into disorder and polaron contributions whose relative weight depend non-linearly on the σ/E_a ratio, and (ii) the σ/E_a ratio governs also the carrier concentration dependence of the charge-carrier mobility in the large-carrier-concentration transport regime as realized in organic field-effect transistors. The carrier density dependence becomes considerably weaker when the polaron energy increases relative to the disorder energy, indicating the absence of universality that is at variance with earlier results [3].

1. I. Fishchuk, V.I. Arkhipov, A. Kadashchuk *et al.*, Phys. Rev. B **76**, 045210 (2007).
2. I.I. Fishchuk, A. Kadashchuk, and H. Bässler, phys. stat. sol. (c) **5**, 746 (2008).
3. J. Cottaar, L.J. A. Koster, R. Coehoorn, and P.A. Bobbert, Phys. Rev. Lett. **107**, 136601 (2011).

SILICON PLANAR STRUCTURES AS DETECTORS FOR MICROBEAM RADIATION THERAPY

I. E. Anokhin, O. S. Zinets

Institute for Nuclear Research, National Academy of Sciences of Ukraine, Kyiv

Nowadays microbeam radiation therapy is widely used for cancer treatments [1]. It allows minimizing the side effects of irradiation using highly spatially fractioned X-ray beams of micrometers sizes. The extremely high dose rate (~20 kGy/s), laterally fractionated radiation field and steep dose gradients utilized in this therapy require the real-time readout and a high spatial resolution.

In the present work responses of silicon planar structures under different geometry of irradiation (front and lateral) have been studied. The spatial resolution and the efficiency of detectors are determined by the charge collection in the space charge region and in the diffusion region. Spatial resolution depends on geometry and sizes of the sensitive volume. The results of the calculations of the diode responses for edge on irradiation geometry for a simple physical model have been presented.

Measured response of a detector $R(x_0)$ (x_0 is the beam scanning position) for a beam with the intensity distribution profile F(x) can be written as follows

$$R(x_0) = \int_{-\infty}^{\infty} U(x_0 - x)F(x)dx = \int_{-\infty}^{\infty} U(x')F(x_0 - x')dx' ,$$

where $U(x_0 - x)$ is a response function on δ-function beam profile.

Analysis of the response with known functions $F(x)$ and $U(x_0 - x)$ allows obtaining required the position resolution of detectors.

The diode response $R(x_0)$ is proportional to the diode current and is determined by absorption x-ray in the diode and charge collection in the space charge region (SCR) and the diffusion region.

The contribution from space charge region is equal to the current

$$J_{SCR} = \int_0^{w_{scr}} g(x, x_0)dx ,$$

where $g(x, x_0)$ is the generation rate of electron-hole pairs under irradiation, w_{SCR} is the width of SCR.

Contribution of the generation in the diffusion region to the diode current is

$$J_{diff} = eD_n \left.\frac{d\Delta n(x, x_0)}{dx}\right|_{x=w_{scr}} ,$$

where $\Delta n(x, x_0)$ is the excess carriers density in the diffusion region.

In the case of a low resistivity base of a diode the $\Delta n(x, x_0)$ were found from the solution of diffusion equation with corresponding boundary conditions.

The response function $U(x_0)$ for our model can be obtained analytically as functions of w_{SCR}, the diffusion length (L_{diff}) and width of the detector base (w_{base}).

The total response of diode is

$$J_{total}(x_0) = J_{SCR}(x_0) + J(x, x_0)\big|_{x=x_0} .$$

The measured response of sequences of microbeams [2] (Fig. 1a) may be described analytically using the stepwise response function. The calculated response on the sequence of rectangular microbeams is shown in Fig. 1b.

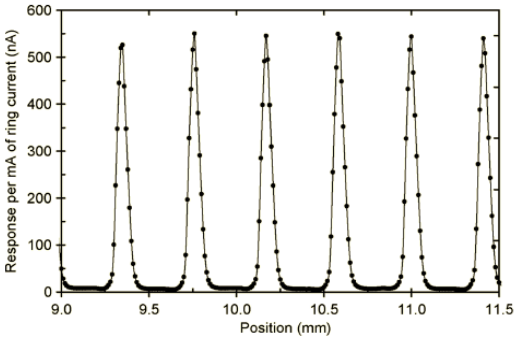

Fig. 1a. The experimentally measured central microbeams.

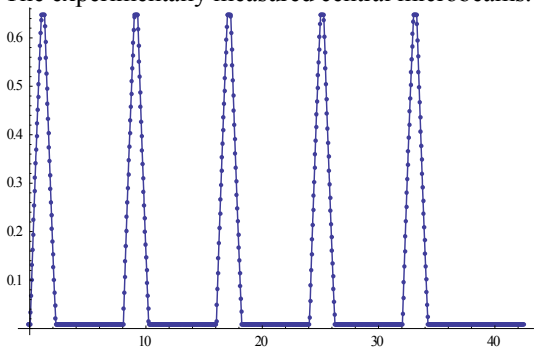

Fig. 1b. The calculated response for rectangular beams (w_{beam} = 62 μm, $w_{SCR} + L_{diff}$ = 62 μm, w_{base} = 50 μm).

Comparison of the experimental results with the analytical ones shows that real beams have rectangular profile with the beam width approximately equal to the width of the response function (~$w_{scr} + L_{diff}$).

Details of calculation have been presented in [3].

The experimentally observed response can be well described in a simple physical model.

1. E. Bräuer-Krisch, R. Serduc, E.A. Siegbahn *et al.*, Mutation Research **704**, 160 (2010).
2. M.L.F. Lerch, M. Petasecca, A. Cullen *et al.*, Radiation Measurements **46**, 1560 (2011).
3. I. Anokhin, O. Zinets, A. Rozenfeld *et al.*, IEEE NSS-MIC 2013, Conference records NP-44, p.164.

IRRADIATION EMBRITTLEMENT OF WWER-1000 RPV WELDS AT HIGH NEUTRON FLUENCE: SURVEILLANCE TEST EXPERIENCE

V. M. Revka, L. I. Chyrko, O. V. Trygubenko

Institute for Nuclear Research, National Academy of Sciences of Ukraine, Kyiv

Thirteen NPP units with WWER-1000 reactor pressure vessel are operated in Ukraine now. In order to ensure RPV safe operation during the design life time the changes in mechanical properties of RPV beltline materials are periodically assessed in line with the surveillance program requirements. For this purpose the static tension, Charpy impact and static fracture toughness tests are carried out. The radiation hardening and embrittlement rate of RPV materials are assessed using surveillance test data.

In this paper the Charpy impact test data are considered for unit 3 and 4 of Zaporizhya NPP. The experimental results for weld metal were included to the analysis. The WWER-1000 RPV welds are fabricated of Cr-Ni-Mo steel (wire Sv-12Ch2N2MAA). These welds have the high nickel (1,55 and 1,7 % wt) and medium manganese (0,67 and 0,65 % wt) contents for the NPP, unit 3 and 4, respectively. The copper content in materials is not more than 0,05 % wt. The Charpy V-notch specimens were irradiated with the maximum lead factor of 3,5 in the neutron fluence range (8,6 ÷ 75,5)·10^{22} m^{-2} at the temperature about 300°C. The highest fluence was accumulated in specimens during 24 fuel cycles (~ 154154 effective hours).

The design of the surveillance assemblies and their location in WWER-1000 reactor pressure vessels lead to their irradiation with the non-uniform neutron flux. As a consequence there is a relatively high scatter of neutron fluence for the specimen sets which are used to evaluate the radiation shift of transition temperature. To meet PNAE G-7-002-86 requirements regarding the fluence scatter the reconstituted specimens have been tested in addition to the standard surveillance program. The electron beam welding technique was applied for the specimen reconstitution.

The analysis of tensile test data has shown the fluence dependences of yield strength increase is consistent with hardening model $\Delta R_{p0.2} = B_F \cdot (F)^{1/3}$. Furthermore, it has been found out that ZANPP-4 RPV weld is more susceptible to irradiation than ZANPP-3 RPV with the yield strength increase. This outcome is most probably related to the higher Ni and Cu content for ZANPP-4 RPV weld comparing to ZANPP-3.

In addition the Charpy impact tests were carried out to estimate the ductile-to-brittle transition temperature shift ΔT_F and the irradiation embrittlement coefficient A_F (which is a functional equivalent of the chemistry factor) for the studied materials. The maximum shift ΔT_F owing to the neutron irradiation is 71°C. The analysis of fluence dependences of the transition temperature shift has shown the design embrittlement curve in the form of $\Delta T_F = A_F \cdot (F)^n$ with the power exponent n = 1/3 to describe well the experimental results (see Figure).

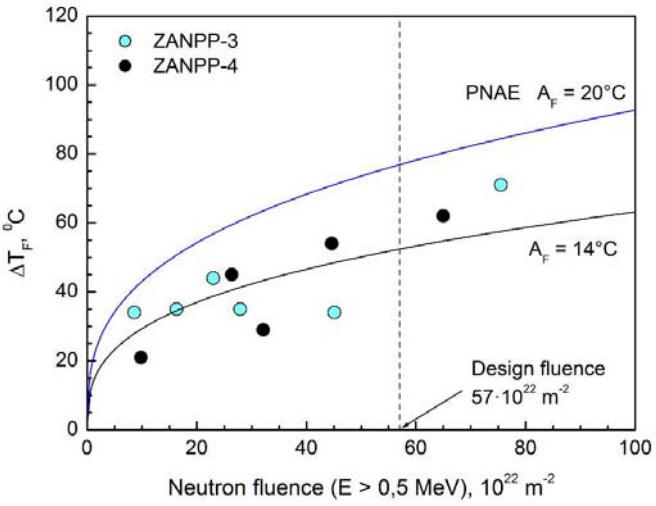

Irradiation embrittlement rate for WWER-1000 RPV weld metal (ZANPP-3 and ZANPP-4).

Furthermore, the surveillance test data for the studied welds allow to conclude that the enhanced embrittlement related to late blooming phases is not observed in spite of high nickel content. The irradiation embrittlement rate is in line with PNAE G-7-002-86 design requirements (A_F = 20°C) up to the neutron fluence 75,5·10^{22} m^{-2}. In addition, the fracture toughness test data for the high fluence values confirm the Charpy impact test results. This outcome can be explained by relatively low Mn content (~ 0,65 % wt) in weld metal.

RPV STEEL STRENGTH CHARACTERISTIC MODIFICATIONS UNDER LONG-TERM IRRADIATION

V. M. Revka, O. V. Trygubenko, Yu. V. Chaikovskyi, L. I. Chyrko

Institute for Nuclear Research, National Academy of Sciences of Ukraine, Kyiv

Understanding the mechanisms of the radiation damage and the change of mechanical properties of nuclear reactor vessel steels is the important task for the whole reactor facility safe operation substantiation. Of late more and more attention is given to the irradiation effect on the vessel material hardening [1]. This issue has been indeed actual during several decades but the majority of works are devoted to the effect of the accelerated irradiation on the steel hardening [2].

The possibility to analyze the RPV steel degree of hardening in the conditions of the long-term neutron irradiation by means of the testing the unloaded from the reactor surveillance specimens that accumulated the fluence close to the design one has appeared recently. The surveillance specimens are irradiated in the conditions similar to those of the reactor vessel inner wall (fluence, rate of fluence rise, temperature) Therefore, the results of their testing will present the most precise characteristics of the reactor vessel metal strength after irradiation.

The aim of this paper is determination of the irradiation effect on the RPV steel hardening, i.e. both obtaining the experimental dependence of the strain-hardening coefficient on the fast neutron fluence at the long-term irradiation of a metal during the power reactor operation and comparison of the RPV steel hardening data obtained by the surveillance specimens testing with the known in the literature experimental data obtained under the accelerated irradiation.

To obtain the strength characteristics uniaxial tensile testing of 3 mm in diameter and with 30 mm effective length cylindrical specimens has been carried out. The specimens were irradiated in the reactor at the temperature of ~ 300°C during 24 fuel campaigns at the neutron flux density ~ 10^{15} neutr/m^2/s. During this period the maximum accumulated by the base metal fast neutron fluence (E > 0,5 MeV) constituted $55{,}6\cdot10^{22}$ neutr/m^2 and that of the weld metal was $73\cdot10^{22}$ neutr/m^2.

The strain-hardening coefficient m was determined by the formula

$$R = K\cdot\varepsilon^m,$$

where R is a tensile stress; K is a strength factor; ε is a specimen deformation.

The results of investigations show the m value to decrease with the accumulating the fluence for the base and weld metals (see Figure), i.e. the section of the chart corresponding to the specimen uniform elongation becomes more sloping and the yield point limit value approaches the strength boundary R_m, this is the result of the steel hardening under the irradiation effect.

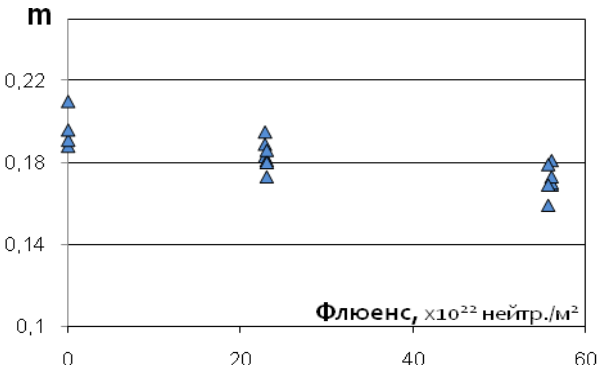

Coefficient m vs fast neutron fluence for weld metal at test temperature 350 °C.

Besides, the comparison of the steel hardening levels owing to the accelerated irradiation in the research reactors and the long-term irradiation in the commercial reactors during operation demonstrates the relation change of $R_{p0,2}/R_m$ to be practically the same in both cases. But it should be pointed that such a change is rather noticeable since the stable growth of $R_{p0,2}/R_m$ and coefficient m decrease are observed with the fluence accumulation.

1. A. Ballesteros, R. Ahlstrand, C. Bruynooghe *et al.*, Progress in Nuclear Energy **53**, 756 (2011).
2. N.N. Alekseenko, A.D. Amaev, I.V. Gorynin, and V.A. Nikolaev *Radiation damage of water-water reactor vessel steel*, edited by I.V. Gorynin (Energoizdat, Moscow, 1981), 192 p.

WWER-1000 RPV HEAT AFFECTED ZONE MECHANICAL PROPERTIES ASSESSMENT BASED ON SURVEILLANCE TEST DATA

V. M. Revka, L. I. Chyrko, O. V. Trygubenko

Institute for Nuclear Research, National Academy of Sciences of Ukraine, Kyiv

According to the surveillance program requirements in Ukraine a radiation embrittlement of RPV materials is being evaluated using surveillance test data for base and weld as well as heat affected zone metal. In order to estimate the radiation embrittlement rate the regulatory guide PNAE G-7-002-86 requires using the Charpy impact test data. However, an experience has shown that HAZ metal in unirradiated and irradiated condition reveals a high scatter in the test data to get the Charpy curve. It is related to a position of V-notch on the Charpy specimen. This issue does not allow to determinate the radiation shift of transition temperature reliably. So the Charpy impact test data for HAZ metal is not considered in the analysis of RPV material embrittlement.

Nevertheless in this study the surveillance test data for HAZ metal has been analyzed in view point of radiation hardening and embrittlement in comparison to base and weld metal. For the analysis the tensile and Charpy impact test results have been used for nine WWER-1000 reactor pressure vessels for which the HAZ surveillance test data are available.

The RPV materials (base, weld and HAZ metal) for nine NPP units with WWER-1000 type reactor were included in the analysis. Specimens were irradiated in the standard surveillance capsules up to the neutron (E > 0,5 MeV) fluence of $68{,}7\cdot10^{22}$ m^{-2}. Irradiation temperature was about 300°C. The surveillance specimens were irradiated by neutron flux of about 10^{15} m^{-2}/sec that is usual for WWER-1000 type reactor irradiation condition.

The analysis has shown in the most cases the initial T_{KI} temperature for base metal is lower or comparable to that of HAZ metal. In addition the radiation embrittlement rate obtained from surveillance test data for HAZ relative to base and weld metal is represented in Figure where the ratio of A_F coefficients (chemistry factors) for RPV materials (i.e. $\frac{A_F^{HAZ}}{A_F^{Base}}$ and $\frac{A_F^{HAZ}}{A_F^{Weld}}$) is used. For all reactor pressure vessels considered the radiation embrittlement rate for HAZ metal is lower than for base and/or weld metal with the exception of unit Y. This outcome is most probably related to a comparatively high content of copper (0,12 % wt) and phosphorus (0,01 % wt) in the unit Y lower shell. Furthermore, the embrittlement rate of HAZ metal for a unit W reactor pressure vessel is higher in comparison to weld metal that is also unusual for RPV materials considered.

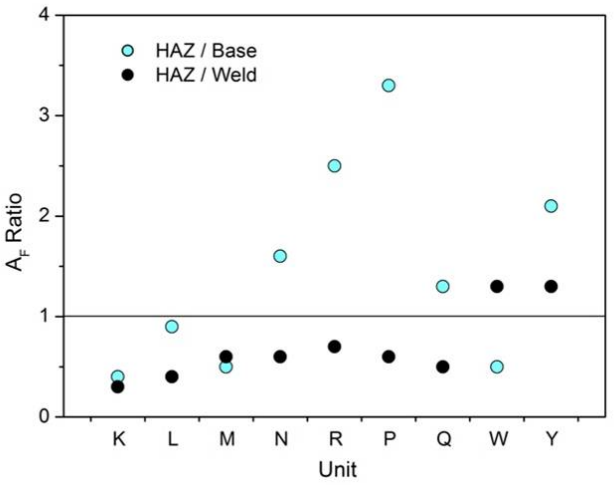

Fig. 1. Radiation embrittlement rate for HAZ relative to base and weld metal.

In addition the analysis has shown the relation between the yield strength increase and transition temperature shift due to irradiation for RPV materials results in a factor of 0,6 in average. This outcome is close to a known empirical correlation $\Delta T_{41J} = 0{,}7\cdot\Delta R_{p0.2}$ for pressure vessel steels [1]. However, for the unit Y heat affected zone metal the high embrittlement rate is not consistent with radiation hardening considering the abovementioned correlation that can be associated with additional radiation damage mechanism.

1. G.R. Odette, P.M. Lombrozo, and R.A. Wullaert in *Effects of Radiation on Materials* (*12th Int. Symp.*), *ASTM STP 870* (Philadelphia, PA, 1985), p. 840.

MIG-053 – COMPACT GAMMA-SPECTROMETER FOR THE ANALYSIS OF FOOD AND BUILDING MATERIALS

O. A. Berzin[3], I. M. Vishnevskyi[1], S. A. Karpenko[2], T. V. Mykytiuk[1], E. E. Petrosyan[1], S. S. Pogulay[1], V. N. Pryymak[2], M. V. Shestakov[4]

[1] Institute for Nuclear Research, National Academy of Sciences of Ukraine, Kyiv
[2] Concern SouzEnergo, Novomoskovsk, Dnipropetrovsk region
[3] Positron GmbH, Zhovti Vody, Dnipropetrovsk region
[4] NPK "Spectrum", Kyiv

Modern gamma-spectrometers are complex and expensive devices with specialized software that requires special training of the user. Usually, gamma-ray spectrometers have the heavy and bulky low-background lead shielding. As often in practice during as field and laboratory measurements do not require high accuracy measurement. The creation of small or portable gamma-ray spectrometers, for work directly on the point of measurement is actually. [1]

In this paper was developed inexpensive compact scintillation gamma-spectrometer MIG-053 (see Figure), for analysis of food products and building materials for the presence of natural and man-made radionuclides. The detector block of the gamma-ray spectrometer is based on the crystal NaI(Tl) 25 × × 25 mm with a resolution of 10 % for the 662 keV. The thickness of the lead shielding is 15 mm, which provides attenuation of gamma-rays in the background to 1.5 times the energy of 1.5 MeV. Based on the accumulated spectra, cesium-137, K-40, and the background were determined by the minimum detectable activity - 17.7 and 230 Bq, respectively. This makes it suitable for the analysis of most food products of all classes and building materials.

Control of the spectrometer is performed using a PC via a specially created program with the ability to import spectrometric data in MS Excel. To calculate the activity of the radionuclide is used method of regression analysis [2]. Program of calculation of the activities is implemented in MS Excel 2010.

Weight MIG-053 protection does not exceed 12 kg, that makes it easy to ship that device and install on-site measurements. MIG-053 spectrometer can be used in medical institutions, research and university laboratories.

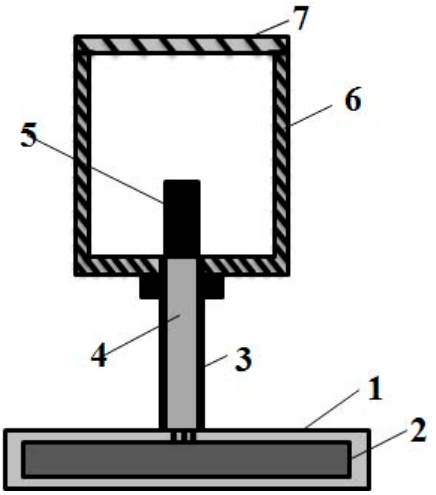

1 - metal stand; *2* - power supply of PMT and analyzer of pulse signals; *3* - a metal tube; *4* – PMT; *5* - crystal NaI(Tl); *6* - lead shielding; *7* - lead cover shielding.

1. A. Bezshyyko, I.M. Vyshnevskyi, R.V. Denisenko *et al.*, Nucl. Phys. At. Energy **12,** No. 4, 400 (2011).
2. N. Draper and H. Smith, Applied Regression Analysis. Multiple regressions, 3rd ed. (Dialectics, M., 2007).

EFFECT OF THERMAL ANNEALING AND COOLING CONDITIONS OF P-DOPED *n*-Si CRYSTALS ON THE TEMPERATURE DEPENDENCES OF THE CHARGE CARRIER MOBILITY IN THE IMPURITY SCATTERING REGION

G. P. Gaidar

Institute for Nuclear Research, National Academy of Sciences of Ukraine, Kyiv

The problem of the control of the physical properties of semiconductors by various treatments is particularly topical regarding silicon because of the development of new technological materials and applications [1, 2]. The single crystals of silicon used in the microelectronics and instrument-making industries materially alter their physical characteristics under the influence of various physical actions [3].

The following are the results of the experiments carried out on Czochralski-grown crystals of P-doped *n*-Si with specific resistance of $\rho_{300K} \approx 0.3$ Ohm cm grown along the [001] direction under nitrogen. The purpose of the carried out experiments is the detection of the influence of the thermal annealing and the cooling conditions on the charge carrier mobility μ within the temperature range of $20 \le T \le 300$ K, which overlapped (for a predetermined level of doping of the crystal) the range from the region of mainly impurity scattering to the region of mainly phonon scattering. High-temperature ($T_{ann} = 1200$°C, $t = 2$ h) and low-temperature ($T_{ann} = 500$°C, $t = 2$ h) annealings were used in this work. The crystals were cooled from T_{ann} to $T = 300$ K in various modes: with a rate of ~1000°C/min (rapid cooling) and ~1°C/min (slow cooling).

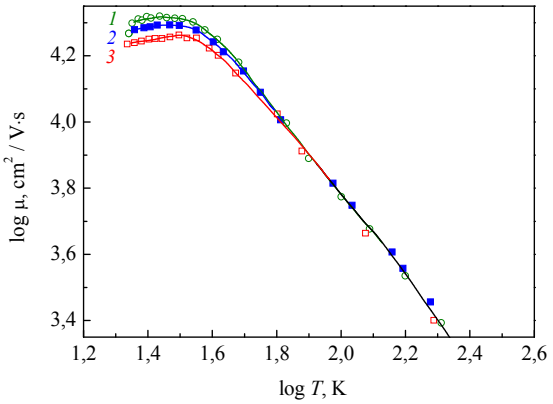

Fig. 1. Temperature dependences of the charge carrier mobility $\log\mu = f(\log T)$ for samples of P-doped *n*-Si ($\rho_{300K} \approx 0.3$ Ohm·cm): virgin (*1*); after high-temperature annealing at 1200°C and cooling: slow cooling (~1°C/min) (*2*); rapid cooling (~1000°C/min) (*3*).

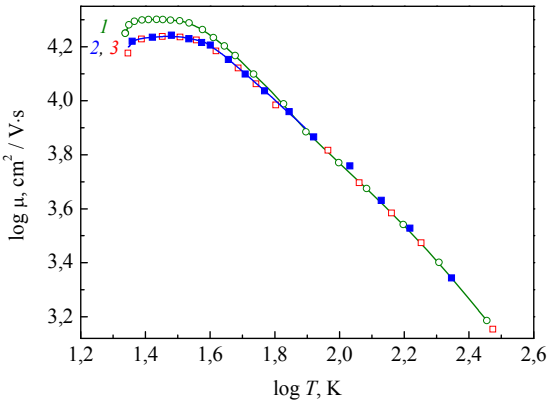

Fig. 2. Temperature dependences of the charge carrier mobility $\log\mu = f(\log T)$ for samples of P-doped *n*-Si ($\rho_{300K} \approx 0.3$ Ohm·cm): virgin (*1*); after annealing at 500°C and cooling: slow cooling (~1°C/min) (*2*); rapid cooling (~1000°C/min) (*3*).

Electrical conductivity and Hall measurements were carried out for the virgin crystals and the crystals after the designated thermal annealings (with the respective cooling rates from the temperature of T_{ann}). The dependences of the charge carrier mobility on the temperature $\log\mu = f(\log T)$ calculated based on the data of the Hall measurements for all these cases are exhibited by the respective curves in Fig. 1 (for the crystals annealed at 1200 °C) and Fig. 2 (for the crystals annealed at 500 °C).

It is found that, in the region of mainly impurity scattering, the behavior of the charge carrier mobility $\mu = \mu(T)$ of the P-doped *n*-Si (Cz) at cooling with various rates on the temperatures of the thermal annealing essentially depends on the temperature of the annealing of the silicon crystal that was cooled further. Second, the dependences $\mu = \mu(T)$ within the area of mainly impurity conductivity of the crystals of *n*-Si annealed under high temperatures (1200 °C) appear to be more sensitive to the character of the cooling of the samples or to the temperature of the annealing than the samples annealed at lower (500 °C) temperatures.

The results obtained in this work should be taken into account both at the development and substantiation of the technology of solid-state devices manufacturing and at determining the quality of the source raw materials that are the basis of the devices development.

1 S. Oda, Mat. Sci. Eng. B **101**(1-3), 19 (2003).
2 J. Vanhellemont, E. Simoen, J. Electrochem. Soc. **154**(7), H572 (2007).
3 V. M. Talanin and I. E. Talanin, Izv. Vyssh. Uchebn. Zaved., Materialy Elektronnoi Tekhniki (4), 4 (2002).

DOSE EFFECTS IN SILICON IRRADIATED WITH HIGH ENERGY LIGHT IONS

V. I. Varnina[1], A. A. Groza[1], P. G. Litovcheno[1], L. S. Marchenko[1], M. B. Pinkovska[1], V. M. Popov[2], M. I. Starchyk[1], H. G. Shmatko[1], M. L. Dmytruk[3], O. S. Kondratenko[3]

[1] Institute for Nuclear Research, National Academy of Sciences of Ukraine, Kyiv
[2] Research Institute of Microdevices, Kyiv
[3] Institute of Semiconductor Physics, National Academy of Sciences of Ukraine, Kyiv

Study of optical and structural properties of Si irradiated with 6.8 MeV hydrogen (protons) and 27.2 MeV helium (a-particles) ions with nearly the same projective range had shown that at high doses new conditions of radiation defects' creation appeared due to defects' interactions.

When proton fluence increases from $1{,}9 \cdot 10^{17}$ см$^{-2}$ to $3 \cdot 10^{17}$ см$^{-2}$, the 477 см$^{-1}$ line (forbidden previously by the crystal symmetry law) is discovered and bands, connected with one-phonon and Si-H-bonds' bounded absorptions in IR- absorption spectra vanish (Fig. 1). It testifies about decrease of the role of point defects and increase of the probability of their interactions.

From selective etching experiment and raster electron microscopy the "walls" of defects placed perpendicularly to the direction of irradiation were observed in the projective range of ions (Fig. 2). Number of walls depends on ion beam intensity.

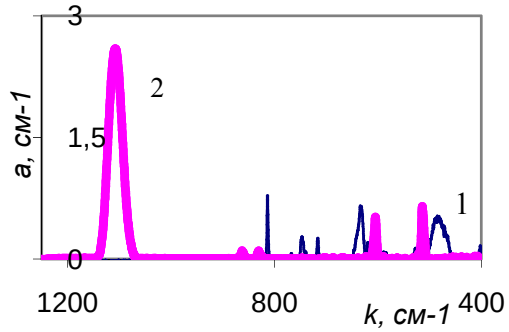

Fig. 1. Differential absorption spectra of Si for proton doses: *1* - $1.9 \cdot 10^{17}$ cm^{-2}; *2* - $3 \cdot 10^{17}$ cm^{-2}.

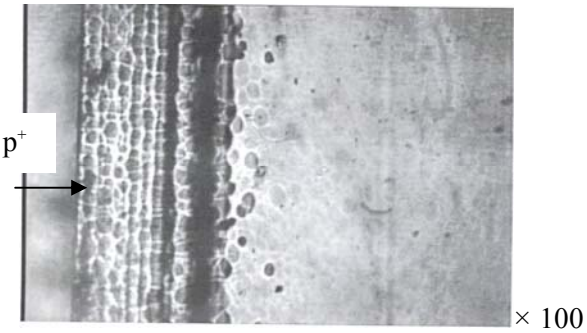

Fig. 2. The picture of selective etching of Si irradiated with a-particles, fluence 1×10^{17} см$^{-2}$.

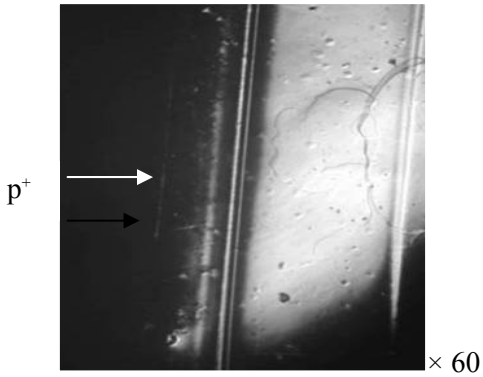

Fig. 3. The picture of selective etching of Si irradiated with protons, fluence $3{,}0 \cdot 10^{17}$ см$^{-2}$.

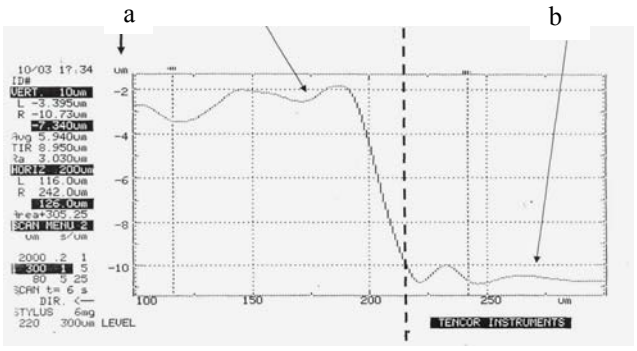

Fig. 4. Microprofilogram of the surface (cross-section) of alpha-irradiated silicon in the ion projective range (*a*) and beyond it (*b*). The dashed line points the straggling position.

In the case of $(3 - 3{,}5) \cdot 10^{17}$ cm^{-2} proton irradiation the "wall"-like defects were extended beyond ion stopping region at the depth equaled to the double ion projective range (Fig. 3).

For α-particles $1 \cdot 10^{17}$ см$^{-2}$ such effect was observed only by raster electron microscopy.

Microprofilogram of the surface (cross-section) of alpha-irradiated silicon fixes the essential difference of surface profile in the pass and beyond ion projective range due to the creation in the first case vacancy complexes and helium deposition (Fig. 4).

Received from multiangle monochromatic ellipsometry the sharp changes of silicon complex refractive index at fluences $1 \cdot 10^{17}$ cm^{-2} for protons as well as for a-particles testify also about changes of conditions of defects' creation.

Summing, at high energy proton and a-particle irradiation of Si new stage of defects' ordering due to their self organization appears. The spreading of defect "walls" beyond ion projective range testifies about long range effect.

ELECTRIC-OPTICAL PROPERTIES OF $GaAs_{1-x}P_x$ LIGHT EMITTING DIODES

O. V. Konoreva, V. P. Tartachnyk, E. V. Malyj, I. V. Petrenko, V. M. Popov*, M. B. Pinkovska

Institute for Nuclear Research, National Academy of Sciences of Ukraine, Kyiv
**Research Institute of Microdevices, Kyiv*

GaP light-emitting diodes due to their simplicity and cheapness are widely used in industry and housekeeping. Diode structures fabricated on the base of GaAs-GaP solid solutions and geterostructures makes it possible to widen the spectral luminescence band and to shift it maximum into necessary direction. While doping the material by izoelecton nitrogen impurities the luminescent centres, the exciton bond energy on which is fixed according to the bottom of C-zone, ensure the receiving of effective orange, red and yellow emitters. High brightness is obtained if x value in $GaAs_{1-x}P_x$ is close to 0.4, when material becomes flat-zone-type and probability of luminescent recombination grows.

As main luminescent and electrical properties of GaP LEDs had been studied before it was desirable to compare its with characteristics of devices made on composite materials.

In given paper the results of electrical-optical characteristics of orange, red and yellow LEDs desighed on the base of solid solution $GaAs_{1-x}P_x$ were studied. Electroluminescence spectra and current-voltage characteristics of diodes were measured in 77-300 K temperature interval.

Spectral curve posess emitting lines of excitons and their phonon replica. The most intensive is the line, connected with recombination of exciton, bounded on the pair of neghborous nitrogen atoms. The intensity of the line displais the sharp temparature dipendence and drops while temperature increases.

As in the case of GaP LEDs, the regions of the negative defferential resistance (NDR) appear on voltage-current characteristics while measuring in the current generating mode at temperatures below 145K (see Figure). The direct current characteristics of $GaAs_{1-x}P_x$ LEDs desintegrates onto two separate parts.

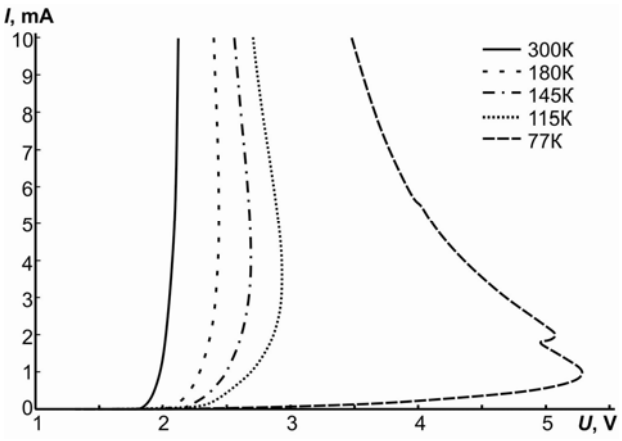

Direct part of voltage-current characteristics of $GaAs_{1-x}P_x$ LEDs at different temperatures.

One can consider that the pecularities observed are formed in the process of capture of free charge carriers by the deep levels located in the borders of i-layer of p-n- junction.

The existance of LEDs in the instability conditions might be used in order to desighn on its origin the generator of low temperature light vibrations.

ANALYSIS OF MODERN METHODS FOR REGISTRATION OF IONIZING RADIATION AND THE FUTURE TRENDS FOR DEVELOPMENT OF SEMICONDUCTOR DETECTORS

G. P. Gaidar, O. V. Tretyakova, I. M. Vyshnevskyi

Institute for Nuclear Research, National Academy of Sciences of Ukraine, Kyiv

With the development of methods for registration of ionizing radiation, their role increases in the study of various phenomena, and now hard to find such field of knowledge where these methods have not been applied. For example, the radiation physics, radiation genetics, radiation chemistry, physics of elementary particles, astrophysics, medicine, geology and other areas are directly connected with the use of radiation detection methods.

In contrast to measurements of many continuous physical quantities in the classical physics (mass, speed, distance, time), measuring of ionizing radiation characteristics has a discrete character. This is due to the fact that all carriers of such radiation are the separate particles or quanta of the electromagnetic field. By the continuous quantities we can pass only in the integral approximation. Depending on the type of particles that must be registered and the intensity of the radiation fields, different types of detectors are used, respectively.

The authors made a detailed analysis of modern methods for registration of ionizing radiation, the features of semiconductor detectors were considered. Their place among other detection methods was determined; the future trends for their development were discussed, as well as the material for publication as a review was prepared. Special attention is drawn to the study of different types of detectors, which are developed and investigated depending on the specific nuclear-physics problems directly in KINR of NAS of Ukraine, particularly in the Departments of High Energy Physics, Nuclear Structure, Radiation Physics, in the Laboratory of Plasma Technologies.

Modern methods of research on the charged particle beams and synchrotron radiation make rigid terms regarding the size and stability of the beam position in the space. The technology for production of hyperfine (2 μ) metal-film microstrip detectors (MMD) based on the microelectronic photolithography and plasma-chemical etching, capable to register the ionizing radiation fluxes over a wide energy range and intensity, was developed in KINR of NASU.

In comparison with known sensors of other type, MMD have an indisputable advantage [1], since they are characterized by parameters such as transparency, radiation hardness (> 100 MGy), high spatial resolution (up to 2 μ), a unique production technology, low operating voltage (up to 20 V) [2]. MMD prototypes made by the developed technology have been successfully tested on the beam of synchrotron radiation in the research centre DESY (Hamburg, Germany).

Among the devices of nuclear spectrometry an important place is occupied by semiconductor detectors [3]. In KINR of NASU the following types of detectors with different operational characteristics are developed and manufactured: surface-barrier detectors of total absorption (E-detectors) based on high-resistance silicon of n and p type conductivity for spectrometry of nuclear radiation; detectors of specific losses of charged particles (dE/dx-detectors) for the use in telescopes to determine the mass spectrum of charged particles that are involved in the complicated nuclear reactions; drift silicon-lithium detectors (Si(Li))-detectors) based on silicon compensated with lithium for spectrometry of charged particles. Detectors have high energy resolution, considerable working area and wide range of sensitive area thickness.

Detectors designed and manufactured in KINR of NAS of Ukraine are used in various fields of science and technology (spectrometry of nuclear radiation, detectors of neutron, α-, β-, γ-radiation, precise measurements of the spatial distribution of radiation fields, etc.), in the nuclear-physics measurements on accelerators of the charged particles (Dubna, CERN).

According to the analysis conducted by the authors of the review, priority directions of research for getting more perfected semiconductor detectors, in particular, based on silicon, were determined.

1. V. Pugatch, V. Aushev, C. Bauer *et al.*, Nucl. Instr. Meth. **A535**, 566 (2004).
2. O.S. Kovalchuk, V.M. Pugatch, O.A. Fedorovych *et al.*, in *Book of Abstracts. Annual Scientific Conference* (*KINR of NAS of Ukraine, 28 January – 1 February, 2013*), p. 17.
3. G. Lutz, *Semiconductor radiation detectors* (Springer, 1999), 350 p.

Abstracts of works on plasma physics

GEODESIC ACOUSTIC MODE IN TOKAMAKS: LOCAL CONSIDERATION AND EIGENVALUE ANALYSIS*

Ya. I. Kolesnichenko, B. S. Lepiavko, V. V. Lutsenko

Institute for Nuclear Research, National Academy of Sciences of Ukraine, Kyiv

A set of MHD equations describing the Geodesic Acoustic Mode (GAM) in tokamak plasmas is derived. The obtained equations take into account the presence of the energetic ions and allow to study energetic-ion-driven GAM instability perturbatively or non-perturbatively (EGAM mode). They are applicable to plasmas with $\overline{\beta} q^2 \le 1$, where $\overline{\beta} = \beta_s / (1+\beta_s)$, $\beta_s = c_s^2 / v_A^2$, c_s is the sound velocity, v_A is the Alfvèn velocity, q is the tokamak safety factor. Using these equations, GAM/EGAM instability is studied in a local approach and by means of the eigenvalue analysis. It is shown that β-coupling (the coupling of Fourier harmonics of the perturbation due to finite β-ratio of the plasma pressure to the magnetic field pressure - and the curvature of the field lines) can be responsible for the radial structure of the GAM-mode.

A conclusion is drawn that conditions for the GAM/EGAM instability to arise are mildest in the case of counter-injection of energetic ions with pitch angles $\chi^2 < 0.6$ and large ratio of Larmor radius of the energetic ions to a characteristic length of inhomogeneity of these ions. A numerical code solving the derived equations is developed. Specific calculations are carried out for tokamaks with a non-monotonic safety factor. On the other hand, it is found that due to the presence of the energetic ions the GAM / EGAM continuum can have an extremum even when the safety factor, $q(r)$, is monotonic, which indicates that global modes can exist also in this case (see Figure).

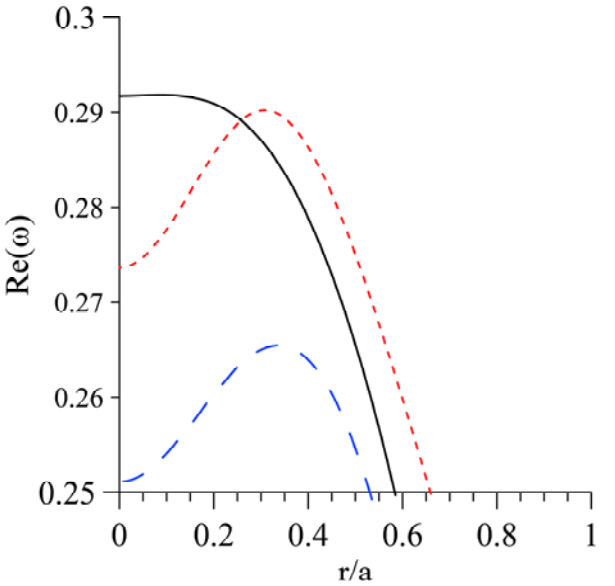

Dependence of an EGAM continuum branch on the radial profile of the energetic ions when $n_\alpha(0)/n_i(0) = 5$ % and $n_i(r) \propto n_i(0)\sqrt{1-r^2/a^2}$: solid line (black), the energetic ions are absent; dotted line (red), $n_\alpha(r) = n_\alpha(0)(1 - r^2/a^2)^2$; dashed line (blue), $n_\alpha(r) = n_\alpha(0)(1 - r^2/a^2)^{1/2}$. We observe that (i) a considerable positive slope of $\omega(r)$ in the region $r/a < 0.4$ is formed due to energetic ions; (ii) the frequency of the maximum is approximately the same in the absence of the energetic ions and in the presence of these ions with a peaked radial distribution.

* This work is published in Plasma Phys. Control. Fusion **55**, 125007 (2013).

FAST ION PUMP OUT INDUCED BY SATURATED INFERNAL MODE

V. S. Marchenko

Institute for Nuclear Research, National Academy of Sciences of Ukraine, Kyiv

The so called "hybrid" regime attracted much attention in tokamak research [1]. Such equilibria are characterized by the flat profile of the safety factor, q, in the wide central core, with $q \sim 1$ in this region. The main advantage of the hybrid shots is the absence of sawteeth, which are the main triggers of the harmful neoclassical tearing modes.

When q in the shear-free core approaches 1, hybrid equilibria become prone to the so called "infernal" modes (IM) [2, 3]. Due to absence of the mode rational surface, IMs quickly saturate by increased bending of perturbed field lines and form the long-lasting equilibria with helical distortion of the central core up to 1 cm.

Strong enhancement of the fast ion losses in the presence of saturated IMs has been observed in the MAST tokamak (see Figure from [4]). In the present work it is shown that such enhancement can be caused by convection of the well-passing fast ions, which are trapped into Doppler-precession resonance, $k_{\|}v_{\|} + \omega_d(r_*) = 0$, with finite-amplitude infernal mode. Convection arises during slowing down of resonant particle on electrons, due to outward shift of resonance position, $\partial r_* / \partial v < 0$.

Averaged over flux surface and over distribution of particles in velocity space, convection speed is given by

$$V_p = \frac{16}{\pi \ln(\varepsilon_\alpha / \varepsilon_c)} \nu_s \sqrt{A}, \qquad (1)$$

where $\varepsilon_\alpha(\varepsilon_c)$ is the injection (critical) particle energy, ν_s is the slowing down rate, and $\sqrt{A}$ is the radial width of the resonance determined by the diamagnetic part of the precession frequency, ω_d.

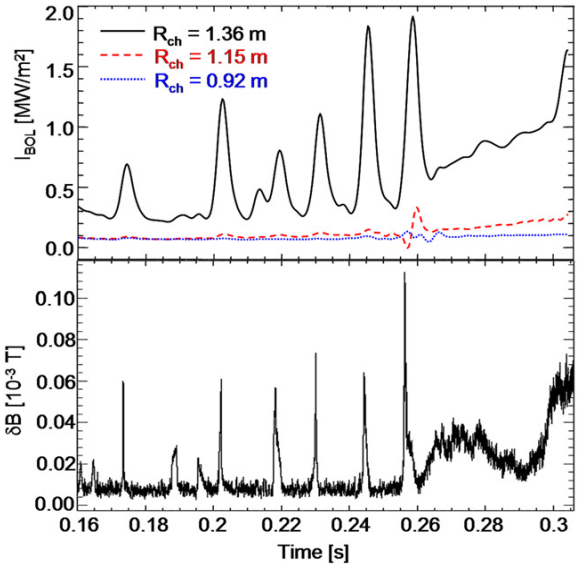

Fast ion losses seen by counter-viewing bolometer during MAST discharge 21781. A peak in the fast ion losses is seen at each fishbone chirp, and the loss rate increases steadily after infernal mode onset (255 ms).

For parameters of the experiment [4], Eq. (1) yields V_p = 5 - 10 m/s, in reasonable agreement with observations. Although detrimental for the modern spherical tori, this transport mechanism can be useful in the hybrid scenario for the fusion reactor ITER from the point of view of helium ash removal.

1. E. Joffrin, Plasma Phys. Control. Fusion **49**, 629 (2007).
2. R.J. Hastie and T.C. Hender, Nucl. Fusion **28**, 585 (1988).
3. F.L. Waelbroeck and R.D. Hazeltine, Phys. Fluids **31**, 1217 (1988).
4. I.T. Chapman *et al.*, Nucl. Fusion **50**, 045007 (2010).

CONVECTIVE AND DIFFUSIVE LOSS OF FAST IONS IN TOKAMAKS

V. O. Yavorskij[1,2], V. Ya. Goloborod'ko[1,2], K. Schöpf[2]

[1] *Institute for Nuclear Research, National Academy of Sciences of Ukraine, Kyiv*
[2] *Institute for Theoretical Physics of Innsbruck University, Innsbruck, Austria*

Fast ions (FIs) confined in tokamak plasmas subject to a substantial convective and diffusive radial transport [1 - 3]. This transport can result both in significant losses of energetic ions from the plasma as well as in essential modification of the distributions of confined FIs. Present study aims investigation of the joint effect of radial convection and diffusion of charged fusion products (CFPs) on their losses from tokamak plasmas. Evaluated is also effect of radial transport on the CFPs radial profiles at the plasma edge.

In quasi stationary tokamak plasmas the charged fusion product behaviour can be described by the following Fokker - Planck equation for distribution function F in constant-of-motion coordinates $\{r_{max}, E, \lambda\}$ [3]

$$\partial_\tau f = \partial(df - D\partial_x f) + f_0\delta(\tau) \qquad (1)$$

with $x = 1 - r_{max}/a$, $\tau = d_E(1 - E/E_0)$, $f = g^{1/2}d_E F$, d_E the slowing down rate, f_0 the initial distribution function, $g^{1/2}$ the Jacobian and d, D correspondingly the convective and diffusive coefficients. In Eq. (1) we supposed an isotropic in velocity distribution of CFPs. For simplest case $d = \text{const}$, $D = \text{const}$, $f_0 = \eta(x)$, where $\eta(x)$ is a Heaviside step function, and for boundary conditions $(0) = 0$, $f(x\to\infty) = 1$ the solution of Eq. (1) is given by

$$f = \exp(-y/2)\sum_{\sigma=\pm1}\Psi_\sigma(y,z), \qquad (2)$$

where $\Psi_\sigma = \sigma\exp(\sigma y/2)\{2 - \text{erfc}[(z - \sigma y/z)/2]\}/2$, $y = dx/D$, $z = d\sqrt{\tau/D}$, erfc(x) – error function. Figure, *a* demonstrates the radial profiles of CFP distribution at different energies in case of pure diffusive transport. Radial diffusion seen to strongly influence the profiles of CFPs confined at the plasma edge. Effect of radial convection for partly thermalized CFPs at $D\tau$=0.01 is displayed in Figure, *b*. Evident is a substantial degradation of the confinement of peripheral fast ions in the case of outward convection (d/D= -10) as well as improvement of confinement at inward convection (d/D = +10).

Conclusions:

1. Convective transport essentially affects the radial profiles of charged fusion products at the plasma edge.
2. Outward radial convection can significantly enhance the CFP loss from tokamak plasmas.
3. Effect of joint action of radial diffusion and convection is important for interpretation the fast ion loss measurements in tokamaks.

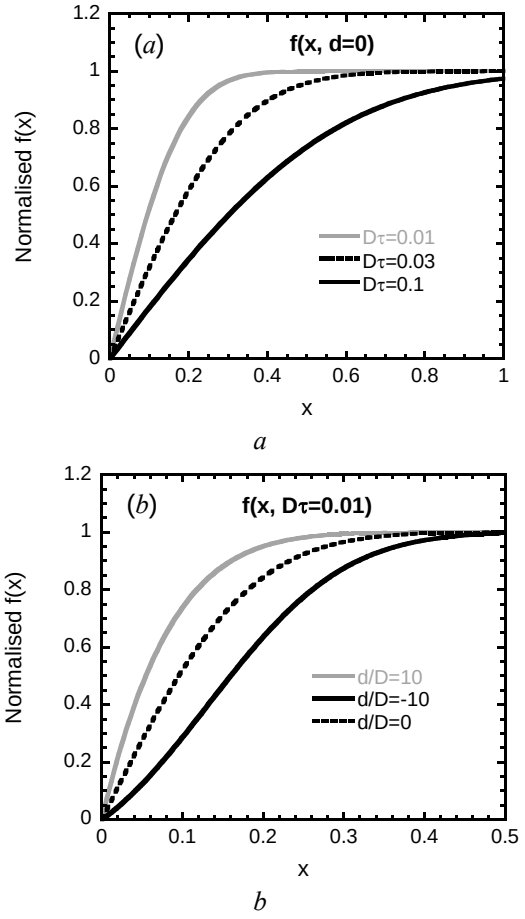

Fig 1. Radial profiles of charged fusion product distribution at different energies ($D\tau$=0.01, 0.03, 0.10) in case of pure diffusive transport – (*a*). Profiles of partly thermalized CFPs ($D\tau$=0.01) depending on the value of radial convection (d/D=–10, 0, 10) – (*b*).

1. S. Zweben *et al.*, Nucl. Fusion **40**, 91 (2000).
2. M. García-Muñoz *et al.*, Phys. Rev. Lett., **104** 85002 (2010).
3. V. Yavorskij *et al.*, Physics of Plasmas, **6** 3853 (1999).

HALL SPIN-UP MECHANISM AND STABILIZATION OF RFP KINKS

A. A. Gurin

Institute for Nuclear Research, National Academy of Sciences of Ukraine, Kyiv

Recent results on the reversed field pinch (RFP) program indicate the important role of the two-fluids, e.g., Hall effects and the plasma rotation in the organization of dynamic quasi-single mode equilibrium [1]. In this paper we propose a model that combines these effects. To describe the spectrum of kinks, the boundary value problem is posed which includes in addition to plasma flows, $V_\theta(r)$ and V_z (r), the Hall effects. Unstable disturbances that in the standard MHD theory of immovable ideal plasma meet the zero frequency, in the Hall MHD theory acquire a finite frequency. Its value is small in Alfven scale, but is consistent with the experimentally observed values and allows applying the procedure of averaging on oscillations in order to find solutions saturated on a time scale of relaxation. Moreover, it appears that the condition of the momentum θ- and *z*-balance of plasma and magnetic field, which in ideal one-fluid plasma, even with the unstable oscillations, is given by the trivial equation: $0 = 0$, in the case of the limited value of the Hall parameter becomes more meaningful. In this paper, the plasma velocities are determined numerically from the momentum balance equations presented as quadratic forms averaged over fluctuations. Using these velocities to the boundary value problem reveals the stabilizing effect of the plasma motion induced by each of the unstable modes. The iterative procedure minimizing increments permits us to call the amplitudes that define the marginal kink stability.

The linearized version of the Hall MHD theory for a cylindrical plasma with a finite value of the parameter beta and arbitrary flows $V_\theta(r)$ and V_z (r) is reduced to the 4-th order differential problem $y'_i(r) = \Sigma j M_{ij}(r|\omega)\cdot y_j(r)$ under condition $y_1(1|\omega) = 0$ where $i, j = 1, \ldots, 4$, $Y(r) = \{\xi_{er}, (r\xi_{er})', \delta G, \delta P\}$, ξ_{er} is the electron displacement: $\delta V_{er}(r) = - i\omega_e(r)\xi_{re}(r)$, where $\omega_e = \omega - \mathbf{kV}_e = \varpi + \mathbf{kU}$, $\varpi = \omega - \mathbf{kV}$, $\mathbf{k} = (0, k_z, -m/r)$. **U** is the current velocity introducing the Hall difference ion and electron mean flows: $\mathbf{U} = \mathbf{V}\text{-}\mathbf{V}_e = \mathrm{rot}\mathbf{B}/N\sqrt{\Pi}$, $\Pi = 4\pi Ne^2a^2/Mc^2$ is Braginskii - Hall parameter, *a* is a plasma radius, *M* is the proton mass, *N* is density. δG, δP are expressed through the magnetic, $[\delta\mathbf{B},\mathbf{k}]_r$, and pressure disturbances.

To find the flows of ideal quasi-steady plasma, it is enough to use averaging procedure for non-radial components of the plasma momentum balance in which the time derivates terms can be omitted. From the single-mode calculations of MHD stresses, one can obtain explicit local expressions $V_\theta(r)$ and V_z (r). Substituting these flows into the code resolving the boundary problem for unstable kinks, and applying the iterative procedure, it is possible to determine the amplitudes that determine the marginal kink stability in the single-mode approximation. The results are plotted in Figure.

1. J.S. Sarff, A.K. Almargi, J.K.Anderson *et. al*. Nucl. Fusion **53**, 104017 (2013).

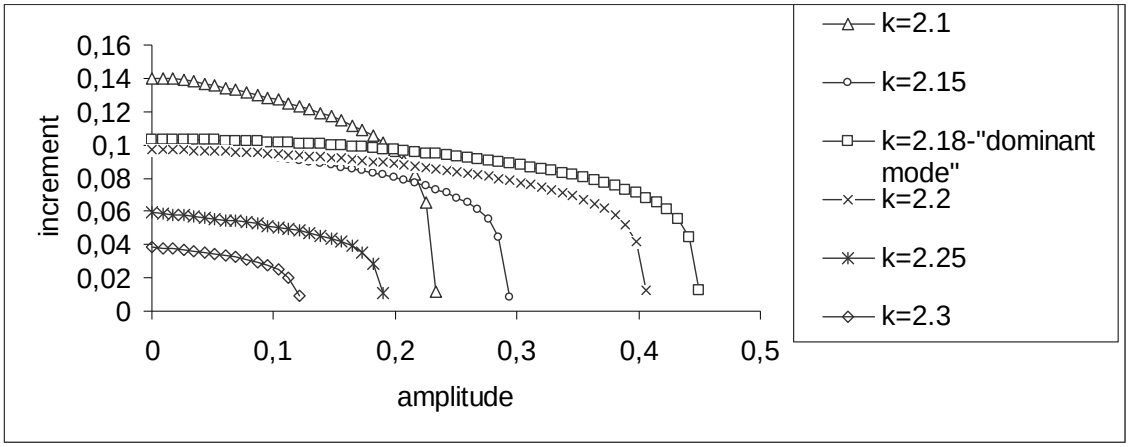

Stabilization of different modes under influence of flows generated with the amplitude $y_1(0)$ at the plasma axis under the parameters $\Pi = 40$, $\beta_0 = 0$.

EFFECT OF MAGNETIC ISLANDS ON THE ENERGETIC ION TRANSPORT IN TOKAMAKS WITH MAGNETIC SHEAR REVERSAL

O. S. Burdo, Ya. I. Kolesnichenko, M. H. Tyshchenko, Yu. V. Yakovenko

Institute for Nuclear Research, National Academy of Sciences of Ukraine, Kyiv

The effect of wide magnetic islands on plasma particles – energetic and thermal ions – is investigated. Magnetic islands often arise in tokamak plasmas. Moreover, there is an opinion that the neutron emission drops during the so-called TAE-avalanches are due to redistributions of injected energetic ions, which are caused by magnetic islands arising as a result of nonlinear interactions between the modes of the avalanches.

In this work, the effect of magnetic islands on the particle motion is simulated in the guiding-centre approximation with the Hamiltonian code ORBIT [1]. The interaction of a resonance island (which arises in the phase space of the particle motion) with satellite islands, which arise due to toroidicity, can result in stochastic motion of particles. This route to stochasticity is known [2], but it was unexpected that when the width of the magnetic island is large enough (of order of the distance to the satellite drift islands), even the motion of ions with thermal energy is stochastized (in spite of the absence of magnetic field stochasticity). A typical example is shown in Fig. 1.

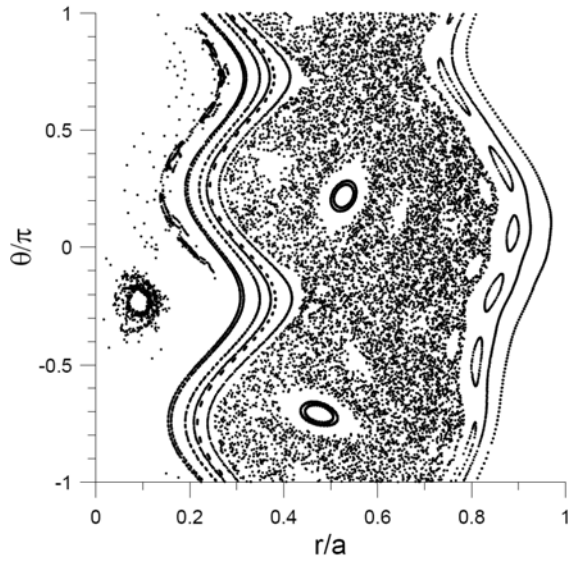

Fig. 1. Poincaré map of motion of 300-eV deutrons in the NSTX spherical torus for a magnetic perturbation with and $\alpha_0 = 4 \cdot 10^{-3}$ (m and n are the poloidal and toroidal mode numbers, respectively; α_0 is the normalized perturbation amplitude).

Since the appearance of TAE-avalanches correlates with non-monotonic radial profiles of the magnetic winding number (safety factor) q, non-monotonic q-profiles were paid special attention in the simulations. It was found that shear reversal can enhance the redistribution (Fig. 2). This effect is sensitive to the toroidal precession of the ions (thus, to their energy) and to $q_{\min}$ (the value of q at the minimum point). It is planned to apply these results to the explanation of experiments on the spherical torus NSTX.

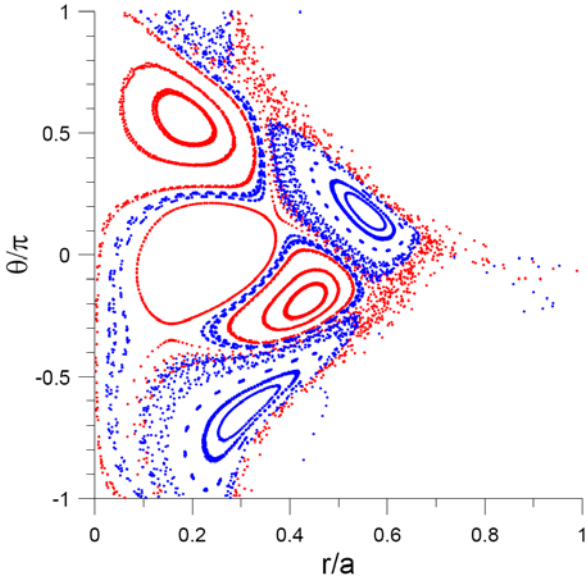

Fig. 2. The same as in Fig. 1 but for 30-keV ions and $\alpha_0 = 3 \cdot 10^{-4}$ in a configuration with $q_{\min} = 1.75$.

This work was reported at the 13th IAEA Technical Meeting on Energetic Particles in Magnetic Confinement Systems (Beijing, China, 17 - 20 September 2013).

1. R.B. White and M.S. Chance, Phys. Fluids **27**, 2455 (1984).
2. H.E. Mynick, Phys. Fluids B **5**, 1471 (1993).

PLASMA ACCELERATION IN A ROTATING ELECTRIC FIELD

Ya. I. Kolesnichenko, T. S. Rudenko

Institute for Nuclear Research, National Academy of Sciences of Ukraine, Kyiv

One of theoretical proposed mechanisms of the plasma acceleration in plasma thrusters is based on the use of the azimuthal plasma current j_z produced by a rotating electric field (REF) [1, 2]. Due to this current and the presence of the radial component of the equilibrium magnetic field B_r the trust arises as a result of Lorentz force along the axis of the thruster, $(j_\theta \times B)_z = - j_\theta \times B_r$. The advantage of this method is that the plasma acceleration is elecrodeless, which increases the service life of the thruster. For the verification of this method an experiment described in Ref. [2] was held. It was turned out, however, that the effect of REF was small or even absent. The reason for this was not known. Therefore, a conclusion was drawn that a more detailed theoretical study is required in order to find optimal conditions for the thrust production. This motivated us to carry out the present work.

The analysis in Refs. [1, 2] was carried out in the assumption that the perturbed magnetic field is absent, i.e., the electrostatic approximation was used. We refused from this assumption. New relations for the average poloidal current and concomitant trust were obtained. It follows from them that the magnetic contribution can be important and it can even dominates in the near axis region. This is the case only at a certain direction of the rotation of the electric field. An analysis of parameters was made. A condition necessary for the observation of effects of REF (when the REF thrust exceeds the one of the diamagnetic current) was obtained. It seems possible the discovered strong dependence of the thrust on the direction of the rotation of the electric field may explain why the REF effect was small in the experiment of Ref. [2]. Hopefully, the obtained relations can be used for optimization.

1. Shunjiro Shinohara, Tohru Hada, Taisei Motomura *et al*., Physics of plasmas **16**, 057104 (2009).
2. Takahiro Nakamura *et al.*, JSASS Aerospace Tech. Japan **10**, No. 28, pp. Tb_17-Tb_23 (2012).

CAN STOCHASTICITY OF FIELD LINES BE RESPONSIBLE FOR SAWTOOTH CRASHES ?

Ya. I. Kolesnichenko, Yu. V. Yakovenko

Institute for Nuclear Research, National Academy of Sciences of Ukraine, Kyiv

The aim of the work is to contribute to understanding whether the partial reconnection of magnetic field lines during crashes of sawtooth oscillations in tokamaks can result from the stochasticity of the magnetic field lines. It is shown numerically that a joint action of effects of frozen-in magnetic field lines and satellite harmonics of the magnetic perturbation can lead to wide-spread stochasticity; the stochasticity occupies, in particular, the near-axis region – which is a necessary condition for drops of the central temperature of the plasma during sawtooth crashes with incomplete reconnection (see Fig. 1). In addition, it is found that the confinement time in the sawteeth region is small enough to explain theheat loss (see Fig. 2). In spite of this, the question in the title of the work is still open. The matter is that, first, our calculations were carried out with a special choice of the perturbation and for low central safety factor and, second, as shown in this work, previous theories investigating field line stochasticity cannot explain crashes with partial reconnection.

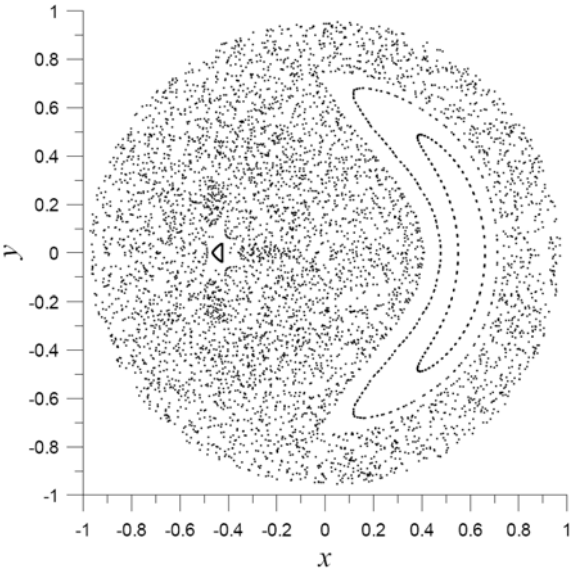

Fig. 1. A Poincaré map of magnetic field lines with allowing for frozen-in field lines for the cental safety factor $q_0 = 0.6$. Satellite harmonics $m = n \pm 1$ with the amplitudes less by a factor of $\varepsilon_s = 0.1$ than those of the main harmonics $m = n$ were added. Stochasticity occupies almost the whole sawtooth region except for the island.

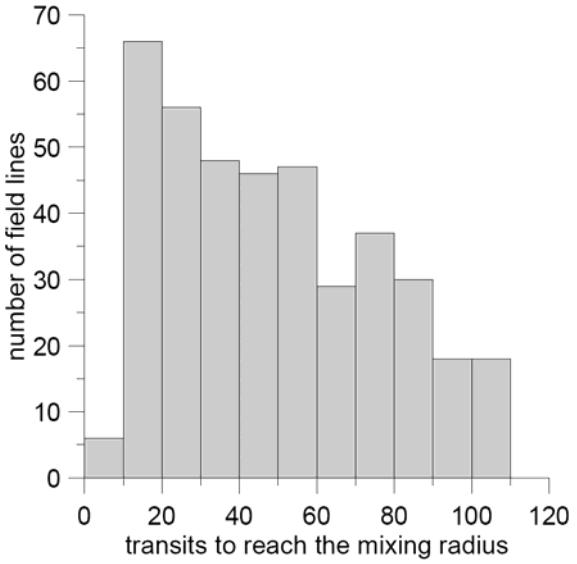

Fig. 2. Histogram of the lengths in toroidal transits ($2\pi R$ with R the major radius of the torus) for which field lines starting at the distance of $r \approx 0.1\, r_{mix}$ from the magnetic axis displaced by the crash reach the plasma mixing radius, $r = r_{mix}$. The calculations were carried out for the same parameters as in Fig. 1.

This work is published in Plasma Physics and Controlled Fusion **55**, 115006 (2013).

INVESTIGATION OF STOCHASTIZATION OF FAST ION MOTION BY HIGH-FREQUENCY PLASMA INSTABILITIES AND SPATIAL ENERGY CHANNELLING IN THE ITER REACTOR

M. H. Tyshchenko, Yu. V. Yakovenko

Institute for Nuclear Research, National Academy of Sciences of Ukraine, Kyiv

One can expect that fast ions (alpha particles and ions produced by neutral beam injection) will excite a wide range of instabilities in ITER. A possible way to predict the consequences of these instabilities is to use the experience gained in experiments on existing devices. In particular, in experiments on the spherical torus (spherical tokamak) NSTX, high frequency instabilities were observed. The instabilities with higher frequencies (predominantly $f \geq 600$ kHz) and smaller toroidal mode number ($|n| \leq 5$) were identified as CAEs (compressional Alfven eigenmodes); those with $f \leq 600$ kHz, $n = -5$ to -8, as GAEs (global Alfven eigenmodes) [1, 2]. It was pointed out that these energetic-ion-driven instabilities can channel the energy of energetic ions outside the region where these ions are located [3]. It is likely that the spatial energy channelling can explain experiments on the spherical torus NSTX where a broadening of the temperature profile and even a drop of the temperature at the plasma center with increasing injected power were observed, which correlated with the appearance of multiple Alfven instabilities [2].

The aim of this work is to study the conditions in which similar modes can cause energy channelling in ITER. We evaluate the number and the amplitudes of modes needed to produce a wide stochastic region in the fast-ion phase space, so that the waves are able to receive a major part of the power of injected ions.

We concentrate on injected fast ions; thus, we are interested in resonances of passing particles. Multiple modes produce stochastic transport in limited domain where modes overlap. A guiding center code was created to study overlap of resonances of multiple waves. The idea is that we turn on and off the wave adiabatically, and then find the phase space regions where the particles' positions have changed. This gives us a possibility to find energy intervals in which the particles are displaced by stochasticity and/or resonance islands. When these regions are wide, the fast ions particles transfer their energy predominantly to the modes (rather than to electrons via collisions), which is a necessary condition of strong energy channeling.

Comparison of the results of analytical calculations and numerical simulations shows good agreement.

1. N. A. Crocker *et al.* Nucl. Fusion **53**, 043017 (2013).
2. D. Stutman *et al.* Phys. Rev. Lett. **102**, 115002 (2009).
3. Ya.I. Kolesnichenko *et al.* Phys. Rev. Lett. **104**, 075001 (2010).

TEMPORAL EVOLUTION OF NBI IONS DISTRIBUTION FUNCTION IN JET

V. Ya. Goloborod'ko[1], V. O. Yavorskij[1], K. Schöpf[2]

[1] *Institute for Nuclear Research, National Academy of Sciences of Ukraine, Kyiv*
[2] *Institute for Theoretical Physics of Innsbruck University, Innsbruck, Austria*

In future tokamak-reactors that are now under construction (ITER) or design (DEMO) a substantial population of charged fusion products will be present in plasma, predominantly fusion born energetic alpha particles. Analysis of experimental data from previous generation of tokamak-reactors such as TFTR [1], JET [2] etc. shows that energetic alpha particles may destabilise toroidal Alfven eigenmodes (TAE) that cause space redistribution and radial transport enhancement of plasma ions. The conditions for TAE destabilisation and their evolution depends on the distribution of fast ions in phase space as well on modes dissipation mechanisms. One of the most important mechanisms of TAE modes dissipation is Landau mode damping on the injected ions. The efficiency of such damping strongly depends on inhomogeneity of NBI ions distribution function in phase space. In present-day tokamak-reactors temporal evolution of equilibrium and plasma parameters during NBI injection also essentially affects the distribution of injected ions. The present paper is focused on the possibility to carry out the similarity DT experiments on the tokamak-reactor JET for the investigation the conditions for TAE modes destabilisation in tokamak-reactor ITER by fusion alpha-particles. One of the goals of this experiment will be the minimisation of mode damping caused by phase space distribution of injected ions for investigation of temporal behaviour of alpha driven TAE modes. In present report the evolution of distribution functions of NBI deuterons and tritons in 50/50 DT JET plasma calculated with codes SNBI and FIDIT for real temporal behaviour of equilibrium and plasma parameters in JET shot #40214 is presented. Time evolution of some shot parameters are shown in Fig. 1. The obtained distribution functions of NBI ions demonstrated in Fig. 2 may be used for the calculation of TAE modes damping rates due to beam injection.

The objective of the work is codes development for calculation of NBI sources and distribution functions of injected ions in real discharge conditions in tokamak-reactor JET.

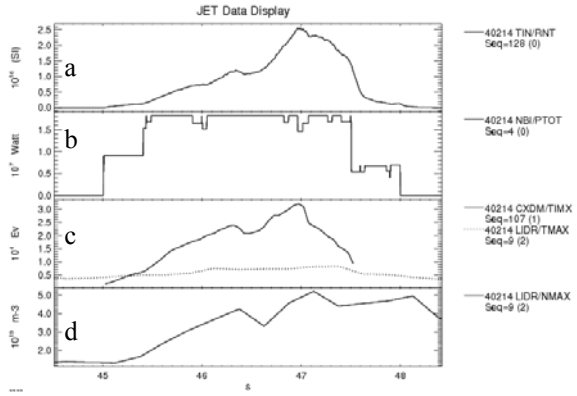

Fig. 1. Evolution of some JET shot #40214 parameters: *a* – neutron yield; *b* – total NBI power; *c* – maximal bulk ion temperature; *d* – maximal bulk ion density.

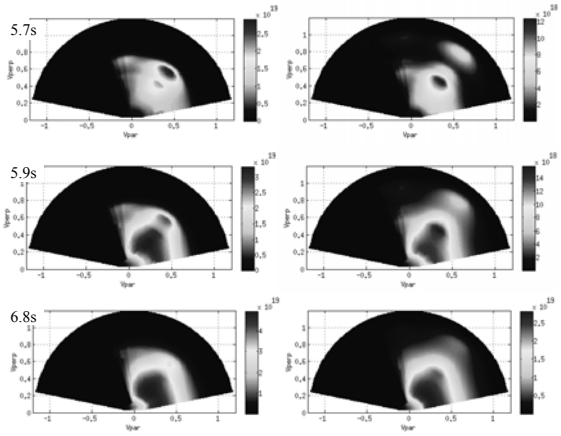

Fig. 2. Temporal evolution of distribution functions of NBI deuterons (left column) and tritons (right column) injected in JET plasma during shot #40214.

1. G.Y. Fu, C.Z. Cheng, R. Budnz *et al.*, Phys. Plasmas **3**, 4036 (1996).
2. S.E. Sharapov, D. Borba, A. Fasoli *et al.*, Nucl. Fusion, **39**, No. 3, 373.

COOLING AND TRANSPORT OF ENERGETIC IONS DUE TO THE GLOBAL GEODESIC ACOUSTIC MODE

Ya. I. Kolesnichenko, V. V. Lutsenko, B. S. Lepiavko

Institute for Nuclear Research, National Academy of Sciences of Ukraine, Kyiv

It is shown that the destabilization of Geodesic Acoustic modes (GAM or E-GAM) by passing energetic ions in tokamaks can be accompanied with a considerable energy transfer from these ions to the mode.

This is the case when the mode is global and plasma density perturbation is large, which provides wave-particle interaction in a wide phase-space region. The mode-induced slowing down of the energetic ions leads to a radial shift outwards / inwards of the ions moving in the direction counter- / co- to the plasma current, in spite of the fact that the canonical angular momentum of the particles is conserved during GAMs (see Figure).

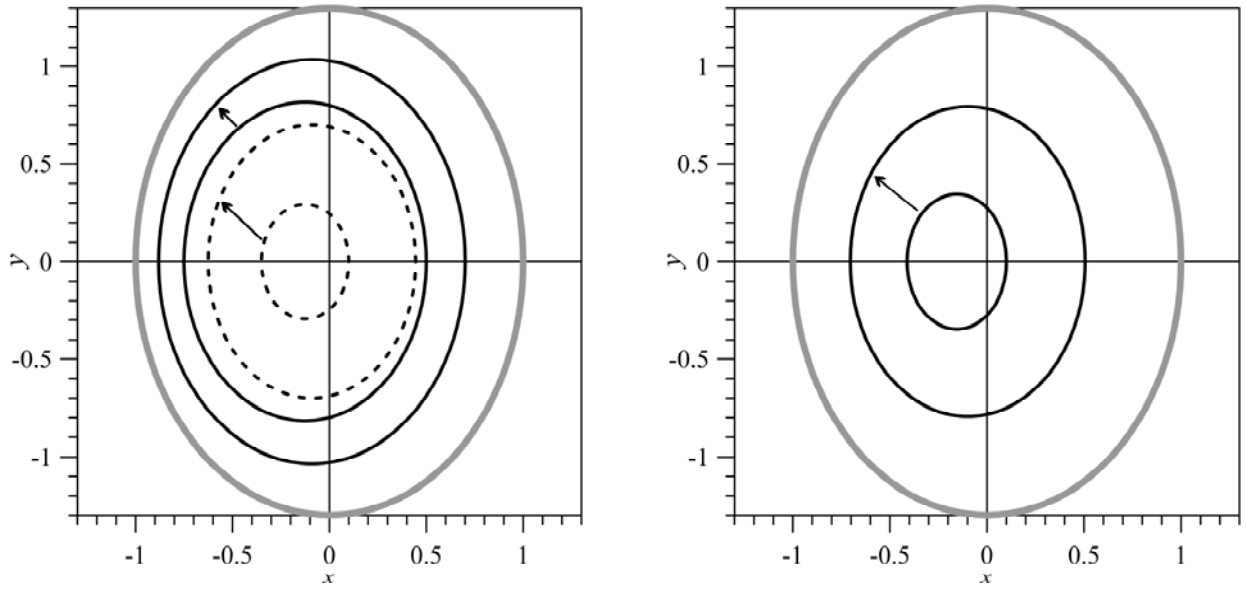

Orbits of passing *75*-keV deuterons moving in the direction counter to the plasma current in a DIII-D like tokamak before and after the slowing down when $\varepsilon^f = 0.5\ \varepsilon^i$, $P_\varphi^f = P_\varphi^i$, and $\mu^f = \mu^i$: left panel, $q\ (r) = 3.5$, $\lambda^i = 0.2$; right panel, $q(r)$ which took place in the E-GAM DIII-D experiment [1], $\lambda^i = 0.35$. The edge of the plasma is shown by a grey thick line, $x = (r/a)\cos\theta$, $y = \kappa\ (r/a)\sin\theta$. The arrows are directed from the initial orbits to final ones (i.e., to the orbits after the slowing down). The following tokamak parameters were used: $B = 2\ T$, $a = 60$ cm, R_0=170 cm, $\kappa = 1.3$. It was assumed that the flux surfaces are concentric ellipses.

1. R. Nazikian *et al*., Phys. Rev. Lett. **101**, 185001 (2008).

PLASMA LENS FOR LARGE AREA ELECTRON BEAMS MANIPULATING

I. V. Litovko[1], A. A. Goncharov[2], A. M. Dobrovolskiy[2], V. I. Gushenets[3], E. M. Oks[3]

[1] *Institute for Nuclear Research, National Academy of Sciences of Ukraine, Kyiv*
[2] *Institute of Physics National Academy of Sciences of Ukraine, Kyiv*
[3] *High Current Electronics Institute SB Russian Academy of Sciences, Tomsk, Russia*

Recently [1] we proposed and explored a new original plasma-optical tool for negative charged particle beams focusing and manipulating with a dynamic cloud of non-magnetized free positive ions and magnetically isolated electrons produced by a toroidal plasma source like an anode layer thruster. In such kind systems the electrons are separated from ions by relatively strong magnetic field in the discharge channel. The accelerated ions are weakly affected by the magnetic field owing to their mass.

Here we describe the current status of ongoing research and development of the wide aperture electrostatic plasma lens (PL) with positive space charge cloud for focusing and manipulating large area (diameter 6 cm), non-relativistic (up to 20 keV) electron beam(e-beam) in wide range of beam current (I_b from 100 mA to 100A). The plasma electron source based on electron extraction from vacuum arc discharge with hollow anode was used for generation of this beam. The lens is based on the main plasma optical principle meaning that electrons are magnetically insulated and non-magnetized positive ions creating a controlled uncompensated dynamical space charge cloud.

For relatively low-current mode ($I_b \leq 1A$) for which electron beam space charged less than positive space charged PL it realize electrostatic focusing passing e-beam. Focusing of the e- beam by electrostatic PL was separated from magnetic focusing experimentally and the compression factor was up to 5. In Fig 1 are shown calculated e-beam trajectories under beam passing through PL and magnetic lens (ML) only for this case under experimental conditions [2].

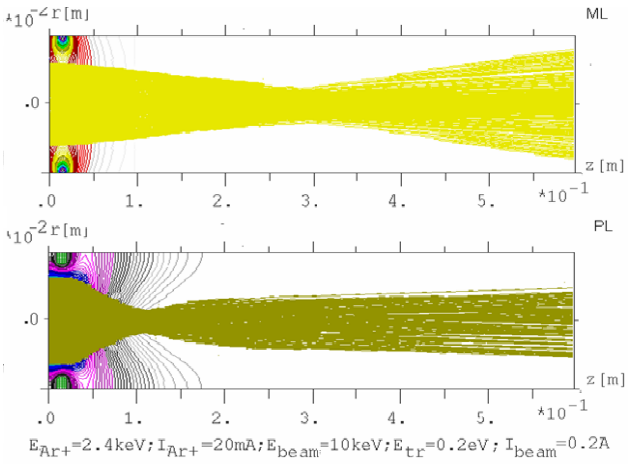

Fig. 1. The e-beam trajectories (low-current mode) under passing e-beam (I_b = 0.2 A, E_b = 10 keV) through ML (*top*) and PL (*down*) with the same magnetic field.

In case of high-current mode when e-beam space charge much more than space charge PL the lens operates in plasma mode to create transparent plasma accelerating electrode and compensate space charge propagating electron beam. The lenses magnetic field in this case use for effective focusing e-beam. Under described experimental conditions the maximal compression factor was up to 30x and beam current density at the focus was about 100 A/cm^2. In Fig. 2 are shown are shown calculated e-beam trajectories under beam passing through PL and magnetic lens (ML) only for this case under experimental conditions [3].

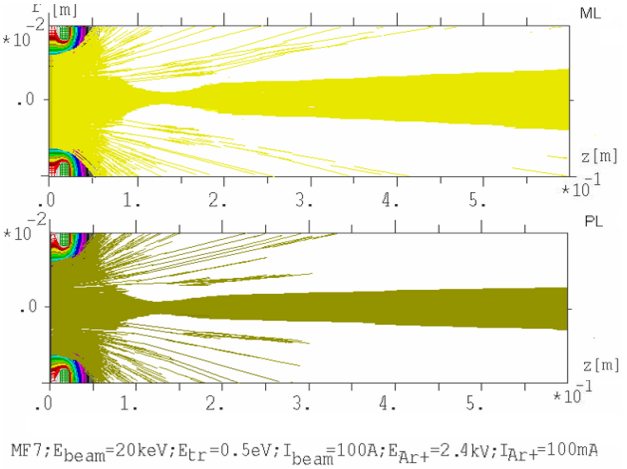

Fig. 2 The e-beam trajectories (high-current mode) under passing e-beam(I_b = 100A, E_b = 10 keV) through ML (top) and PL (down) with the same magnetic field.

Thus our simulation demonstrates the presence of space charge PL improved beam focusing in comparison with magnetic focusing solely. The swithing on PL reduces beam losses and improves beam tranport, because of lens is produced plasma density required for the electron beam stable transport.

The results of the computer simulation are shown good agreement with experimental data. Obtained experimental results demonstrate the possibility to create a low-cost high-effective tool for negatively-charged particle beam focusing without influence of momentum aberrations.

1. A. Dobrovolskiy, S. Dunets, A. Evsykov *et al.*, Rev. Sci. Instrum., **81**, issue 2B, 704 (2010).
2. A. Goncharov, A.M. Dobrovolskiy, S.P. Dunets *et al.*, Rev. Sci. Instrum. **83,** 02B723, (2012).
3. V. Gushenets, A. Goncharov, A. Dobrovolskiy *et al.*, IEEE Trans. Plasma Sci. **41**, #4, part 3, 2171 (2013).

ION ENERGY DISTRIBUTION IN PLASMA OF NONSELF-SUSTAINED ARC DISCHARGE

A. G. Borisenko, Yu. S. Podzirey

Institute for Nuclear Research, National Academy of Sciences of Ukraine, Kyiv

The physical processes occurring in widely used vacuum arc discharge in vapor of a cathode material that leads to presence of the cathode material drops at created plasma streams. Therefore such streams appear unacceptable for the solution of some technological problems and require development and usage of different methods of additional filtering. However, the filtering of streams not only promotes removal of the dropwise phase, but also leads to the significant decrease of intensity of plasma flow at the outlet of the filter [1, 2]. The nonself-maintained arc discharge in vapors of anode material allows one to create drop-free plasma flows of solid state materials for use in various practical applications [3]. This discharge also allows change in wide range of the ionization coefficient of plasma flows, that is a part of ions in a oral flow of plasma. As it known, the ion energy and their part in the plasma flow, especially at the initial stage of the deposition process, affect the processes of formation of point defects on the surface of the substrate and also on the surface diffusion processes, formation of metal clusters, further growth and structure of the film. Therefore, energy management and the proportion of the ions in the plasma stream may be used as an additional method of purposeful change of their structure and properties. However, any data about the energies of ions in plasma streams created by such discharge are absent. Therefore their study is important both with fundamental, and with applied the points of view.

Implemented experimental researches of main characteristics and energy specters of ions of plasma nonself-maintained arc discharge in vapors of nickel anode have displayed that in created plasma streams ions with energy is equal or increases voltage or discharge are absent. This shows that in experimental conditions ions that come from surface of the anode are absent also. The resulted data conclude that main physical process that form working environment of discharge of such type is vapor of working material from the anode. The most probable mechanism of forming of plasma flows is ionization of atoms of working material directly in discharge zone. Also concluded that increase of discharge current leads to decreasing of average energy of directed ionic motion (see Figure).

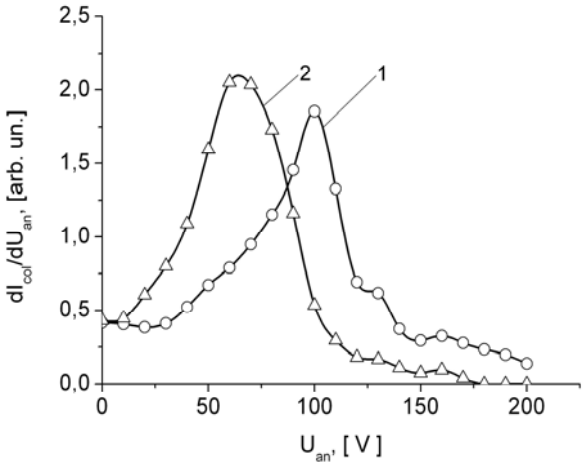

Energy specters of ions of plasma at different current discharges: *1* - I_P = 12 A; *2* – 20 A.

Speed of deposition of nickel films on dielectric substrates and meanings of ionization plasma flows coefficients at current discharge till 35 A show that such discharge allows to create non-drop and highly ionized flows of metallic plasma and to supply high speed of film spraying that are equal to possibilities of vacuum arc cathode.

1. R.L. Boxman, D.M. Sanders, and P.J. Martin. *Handbook of Vacuum Arc Science and Technology* (Noyes Publications, Park Ridge, N.J., 1995).
2. A. Anders. *Cathodic Arcs: From Fractal Spots to Energetic Condensation* (Springer, New York, 2008) ISBN 978-0-387-79107-4.
3. A.G. Borisenko, V.A. Saenko, and V.A. Rudnitsky, IEEE Trans. Plasma Science **27**, No. 4, 877, 1999.

TRANSFORMATION OF LANGMUIR WAVES IN TURBULENT PLASMA IN THE PRESENCE OF UPPER-HYBRID PUMP

V. N. Pavlenko, V. G. Panchenko, N. A. Beloshenko

Institute for Nuclear Research, National Academy of Sciences of Ukraine, Kyiv

An important instrument for studying the properties of matter is the scattering and transformation of electromagnetic radiation. A completely homogeneous medium cannot scatter radiation because any scattering or transformation processes may occur due to turbulence or inhomogeneities in the medium. So in plasma with certain fluctuation level the propagation of electromagnetic waves can lead to radiation of waves (with new frequencies and wavenumbers in comparison with incident wave) and new type of waves – transformed waves [1].

In the present paper we investigate the transformation process of longitudinal Langmuir wave into the transverse electromagnetic wave in turbulent plasma subjected the upper hybrid pump. The case when an upper hybrid pump wave decays into daughter and ion – sound waves is considered. Note that the main contribution to the intensity of electromagnetic radiation which has been calculated is given by the high-frequency turbulent fluctuations at upper hybrid frequency. It is shown that the frequency of such radiation is closen to be near double electron Langmuir frequency $2\omega_{pe}$.

The intensity of such radiation is connected with the transformation coefficient $d\sum_{l\to t}$ by the relation [2]

$$I \sim V\iint d\sum_{l\to t} S\frac{d^3k'd\omega'}{(2\pi)^3 2\pi}, \qquad (1)$$

where S is the energy density fluctuations.

We suppose that the plasma is subjected to a magnetic field $\vec{B}_0 = B_o\vec{z}$ and a pump wave electric field $E(t) = E_0\vec{y}\cos\omega_0 t$. Consider the case when the pump wave frequency is close to the upper hybrid frequency:

$$\omega_{UH} \approx (\omega_{pe}^2 + \Omega_e^2)^{1/2}, \qquad (2)$$

where ω_{pe} is the electron Langmuir frequency and Ω_e is the electron gyrofrequency. Here $\omega_{pe} > \Omega_e$, i.e. we have the case of weakly magnetized plasma.

We consider the decay of the pump wave into daughter uuper hybrid and ion – sound wave [3]:

$$\omega_0 = \omega_{UH} + \omega_s, \qquad (3)$$

where $\omega_s = \left|\vec{k}\right| v_s$ and $v_s = (T_e/m_i)^{1/2}$ is the ion – sound velocity. Assume that the damping rate of the upper hybrid wave $\gamma_{UH} \approx \nu_{ei}$, where ν_{ei} is the collision frequency between ions and electrons.

Using the fluctuation-dissipative theorem, carrying out the integration over k' and taking into account (3) finally we obtain the dependence of the radiation intensity on the ionic temperature anisotropy:

$$I \sim V\left(\frac{e^2}{mc^2}\right)^2 N\frac{\omega_{pe}T_e^2k'^2}{e^2}\mu^2\frac{\omega_s^2}{\gamma_{UH}\gamma_s}(k'r_{De})^2, \qquad (4)$$

Notice must be taken that the frequencies of transformed electromagnetic waves according to (2) are closed to double plasma electron frequency $2\omega_{pe}$. This allows to propose one of the probable mechanism for the interpretation the electromagnetic radiation from the solar crown.

The results of this paper give us the possibility to explain the nature of radiation from the various space objects.

1. A.I. Akhiezer, I.A. Akhiezer, R.V. Polovin *et al.*, *Plasma Electrodynamics* (Pergamon, Oxford, 1975).
2. V.N. Pavlenko and V.G. Panchenko, Physica Scripta (2014) to be published.
3. H. Wilhelmsson, V.N. Pavlenko, and V.G. Panchenko, Physica Scripta **44,** 599 (1991).

THE STUDY OF CHARACTERISTICS OF HELICON DISCHARGE IN SYSTEM WITH PLANAR ANTENNA IN THE MEDIUM OF METHANE AND IT'S MIXTURES WITH HYDROGEN

V. M. Slobodyan[1], V. F. Virko[1], K. P. Shamrai[1], I. V. Korotash[2], L. S. Osipov[2], D. Yu. Polotsky[2], E. M. Rudenko[2], V. F. Semenyuk[2]

[1] Institute for Nuclear Research, National Academy of Sciences of Ukraine, Kyiv
[2] G. V. Kurdyumov Institute for Metal Physics, National Academy of Sciences of Ukraine, Kyiv

Systems based on helicon discharge are effective sources of dense plasmas and are widely used in practice, including nanotechnology. In particular, in [1] the synthesis of carbon nanostructures (CNT) was carried out using standard helicon source, in which the exciting antenna covered the dielectric chamber and excited discharge in methane or its mixtures with hydrogen. Helicon source with the flat (planar) exciting antenna located at the end of the metal discharge chamber allows more efficiently generate the plasma and constructively is easier for process applications than standard. The purpose of this study is to investigate experimentally the possibility of using just such discharge system for creating process medium (plasma discharge in methane and its mixture with hydrogen), which provides for the formation of carbon nanostructures.

The discharge chamber of the research source is a 20-cm-diam, 30-cm-long grounded metal cylinder closed on top by a quartz window. The 11.5-cm-diam double-turn planar antenna supplied from an rf generator of frequency 13.56 MHz and up to 2 kW power is located above the window. The chamber is confined from below by a 15-cm-diam metal electrode (substrate holder), which was either at a floating potential or negatively biased down to −100 V. The magnetic field of various configurations and maximum strength up to 250 G was produced by four solenoids with independent power supplies. The working gas was methane, hydrogen and their mixtures.

It is established that, in contrast to the heavy monatomic inert gases (Ar, Kr, Xe), in a helicon source with planar antenna the intense discharge in methane and hydrogen is available to be maintained only in the rather narrow range of pressures, ≤ 1.5 Pa, and the optimum plasma density is achieved at 0.6 - 0.9 Pa. The magnetic field range for the existence of the discharge is limited by 60 - 80 G at RF power of 1 kW. The maximum plasma density for methane reaches $(2\div5)\cdot10^{11}$ cm^{-3}, and for hydrogen of 1.5 - 2 times lower (in argon under similar conditions the density reaches greater than 10^{12} cm^{-3}). Electron temperature for discharge in methane is ~ 5 eV, in hydrogen - ~ 8 eV. The discharge conditions and plasma parameters, in general, are similar to the data of [1], where standard helicon source was applied. Discharge in a mixture of methane and hydrogen in various proportions was also realized. The properties of such discharge were generally similar to those that occur in the discharges in methane and hydrogen separately. It is established that the dependence of plasma density on the magnetic field for both gases and their mixtures has the jumping form. Measured at different magnetic fields radial distributions of plasma density indicate existence of both an intense mode with peaked radial profile of plasma density (magnetic field ≤ 30 G) and a moderate mode with an on-axis decrease on the radial density profile (magnetic field ≥ 50 G). The latter mode is of interest for practical applications because it provides a more uniform radial distribution of plasma density. It is shown that the magnetic field configuration is a significant factor that affects the discharge characteristics. It is established the optimum configuration of the magnetic field, which provides the best conditions for maintaining a discharge in methane and the highest plasma density (Figure).

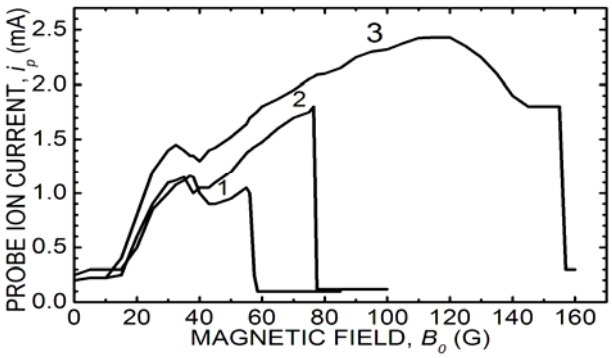

The series of dependences of probe ion current on the magnetic field for different magnetic field configurations: *1* - uniform magnetic field; *2* - nonuniform magnetic field (usual configuration); *3* - nonuniform magnetic field (the optimal configuration).

Obtained results confirm the promise of applications of helicon sources with planar antenna for process of the formation of CNT.

This work was performed by the joint project #5713 of the NAS of Ukraine and the STC in Ukraine.

1. G. Sato *et al.*, *Thin Solid Films* **506-507**, 550 (2006).

DEVELOPMENT OF TURBULENT MIXING IN THE EXPLODING WIRE-INITIATED PULSED DISCHARGE IN LIQUID MEDIA

P. V. Porytskyy, P. D. Starchyk

Institute for Nuclear Research, National Academy of Sciences of Ukraine, Kyiv

Development of hydrodynamic instability in pulsed discharges is the result of accelerated plasma repulsion of dense surrounding environment of the discharge channel due to the pulsed supply of energy to it. In each case, when the plasma undergoes heat sufficient for its accelerated expansion, the conditions are created for the growth of Rayleigh - Taylor hydrodynamic instability [1]. Plasma flows outward in the form of bubbles, and between them, inside the discharge channel the spread of cold jets takes place. Formed in discharges shock waves and shear flows further create the possibility of development of other types of instabilities [2] and the turbulent mixing (TM) undergoes in the contact zone.

A current study of the influence of discharge conditions on the development of turbulence has shown that spatial distributions and growth rate of developing perturbations depend not only on the inhomogeneous structure of channels [3] but it is determined by initial heterogeneity of discharge channels. In triggered spark discharges initial corrugations of discharge channels are so large that their structure completely determines the dynamics of the plasma channel and separates the vortex formation. In the case when the discharge is initiated by exploding wires (EW) the striations character causes the destruction of channel and also generates TM, but the sizes of excitations are incomparable smaller than that at the spark discharges. Since the depth of the zone TM is comparable with the dimensions generated disturbances in this case, it is localized in the surface layers of the discharge channel. By increasing the rate of energy input in the EW may be reached such degree of dispersion of its destruction, in which the perturbation generating TM does not grow and the surface of the plasma channel shines practically uniform. The Figure below shows the general form images of discharge channels initiated by tungsten wire 20 μm in diameter at different initial strength of electric fields E_0. With a smaller initial strength E_0 on the surface of the channel structure is clearly observed perturbations formed by the end of the first period of oscillatory discharge.

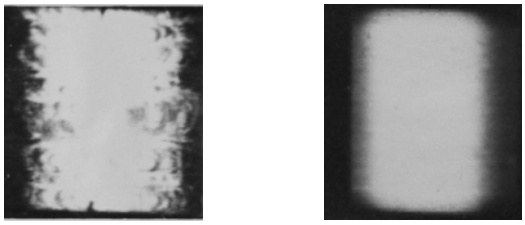

E_0 = 0.75 kV/cm E_0 = 7.5 kV/cm

Applying a higher voltage increases the dispersion and destruction EW achieves the conditions under which the perturbations are not fixed within the limits of high-speed camera resolution.

Dynamics of development and structure of TM-zone as a whole are determined by processes that characterize the development of instabilities in generating mixing. The region with plasma bubbles is about 2÷3 times thinner than layer, in which the plasma is mixed with jet fluid vortices. Also the rearrangement of perturbation spectra takes place in time from short-wave character into the long-wave one. As a result, the wavelength distribution of oscillations generated by perturbations, eventually shifted to the long-wave side. Over time in accordance with the hydrodynamics of the explosion in the fluid, the pattern of development of the turbulence is replaced by a damping stage.

The determining influence of the processes at the beginning of the discharge on the dynamics of development properties of TM inhomogeneities produced in the plasma channel, is confirmed by experiments with made-up corrugations of exploding wires. If the size of the perturbations exceeds a certain size-threshold for the level of their development it was observed during the entire time of discharges for all sufficiently values E_0

1 S. Chandrasekhar, *Hydrodynamic and Hydromagnetic Stability* (Clarendon Press, Oxford, 1961), 652 p.
2 N.A. Inogamov, A.J. Demyanow, E.E. Son, *Hydrodynamic mixing* (Publishing House of MIPT, Moscow, 1999), 464 p.
3 P.D. Starchyk and P.V. Porytskyy, Problems At. Sci. & Techn. Ser. «Plasma Phys.» No. **6(82)**, 214 (2012).

HELICON DISCHARGE FOR LINEARLY UNIFORM PLASMA PRODUCTION

V. F. Virko, V. M. Slobodian, Yu. V. Virko, M. A. Beloshenko, K. P. Shamrai

Institute for Nuclear Research, National Academy of Sciences of Ukraine, Kyiv

Presently, in plasma technological processes the discharges excited by circularly polarized waves − helicons − are widely used [1]. These discharges are generated with the aid of inductive antennas usually placed on the cylindrical surface of dielectric discharge chamber. The radial plasma density distributions in the helicon discharges are essentially nonuniform. But at the same time the plasma technology development demands uniform processing of more and more large area surfaces, as the displays, solar batteries, light panels and so on. For their treatment the discharge, excited by an inductive antenna shaped as a flat spiral on a flat vacuum window surface (so called *transormerly coupled plasma* or *TSP* – discharge) was proposed. Unfortunately, this device cannot be enlarged arbitrarily for the quartz window thickness capable of stand against the atmospheric pressure unacceptably grows. A possible way out consists in the creation of axially uniform plasma. Then, drawing a surface in the transversal direction we can uniformly process a large area.

In this work some modification of the helicon discharge, which can produce the linearly uniform plasma, is proposed and explored. The discharge is excited with assistance of a linear inductive antenna which consists of two parallel conductors with antiphase RF currents. The antenna conductors were situated in two quartz tubes passing through the vacuum volume on the distance 3 cm one from another, perpendicularly to the external magnetic field. The metal discharge chamber had a cubic form with the edge length of 22 cm. External magnetic field was produced by two rectangular coils and was uniform within the chamber. The experiments were carried out in Argon gas at a pressure of 0.65 Pa (5 mTorr), in the range of magnetic field 0 - 10 mT and RF power up to 1 kW on the frequency 13.56 MHz.

In the above mentioned conditions the possibility of excitation by the linear antenna of a stable discharge with sufficient intensity has been shown. It was established that during increasing the magnetic field the beginning growth of the plasma density is accompanied by its abrupt step-like decreasing and finishes with complete cease of the discharge. The critical magnetic fields corresponding to these density jumps grow with increasing of the RF generator output power. Such a behavior is characteristic to the axially bounded helicon discharges and results from change of the modes of standing helicon waves along magnetic field. By means of moveable magnetic probes the spatial distributions of amplitudes and phases of the RF wave magnetic fields were investigated in three mutually perpendicular directions. The measured distributions along the external magnetic field correspond to standing helicon waves that is confirmed by antiphase of oscillations in the adjacent maximums. The wavelength dependence on the plasma density and the magnetic field strength qualitatively agrees with the helicon wave dispersion. Study of the ion saturation current to the probe along the antenna showed that there were some regimes, at which the plasma density was uniform (with accuracy 1.5 - 2 %) on the significant part of the antenna length. At the same time it was revealed that at slight changes in such parameters as the RF power, matching conditions or the magnetic field strength the uniformity might be lost and the density profile along the antenna became nonuniform. It was found that these regimes were distinguished by the standing wave patterns. The conditions for obtaining the uniform density profile need further investigations. The ion current density achieved in the conditions presented at the distance 10 cm from the antenna was 20 mA/cm^2 that corresponded to the plasma density of $8 \cdot 10^{11}$ cm^{-3}.

Thus, a new variety of inductive discharge excited in the magnetic field by the linear conductors with RF currents was proposed, its helicon wave nature was demonstrated. The existence of regimes with linearly uniform plasma on a considerable part of the antenna length has been shown. It was realized a convenient design of the discharge with the inductive antenna immersed in plasma. At further improvement and increase of dimensions the proposed system may be used in plasma-technological equipment for uniform processing of large scale surfaces by its moving across the antenna.

1. M.A. Liberman and A.J. Lichtenberg, *Principles of Plasma Discharges and Materials Processing* (Wiley, New York, 1994).

ABOUT THE HEATING TEMPERATURE OF THE SUBSTRATE AT SYNTHESIS OF DIAMOND-LIKE FILMS

V. V. Gladkovskiy, E. G. Kostin, B. P. Polozov, O. A. Fedorovich

Institute for Nuclear Research, National Academy of Sciences of Ukraine, Kyiv

In recent years exists significant progress in the development of plasma technology of the diamond-like films (DLF) producing and in the methods of their analysis. Stimulus for the development of this technological trend served a collection of unique physical and chemical properties of diamonds and the possibility of their use in various fields of science and technology.

As is well known, properties of the film materials depend on the deposition conditions. This allows to get materials with given collection of mechanical, electric and optical characteristic, which, in turn, opens broad prospects for their use. The defining parameters that affect the structure and properties of DLF are energy of particles, chemical composition of the plasma, vacuum conditions and substrate temperature [1]. It is known, the structure of obtained films and the ratio in them of (sp^3) and (sp^2) - bonds determined by the substrate temperature [2].

Experimental installation for obtaining of diamond-like films from gas phase was constructed and tested in the Institute for Nuclear Research of the National Academy of Sciences.

The high-frequency diode discharge (13.56 MHz) into controlled crossed magnetic and electric fields was taken as a basis for installation. The discharge is excited in mixtures of $H_2 + CH_4$ or $H_2 + CH_4 + Ar$ in different proportions. Working pressure in the chamber was 10^{-1} - 10^{-2} Torr [3].

The temperature of substrate was measured without of plasma using an optical pyrometer and thermocouple. Measurements of the additional heating of the substrate by plasma under discharge switched on by any of the two methods were not obtained. It is associated with the high-frequency current skin-effect on the surface of thermocouple and its additional heating, with deposition on the ends of the insulation of the conductive carbon, which can lead to an understatement of the measurement results. Intense glow of plasma prevents temperature control by using an optical pyrometer is OPPÌR-09.

The problem with the skin effect and electromagnetic interference was decided by shielding of thermocouple surface by metallic plate at the measuring point, as well as the location of the thermocouple under the metal electrodes with a floating potential which their shield. Due to double insulation of thermocouple wires by two hollow porcelain tubes it was eliminated the carbon coating of insulation ends.

Research was conducted with the following values of the current discharge I_d = 0, 4, 6 and 8 A.

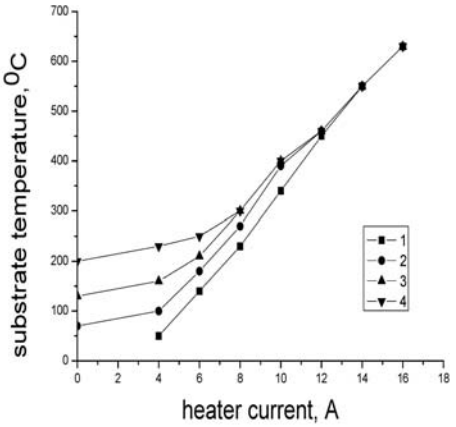

Substrate temperature at different discharge currents.

The dependence of substrate temperature is shown in the Figure at different values of discharge current. Curve *1* is the value of the substrate temperature without discharge. Curves *2* - *4* are obtained at different values of current discharge. From the picture, you can see that the discharge does not affect the substrate temperature at temperature 600 °C.

1. I.A. Sypchenko, Voprosy proektirovaniya i proizvodstva konstryktsii letatel'nykh aparatov: Sb. nauch. tr. Nau. aerokosm. un-ta im. N.E. Zhukovskogo "KhAU", Iss. **3(63)**, 296, 2010.
2. S.O. Rudchenko, V.E. Pukha, and V.V. Starykov, Visnyk KhNU, № 1019 seriya "Fizika", Iss. **16**, 89 (2012).
3. L.S. Maksymenko, O.N. Mishchuk, I.E. Matyash *et al.*, Tekhnologiya i konstruirovanie v elektronnoi aparature **1**, 3 (2013).

CORRELATION BETWEEN REDUCTION COEFFICIENTS OF DECAY DENSE PLASMA WITH FEWER OBSERVED IN THE SPECTRUM LINES

O. A. Fedorovich, L. M. Voitenko

Institute for Nuclear Research, National Academy of Sciences of Ukraine, Kyiv

Dense plasma decay processes are studied insufficiently. In [1 - 4] it was shown that the decay coefficients (C_d) obtained in dense plasma pulsed discharge in water for several orders of magnitude lower than that calculated for ideal plasma.

Experimentally there was not received unambiguous dependence of values C_d on the plasma temperature T [5], on the pressure in the channel, on the concentration of atoms in dense plasma and on its degree of nonideality. The equal values C_d were obtained for the equal values N_e , when the T varied from $6 \cdot 10^4$ K to $6 \cdot 10^3$. According to the classical formulas distinction must be $3 \cdot 10^4$ times [6]. Dependence of C_d from the degree of plasma nonideality (Γ) plasma was obtained ambiguous - the same values of the degree of nonideality corresponded to several decay coefficients. And for some discharges modes even "hysteresis loop" was obtained (when there was a decrease of the decay coefficients with increasing degree of plasma nonideality Γ). The nonideality parameter Γ depends on the electron density and temperature, but rather on their ratio. Therefore, by varying this ratio, it was possible to get the same value of nonideality parameter Γ with very different plasma parameters. It is an impossible and the good agreement of the theoretical description of the experimental dependence of parameters Γ is in [7]. In dense plasma experimental values C_d uniquely depend only on the electron density (N_e), as described by the empirical formula in [3].

Significant increase of C_d correlates with consistent appearance of hydrogen lines H_α (50 ms), H_β (54 ms), H_γ (63 ms) in the emission spectra of the hydrogen-oxygen plasma. Plasma becomes transparent in the continuous spectrum, but in radiation of the line H_α else opaque. Similar results were observed in tungsten plasma recombination. At the initial stage of discharge, when the values of pressure, electron concentration and temperature are highest, plasma is almost not recombining.

Though there is no radiation in the continuous spectrum and no absorption lines. With absorption line appearance (with the lower transition from the ground state to the first excited) recombination starts to go and the intensity of the continuous spectrum due to the appearance of free-bound transitions increases. Continuum intensity due to free-free transitions is very low, as distance between individual ions little and no significant deviations from the straight path of electrons in the fields of closely spaced ions. For large values of N_e recombination is possible only on the unexcited (ground) state of the atom, but the cross section for this process is very small. For the first time the possibility of the influence of nonideality on the recombination coefficient was noted in [8].

It was assumed that the decrease of recombination coefficients occurs because the non-realization of the upper layers (the optical gap ΔE) in the spectrum of the hydrogen and because there is a strong dependence of the recombination coefficients on the plasma temperature. But calculations based in [8] are not fully explaining the large discrepancy with the experimental data.

When we calculate the recombination coefficients we must consider only those levels of atoms, which are observed experimentally [9]. It is necessary to use a formula which takes into account recombination on each individual level, which includes the excitation potentials of the experimentally observed lines.

1. O.A. Fedorovich and L.M. Voitenko, Ukrainian Journal of Physics **53**, No. 5, 450 (2008).
2. O.A. Fedorovich and L.M. Voitenko, Problems of atomic science and Technology **7**, No. 4 (68) 354 (2010).
3. O.A. Fedorovich and L.M. Voitenko, Problems of atomic science and Technology No. **1(71)**, 122 (2011).
4. O.A. Fedorovich and L.M. Voitenko, in *Proc. XV Int. Sci. Conf. «Fircks»* (Nikolaev, 2011), p. 66.
5. O.A. Fedorovich and L.M. Voitenko, in *Proc. XV Int. Sci. Conf. «Fircks»* (Nikolaev, 2011), p. 62.
6. C.L. Johnson and E. Hinnov, J. Quant. Spectrosc. and Radiat. Trasfer., **13**, 333 (1973).
7. A. Lankin and G. Norman. Contribution to Plasma Physics **49**, No. 10, 723 (2009).
8. Y.K. Kurilenkov, High Temperature **18**, No. 6, 1312 (1980).
9. O.A. Fedorovich and L.M. Voitenko, Problems of atomic science and Technology **4 (86)**, 217 (2013).

INVESTIGATION OF Ar PRESSURE EFFECT IN MAGNETRON DISCHARGE ON STRUCTURE AND OPTICAL PROPERTIES OF TiO_2 FILMS

E. G. Kostin[1], A. A.Goncharov[2]

[1] *Institute for Nuclear Research, National Academy of Sciences of Ukraine, Kyiv*
[2] *Institute of Physics, National Academy of Sciences of Ukraine, Kyiv*

Earlier [1], gas discharge, generated in an in a cylindrical inverted DC magnetron, has been used for synthesis of TiN films. In [2] were performed investigation of plasma optical characteristic and discharge parameter of this magnetron for TiO_2 films synthesis. This report is examination of interrelation between films deposition conditions, such as discharge pressure, and films structure and optical properties. To monitor the synthesis of the films, we used a Plasma Spec spectrometer [1]. Reactive gas (O_2) flow, required to produce stoichiometric TiO_2 films, was determined on the location of singular points on the curves of the discharge voltage and atomic oxygen line (777, 2 nm) intensity. Physical meaning and location of these singular points discussed in [2].

Composition of the films deposited at a substrate temperature 400 °C corresponds to the anatase TiO_2 with typical for this phase lines. At temperature 300 °C the films were amorphous. From the spectra in Fig. 1, you can see the influence of argon pressure on the position and broadening of anatase line.

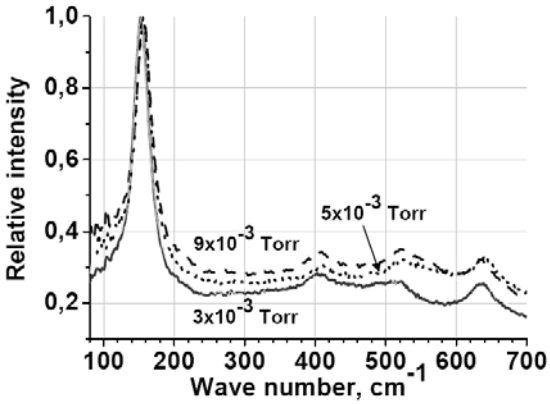

Fig. 1. Raman spectra TiO_2 films deposited at substrate temperatures 400°C and pressures $3\cdot10^{-3}$, $5\cdot10^{-3}$, $9\cdot10^{-3}$ Torr.

Comparison of these Raman spectra with the bulk anatase spectrum shows the "blue" shift of position of all registered lines, that inherent for small crystallite size. With decreasing of argon pressure there is a decrease in the background under the line Eg1, reducing the "blue" shift and line widths. Decrease in background means decrease of disordered (amorphous) crystalline fraction in the film volume, and a decrease in the "blue" shift of Eg1 line means an increase in crystallite size at lower argon pressure. Physically, the effect of the argon pressure is explained by Ti atoms scattering on Ar atoms on the way towards substrate with a loss of energy. As a result, they lose the ability to migrate along the surface of the substrate and lose the opportunity to integrate in an ordered crystalline structure during thermalization of their energy. The estimations of Ti atoms free path for gas temperature 500 K show that quantity of particle, reaching substrate without scattering is 15, 8 % for 2, $5\cdot10^{-3}$ Torr, 2, 5 % for $5\cdot10^{-3}$ Torr and 0, 13 % for $9\cdot10^{-3}$ Torr.

Fig. 2 shows the refractive index dispersion of the TiO_2 films, calculated from the optical transmittance.

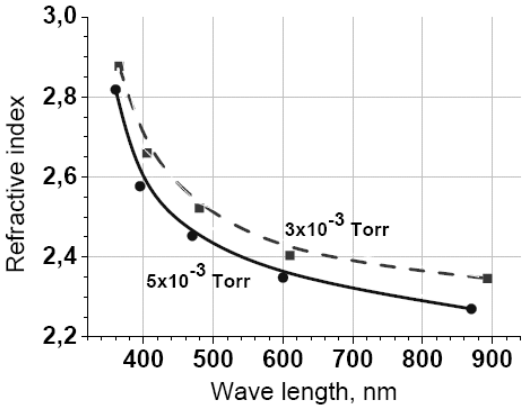

Fig. 2. Refractive index of films deposited at substrate temperatures 400°C and pressures 2, $5\cdot10^{-3}$, $5\cdot10^{-3}$ Torr.

It is known that refractive index is directly related to optical films porosity. From the Fig. 2 data it can be concluded that at a lower pressure less porous film formed. This agrees with the fact that than scattering of Ti atoms less so with greater energy they enter on substrate and can be embedded in a dense structure.

1. A.A. Goncharov, A.V. Demchishin, E.G. Kostin *et al.*, Tech. Phys. **52**, No. 8, 1073 (2007).
2. A.A. Goncharov, A.N. Evsjukov, E.G. Kostin, E. K. Frolova, Ukr. J. Phys. **55**, No. 6, 677 (2010).

Abstracts of works on radioecology and radiobiology

LIPID PEROXIDATION IN RAT BLOOD FOR A SINGLE ENTER DIFFERENT DOSES OF ^{131}I

Yu. P. Grynevych, A. I. Lypska, S. V. Teletska, T. V. Tsyganok

Institute for Nuclear Research, National Academy of Sciences of Ukraine, Kyiv

Iodine - a trace mineral that is essential for the functioning of the thyroid gland (TG) - the most important organ of the endocrine system that synthesizes hormones for normal functioning of most organs and systems. Iodine as a structural component of thyroid hormones determine the activity of course a wide range of metabolic processes in the body. Its accumulation in the TG correlates with the level of iodide in the blood through the complex regulatory mechanisms and controlled by the central nervous system. Radiation damage TG evident increase of the functional activity of the gradual transition in hypothyroid condition in which inhibited the biosynthesis of thyroid hormones thyroxine and triiodothyronine - major regulators oxidation - reduction processes in the body, which played a leading role in the formation of primary physical and chemical reactions on the effect of radiation. This work is a continuation of the flow loop studies of the mechanism of free radical processes (FRP) in the blood of animals for effects on the body ^{131}I. VRP different doses for oral conditions (through a tube) injection of an aqueous solution of sodium iodide 1I activity 3.32 kBq, 19.2 kBq , 65 kBq per animal hemolisate investigated in rat blood - male Wistar weighing 200±15 g induced by H_2O_2 chemiluminescence (CL) [1] for the parameters of the maximum intensity of luminescence (I_{max}) and its light sum (Σ_{300}) for 5 min dynamics experiment at 0.125 (3H) per 1, 3, 7, 8, 14 and 30 days from the start injection of the isotope. Antioxidant link FRP studied the activity of catalase [2]. Blood for research (20 mkl) taken from the tail vein of animals.

Dynamics of FRP in the peripheral blood of rats tends to undulating changes in CL, amplitudes are not significantly (within measurement error) depends on the imposed activities ^{131}I.

Thus, doses of 3.32 kBq and 19.16 kBq maximum value I_{max}, Σ_{300} and registered on 3rd and 14th days of experiment and at a dose of 65 kBk on the 1st and 14th, while the minimum - 7 - 8 days. Recovering kinetic parameters of CL reactions observed from 14 days (3.32 kBq per I_{max}) and 30 (19.2 kBq), day of the experiment. Undulating change in intensity FRP obviously floor, connected both with wavy isotope redistribution between organs and tissues, as features of the process of its output, and a slight deviation from their control - low in the isotope in blood. It should be noted that in 24 hours after exposure TG reduced activity of thyroid peroxidase and thyroid status, which is the most significant reduction in remote period and phase changes occurring in the blood of thyroid hormones that control the processes of peroxide. Amplitudes due I_{max} functional activity of key antioxidant enzymes - superoxidedismutase and active catalase conjugated with it. Her activity in the blood of rats nonsignificantly changed during the experiment and the doses administered were oppositely directed changes to the CL of the blood. As a result of this turn of the FRP kept intact cell membrane, their transport, and energotrans-formation, receptor function. Thus, in this presents studies, as in the past, it is proved that the single input ^{131}I in the specified activity does not significantly affect the dynamics of the flow hemolisate FRP in blood and does not lead to significant impairment prooxidant - antioxidant balance.

1. Ya. I. Serkiz, M. O. Druzhyna, A. P. Hryenko *et al. Chemiluminescense of blood at radiation impact.* (Nauk. Dumka, Kyiv, 1989).
2. M. A. Koroliuk, L. I. Ivanov, I. G. Mayorov *et al.*, Lab. Case. **1(16)** (1988).

EVALUATION RADIATION EXPOSURE IN CASE OF FIRE AT OBJECT "UKRYTIA"

S. I. Azarov[1], V. L. Sydorenko[2]

[1] *Institute for Nuclear Research, National Academy of Sciences of Ukraine, Kyiv*
[2] *Public Administration in Sphere of Civil Protection, Kyiv*

There is a probability of occurrence and development of fire object "Ukrytia" that can appear causes of physical barriers, tightness and release of radioactive combustion products outside the object "Ukrytia" [1].

Radioactive combustion products during a fire indoors facility were collected on filters area of approximately 0.05 m^2 with air pumping capacity of 10^3 m^3/day. The filters were then sent to the laboratory radiometric to Chernobyl, where they spent their γ-spectrometry for ultra-pure germanium detector with energy of 1.9 keV sensitivity to gamma-ray lines of ^{60}Co and efficient registration of 52 %. Registration, processing and delivery of information carried spectrometric analyzer Nokia Lp4900B. The limit of detection of ^{137}Cs – 0.048 mBq/m^3 the relative level of accuracy of measurement of specific activity in samples of less than 10 %. The total activity of filters was measured no sooner than three days after sampling, that after the collapse of short-lived daughter products of natural noble gas radon and argon. Activity size distribution of radioactive particles held impactors of 3 m^3/min air flow. Concentration and separation of transuranic elements with carriers of the aerosol filters and solutions carried out by radiochemical methods.

The expression for calculating the dose of internal irradiation by inhalation of radionuclides in the human body, without the use of personal protective equipment [2]:

$$E^{inhal} = w\,t \sum_i \sum_j e_\tau^{i,j} \frac{C_{eq}^{\Sigma}\, P_{eq}^{i,j}}{100},$$

where w – breathing man; t – time-stays of personnel in an emergency area; $e_\tau^{i,j}$ – dose per unit activity inhaled by revenues due to i radionuclide j type absorption by the body; C_{eq}^{Σ} – the concentration of a mixture of radionuclides in air; $P_{eq}^{i,j}$ – the percentage of i nuclide j type in the air.

Inhalation dose coefficients for radionuclides ^{137}Cs, ^{90}Sr and transuranic elements were calculated using the program IMBA, developed by NRPB [3].

The total dose rates from inhalation were found for the main design scheme (see Table).

According to disperse radioactive composition of volatile particles were distributed as follows: aerosols with AMAD of 1 micron – 1 %, from 1 to 15 μm – 95 %, more than 15 μm – 4 %.

The total dose rates from inhalation intake of individual

Diagram	E^{inhol}, mcSv/Bq	Source
Two-tiered division, class S	0.43	[4]
АМАД, СГВ, клас S - d_m = 0,5 μm, σ_g = 2.45	0.30	[3]
- d_m = 1,0 μm, σ_g = 2.48	0.26	[3]
- d_m = 5,0 μm, σ_g = 2.5	0.15	[3]
АМАД, СГВ - d_m = 1,0 μm, σ_g = 2.5	4.2	[2]

AMAD – Active median aerodynamic diameter aerosols (d_m); SGD – standard geometric deviation (σ_g).

Doses of internal irradiation were determined by inhalation of radionuclides in the human body. The density of particles of prostate cancer was taken as 0.32 kg/m^3, form factor – 1.5, the rate of breathing person – 1.2 m^3. It was assumed that the proportion of radioactive substances initially precipitated in the lungs, is transferred into the gastrointestinal tract. The corresponding values for the account of the transfer of the gastrointestinal tract in plasma were taken equal to 0.1 for ^{137}Cs and ^{90}Sr and 10^{-5} for $^{239+240}$Pu.

Comparison of the calculated total effective dose from inhalation statutory annual individual effective dose of internal exposure to personnel, which should be no more than 3.0 mSv, showed that suppression of fire in the room 402/3 object "Ukrytia" in 10 hours you can get a total dose of more acceptable and to extinguish the fire in the room 805/3 Received dose commensurate with acceptable levels of daily stress [5].

1. S. I. Azarov and V. V. Tokarevsky, Nuclear engineering international **40(491)**, 38 (1995).
2. *Норми радіаційної безпеки України* (*НРБУ-97*): 135 (2000).
3. A. Birchall, M. Puncher, A. C. James *et al*., RPD **105**, 421 (2003).
4. С. И. Азаров, Атомная энергия **90(4)**, 296 (2001).
5. Ю. В. Литвинов, С. І. Азаров та В. Л. Сидоренко, СНУЯЕтаП **2(46)**, 125 (2013).

МОДЕЛЬ ДЛЯ ДОСЛІДЖЕННЯ ЦИТОГЕНЕТИЧНИХ ЕФЕКТІВ РАДІОНУКЛІДІВ У ЛІМФОЦИТАХ ПЕРИФЕРІЙНОЇ КРОВІ ЛЮДИНИ В ЕКСПЕРИМЕНТАХ *in vitro*

Л. К. Бездробна, В. І. Федорченко, В. А. Агеєв, Т. В.Циганок, Л. В. Тарасенко, В. А. Курочкіна, Т. В. Мельник

Інститут ядерних досліджень НАН України, Київ

Мета роботи: розробка моделі для дослідження цитогенетичних ефектів радіонуклідів у лімфоцитах периферійної крові людини в експериментах *in vitro*.

Відпрацьовано умови та розроблено й виготовлено установку для інкубації зразків гепаринізованої венозної крові людини з радіонуклідами для проведення досліджень з вивчення залежності спектра й частоти індукованих хромосомних пошкоджень у лімфоцитах крові від дози опромінення.

Головною частиною установки є касета, виготовлена з дюралевої заготовки (діаметром 100 мм), яка має по периферії 6 гнізд для розміщення флаконів зі зразками крові і по центру гніздо для термометра, призначеного для контролю температури в касеті. Для запобігання взаємного опромінення зразків крові з радіонуклідами передбачено обгортання флаконів листовим свинцем необхідної товщини. Для постійного перемішування крові касету зафіксовано на сталевій горизонтальній осі, що вільно перекручується між двома підпорами, закріпленими на масивній платформі. Обертання осі касети здійснюється від редукторного електродвигуна РД-54 з частотою обертання 10,8 об/хв. Установку розміщено в термостаті (37 °С), а електродвигун – поза термостатом вертикально над його електронним блоком. Для введення осі електродвигуна в камеру термостата використали отвір у термостаті, що призначений для контрольного термометра. Вісь електродвигуна з'єднано з віссю касети через шестерінчастий поворот на 90° (див. рисунок). Фіксація флаконів зі зразками крові при обертанні касети забезпечується прижимною кришкою на двох гвинтах.

Показано, що за умов інкубації крові (3 мл) з фізіологічним розчином (0,5 мл), що буде використовуватися в подальшому для розведення радіонукліда, і поживним середовищем RPMI-1640 (1,5 мл) із гентоміцином (6 одиниць на 1 мл загальної суміші) упродовж 48 год при 37 °С при постійному перемішуванні та проведенні процедур, що імітують відмивання клітин крові від радіонукліда, лімфоцити крові зберігають життєздатність. Для цього після закінчення інкубації вміст флаконів переносили у стерильні центрифужні пробірки, додавали 2 мл фізіологічного розчину (37 °С), перемішували та центрифугували 10 хв при 1000 об/хв. Надосад видаляли, залишаючи у пробірці 3 мл осаду клітин, додавали поживне середовище (5 мл, 37 °С), перемішували й центрифугували. Процедуру відмивання проводили у стерильних умовах і повторювали двічі. Осад ресуспендували.

Мікроскопічний аналіз мазків суспензії відмитих клітин крові не виявив морфологічних змін лімфоцитів.

Тестування лімфоцитів на пошкодження цілісності клітинних мембран за фарбуванням трипановим-синім [1] показало, що більше 99,5 % лімфоцитів мають неушкоджену мембрану.

Після культивування відмитих клітин крові в поживному середовищі з фітогемаглютиніном відповідно до стандартного протоколу [2] було виявлено достатню кількість метафазних пластинок, що відповідали вимогам для проведення цитогенетичного аналізу.

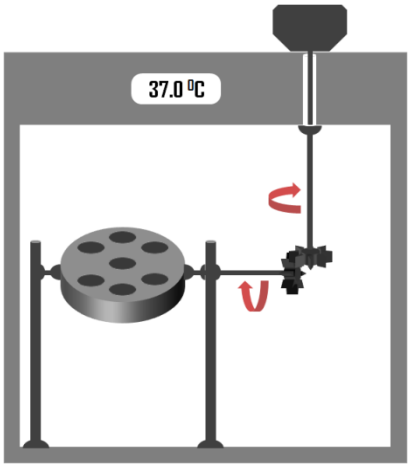

Схема установки для інкубації зразків крові людини у термостаті.

1. *Лимфоциты: Методы*, пер. с англ.; под ред. Дж. Клауса (Мир, М. 1990), 395 с.
2. *Cytogenetic dosimetry: applications in preparedness for and response to radiation emergencies* (IAEA, Vienna, 2011), 229 p.

RADIOBIOLOGICAL EFFECTS IN SMALL RODENTS – CONSTANT INHABITANTS OF CNPP RADIATION-POLLUTED REGION

O. O. Burdo[1], A. I. Lypska[1], O. A. Sova[1], N. K. Rodionova

[1] Institute for Nuclear Research, National Academy of Sciences of Ukraine, Kyiv
[2] R. E. Kavetsky Institute of Experimental Pathology, Oncology and Radiobiology National Academy of Sciences of Ukraine, Kyiv

Complex radiological research (including in-field and laboratory ones) of small rodents – constant inhabitants of CNPP radiation-polluted region were made. Trapping of animals performed in areas with uneven distribution of radiation fields, the background radiation in some areas was able to vary by more than 5 times.

Species diversity of the small rodents was studied using karyotyping and morphological characteristics. Shown that most representative type of CNPP region is red vole (*Clethrionomys glareolus*). γ-β-spectrometric studies, the levels of accumulation and specific activity of ^{137}Cs and ^{90}Sr ^{137}Cs in the body of animals were conducted. Radioactive contamination of the animals varied widely from 200 to 1450 Bq/g ^{137}Cs, 100 - 1700 Bq/g ^{90}Sr. Individuals with abnormally high content of radionuclides were also observed. Absorbed radiation doses originating from Chernobyl radiation factor were calculated.

A comparative analysis of cytogenetic, morpho-physiological and hematologic parameters of animals from contaminated and background areas was made.

In experimental animals the frequency of mononuclear cells with MNwas in 8 - 13 times higher than the spontaneous level; also cells with a large number of MN per cell were observed (Fig. 1). These changes indicate a violation of cytogenetic homeostasis. Increased level of cytogenetic disorders may be due to both the direct effect of radiation, and with a decrease in the functional activity of the immune system that monitors the cytogenetic homeostasis.

Hematological studies have established that the concentration of leukocytes in animals from contaminated areas were not statistically different from the control group. The number of erythrocytes in irradiated animals was within reference values. Nevertheless were observed qualitative disturbances of peripheral blood red cell units - pronounced anizopoykilotsytoz, polychromatophilia of red blood cells, indicating a disruption of the maturation processes of erythroid precursor cells and coincides with an increase in level of cytogenetic abnormalities in bone marrow cells. In the spleen of animals with a high content of incorporated radionuclides registered an erythroid precursor cells.

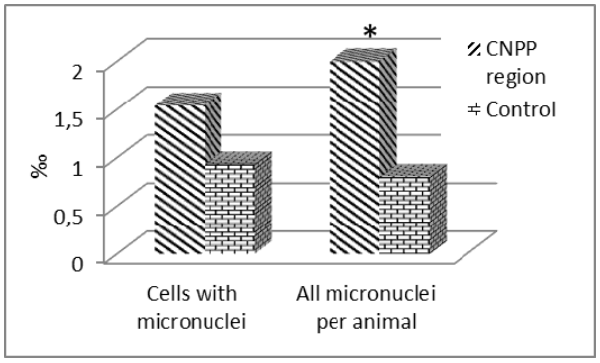

Fig.1. Results of cytogenetic studies of bone marrow cells voles ‰ (CNPP region, Control), *p≥0,05

Analysis of morphological parameters showed that mass indexes of the internal organs of animals from the Chernobyl exclusion zone are substantially different from control levels (Fig. 2).

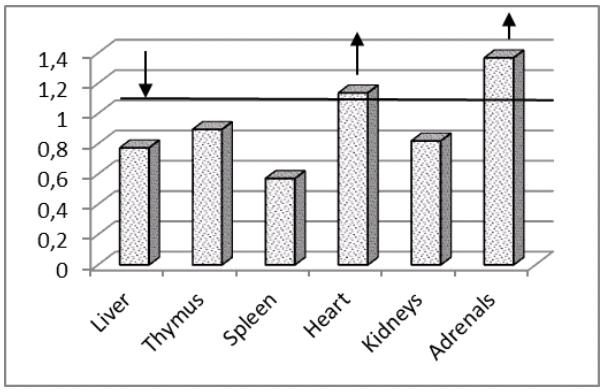

Fig. 2. The ratio of average mass index of the internal organs of experimental and control groups.

Such index ratio of the internal organs testifies to infringement of the energy balance.

The set of these results and the literature data indicates complex adaptative processes in populations of animals within the zone of radioactive contamination.

DOSE-DEPENDENT CHANGES IN EFFECTIVE HALF-LIFE PERIOD OF ^{131}I FROM LABORATORY RATS THYROID GLAND

I. P. Drozd, O. A. Sova

Institute for Nuclear Research, National Academy of Sciences of Ukraine, Kyiv

In 2011, we conducted a series of experiments with a single oral administration of iodine with three different activities, namely, 3.3, 19.2 and 114.8 kBq/animal to laboratory rats.

Thus on the 80th day in the thyroid gland (TG) formed a dose of 0.86, 6.62 and 32.11 Gy.

As a result it was determined that, with an increase of absorbed in thyroid dose, an increase in the effective half-life period of the isotope from the body (T_{ef}) is observed, which can be described by a power function:

$$T_{ef} = 2.71109\, D^{0.16168},$$

where D - absorbed dose, Gy [1].

This growing can be explained by the gradual development of iatrogenic hypothyroidism, caused by a moderate damage of thyroid gland tissues, resulting in reduced production of thyrotropic hormones and thus reduce the release of iodine into the bloodstream.

However, there are messages in literature, that are based on repeatedly experimentally proven facts, that for a very large dose (hundreds of Gray) T_{ef} decreases rapidly with increasing dose [2]. This is due to progressive destruction of TG tissue and loss of ability to retain iodine.

The question is: at what dose value begins the TG destruction and, consequently, T_{ef} reducing? This is important for understanding the process of absorbed dose formation in TG. In the scientific literature such data is absent. So we set an experiment with single injection of sodium iodide (^{131}I) in an amount 327 kBq/animal to laboratory rats. 25 animals – mature male rats Wistar, weighing 240 ± 30 g were involved in the experiment. The animals were sacrificed according to schedule, with the requirements of Art. 26 Law of Ukraine "On protection of animals from cruelty." The method of gamma-ray spectrometry determined the content of the isotope in the thyroid in dynamics of experiment. We determined T_{ef} according to obtained data.

The maximum absorbed dose on the 80th day was 68.5 Gy. As a result, it was found that T_{ef} decreased by 11 % and amounted 4.3 compared to 4.85 with a dose 32 Gy.

Having a reference points for doses above 400 Gy, taken from [2] and using our own experimental data, and assuming that the radiation-induced TG tissue destruction goes exponentially, we found the minimum dose at which destruction begins lies in the range 32 - 37 Gy.

Dynamics of T_{ef} changes are shown on Figure.

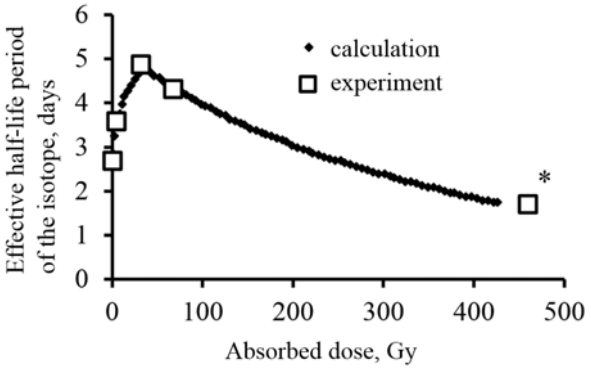

* Published data.

The dependence of the values of the effective half-life period of ^{131}I from the thyroid from absorbed dose in the organ.

Found that the absorbed dose of 750 ± 50 Gy leads to complete destruction of thyroid tissue.

Patterns of accumulation and retention of radioactive iodine in thyroid, that were found, we subsequently used in interpreting the results of experiments with long-term oral intake of ^{131}I.

1. *Annual Report-2011* (Institute for Nuclear Research, Kyiv, 2012), p. 118.
2. *Распределение, кинетика обмена и биологическое действие радиоактивных изотопов йода.* Сб., под ред. Л. А. Ильина, Ю. И. Москалева (Медицина, М., 1970), 240 с.

IRRADIATION OF BLOOD CELLS AT THE INTAKE OF RADIONUCLIDE (DOSIMETRIC MODEL)

I. P. Drozd, A. I. Lypska, O. A. Sova

Institute for Nuclear Research, National Academy of Sciences of Ukraine, Kyiv

In radiobiological and biomedical researches it is often necessary to know the radiation dose of blood cells (BC). It is especially useful for dosimetric support in field of radiation hematology and cytogenetics.

This problem should be referred to the field of microdosimetry, because BC have small sizes, different forms and various kinetic properties.

However, there are no generally accepted methods for circulating blood cells doses calculating in available literature. This report sets out a methodical approach to the assessment of absorbed doses in BC using macrodosymetric parameters.

It is known that the absorbed dose is the energy of radioactive decay, emitted in volume V for time t, referred to the mass of the substance m, contained in this volume. We believe that BC are uniformly distributed in indicated volume. Then, using such quantities as average number of BC of this type in volume blood unit, average volume of one BC, density of the culture, that consists of this type BC, and energy of radiation, which is released at time t in volume, that is occupied with particular BC, we can calculate average absorbed dose in this BC. Also, we believe that all types of BC, except red blood cells and platelets, the average volume of which is known and described in reference sources, are spherical formations. Time t in this case corresponds to the average circulation time of this BC.

If radioactive isotope with activity Q (Bq) is contained in 1 liter of blood, radiation energy (J), which is absorbed in this volume, can be determined as:

$$E = \int_0^t Q_0 \cdot 1{,}6 \cdot 10^{-13} \cdot E_{ef}\, dt$$

where E_{ef} – effective energy (MeV/decay), that is released in each act of radionuclide decay.

Energy, which is absorbed in population of k-type BC contained in 1 liter of blood:

$$E_k = E \cdot V_k,$$

where V_k – is volume of all together k-type BC.

Energy, which is absorbed in one k-type BC:

$$e_k = E_k / n_k,$$

where n_k – number of k-type BC contained in 1 liter of blood.

Dose (Gy) absorbed at time t in the same k-type BC will be:

$$d_k = \frac{e_k}{\rho \cdot v_k},$$

where v_k – volume of one k-type BC; ρ – density of culture of k-type BC.

Each type of BC has a specific, peculiar only to him bloodstream circulation time.

The maximum absorbed doses in different types of BC, which are calculated, as an example of this method, for male rat (for the entire period of their circulation in the bloodstream) for the cases of single-and long-term intakes of ^{131}I, are shown in the Table.

Maximum doses, absorbed in blood cells after one time and long-term intakes of ^{131}I

Blood cells		The maximum doses (Gy) for the time of BC circulation in bloodstream	
		after one time ^{131}I intake in the amount 114.8 kBq	with long-term daily intake of ^{131}I in the amount of 29.3 kBq
Erythrocytes		0,001629	0,003015
Platelets		0,000940	0,000543
Leukocytes	Neutrophils	0,000115	0,000012
	Monocytes	0,000221	0,000036
	Eosinophils	0,000245	0,000044
	Basophils	0,000435	0,000124
	Lymphocytes	0,001361	0,002539

KINETICS OF IODINE-131 AND DOSE FORMATION IN ORGANISMS OF LABORATORY RATS AT THE PERMANENT INTAKE OF ISOTOPE

I. P. Drozd, A. I. Lypska, O. A. Sova, V. A. Shytiuk, L. K. Bezdrobna, O. O. Burdo, L. I. Kuptsova, V. A. Kurochkina, T. V. Melnyk, L. V. Tarasenko, L. A. Temenik, T. V. Tsyganok

Institute for Nuclear Research, National Academy of Sciences of Ukraine, Kyiv

The processes of accumulation and excretion of ^{131}I in the organs and tissues of male Wistar laboratory rats by peroral daily intakes of 29.3 kBq isotope were studied. The experiment lasted 15 days. The solution of NaI in distilled water was administrated orally through a tube to animals, and then they were fed. We used rats with stable homeostasis, weighing 270 ± 40 g. Animals were sacrificed (5 pcs. each time) on 1, 2, 3, 7 and 15 days after the start of administration of the isotope in compliance with Art. 26 Law of Ukraine "About protection of animals from cruelty". Content of isotope was measured in organs and tissues by γ-spectrometry method. According to the averaged for 5 animals measurements, the graphic of isotope accumulation in organs and tissues was built and comprehensively analyzed. Example of the ^{131}I accumulation in thyroid gland (TG) analysis is shown on Fig. 1.

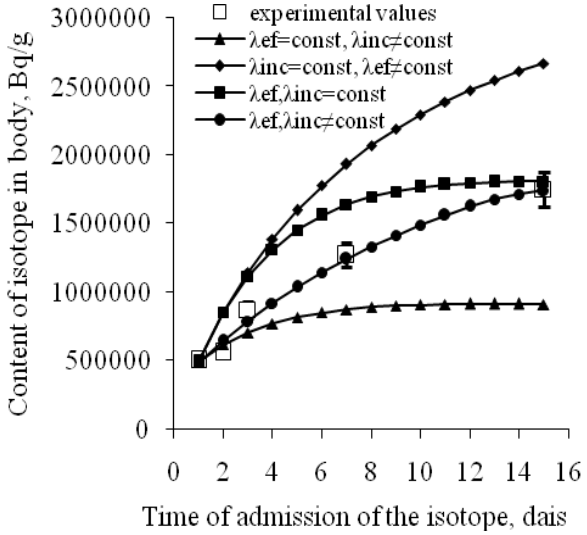

Fig. 1. Analysis of the accumulation of ^{131}I in TG: λinc - describes amount the isotope entering into the TG; λef - rate of excretion from TG.

We found that the proportion of isotope transported to the organ and the excretion rate of the isotope is not constant and depend on the dose of TG irradiation.

Isotope accumulations in main depots curves are informative. We have experimentally proved that, in addition to TG, hypoderm should also be considered as a main depots. On the second day from the beginning of the injection dominates the accumulation of iodine in the hypodermis, which plays role as a body depot for reservation of various substances, including trace elements, among these is iodine (Fig. 2). If necessary, obviously hypodermis becomes a reserve source of iodine for the thyroid gland and some other organs.

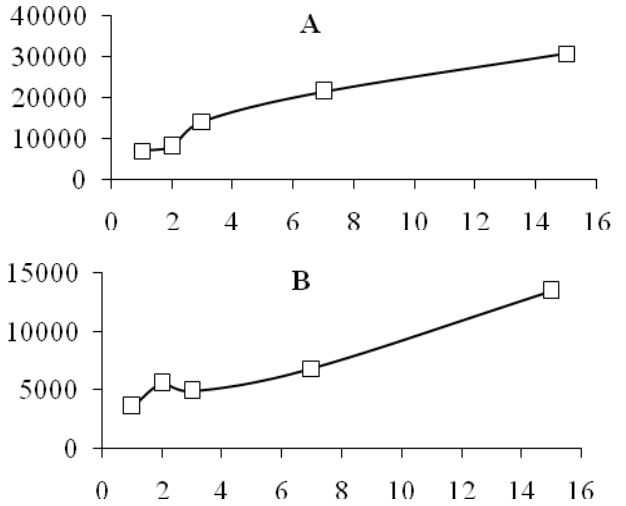

Fig. 2. The iodine accumulation dynamics in TG (A) and hypoderm (B). On the horizontal axis - time of admission of the isotope, days; vertical axis - the absolute content of isotope, Bq.

Using the expressions $N = \int_0^t q(t)dt$ and $D = 1{,}6 \cdot 10^{-10} \cdot N \cdot E_{ef}$, where $q(t)$ - specific activity in the organ, E_{ef} – effective energy we determined the cumulative amount of radioactive decays (N) and absorbed dose (D) in the organs and tissues at the time t.

Calculations showed that at 15 days: absorbed in TG dose was 51 Gy; in stomach walls and hypoderm - about 3 orders of magnitude, in kidney, liver, lung, spleen, bone, red bone marrow, thymus, wall of intestine - about 4 and in muscle tissue - about 5 orders of magnitude smaller, than in TG.

Since absorbed in TG dose after internal intake of ^{131}I can reach very high values, this is used for radiotherapy of TG cancer in humans. However, for radiotherapy regulations development that would take into account individual patient it is necessary to conduct a thorough analysis of dose formation.

INVESTIGATION OF MIGRATION PROCESSES IN AREAS WITH DIFFERENT LEVELS OF RADIOACTIVE CONTAMINATION

N. V. Kulich, A. I. Lipskaya, V. I. Nikolaev, V. A. Shityk

Institute for Nuclear Research, National Academy of Sciences of Ukraine, Kyiv

The current state of contamination by anthropogenic radionuclides is explored in ChNPP near zone. The investigation is performed on the four monitoring landfills located at different distances from the ChNPP (from 2 to 25 km). Radiometric measurements were made at soil sampling points. The exposure rate at some points differs more than in 100 times. Soil samples for research are collected step-by-step to the 30 cm depth (0 - 2 cm; 2 - 4 cm; 4 - 7 cm; 7 - 10 cm; 10 - 15 cm; 15 - 20 cm; 25 - 30 cm) by envelope technique at points without anthropogenic influence. Soils on investigated landfills are mostly lightlyturfed lightlyhumused sands and dewed sand soils.

γ-β-spectroscopic investigations of soil samples is done, then spectral consistency and activities of radionuclides are determined. Distribution of radionuclides ^{90}Sr; ^{137}Cs; ^{241}Am is investigated at soil horizon on landfills both with maximum and minimum level of contamination. It was fond that on all investigated areas main quantity of radionuclides are located in the root-inhabited layer of soil. The similarity is observed in the behavior of ^{90}Sr; ^{137}Cs; ^{241}Am in soils. This, may be, is determined by the fact that the migration of radioactivity to the depth of soil is done by migration of fuel particles, which contain ^{90}Sr; ^{137}Cs; ^{241}Am.

The spectral investigation data and diffuse-convection model are used to calculate environmental periods of half-purification of 5 cm soil layer ($T_{1/2env}$) from ^{90}Sr; ^{137}Cs; ^{241}Am. It is shown that $T_{1/2env}$ is almost equal for all investigated radionuclides in the layer in spite of significant differences in radioactive contamination levels of areas. Periods of half-purifications can be divided in two groups with $T_{1/2env}$ equal to 30 and 60 years. The environmental period of half-purification of 5 cm soil layer, $T_{1/2\ env}$, is determined from obtained data for ^{90}Sr; ^{137}Cs; ^{241}Am.

Activity and period of half-purification $T_{1/2env}$ for ^{90}Sr, ^{137}Cs, ^{241}Am in investigated layers

Ladnfill	Activity, Bk/sample			Period of half-purification $T_{1/2env}$, years		
	^{137}Cs	^{90}Sr	^{241}Am	^{137}Cs	^{90}Sr	^{241}Am
Yanov 1-1	5866	2450	113	36	42	40
Yanov 1-2	57000	14063	578	71	80	71
Yanov 1-3	17497	11438	843	53	65	120
Yanov 2-1	13560	4572	100	75	74	67
Yanov 2-2	12304	8151	384	56	68	69
Yanov 2-3	13063	2765	234	42	58	65
Yanov $_{pine}$	7642	2281	266	69	54	114
Yanov $_{1\ 2010}$	2008	704	39	57	39	74
Yanov $_{2\ 2010}$	1839	1330	30	28	26	26
Chistogalovka$_1$	1139	615	27	28	26	28
Chistogalovka $_2$	3315	1116	98	30	28	31
Izumrudnoe$_1$	260	73	6	29	26	27
Izumrudnoe $_2$	160	246	4	26	32	23
Skazochnoe$_1$	55	13	0,3	61	34	52
Skazochnoe $_2$	115	20	3	42	31	47

RESEARCH OF THE RADIONUCLIDES FORMS IN SOIL-PLANT COMPLEXES OF THE NEAREST CHERNOBYL NPP ZONE

V. I. Nikolaev, V. A. Shytiuk, A. I. Lypska, N. V. Kulich

Institute for Nuclear Research, National Academy of Sciences of Ukraine, Kyiv

Physicochemical forms of radionuclides, which got into the environment as a result of the accident on Chernobyl NPP are changing under the influence of external environmental factors. Consequently, that changes their migration capacity and bioavailability. Determination of radionuclides forms that affect the intensity and mechanism of migration is an actual problem.

Complex radioecological studies were conducted on the territory of research polygon near Chernobyl zone with non-uniform radioactive contamination, exposure dose was 600 - 5000 mcR/h. Soil and plant samples were collected for studies in the same areas. After the standard laboratory sample preparation, γ- and β-spectrometric studies of soil and vegetation samples were carried out.

Activity of the radionuclides in the experimental samples was measured on γ-spectrometer CANBERRA and β-spectrometer "SEB-50". Processing of the spectra was carried out, using program WINSPECTRUM and "Beta fit".

For estimation of forms of the radionuclides in soils and plants researches using the sequential chemical extraction were carried out. Extraction of radionuclide fractions in the soil samples were performed in the following order: water soluble, exchange, organic, mobile, fixed and mineral balance. The following forms were determined in plants: exchange-adsorption, organic and mineral remainder. Radionuclides, which passed to the contact solution considered as "mobile" form and those, which remained in mineral remainder are "non-exchange".

Isotopic composition and content of technogenic radionuclides in soil, plants and forest litter were studied. The activity of radionuclides ^{137}Cs, ^{90}Sr and ^{241}Am in the extracted fractions was determined.

It was established that the main content of ^{137}Cs and ^{90}Sr in soils are represented in non-exchange and fixed forms, and only ~ 20 % of radionuclides - biologically available forms. Table presents the data on the distribution of forms of radionuclides in soils.

This distribution is probably due to the fact that significant part of the radionuclides in the soil are still composed in the fuel particles and weakly leached with contact solutions.

Forms of radionuclides in soils of research polygon

Forms	^{137}Cs,	^{90}Sr	^{241}Am
Water soluble	0,20 ±0,01	0,25 ±0,05	0,5±0,2
Exchange	0,31 ±0,02	9,35 ±0,8	1,0±0,5
Organic	0,49 ±0,03	2,4 ±0,45	7,0 ±0,2
Mobile	2,5 ±0,5	7,5 ±0,7	45 ±5
Fixed	12,5 ±1,5	2,5 ±0,5	20 ±2
Mineral remainder	84 ±5	78 ±8	26,5 ±3

In plants radionuclides are mainly represented in exchange-adsorption and organic forms (85 - 90 %). Thus, the main part after death of the plant can easily be involved in the redistribution chain "soil-plant-animal". The Figure presents the forms of the radionuclides in plants.

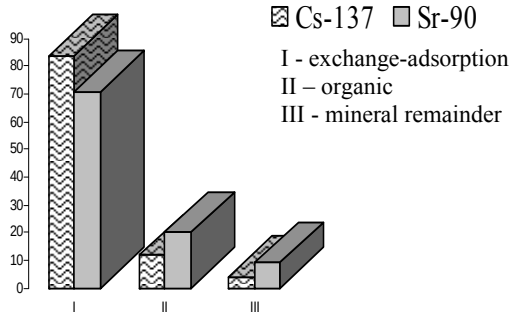

The forms of ^{137}Cs and ^{90}Sr in plants.

Spectrometric study of forest litter extracts revealed a significant content of radionuclides in the contact solution. In the litter of fixed forms is only 19-21%. This indicates that litter is an additional source of mobile forms of radionuclides.

According to our research significant part of the radionuclides in the soil are represent in non-exchange forms and in the near future will not be included in the redistribution.

Therefore, the forms of radionuclides in soils determine their bioavailability and migration in soil-plant complex.

PARAMETERS OF ^{137}Cs KINETICS IN RATS' ORGANISM AND RADIATION DOSES OF ORGANS AND TISSUES CALCULATION PROGRAM

V. I. Pastushenko, M. V. Naychuk, A. I. Lypska, I. P. Drozd

Institute for Nuclear Research, National Academy of Sciences of Ukraine, Kyiv

Important and actual direction of experimental radio-biology researches is a dosimetry and programmatic-mathematical modeling. For correct interpretation of radiogenic violations in an organism for a receipt ^{137}Cs it is necessary to know the doses taken in directly in every organ, and dynamics of their forming. For description of kinetics of Cesium in the organism of animals it is offered the multichamber model of metabolism, that takes into account the functional features of organs, fabrics and transport liquid (to blood), is built on the basis of theory of chamber models. In this radionuclide kinetics is described by the system of the first-order differential equalizations (SDE), made on the basis of balance of activities in chambers.

$$\frac{d\vec{q}}{dt} = \Lambda \vec{q}(t),$$

where: Λ - matrix of the system, the undiagonal elements of that are transition constants of radionuclide between chambers (λ_{ij}); $\vec{q}(t)$ - vector components of that describe content of radionuclides in organs.

SDE was solved by Runge-Kutta using the built-in ode45 function in the MATLAB environment. This feature allows solving a given SDE by successive approximations of the given vector of initial values for a given range of periods. It was chosen as the most optimal for this objective because it allows the fastest and most accurately resolving of the problem.

The absorbed dose in the organ or tissue was determined by the expression

$$D = 1.6 \cdot 10^{-13} \cdot E_{ef} \cdot C_0 \cdot t,$$

where E_{ef} - effective energy; $C_0 \cdot t$ - number of decays at time t, which represents the value of the integral under the activity curve divided by the average mass of organ at that time; $1.6 \cdot 10^{-13}$ - conversion coefficient (number of J in 1 MeV).

The use of the developed program significantly increases the express method, the accuracy and reliability of the determination of internal radiation doses, what will allow correct interpretation of radiobiological dependences "dose - effect".

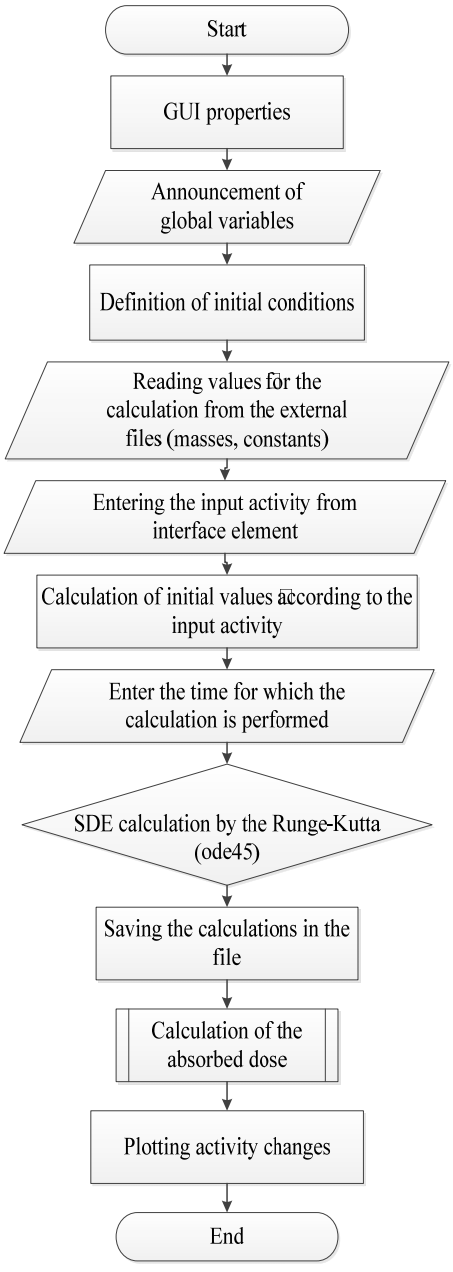

Block diagram of the complete source code.

ОПРЕДЕЛЕНИЕ УРАНА, РАДИЯ-226 И КОЭФФИЦИЕНТА РАДИОАКТИВНОГО РАВНОВЕСИЯ В ОБРАЗЦАХ УРАНОВЫХ РУД И ПУЛЬПЫ РУД ПОСЛЕ ВЫЩЕЛАЧИВАНИЯ

И. А. Малюк, А. Ф. Рудик, В. В. Тришин

Институт ядерных исследований НАН Украины, Киев

Определение с высокой точностью содержания урана, ^{226}Ra и коэффициента радиоактивного равновесия ($К_{РР}$) в рудах вызывает интерес как при поиске урановых месторождений (особенно с нарушенным радиоактивном равновесием, что имеет место при технологиях подземного выщелачивания), так и в ядерной криминалистике, поскольку эти параметры являются характерными признаками (сигнатурами) урановых руд.

В нашей работе [1] изложены принципы, а со временем усовершенствована и завершена разработка метода одновременного измерения урана, ^{226}Ra и $К_{РР}$ на основе деконволюции суммарного пика с энергией 185,7 и 186,2 кэВ радионуклидов ^{235}U и ^{226}Ra с использованием гамма-спектроскопии высокого разрешения. На рисунке приведен пример деконволюции суммарного пика в гамма-спектре руды с $К_{РР} = 1$.

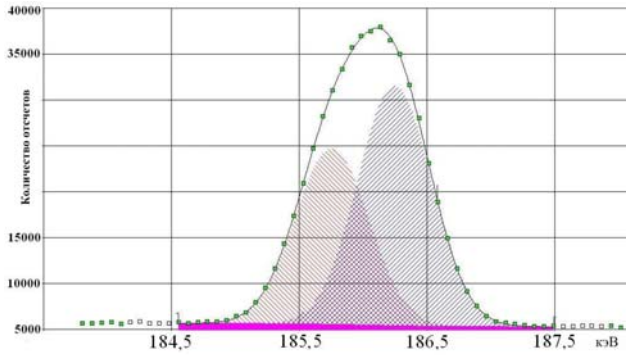

Рис. 1. Деконволюция суммарного пика 186 кэВ в гамма-спектре урановой руды с $К_{РР} = 1$.

Оригинальной чертой и ключевым элементом метода является способность с высокой точностью определять отношение интенсивности гамма-квантов с энергией 185,7 и 186,2 кэВ в пробах урановых руд. Показано, что достаточно точным приближением к этому отношению является выражение

$$\xi = \frac{S_{185}^{235U}}{S_{186}^{226Ra}},$$

где S_{185}^{235U} и S_{186}^{226Ra} – количество импульсов, полученных в результате деконволюции суммарного пика с энергией 185,7 кэВ и 186,2 кэВ в гамма-спектре пробы.

Отношение ξ позволяет рассчитать $К_{РР}$ в пробе произвольной геометрии без использования стандартных образцов (со) и определять концентрации урана и ^{226}Ra в рудах с использованием таких образцов в идентичных геометриях измерения, благодаря чему сводятся к минимуму неопределенности рассчитанных величин.

Массовая доля урана в исследуемой пробе рассчитывается по формуле:

$$\omega^{u} = \frac{\left(1+\frac{1}{\xi_{co}}\right) S^{\Sigma} \cdot t_{co} \cdot m_{co} \cdot \varepsilon_{co}}{\left(1+\frac{1}{\xi}\right) S_{co}^{\Sigma} \cdot t \cdot m \cdot \varepsilon} \omega_{co}^{u},$$

где ω_{co}^{u} – массовая доля урана в стандартном образце; m, m_{co}, t, t_{co}, ε, ε_{co} – масса, время измерения и эффективность регистрации гамма-квантов для пробы и стандартного образца соответственно.

По этому методу было проведено определение $К_{РР}$ и содержания урана в образцах руд и пульпы этих руд после выщелачивания, полученных из Восточного горно-обогатительного комбината (г. Желтые Воды). Результаты приведены в таблице.

Концентрация урана и $К_{РР}$

Вид образца	Код образца	Концентрация урана, % (мас.) (P = 0,95)	$К_{РР}$ (P = 0,95)
Объединенная проба урановой руды	Р1	0,085 ± 0,002	1,00 ± 0,02
	Р2	0,085 ± 0,002	1,00 ± 0,02
	Р3	0,085 ± 0,002	1,00 ± 0,02
	Р4	0,098 ± 0,002	1,00 ± 0,02
Пульпа руды после выщелачивания	П1	0,029 ± 0,002	2,5 ± 0,2
	П2	0,030 ± 0,002	2,6 ± 0,2
	П3	0,025 ± 0,002	2,9 ± 0,2
	П4	0,041 ± 0,002	2,2 ± 0,2

1. И. А. Малюк, А. Ф. Рудик и В. В. Тришин. Метод одновременного измерения урана, радия-226 и коэффициента радиоактивного равновесия в пробах урановых руд с использованием гамма-спектрометрической системы U-Pu InSPECTOR. Щорічник-2012 (ІЯД НАН України, К., 2013), С. 132.

РОЗРОБКА СИСТЕМИ УПРАВЛІННЯ ЯКІСТЮ ПРИ ВИРОБНИЦТВІ РАДІОФАРМПРЕПАРАТІВ В ІНСТИТУТІ ЯДЕРНИХ ДОСЛІДЖЕНЬ НАН УКРАЇНИ

В. В. Тришин, О. В. Божок, Л. К. Бездробна, Г. Я. Мінчук, В. А. Агеєв

Інститут ядерних досліджень НАН України, Київ

Одночасно з організацією робіт із виробництва радіофармпрепаратів (РФП) у лабораторії радіонуклідів та РФП Центру екологічних проблем атомної енергетики ІЯД НАН України розробляється система управління якістю (СУЯ) продукції, що буде вироблятися. СУЯ розробляється з метою забезпечення відповідності якості РФП їхньому призначенню. Ефективне функціонування СУЯ особливо важливе при виробництві РФП, діючою речовиною яких є короткоживучі радіонукліди (наприклад, діагностичний РФП пертехнетат натрію ^{99m}Tc). У таких випадках застосування РФП починається до закінчення всіх випробувань з контролю їхньої якості.

СУЯ передбачає: постановку задач у сфері якості вищим керівництвом; інформування персоналу та його відповідну кваліфікаційну підготовку; постійний моніторинг усіх видів діяльності щодо виконання поставлених вимог; самовдосконалення шляхом розробки та реалізації коригувальних і запобіжних дій; проведення внутрішніх аудитів; регулярний нагляд з боку керівництва.

На даному етапі розроблено концептуальну модель СУЯ виробництва РФП. Як базовий документ обрано міжнародний стандарт ISO 9001 [1]. У ході розробки моделі використано інформаційні матеріали щодо впровадження СУЯ на фармпідприємствах України. Розробка та впровадження СУЯ при виробництві РФП мають свої особливості у зв'язку з необхідністю виконання радіофармацевтичним виробництвом окрім вимог галузевого стандарту - Належної виробничої практики (GMP) [2] ще й дотримання Загальних вимог до системи управління діяльністю у сфері використання ядерної енергії [3]. Виходячи з цього, розроблена нами модель СУЯ базується на трьох стандартах [1 - 3], що дало змогу врахувати вимоги трьох складових: фармацевтичної, радіаційної, загального управління виробництвом у сфері якості. Структурною основою СУЯ стала модель ISO 9001, в яку вбудовано необхідні галузеві вимоги. Розроблена модель ґрунтується на процесному й системному підході, використанні принципу Е. Демінга (цикл PDCA "Plan - Do - Check - Act" "Плануй - Виконуй - Перевіряй - Дій") як до кожного процесу, так і системи в цілому. Даний підхід передбачає визначення та формування мережі взаємопов'язаних і взаємодіючих процесів при виробництві РФП, де чітко встановлені "входи" і "виходи" кожного процесу, параметри та критерії оцінювання й аналізування, розподіл повноважень і відповідальності. "Системний підхід до управління" реалізовано шляхом створення процесної моделі, регламентації здійснення процесів, розробки задокументованих процедур різних рівнів і показників для оцінки їхньої результативності та застосування заходів для постійного вдосконалення.

Створення завдяки СУЯ таких внутрішніх відносин між всіма видами діяльності (процесами), коли вихід процесу оцінюється за встановленими критеріями перш ніж стати входом відповідного наступного процесу, забезпечення зрозумілості та чіткості для виконавців алгоритмів процесів зменшує кількість помилок і невідповідностей, залучає до відповідальності за якість та дотримання встановлених правил кожного учасника процесу. Усе це забезпечить реальне отримання високої якості РФП та задоволення вимог споживачів, радіаційну безпеку персоналу, екологічні вимоги.

1. *ДСТУ ISO 9001*-2009 (Держстандарт України, К., 2009), 20 с.
2. *Лікарські засоби. Належна виробнича практика.* Настанова СТ-Н МОЗУ 42-4.0:2011 (МОЗ України, К., 2011), 280 с.
3. *Про затвердження Загальних вимог до системи управління діяльністю у сфері використання ядерної енергії.* Наказ від 19.12.2011 № 190 (ДІЯР України, К., 2011), 10 с.

DEVELOPING OF NUCLEAR FORENSICS DATABASE BASED ON OPEN SOURCES OF INFORMATION

O. V. Gaidar, V. V. Tryshyn, A. I. Ustinov

Institute for Nuclear Research, National Academy of Sciences of Ukraine, Kyiv

Implementation of evidence-based peer reviews, trend analysis of the situation and development of predictive models requires processing of large amounts of information that can be presented in various forms: data tables, text documents, cartographic materials, graphs and charts, photographs, audio and video.

In the case when a database is based on data from literature sources it is required the solving of a number of specific problems, including: to store data of different types and completeness, to avoid duplication of information and prevent its loss, to establish comprehensive system of relationships between data, to develop of structured vocabulary of terms and definitions.

Nuclear forensics is one of the fields in which such analytical systems are urgently required. Nuclear forensics investigation is more than the characterization of the material, which is simply a determination of the physical nature of the sample. For the final attribution and interpretation of the evidences and material properties, it also requires an involvement of knowledge and expertise from the broad scientific, forensic and nuclear technology related areas.

The INR of NAS of Ukraine, in accordance with the Cabinet of Ministries Decree designated as the main expert organization for the study and characterization of nuclear and other radioactive materials seized from illicit trafficking in Ukraine. In presidential decree about the national plan for realization of the provisions of Seoul summit communiqué it is supported the subsequent improving of technical capabilities of nuclear forensics laboratory, based in KINR, facilitation of international cooperation and creation a database of nuclear material characteristics, radioactive sources and shielding containers.

Now, in INR NAS of Ukraine the pilot project of database for nuclear forensics in Ukraine is under developing to support nuclear forensic studies of nuclear and other radioactive materials, which are found outside of regulatory control.

The general scheme of the pilot version of database is based on a client - server architecture. The client part of system is based on standard Internet browsers and does not require any special software to be developed. The proposed architecture for the web server is similar to the common open source server architecture (LAMP) which comprises: Linux – the server's operating system; Apache – the web server component; MySQL – a relational database; PHP – the application layer.

In general, the proposed architecture is only one of many possible variants for the development of this type of system. It is assumed that during the development of the database, components may be added, extended or replaced. The main principals of the pilot version are its easy transfer for different operation systems and utilization of the most general data types, commands and procedures. If general data types, commands and procedures are used, the database will be versatile and the operation system used in the future could be Linux, BSD, FreeBSD, Windows; as a web server Apache, Comanche, Nginx; Microsoft (IIS), script or CGI-program can be released in Perl, C/C++, etc. Additionally, multiple database management systems could be used: MySQL, Interbase, PostgreSQL, MS SQL, Oracle, etc.

To avoid significant changes of database structure in the process of database utilization, our approach to introducing new objects or their attributes to the database is based on the conception of a relational database with a limited number of tables and the utilization of a comprehensive scheme of relationships. We assume, that this proposed approach will enable us to complete both present and future tasks without considerable modifications of database structure and corresponding significant efforts for implementation.

Careful consideration is being used to populate the database with data. As a result of discussions with potential users of the database and the preliminary analysis of data from open sources, a basic set of data has been selected. Also special attention is paid for selection of existing sets of terms and definitions, and approved by international community approaches for data systematization.

It has been developed a structure for the database, which covers a wide range of objects and metadata (which can exchange roles), as well as relations between data in order to maximize the flexibility of the database for its future applications.

INVERSION FACTOR IN THE COMPARATIVE ANALYSIS OF DYNAMICAL PROCESSES IN RADIOECOLOGY

O. L. Zarubin, N. N. Zarubina

Institute for Nuclear Research, National Academy of Sciences of Ukraine, Kyiv

We have studied levels of specific activity of radionuclides in fish and fungi of the Kyiv region of Ukraine since 1986 till 2013, including 30-km alienation zone of Chernobyl Nuclear Power Plant (ChNPP) after the accident. The radionuclides specific activity dynamics analysis for 10 species of freshwater fishes of different trophic levels and at 7 species of higher fungi was carried out for this period. Multiple research of specific activity of radionuclides in fish was carried out on the Kanevskoe reservoir and cooling-pond of ChNPP, in fungi – on 6 testing areas, which are situated within the range of 2 to 150 km from ChNPP. The basic attention was given to accumulation of ^{137}Cs.

We have established that dynamics of specific activity of ^{137}Cs within different species of fish in the same reservoir is not identical. Dynamics of specific activity of ^{137}Cs within various species of fungi of the same testing area is also not identical. Dynamics of specific activity of ^{137}Cs with the investigated objects of various testing dryland and water areas also varies.

Authors suggest an inversion factor to be used for comparison of dynamics of specific activity of ^{137}Cs, which in case of biota is a nonlinear process: K_{inv} = = A0 / At, where A0 stands for the value of specific activity of the radionuclide at time 0; At – corresponding value at time t; At – activity of radionuclide at time t. Therefore, K_{inv} reflects ratio (inversion) of specific activity of radionuclides to its starting value as a function of time, where Kinv > 1 corresponds to increase in radionuclides' specific activity and Kinv < 1 corresponds to its decrease.

For example, K_{inv} of ^{137}Cs in *Rutilus rutilus* (L.) in the Kanevskoe reservoir was equal to 0.57, and 13.33 in the cooling-pond of ChNPP, at *Blicca bjoerkna* (L.) 0.95 and 29.61 accordingly in 1987 – 1996.

In 1987 - 2011 K_{inv} of ^{137}Cs at *R. rutilus* in the Kanevskoe reservoir equaled 6.80, and in the cooling-pond – 28.70; at *B. bjoerkna* 11.53 and 59.88 accordingly.

At the same time (1987 - 2011) K_{inv} of ^{137}Cs in the water of the Kanevskoe reservoir was equal to 41.12, in the water of the cooling-pond – 72.30.

During 1987 - 2011 K_{inv} of ^{137}Cs at *Suillus Luteus* (L.: Fr.) *S. F. Gray* at the testing area "Janov" (2 km from ChNPP) was equal to 17.21, and at "Stayky" (150 km from ChNPP) – 4.33; at *Boletus edulis* (Bull.: Fr.) accordingly 7.44 and 5.12.

Thus, this universal and simple K_{inv} can be used to solve a wide range of the problems connected with tentative estimation and comparison of dynamics of identical processes for any selected interval of time.

SPECIFIC ACTIVITY OF ^{137}Cs AT THE BIOTA OF COOLING-POND OF ChNPP AT THE PRESENT STAGE OF ITS TRANSFORMATION

O. L. Zarubin, N. E. Zarubina, V. A. Kostiuk, I. A. Maliuk

Institute for Nuclear Research, National Academy of Sciences of Ukraine, Kyiv

The strong-willed decision of the President of Ukraine the Chernobyl atomic power station has stopped to develop the electric power in the end of 2000. Therefore reasonably there is a question on necessity of maintenance of operational characteristics of its cooling-pond (CP). Various scenarios of the termination of maintenance of a water level of CP that will lead to drainage of a considerable part of its bottom accordingly, to redistribution of radioactive nuclides in a transformed ecosystem of CP, are developed now. The area of CP will be reduced several times at the expense of the termination of replenishment by water from the river Pripyat. Engineering works on cutting off of water in taking and water waste canals from the basic part of CP are spent with 2012.

Therefore, a studying of specific activity of radioactive nuclides of "a zero background», including content of ^{137}Cs in a biota of CP, in a period a transformation of CP to some closed reservoirs is obviously necessary.

Selection, preparation and measurements of samples it is executed by employees of INR of NAS of Ukraine on standard procedures.

Levels of ^{137}Cs specific activity at fishes of CP were in limens 0.77-7.61 kBq/kg of crude, natural mass in 2011-2012. As well as earlier, since 1990, the maximum of ^{137}Cs specific activity is characteristic for fishes of high trophic levels.

Specific activity of ^{137}Cs in mollusks of genus *Dreissena* was at level 0.30 - 0.93 kBq/kg of crude, natural mass in this period.

Specific activity of ^{137}Cs in these aquatic organisms essentially has not varied and at fishes compounded 0.92 - 4.37 kBq/kg; at mollusks – 0.13 - 0.4 kBq/kg by May 2013.

Specific activity of ^{137}Cs in vegetation of CP in 2011 - 2012 varied: a surface part of *Phragmites australis* (Cav.) – 0.42 - 1.32 kBq/kg, *Myriophyllum picatum* – 6.80 - 10.11 kBq/kg of air-dry mass at natural humidity.

Specific activity of ^{137}Cs in vegetation has considerably increased and in some samples has compounded: encrustations – to 21.00 kBq/kg, *M. spicatum* – to 23.64 kBq/kg, *P. australis* – to 85.12 kBq/kg of air-dry mass at natural humidity to 5 May 2013.

These samples have passed additional measurements in INR of NAS of Ukraine and in "Ecocenter" (Chernobyl) for check of reliability of the received results. Distinctions are in limens of an error of measurements (7 - 15 %).

Now we cannot explain such sharp increase of ^{137}Cs specific activity in water vegetation of CP. Researches preceded.

INFLUENCE OF THE AMOUNT OF PRECIPITATION AND AIR TEMPERATURE ON MAGNITUDE OF SPECIFIC ACTIVITY OF ^{137}Cs IN SOILS

N. E. Zarubina

Institute for Nuclear Research, National Academy of Sciences of Ukraine, Kyiv

Research of weather effect (amount of precipitation) throughout a year on fluctuations of content of ^{137}Cs in soil of forest ecosystems in terrain of the alienation zone of ChNPP (AZ) was the work purpose.

Soils were sampled on three testing areas in terrain of AZ: "Lelev" – the 10-km zone around ChNPP; "Paryshev", "Ditjatky" – 30-km zone. Sampling was spent monthly on testing areas "Paryshev" and "Ditjatky" to the period from September, 2007 till the end of December, 2012. Sampling on testing area "Lelev" was spent monthly, from June, 2008 till the end of December, 2012.

Sampling and preparation of samples of soil were spent according to procedures [1, 2]. Soils were sampled by an envelope method. Preparation of soils for measurements was spent in laboratory. Soils were dried up to air-dry mass, homogenized, packaged in the calibrated ware (a mass of samples was 30 - 50 g for a forest litter and 170 - 230 g for under laying soil layers). Measurement of ^{137}Cs content in samples of soils (layer-by-layer) was spent in INR of NAS of Ukraine on standard procedures of gamma spectrometry.

Long-term researches of ^{137}Cs accumulation in different layers of forest' soils in territory of AZ have shown that throughout a calendar year this magnitude changes. Fluctuations of values of specific activity of ^{137}Cs in tree' waste, a litter, soil 0 - 5 cm and soil 5 - 10 cm can reach one mathematical order of magnitudes [3].

For influence definition (or its absence) meteorological factors on change of ^{137}Cs content in soils throughout a year, correlation coefficients have been calculated between the content of ^{137}Cs in various layers of soils and meteorological factors – an amount of precipitation for different spans (2 months, 1 month, 2 weeks, 1 week, 5, 3 and 1 day), preceding sampling; temperature of air at the moment of sampling.

Correlation coefficients between the investigated parameters $<\pm$ 0.3 on all testing areas. Proceeding from magnitude of the received coefficients, it is possible to confirm, that the amount of precipitation and air temperature practically do not influence to magnitude of content of ^{137}Cs in different soil layers.

Exception is presence of weak communication between temperature of air and the content of this radionuclide in tree' waste and a layer of soil 5 - 10 cm on testing area "Ditjatky" (the correlation coefficient is equal - 0.35 and - 0.33 accordingly). On the same testing area there is a weak positive communication between an amount of precipitation for 14 days preceding sampling and the content of ^{137}Cs in a layer of a litter = 0.35. Probably existence of weak negative communication (r = -0.30) between an amount of precipitation for 7 days and the content of ^{137}Cs in a layer of soil 0 - 5 cm on testing area "Lelev".

Practical absence of influence of such abiotic factors as the amount of precipitation and air temperatures on fluctuations of ^{137}Cs content in soil speaks about probable existence any, till now not certain biological factor which influences the content of this radionuclide in different soil layers throughout a calendar year.

It has not been established authentic dependence of influence of meteorological factors (an amount of precipitation and air temperature) on levels of specific activity of ^{137}Cs in soil (layer-by-layer) in territory of testing areas of AZ.

1. Ю. В. Хомутинин, В. А. Кашпров и Е. И. Жебровская, *Оптимизация отбора и измерений проб при радиоэкологическом мониторинге* (УкрНИИСХР, К., 2001), 160 с.
2. *Методичні рекомендації* "*Пробовідбір повітря, води, грунту, донних осадів та атмосферних випадань для визначення вмісту радіонуклідів*" (К., 1998), 29 с.
3. Н. Є. Зарубіна, у *Матер. VIII міжнар. конф. "Екологічна безпека: проблеми і шляхи вирішення*", (2012), с. 142.

ВЛИЯНИЕ НАНОРАЗМЕРНЫХ МАГНИТОЧУВСТВИТЕЛЬНЫХ КОМПОЗИТОВ, СОДЕРЖАЩИХ ГАДОЛИНИЙ-157 НА МОРФОФУНКЦИОНАЛЬНЫЕ СВОЙСТВА КЛЕТОК *IN VITRO*

Г. И. Лавренчук[1], Д. Д. Гапеенко[1], Ю. Б. Шевченко[2], В. В. Тришин[2], А. Л. Петрановская[3], Е. В. Пилипчук[3], П. П. Горбик[3]

[1] Государственное учреждение «Национальный научный центр радиационной медицины НАМН Украины», Киев
[2] Институт ядерных исследований НАН Украины, Киев
[3] Институт химии поверхности им. О.О. Чуйко НАН Украины, Киев

Активный поиск биосовместимых наноматериалов для целевой доставки молекул бора-10 или гадолиния-157 к клеткам опухоли при нейтронозахватной терапии сосредоточен, в частности, в области синтеза магниточувствительных твердотельных частиц. Накапливается все больше как позитивных, так и негативных сведений о молекулярных и клеточных эффектах таких наноразмерных частиц.

Разработана методика и синтезированы магнитные жидкости состава: 1 – магнетит/диэтилентриаминпентауксусная кислота (ДТПК)/гадолиний/олеат Na, 2 – магнетит/*мезо-2,3*-димеркаптосукциновая кислота (ДМСК)/гадолиний/олеат Na и 3 – магнетит/олеат Na. Полученные водные полидисперсии имели размеры частиц от 2 до 22 нм с максимальным содержанием фракции ~7,5 нм. При этом предлагаются методы управления движением и свойствами наночастиц посредством прикладываемых магнитных полей.

Проведены экспериментальные исследования влияния различного содержания (от 15 до 0,15 мкг/мл) (рисунок) этих нанокомпозитов в питательной среде на морфофункциональные характеристики культуры клеток (линия L929), которые продемонстрировали изменения структуры монослоя, формы клеток и ядра, степени вакуолизации цитоплазмы, места накопления наночастиц, а также выживаемости, пролиферативной и митотической активности клеток.

Показно, что инкубация клеток с наночастицами содержащими гадолиний, несмотря на невысокую цитотоксичность (гибель клеток не превышала 20 %), при воздействии концентраций исследуемых наночастиц 15 и 1,5 мкг/мл в культуре клеток возникало значительное количество патологических митозов, что приводило соответственно к образованию многоядерных (3 – 6 ядер) гигантских клеток, которые при пересадке элиминировали с культуры. Наблюдали значительное количество апоптических клеток. Выявлено, что поступление исследуемых наночастиц в клетку, вероятнее всего, происходит путем фаго- или пиноцитоза (но не в вакуолях), а накопление – в эндоплазматическом ретикулюме.

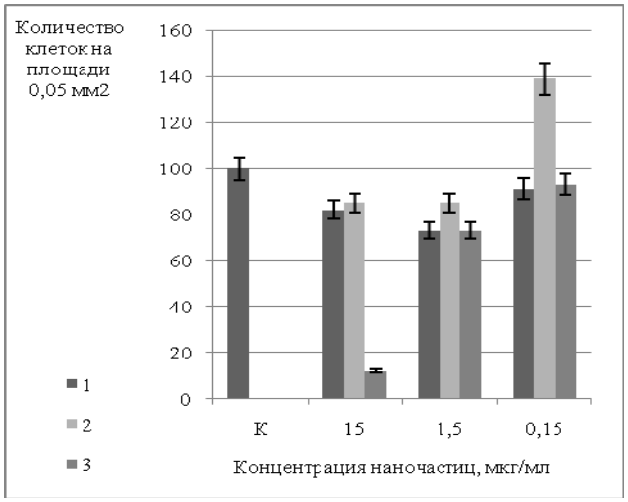

Выживаемость клеток при инкубации с нанокомпозитами в разных концентрациях.

Полученные данные свидетельствуют о перспективности использования разработанных наносистем для решения ряда задач нейтронозахватой терапии.

МОДИФИЦИРУЮЩЕЕ ДЕЙСТВИЕ НЕЙТРОНОЗАХВАТНЫХ АГЕНТОВ НА РАДИОГЕННЫЕ ИЗМЕНЕНИЯ В КЛЕТКАХ *IN VITRO*

Г. И. Лавренчук[1], Ю. Б. Шевченко[2], В. В. Тришин[2]

[1]ГУ "Национальный научный центр радиационной медицины НАМН Украины", Киев
[2] Институт ядерных исследований НАН Украины, Киев

Одним из наиболее перспективных, но и наиболее сложных вариантов лучевой терапии опухолей является нейтронзахватная терапия (НЗТ). Селективная доставка атомов ^{10}B к опухоли позволяет, после воздействия тепловыми нейтронами, рассчитывать на локальное повреждения только самой мишени. Многообещающим направлением является синтез ^{10}B-, и / или ^{157}Gd-содержащих соединений, которые обладают как свойствами нейтронозахватных агентов (НЗА) для нейтронозахватной терапии, так и фотосенсибилизаторов (ФС) для другого бинарного метода, фотодинамической терапии (ФДТ). Целью исследования было в экспериментах в тест-системе клеточной популяции определить дозовую зависимость клеточных реакций при комбинированном воздействии НЗА и радиации.

Исследования выполнены на культуре клеток линии L_{929}. Были использованы (НЗА): 1 - карба-Клозе-додекарборат цезия (реагент А), и супрамолекулярное соединение {5, 10, 15, 20-тетракис [*n*-(1'-карба-*клозо*-додекарборан-1'-ил) тетрафторфенил] 17, 18-дигидропорфирин}натрия (реагент Б) в концентрации 0,1 мкг/мл. Облучали γ-квантами ^{60}Co в дозах 0,5, 1, 2, 3, 4, 5, 7,5 и 10 Гр. Клеточные ответы оценивали в разные сроки культивирования клеток по общепринятым показателям жизнеспособности: пролиферативная и митотическая активность, количество атипичных поликариоцитив, апоптоз.

В результате экспериментальных исследований с применением тест-системы культуры перевивных клеток и ряда показателей их морфофункциональных характеристик были получены зависимости «доза - эффект», установлены характер и особенности сочетанного воздействия на выживаемость и апоптоз клеток НЗА и γ-излучения, которое является сопутствующим для нейтронов спектра деления, с целью прогнозирования интегральной эквивалентной дозы на основе определения и анализа полученных клеточных реакций. Таким образом:

1. Установлено, что при инкубации клеток, облученных в диапазоне доз 0,5 - 10,0 гр с НЗА в концентрации 0,1 мкл/мл наблюдается дозозависимая изменение выживаемости (клоногенной способности) клеток. Дозовые зависимости для всех трех вариантов опытов совпадают на всем дозовой интервале, кроме дозы 5 Гр, что может свидетельствовать об особенностях механизмов инактивации клеток.

2. Обнаружено, что инкубация клеток, облученных в дозе 0,5 Гр, с НЗА не влечет активизации пролиферации и выживаемости клеток по сравнению с отдельным действием излучения.

3. Анализ митотической активности в тест-системе культуры клеток показал, что при сочетанном действии НЗА (карборана и порфиринов) и облучения действуют механизмы воздействия на клетки, которые отличаются от механизмов отдельного действия радиации: вызывают гибель клеток из-за блокирования митоза (или патологию митоза) или через некробиоз.

4. Определение апоптоза в тест-системе культуры клеток показало и доказало, что механизмы инактивации облученных клеток с НЗА разные: для реагента Б преобладающим является гибель клеток путем апоптоза, для реагента А - добавляется еще и некроз.

ЯДЕРНАЯ МАГНИТНАЯ РЕЛАКСАЦИЯ В ДИСПЕРСИЯХ ПАРАМАГНИТНЫХ ЧАСТИЦ

Ю. Б. Шевченко

Институт ядерных исследований НАН Украины, Киев

В работах ряда авторов, среди которых отметим работу Кубо и Томита [1], было проведено строгое квантовомеханическое рассмотрение задачи диполь-дипольного (dd) взаимодействия магнитных моментов ядер и ионов в жидкости и получены классические соотношения, связывающие времена релаксации с молекулярными параметрами системы. Как правило, в парамагнитных растворах dd механизм ядерной магнитной релаксации растворителя является доминирующим. Растущий интерес к наноразмерным обьектам делает актуальным анализ dd-релаксации в дисперсных системах. В качестве примера таких систем можно привести дисперсии нано- и микроразмерных нейтронозахватных агентов и препаратов для радиотерапии в биологических жидкостях. Рассмотрим магнитное взаимодействие произвольного ядра жидкой дисперсионной среды с дисперсной частицей радиуса R_p, в которой случайным образом распределены точечные парамагнитные центры со средней объемной плотностью σ_μ такой, что парные взаимодействия отсутствуют. Это означает, что все магнитные моменты центров $\mu_{эф}$ взаимодействуют с моментом I релаксирующего ядра независимо. Поскольку в настоящей работе мы ограничимся рассмотрением спин-решеточной dd-релаксации, последнее обстоятельство позволяет нам сразу воспользоваться известным выражением для релаксации в парамагнитных растворах при взаимодействии релаксирующего ядра с одним парамагнитным центром, записанным в виде[2]

$$\frac{1}{T_1^{dd}} = \frac{2}{15}\cdot\gamma_I^2\cdot\mu_{эф}^2\cdot\frac{1}{r^6}\cdot\left(\frac{3\tau_{Ic}}{1+\omega_I^2\tau_{Ic}^2}+\frac{7\tau_{Sc}}{1+\omega_S^2\tau_{Sc}^2}\right), \qquad (1)$$

где $\mu_{эф}$ - эффективный магнитный момент парамагнитного центра; γ_I - гиромагнитное отношения ядра; r - расстояние между дипольно взаимодействующими моментами ядра и неспаренного электрона; τ_c - время корреляции, контролирующее это взаимодействие; ω_k , ω_{Se} - ларморовская частота магнитных моментов ядра и электрона. Суммируя по всем $\mu_{эф}$ в объеме частицы, получаем для скорости dd-релаксации в дисперсионной среде:

$$\frac{1}{T_{1p}^{dd}} = \frac{2}{15}\gamma_I^2\mu_{эф}^2\frac{4}{3}\pi\sigma_\mu\cdot\frac{R_p^3}{h^3(h+2R_p)^3}\times$$

$$\times\left(\frac{3\tau_{Ic}}{1+\omega_I^2\tau_{Ic}^2}+\frac{7\tau_{Sc}}{1+\omega_S^2\tau_{Sc}^2}\right). \qquad (2)$$

Здесь h – расстояние между релаксирующим ядром и поверхностью дисперсной частицы. Из формул (1) и (2) следует, что в парамагнитной дисперсии зависимость скорости ядерной релаксации от расстояния h между релаксирующим ядром и парамагнитной частицей носит сложный характер: $1/T_{1p}^{dd}$ пропорциональна $1/h^3$ при $h << R_p$ и $1/h^6$ при $h >> R_p$, тогда как в парамагнитных растворах она пропорциональна $1/r^6$ при всех r. Как видим, при малых расстояниях разница составляет **три порядка**. Это существенное обстоятельство, поскольку время ядерной магнитной релаксации невязких растворителей или дисперсионной среды контролируется именно релаксацией в первой координационной сфере парамагнитных ионов или дисперсных частиц, т.е. при малых r и h соответственно.

1. R. Kubo and K. Tomita, J. Phys. Soc. Japan, **9,** 888 (1954).
2. А.А. Вашман и И.С. Пронин, *Ядерная магнитная релаксационная спектроскопия* (Энергоатомиздат, М., 1986).

ГАДОЛИНИЙ-БОРСОДЕРЖАЩИЕ НАНОКОМПОЗИТЫ НА ОСНОВЕ МАГНЕТИТА

Е. В. Пилипчук[1], А. Л Петрановская[1], П. П. Горбик[1], А. А. Роговцов[2], Ю. Б. Шевченко[3]

[1] Институт химии поверхности им. А.А. Чуйко НАН Украины, Киев
[2] Институт общей и неорганической химии им. В. И. Вернадского НАН Украины, Киев
[3] Институт ядерных исследований НАН Украины, Киев

Сцинтилляторы – вещества, обладающие способностью излучать свет при поглощении ионизирующего излучения (гамма-квантов, электронов, альфа-частиц и т.д.). Основное применение сцинтилляторов – детекторы ядерных излучений, детекторы нейтронов.

Использование бора является эффективным в бор-нейтронозахватной терапии (БНЗТ), и его наличие в нейтронозахватном агенте (НЗА) одновременно с гадолинием является дополнительным активатором процесса нейтронозахватной терапии.

Нанокомпозит $Fe_3O_4/GdBO_3$ синтезирован в результате модифицирования поверхности магнетита боратом гадолиния $GdBO_3$, образующимся в результате взаимодействия ионов Gd^{3+} с гидратированным анионом бора $[B_4O_5(OH)_4]^{2-}$, с последующим гидролизом в $GdBO_3$.

Синтезированные магниточувствительные нанокомпозиты на основе Fe_3O_4, в состав которых входит борат гадолиния, могут выполнять функции неорганического сцинтиллятора и нейтронозахватного агента.

Схема химической реакции, происходящая в процессе синтеза:

$$Na_2B_4O_7 + 2H_2O = 2Na^+ + [B_4O_5(OH)_4]^{2-},$$

$$B_4O_7^{2-} + 11\ H_2O = 4[B(H_2O)(OH)_3] + 2OH^-,$$

$$Gd_2(SO_4)_3 + 2H_3BO_3 = 2GdBO_3 + 3H_2SO_4$$

Разработанный метод допирования магнетита $GdBO_3$ позволяет получить аморфный наноразмерный неорганический сцинтиллятор на его поверхности. Строение и свойства нанокомпозитов изучено комплексом физико-химических методов исследования. Наличие бора и гадолиния подтверждено методами РФС и РФА. Показано, что формирование кристаллической фазы $GdBO_3$ происходит только после отжига при 950 °С.

Количественный анализ элементного состава синтезированного нанокомпозита проводился методом атомно-эмиссионной спектрометрии на высокоскоростном атомно-эмиссионном спектрометре с индуктивно-связанной плазмой SHIMADZU ICPE-9000. Чувствительность и диапазон линейности ICPE-9000 обеспечивает определение большинства элементов на уровне1 - $10 \cdot 10^{-6}$ и ниже при диапазоне линейности 5 - 6 порядков.

Результаты количественного анализа образцов представлены в таблице.

Количественный состав и соотношение Fe/Gd/B в образце$Fe_3O_4/GdBO_3$

Элемент	Концентрация, мг/л	Длина волны, нм	Массовое соотношение Fe/Gd/B
Fe	110	238,204	48/1/0,1
Gd	2,3	342,247	
B	0,26	249,678	

Синтезированные нанокомпозиты могут быть использованы для создания новых типов высокоэффективных лекарственных средств для нейтронозахватной терапии с дополнительными функциями магнитоуправляемой направленной доставки к органам или клеткам-мишеням, а также при гипертермии, комбинированной T_1-, T_2-МРТ-диагностики, и терапии в режиме реального времени.

Publications in peer-reviewed journals

Nuclear physics:

A.P. Lashko, T.N. Lashko

The study of ^{177m}Lu decay

Вопросы атомной науки и техники **3(85),** 129 – 135 (2013)

O.O. Beiyuskina, V.I. Grantsev, K.K. Kisurin, S.E. Omelchuk, Yu.S. Roznyuk, B.A. Rudenko, V.S. Semenov, L.I. Slusarenko, B.G. Struzhko

Distribution of deuterons in the three body break-up reactions in D+D collisions

Вопросы атомной науки и техники **3(85),** 162 – 167 (2013)

T.V. Obikhod, Yu.M. Malyuta

Searches for superparticles at the LHC by application of computer simulation

Вопросы атомной науки и техники **3(85),** 147 – 150 (2013)

О.О. Белюскина, В.И. Гранцев, К.К. Кисурин, С.Е. Омельчук, Ю.С. Рознюк, Б.А. Руденко, Л.И. Слюсаренко, Б.Г. Стружко

Энергетические и угловые распределения дейтронов в реакции D + D → p + n + d

Известия РАН (сер. физ.) **77,** 981 – 987 (2013)

В.Ю. Денисов, В.А. Плюйко

Проблемы физики атомного ядра и ядерных реакций

Издательско-полиграфический центр "Киевский университет", Київ, 412 с, (2013)

А.П. Войтер

Комплексний аналіз ефективної швидкості передачі в адаптивних пакетних радіомережах

Наукові вісті Національного технічного університету України ‘’Київський політехнічний інститут” **6,** 7 – 12 (2013)

В.С. Ольховский

Временной анализ нуклон-ядерного рассеяния в области одного-двух резонансов

Современный научный вестник **32(171),** 129 – 150 (2013)

В.С. Ольховский

О непростой и ещё не совсем законченной истории квантовой механики

Современный научный вестник, Физика, **74(190),** 74 – 89 (2013)

О.І. Феоктістов, В.Т. Купряшкін, Л.П. Сидоренко, М.Ф. Коломієць, О.В. Коваленко, В.А.Лашко

Низькоенергетичні спектри електронів, які виникають при бомбардуванні титанової мішені β-частинками тритію та α-частинками ^{238}Pu

Український фізичний журнал **58,** 10 – 19 (2013)

О.І. Феоктістов В.Т. Купряшкін, Л.П. Сидоренко, В.А.Лашко

Розподіл електронів за енергією в "піку нульової енергії", що виникає при радіоактивному розпаді або при бомбардуванні мішені зарядженими частинками

Український фізичний журнал **58,** 109 – 115 (2013)

V.M. Kolomietz, S.V. Radionov

Stochastic resonance at diffusion over potential barrier

Ядерна фізика та енергетика **14,** 7 – 10 (2013)

С.Ю. Межевич, А.Т. Рудчик, К. Русек, Є.І. Кощий, С. Клічевскі, Г.В. Мохнач, А.А. Рудчик, С.Б. Сакута, Р. Сюдак, Б. Чех, Я. Хоіньскі, А. Щурек

Механізми реакції $^{14}C(^{11}B, ^{9}Be)^{16}N$ при енергії 45 МеВ та потенціал взаємодії ядер $^{9}Be + ^{16}N$

Ядерна фізика та енергетика **14,** 18 – 24 (2013)

А.Т. Рудчик, В.Ю. Каніщев, А.А. Рудчик, О.А. Понкратенко, Є.І. Кощий, С. Клічевскі, К. Русек, В.А. Плюйко, С.Ю. Межевич, Вал.М. Пірнак, А.П. Ільїн, В.В. Улещенко, Р. Сюдак, Я. Хоіньскі, Б. Чех, А. Щурек

Пружне та непружне розсіяння іонів ^{12}C ядрами ^{7}Li при енергії 115 МеВ

Ядерна фізика та енергетика **14,** 25 – 32 (2013)

Т.В.Ковалінська, І.А.Остапенко, В.І. Сахно, А.Г. Зелінський

Шляхи вдосконалення радіаційної техніки для кваліфікації обладнання АЕС

Ядерна фізика та енергетика **14,** 91 – 96 (2013)

А.Е. Вальков, А.К. Зайченко

Расчет равновесных орбит циклотрона У-240
Ядерна фізика та енергетика **14,** 97 – 103 (2013)

Н Ф. Митрохович, В.Т. Купряшкін, Л.П. Сидоренко
Коррелированность направления движения электронов Оже с направлением движения электрона внутренней конверсии
Ядерна фізика та енергетика **14,** 129 – 135 (2013)

О.А. Понкратенко, В.В. Улещенко, Ю.О. Ширма
Енергетична залежність потенціалу взаємодії ядер $^{16}O + {}^{12}C$
Ядерна фізика та енергетика **14,** 239 – 246 (2013)

О.В. Бабак, В.П. Вербицький, О.Д. Григоренко
Потенціали ядерної взаємодії дейтронів з важкими ядрами в моделі однократної згортки
Ядерна фізика та енергетика **14,** 247 – 251 (2013)

М.М. Правдивий, І.О. Корж
Залежність резонансних параметрів ядер від масового числа
Ядерна фізика та енергетика **14,** 252 – 258 (2013)

В.Т. Купряшкин, Л.П. Сидоренко, О.І. Феоктистов, В.А. Лашко
Выход e_0 – электронов с поверхности мишени при бомбардировке ее α- частицами разной энергии в диапазоне от 0,9 до 5,5 МэВ
Ядерна фізика та енергетика **14,** 271 – 275 (2013)

I. Panasenko et al.
CBM Experiment. Characterization Studies of the Detector Modules for Silicon Tracking System
Ядерна фізика та енергетика **14,** 304 – 306 (2013)

І.О. Корж, А.Д. Фурса
Дослідження впливу ефекту змішування станів у непарних ядрах на перерізи прямого непружного розсіяння нуклонів
Ядерна фізика та енергетика **14,** 337 – 344 (2013)

Ю.А. Бережной, В.П. Михайлюк, В.В. Пилипенко, Д.В. Федорченко
Упругое рассеяние дейтронов ядрами в α-кластерной модели
Ядерная физика, **76,** 914 – 923 (2013)

M.S. Borysova, Yu. Karpenko, V. Shapoval, Yu.M. Sinyukov
Tubular Initial Conditions and Ridge Formation
Advances in High Energy Physics **2013,** 209182/1 – 10 (2013)

H.Gomez (on behalf of the SuperNEMO collaboration)
BiPo: A dedicated radiopurity detector for the SuperNEMO experiment
AIP Conference Proceedings **1549,** 94 – 97 (2013)

B. Soule (on behalf of the SuperNEMO Collaboration)
Radon Emanation Chamber: High sensitivity measurements for the SuperNEMO experiment
AIP Conference Proceedings **1549,** 98 – 101 (2013)

J. Busto (on behalf of SuperNEMO collaboration)
Radon adsorption in nanoporous carbon materials
AIP Conference Proceedings **1549,** 112 – 115 (2013)

O.G. Polischuk, A.S. Barabash, P. Belli, R. Bernabei, R.S. Boiko, F. Cappella, R. Cerulli, F.A. Danevich, A. Incicchitti, M. Laubenstein, V.M. Mokina, S. Nisi, D.V. Poda, V.I. Tretyak
Purification of lanthanides for double beta decay experiments
AIP Conference Proceedings **1549,** 124 – 127 (2013)

J.Mott (on behalf of the SuperNEMO Collaboration)
Low-background tracker development for SuperNEMO
AIP Conference Proceedings **1549,** 152 – 155 (2013)

F. Perrot (on behalf of the SuperNEMO Collaboration)
Strategy of HPGe screening measurements in the SuperNEMO experiment
AIP Conference Proceedings **1549,** 173 – 176 (2013)

R. Bernabei, P. Belli, F. Cappella, V. Caracciolo, S. Castellano, R. Cerulli, R.S. Boiko, D.M. Chernyak, F.A. Danevich, C.J. Dai, A. d'Angelo, S. d'Angelo, A. Di Marco, H.L. He, A. Incicchitti, X.H. Ma, V.M. Mokina, F. Montecchia, D.V. Poda, O.G. Polischuk, X.D. Sheng, R.G. Wang, Z.P. Ye, V.I. Tretyak
Crystal scintillators for low background measurements
AIP Conference Proceedings **1549,** 189 – 196 (2013)

F.A. Danevich, A.S. Barabash, P. Belli, R. Bernabei, R.S. Boiko, V.B. Brudanin, F. Cappella, V. Caracciolo, R. Cerulli, D.M. Chernyak, S. d'Angelo, V.Ya. Degoda, M.L. Di Vacri, A.E. Dossovitskiy,

E.N. Galashov, A. Incicchitti, V.V. Kobychev, S.I. Konovalov, G.P. Kovtun, B.N. Kropivyansky, M. Laubenstein, A.L. Mikhlin, V.M. Mokina, A.S. Nikolaiko, S. Nisi, D.V. Poda, R.B. Podviyanuk, O.G. Polischuk, A.P. Shcherban, V.N. Shlegel, D.A. Solopikhin, V.I. Tretyak, V.I. Umatov, Ya.V. Vasiliev, V.D. Virich

Development of radiopure cadmium tungstate crystal scintillators from enriched ^{106}Cd and ^{116}Cd to search for double beta decay

AIP Conference Proceedings **1549,** 201 – 204 (2013)

T.V. Obikhod

MSSM Neutral Higgs Production Cross Section Via Gluon Fusion and Bottom Quark Fusion at NNLO in QCD

American Journal of Modern Physics **2,** 1 – 6 (2013)

T. Alexander, D. Alton, K. Arisaka, H.O. Back, P. Beltrame, J. Benziger, G. Bonfini, A. Brigatti, J. Brodsky, L. Cadonati, F. Calaprice, A. Candela, H. Cao, P. Cavalcante, A. Chavarria, A. Chepurnov, D. Cline, A.G. Cocco, C. Condon, D. D'Angelo, S. Davini, E. De Haas, A. Derbin, G. Di Pietro, I. Dratchnev, D. Durben, A. Empl , A. Etenko, A. Fan, G. Fiorillo, K. Fomenko, F. Gabriele, C. Galbiati, S. Gazzana, C. Ghag, C. Ghiano, A. Goretti, L. Grandi, M. Gromov, M. Guan, C. Guo, G. Guray, E.V. Hungerford, Al. Ianni, An. Ianni, A. Kayunov, K. Keeter, C. Kendziora, S. Kidner, V. Kobychev, G. Koh, D. Korablev, G. Korga , E. Shields, P. Li, B. Loer, P. Lombardi, C. Love, L. Ludhova, L. Lukyanchenko, A. Lund, K. Lung, Y. Ma, I. Machulin, J. Maricic, C.J. Martoff, Y. Meng, E. Meroni, P.D. Meyers, T. Mohayai, D. Montanari, M. Montuschi, P. Mosteiro, B. Mount, V. Muratova, A. Nelson, A. Nemtzow, N. Nurakhov, M. Orsini, F. Ortica, M. Pallavicini, E. Pantic, S. Parmeggiano, R. Parsells, N. Pelliccia, L. Perasso, F. Perfetto, L. Pinsky, A. Pocar, S. Pordes, G. Ranucci, A. Razeto, A. Romani, N. Rossi, P. Saggese, R. Saldanha, C. Salvo, W. Sands, M. Seigar, D. Semenov, M. Skorokhvatov, O. Smirnov, A. Sotnikov, S. Sukhotin, Y. Suvorov, R. Tartaglia, J. Tatarowicz, G. Testera, A. Teymourian, J. Thompson, E. Unzhakov, R.B. Vogelaar, H. Wang, S. Westerdale, M. Wojcik, A. Wright, J. Xu, C. Yang, S. Zavatarelli, M. Zehfus, W. Zhong, G. Zuzel

Light yield in DarkSide-10: A prototype two-phase argon TPC for dark matter searches

Astroparticle Physics **49,** 44 – 51 (2013)

A.P. Lashko, T.M. Lashko, A.M. Savrasov V.O. Zheltonozhsky

Anomalous internal conversion of the K-forbidden 55 keV E1-transition in ^{177}Hf

Eur. Phys. Journal A **49,** 21 (2013)

P. Belli, R. Bernabei, F. Cappella, R. Cerulli, F.A. Danevich, S. d'Angelo, A. Di Marco, A. Incicchitti, G.P.Kovtun, N.G. Kovtun, M. Laubenstein, D.V. Poda, O.G. Polischuk, A.P. Shcherban, V.I. Tretyak

First search for double-β decay of ^{184}Os and ^{192}Os

Eur. Phys. Journal A **49,** 24 (2013)

R. Bernabei, P. Belli, F. Cappella, V. Caracciolo, S. Castellano, R. Cerulli, C.J. Dai, A. d'Angelo, A. Di Marco, H.L. He, A. Incicchitti, M. Laubenstein, X.H. Ma, F. Montecchia, X.D. Sheng, V.I. Tretyak, R.G. Wang, Z.P. Ye

New search for correlated e^+e^- pairs in the α decay of ^{241}Am

Eur. Phys. Journal A **49,** 64 (2013)

A.T. Rudchik, R.M. Zelinskyi, K.W. Kemper, K.A. Chercas, A.A. Rudchik, Val. M. Pirnak, V.A. Plujko, O.A. Ponkratenko

Energy dependence of the 6^Li + 16^O elastic scattering versus that of 7^Li + 16^O

Eur. Phys. Journal A **49,** 74 (2013)

G. Bellini, J. Benziger, D. Bick, G. Bonfini, D. Bravo, M. Buizza-Avanzini, B. Caccianiga, L. Cadonati, F. Calaprice, C. Carraro, P. Cavalcante, A. Chavarria, A. Chepurnov, V. Chubakov, D. D'Angelo, S. Davini, A. Derbin, A. Etenko, K. Fomenko, D. Franco, C. Galbiati, S. Gazzana, C. Ghiano, M. Giammarchi, M. Goger-Neff, A. Goretti, L. Grandi, E. Guardincerri, S. Hardy, Aldo Ianni, Andrea Ianni, V. Kobychev, D. Korablev, G. Korga, Y. Koshio, D. Kryn, M. Laubenstein, T. Lewke, M. Lissia, E. Litvinovich, B. Loer, F. Lombardi, P. Lombardi, L. Ludhova, I. Machulin, S. Manecki, W. Maneschg, G. Manuzio, Q. Meindl, E. Meroni, L. Miramonti, M. Misiaszek, D. Montanari, P. Mosteiro, F. Mantovani, V. Muratova, S. Nisi, L. Oberauer, M. Obolensky, F. Ortica, K. Otis, M. Pallavicini, L. Papp, L. Perasso, S. Perasso, A. Pocar, G. Ranucci, A. Razeto, A. Re, A. Romani, N. Rossi, A. Sabelnikov, R. Saldanha, C. Salvo, S. Schonert, H. Simgen, M. Skorokhvatov, O. Smirnov, A. Sotnikov, S. Sukhotin, Y. Suvorov, R. Tartaglia, G. Testera, R.B. Vogelaar, F. von Feilitzsch, J. Winter, M. Wojcik, A. Wright, M. Wurm, G. Xhixha, J. Xu, O. Zaimidoroga, S. Zavatarelli, G. Zuzel

Lifetime measurements of ^{214}Po and ^{212}Po with the CTF liquid scintillator detector at LNGS

Eur. Phys. Journal A **49,** 92 (2013)

F. Cappella, R. Bernabei, P. Belli, V. Caracciolo, R. Cerulli, F.A. Danevich, A. d'Angelo, A. Di Marco, A. Incicchitti, D.V. Poda, V.I. Tretyak

On the potentiality of the $ZnWO_4$ anisotropic detectors to measure the directionality of Dark Matter

Eur. Phys. Journal C **73,** 2276 (2013)

R. Aaij, V. Iakovenko, O. Okhrimenko, V. Pugatch, et al (the LHCb collaboration)

Implications of LHCb measurements and future prospects

Eur. Phys. Journal C **73,** 2373 (2013)

R. Aaij, V. Iakovenko, O. Okhrimenko, V. Pugatch, et al (the LHCb collaboration)

Measurement of the forward energy flow in pp collisions at $\sqrt{s}$= 7 TeV

Eur. Phys. Journal C **73,** 2421 (2013)

R. Aaij, V. Iakovenko, O. Okhrimenko, V. Pugatch, et al (the LHCb collaboration)

Measurements of the branching fractions of $B^+ \to p\bar{p}K^+$ decays

Eur. Phys. Journal C **73,** 2462 (2013)

R. Aaij, V. Iakovenko, O. Okhrimenko, V. Pugatch, et al (the LHCb collaboration)

Measurement of J/ψ polarization in pp collisions at $\sqrt{s}$ = 7 TeV

Eur. Phys. Journal C **73,** 2631 (2013)

V.M. Kolomietz, A.I. Sanzhur

Thin structure of β-stability line and symmetry energy

Int. Jour. Mod. Phys. E **22,** – 1350003/1 – 12 (2013)

P. Ahmedzade, A. Fainleib, T. Günay, O. Starostenko, T. Kovalinska

Effect of Gamma Irradiated Recycled Low Density Polyethylene on the High and Low Temperature Properties of Bitumen

International Journal of Polymer Science **2013,** 141298/1 – 9 (2013)

P. Ahmedzade, A. Fainleib, O. Grigoryeva, T. Günay, B. Kultayev, O. Starostenko, T. Kovalinska

Modification of Bitumen by Recycled Post-Consumer Low Density Polyethylene with Surface Activated Using Air Ion Irradiation

International Journal of Polymer Science **2013,** 141298/1 – 10 (2013)

G. Bellini, J. Benziger, D. Bick, G. Bonfini, D. Bravo, M. Buizza-Avanzini, B. Caccianiga, L. Cadonati, F. Calaprice, P. Cavalcante, A. Chavarria, A. Chepurnov, D. D'Angelo, S. Davini, A. Derbin, A. Empl, A. Etenko, K. Fomenko, D. Franco, C. Galbiati, S. Gazzana, C. Ghiano, M. Giammarchi, M. Goger-Neff, A. Goretti, L. Grandi, C. Hagner, E. Hungerford, Aldo Ianni, Andrea Ianni, V. Kobychev, D. Korablev, G. Korga, D. Kryn, M. Laubenstein, T. Lewke, E. Litvinovich, B. Loer, P. Lombardi, F. Lombardi, L. Ludhova, G. Lukyanchenko, I. Machulin, S. Manecki, W. Maneschg, G. Manuzio, Q. Meindl, E. Meroni, L. Miramonti, M. Misiaszek, R. Mollenberg, P. Mosteiro, V. Muratova, L. Oberauer, M. Obolensky, F. Ortica, K. Otis, M. Pallavicini, L. Papp, L. Perasso, S. Perasso, A. Pocar, G. Ranucci, A. Razeto, A. Re, A. Romani, N. Rossi, R. Saldanha, C. Salvo, S. Schonert, H. Simgen, M. Skorokhvatov, O. Smirnov, A. Sotnikov, S. Sukhotin, Y. Suvorov, R. Tartaglia, G. Testera, D. Vignaud, R.B. Vogelaar, F. von Feilitzsch, J. Winter, M. Wojcik, A. Wright, M. Wurm, J. Xu, O. Zaimidoroga, S. Zavatarelli, G. Zuzel

Cosmogenic backgrounds in Borexino at 3800 m water-equivalent depth

Journal of Cosmology and Astroparticle Physics **08**:049 (2013)

L. Cardani, N. Casali, S. Nagorny, L. Pattavina, G. Piperno, O.P. Barinova, J.W. Beeman , F. Bellini, F.A.Danevich, S. Di Domizio, L. Gironi, S.V Kirsanova, F. Orio, G. Pessina, S. Pirro, C. Rusconi, C. Tomei, V.I. Tretyak, M. Vignati

Development of a Li_2MoO_4 scintillating bolometer for low background physics

Journal of Instrumentation **08,** P100002/1 – 13 (2013)

F.A. Danevich

Study of neutrino properties and weak interaction in double beta decay experiments

Journal of Kharkiv National University**1040,** 40 – 47 (2013)

R. Aaij, V. Iakovenko, O. Okhrimenko, V. Pugatch, et al (the LHCb collaboration)

Exclusive J/ψ and ψ(2S) production in pp collisions at $\sqrt{s}$=7 TeV

J.Phys.G **40,** 045001/1 – 17 (2013)

R. Aaij, V. Iakovenko, O. Okhrimenko, V. Pugatch, et al (the LHCb collaboration)

A study of the Z production cross-section in pp collisions at $s\sqrt{}$ = 7 TeV using tau final states

Journal of High Energy Physics **01**:111 (2013)

R. Aaij, V. Iakovenko, O. Okhrimenko, V. Pugatch, et al (the LHCb collaboration)
Search for the rare decay $K^0S \to \mu^+\mu^-$
Journal of High Energy Physics **01**:090 (2013)

R. Aaij, V. Iakovenko, O. Okhrimenko, V. Pugatch, et al (the LHCb collaboration)
Measurement of J/ψ production in pp collisions at $\sqrt{s}$=2.76 TeV
Journal of High Energy Physics **02**:041(2013)

R. Aaij, V. Iakovenko, O. Okhrimenko, V. Pugatch, et al (the LHCb collaboration)
First evidence for the annihilation decay mode $B^+ \to D^+_s\varphi$
Journal of High Energy Physics **02**:043 (2013)

R. Aaij, V. Iakovenko, O. Okhrimenko, V. Pugatch, et al (the LHCb collaboration)
Differential branching fraction and angular analysis of the $B^+ \to K^+\mu^+\mu^-$ decay
Journal of High Energy Physics **02**:105 (2013)

R. Aaij, V. Iakovenko, O. Okhrimenko, V. Pugatch, et al (the LHCb collaboration)
Measurement of the cross-section for $Z \to e^+e^-$ production in pp collisions at $\sqrt{s}$=7 TeV
Journal of High Energy Physics **02**:106 (2013)

R. Aaij, V. Iakovenko, O. Okhrimenko, V. Pugatch, et al (the LHCb collaboration)
Measurement of CP observables in $B^0 \to DK^{*0}$ with $D \to K^+K^-$
Journal of High Energy Physics **03**:067 (2013)

R. Aaij, V. Iakovenko, O. Okhrimenko, V. Pugatch, et al (the LHCb collaboration)
Measurement of the fragmentation fraction ratio fs/fd and its dependence on B meson kinematics
Journal of High Energy Physics **04**:001 (2013)

R. Aaij, V. Iakovenko, O. Okhrimenko, V. Pugatch, et al (the LHCb collaboration)
Limits on neutral Higgs boson production in the forward region in pp collisions at $\sqrt{s}$=7 TeV
Journal of High Energy Physics **05**:132 (2013)

R. Aaij, V. Iakovenko, O. Okhrimenko, V. Pugatch, et al (the LHCb collaboration)
Measurement of the $B^0 \to K^{*0}e^+e^-$ branching fraction at low dilepton mass
Journal of High Energy Physics **05**:159 (2013)

R. Aaij, V. Iakovenko, O. Okhrimenko, V. Pugatch, et al (the LHCb collaboration)
Search for CP violation in $D^+ \to \phi\pi^+$ and $D^+s \to K^0s\pi^+$ decays
Journal of High Energy Physics **06**:112 (2013)

R. Aaij, V. Iakovenko, O. Okhrimenko, V. Pugatch, et al (the LHCb collaboration)
Production of J/ψ and Y mesons in pp collisions at $\sqrt{s}$ = 8 TeV
Journal of High Energy Physics **06**:064 (2013)

R. Aaij, V. Iakovenko, O. Okhrimenko, V. Pugatch, et al (the LHCb collaboration)
Precision measurement of D meson mass differences
Journal of High Energy Physics **06**:065 (2013)

R. Aaij, V. Iakovenko, O. Okhrimenko, V. Pugatch, et al (the LHCb collaboration)
Differential branching fraction and angular analysis of the decay $B_s^0 \to \phi\mu^+\mu^-$
Journal of High Energy Physics **07**:084 (2013)

G. Bellini, D. Bick, G. Bonfini, D. Bravo, B. Caccianiga, F. Calaprice, A. Caminata, P. Cavalcante, A. Chavarria, A. Chepurnov, D. D'Angelo, S. Davini, A. Derbin, A. Etenko, G. Fernandes, K. Fomenko, D. Franco, C. Galbiati, C. Ghiano, M. Goger-Neff, A. Goretti, C. Hagner, E. Hungerford, Aldo Ianni, Andrea Ianni, V. Kobychev, D. Korablev, G. Korga, D. Krasnicky, D. Kryn, M. Laubenstein, J. M.Link, E. Litvinovich, F. Lombardi, P. Lombardi, L. Ludhova, G. Lukyanchenko, I. Machulin, S. Manecki, W. Maneschg, E. Meroni, M. Meyer, L. Miramonti, M. Misiaszek, P. Mosteiro, V. Muratova, L. Oberauer, M. Obolensky, F. Ortica, K. Otis, M. Pallavicini, E. Pantic, L. Papp, S. Perasso, A. Pocar, G. Ranucci, A. Razeto, A. Re, A. Romani, N. Rossi, R. Saldanha, C. Salvo, S. Schonert, D. Semenov, H. Simgen, M. Skorokhvatov, O. Smirnov, A. Sotnikov, S. Sukhotin, Y. Suvorov, R. Tartaglia, G. Testera, E. Unzhakov, R.B. Vogelaar, H. Wang, M. Wojcik, M. Wurm, O. Zaimidoroga, S. Zavatarelli, G. Zuzel
SOX: Short distance neutrino Oscillations with BoreXino
Journal of High Energy Physics **08**: 038 (2013)

R. Aaij, V. Iakovenko, O. Okhrimenko, V. Pugatch, et al (the LHCb collaboration)
Measurement of B meson production cross-sections in proton-proton collisions at $\sqrt{s}$ = 7 TeV
Journal of High Energy Physics **08**:117 (2013)

R. Aaij, V. Iakovenko, O. Okhrimenko, V. Pugatch, et al (the LHCb collaboration)

Differential branching fraction and angular analysis of the decay $B^0 \to K^{*0}\mu^+\mu^-$
Journal of High Energy Physics **08**:131 (2013)

R. Aaij, V. Iakovenko, O. Okhrimenko, V. Pugatch, et al (the LHCb collaboration)
Searches for $B_{(s)}^0 \to J/\psi p\bar{p}$ and $B^+ \to J/\psi p\bar{p}\pi^+$ decays
Journal of High Energy Physics **09**:006 (2013)

R. Aaij, V. Iakovenko, O. Okhrimenko, V. Pugatch, et al (the LHCb collaboration)
First observation of the decay $B_c^+ \to J/\psi K^+$
Journal of High Energy Physics **09**:075 (2013).

R. Aaij, V. Iakovenko, O. Okhrimenko, V. Pugatch, et al (the LHCb collaboration)
Study of D_J meson decays to $D^+\pi^-$, $D^0\pi^+$ and $D^{*+}\pi^-$ final states in pp collisions
Journal of High Energy Physics **09**:145 (2013)

R. Aaij, V. Iakovenko, O. Okhrimenko, V. Pugatch, et al (the LHCb collaboration)
First evidence for the two-body charmless baryonic decay $B^0 \to p\bar{p}$
Journal of High Energy Physics **10**:005 (2013)

R. Aaij, V. Iakovenko, O. Okhrimenko, V. Pugatch, et al (the LHCb collaboration)
Measurement of the relative rate of prompt χ_{c0}, χ_{c1} and χ_{c2} production at $\sqrt{s}$ = 7 TeV
Journal of High Energy Physics **10**:115 (2013).

R. Aaij, V. Iakovenko, O. Okhrimenko, V. Pugatch, et al (the LHCb collaboration)
Study of $B_{(s)}^0 \to K_S^0 h^+ h'^-$ decays with first observation of $B_s^0 \to K_S^0 K^\pm \pi^\mp$ and $B_s^0 \to K_S^0 \pi^+ \pi^-$
Journal of High Energy Physics 10:143 (2013)

R. Aaij, V. Iakovenko, O. Okhrimenko, V. Pugatch, et al (the LHCb collaboration)
Precision measurement of the B^0s–$B^{-0}s$ oscillation frequency with the decay $B^0s \to D^-s\pi^+$
New J. Phys. **15,** 053021 (2013)

P. Belli, R. Bernabei, S.V. Budakovsky, F. Cappella, R. Cerulli, F.A. Danevich, S. d'Angelo, A. Incicchitti, M. Laubenstein, D.V. Poda, O.G. Polischuk, V.I. Tretyak
Radioactive contamination of ^{7}LiI(Eu) crystal scintillators
Nucl. Instrum. Meth. A **704,** 40 – 43 (2013)

D.M. Chernyak, F.A. Danevich, V.Ya. Degoda, I.M. Dmitruk, F. Ferri, E.N. Galashov, A. Giuliani, I.M. Ivanov, V.V. Kobychev, M. Mancuso, S. Marnieros, V.M. Mokina, C. Nones, E. Olivieri, G. Pessina, C. Rusconi, V.N. Shlegel, O.P. Stanovyi, M. Tenconi, V.I.Tretyak, I.A. Tupitsyna
Optical, luminescence and thermal properties of radiopure $ZnMoO_4$ crystals used in scintillating bolometers for double beta decay search
Nucl. Instrum. Meth. A **729,** 856 – 863 (2013)

H. Gomez (on behalf of the SuperNEMO Collaboration)
BiPo: A dedicated radiopurity detector for the SuperNEMO experiment
Nucl. Instrum. Meth. A **718,** 52 – 55 (2013)

S. Davini (on behalf of the Borexino Collaboration)
Looking at the Sun's core. CNO and pep solar neutrino detection in Borexino
Nuovo Cim. C **36,** 229 – 233 (2013)

M. Pallavicini, G. Bellini, J. Benziger, D. Bick, G. Bonfini, D. Bravo, M. Buizza-Avanzini, B. Caccianiga, L. Cadonati, F. Calaprice, C. Carraro, P. Cavalcante, A. Chavarria, D. D'Angelo, S. Davini, A. Derbin, A. Etenko, K. Fomenko, D. Franco, C. Galbiati, S. Gazzana, C. Ghiano, M. Giammarchi, M. Goger-Neff, A. Goretti, L. Grandi, E. Guardincerri, S. Hardy, Aldo Ianni, Andrea Ianni, V. Kobychev, D. Korablev, G. Korga, Y. Koshio, D. Kryn, M. Laubenstein, T. Lewke, E. Litvinovich, B. Loer, P. Lombardi, F. Lombardi, L. Ludhova, I. Machulin, S. Manecki, W. Maneschg, G. Manuzio, Q. Meindl, E. Meroni, L. Miramonti, M. Misiaszek, D. Montanari, P. Mosteiro, V. Muratova, L. Oberauer, M. Obolensky, F. Ortica, K. Otis, L. Papp, L. Perasso, S. Perasso, A. Pocar, R.S. Raghavan, G. Ranucci, A. Razeto, A. Re, A. Romani, N. Rossi, A. Sabelnikov, R. Saldanha, C. Salvo, S. Schonert, H. Simgen, M. Skorokhvatov, O. Smirnov, A. Sotnikov, S. Sukhotin, Y. Suvorov, R. Tartaglia, G. Testera, D. Vignaud, R.B. Vogelaar, F. von Feilitzsch, J. Winter, M. Wojcik, A. Wright, M. Wurm, J. Xu, O. Zaimidoroga, S. Zavatarelli, G. Zuzel
Recent results and future development of Borexino
Nucl. Phys. B (Proc. Suppl.) **235,** 55 – 60 (2013)

A. Ianni, G. Bellini, J. Benziger, D. Bick, G. Bonfini, D. Bravo, M. Buizza-Avanzini, B. Caccianiga, L. Cadonati, F. Calaprice, C. Carraro, P. Cavalcante, A. Chavarria, D. D'Angelo, S. Davini, A. Derbin, A. Etenko, D. Franco, K. Fomenko, C. Galbiati, S. Gazzana, C. Ghiano, M. Giammarchi, M. Goger-Neff, A. Goretti, L. Grandi, E. Guardincerri, S. Hardy, Andrea Ianni, A. Kayunov,V. Kobychev, D. Korablev, G. Korga, Y. Koshio, D. Kryn, M. Lauben-

stein, T. Lewke, E. Litvinovich, L.Ludhova, B. Loer, F. Lombardi, P. Lombardi, I. Machulin, S. Manecki, W. Maneschg, G. Manuzio, Q. Meindl, E. Meroni, L. Miramonti, M. Misiaszek, D. Montanari, P. Mosteiro, V. Muratova, L. Oberauer, M. Obolensky, F. Ortica, K. Otis, M. Pallavicini, L. Papp, L. Perasso, S. Perasso, A. Pocar, R.S. Raghavan, G. Ranucci, A. Razeto, A. Re, P.A. Romani, A. Sabelnikov, R. Saldanha, C. Salvo, S. Schoenert, H. Simgen, M. Skorokhvatov, O. Smirnov, A. Sotnikov, S. Sukhotin, Y. Suvorov, R. Tartaglia, G. Testera, D. Vignaud, R.B. Vogelaar, F. Von Feilitzsch, J. Winter, M. Wojcik, A. Wright, M. Wurm, J. Xu, O. Zaimidoroga, S. Zavatarelli, G. Zuzel

Neutrinos from the sun and from radioactive sources

Nucl. Phys. B (Proc. Suppl.) **237,** 77 – 81 (2013)

D. Franco, G. Bellini, J. Benziger, D. Bick, G. Bonfini, D. Bravo, M. Buizza-Avanzini, B. Caccianiga, L. Cadonati, F. Calaprice, C. Carraro, P. Cavalcante, A. Chavarria, D. D'Angelo, S. Davini, A. Derbin, A. Etenko, K. Fomenko, C. Galbiati, S. Gazzana, C. Ghiano, M. Giammarchi, M. Goger-neff, A. Goretti, L. Grandi, E. Guardincerri, S. Hardy, Aldo Ianni, Andrea Ianni, A. Kayunov,V. Kobychev, D. Korablev, G. Korga, Y. Koshio, D. Kryn, M. Laubenstein, T. Lewke, E. Litvinovich, L. Ludhova, B. Loer, F. Lombardi, P. Lombardi, I. Machulin, S. Manecki, W. Maneschg, G. Manuzio, Q. Meindl, E.Meroni, L. Miramonti, M. Misiaszek, D. Montanari, P. Mosteiro, V. Muratova, L. Oberauer, M. Obolenksy, F. Ortica, K. Otis, M. Pallavicini, L. Papp, L. Perasso, S. Perasso, A. Pocar, R.S. Raghavan, G. Ranucci, A. Razeto, A. Re, P.A. Romani, A. Sabelnikov, R. Saldanha, C. Salvo, S. Schonert, K. Simgen, M. Skorokhvatov, O. Smirnov, A. Sotnikov, S. Sukhotin, Y. Suvorov, R. Tartaglia, G. Testera, D. Vignaud, R.B. Vogelaar, F. Von Feilitzsch, J. Winter, M. Wojcik, A. Wright, M. Wurm, J. Xu, O. Zaimidoroga, S. Zavatarelli, G. Zuzel

Solar neutrino results from Borexino

Nucl. Phys. B (Proc. Suppl.) **237,** 104 – 106 (2013)

R. Aaij, V. Iakovenko, O. Okhrimenko, V. Pugatch, et al (the LHCb collaboration)

Evidence for the decay $B^0 \to J/\psi\omega$ and measurement of the relative branching fractions of B^0s meson decays to $J/\psi\eta$ and $J/\psi\eta'$

Nucl. Phys. B **867,** 547 – 566 (2013)

R. Aaij, V. Iakovenko, O. Okhrimenko, V. Pugatch, et al (the LHCb collaboration)

Prompt charm production in pp collisions at $\sqrt{s}$ = 7 TeV

Nucl. Phys. B **871,** 1 – 20 (2013)

R. Aaij, V. Iakovenko, O. Okhrimenko, V. Pugatch, et al (the LHCb collaboration)

Observation of the B^0s$\to\psi(2S)\eta$ and $B^0(s)\to\psi(2S)\pi^+\pi^-$ decays

Nucl. Phys. B **871,** 403 – 419 (2013)

R. Aaij, V. Iakovenko, O. Okhrimenko, V. Pugatch, et al (the LHCb collaboration)

Measurement of the effective B^0s$\to J/\psi K^0$S lifetime

Nucl. Phys. B **873,** 275 – 292 (2013)

R. Aaij, V. Iakovenko, O. Okhrimenko, V. Pugatch, et al (the LHCb collaboration)

Observation of $B_s^0\to\chi_{c1}\phi$ decay and study of $B^0\to\chi_{c1,2}K^{*0}$ decays

Nucl. Phys. B **874,** 663 – 678 (2013)

F.A. Ivanyuk

On the Scission Point Configuration of Fissioning Nuclei

Physics Procedia **47,** 17 – 26 (2013)

J.P. Blocki, A.G. Magner

Transport coefficients for a slow Fermi-particle motion

Physica Scripta **154,** 014006/1 – 5 (2013)

F.A. Ivanyuk, K. Pomorski

On the Poinkare instability of a rotating liquid

Physica Scripta **154,** 014021/1 – 6 (2013)

P. Belli, R. Bernabei, F. Cappella, R. Cerulli, F.A. Danevich, S. d'Angelo, A. Incicchitti, G.P. Kovtun, N.G. Kovtun, M. Laubenstein, D.V. Poda, O.G. Polischuk, A.P. Shcherban, D.A. Solopikhin, J. Suhonen, V.I. Tretyak

Search for 2β decays of ^{96}Ru and ^{104}Ru by ultralow-background HPGe γ spectrometry at LNGS: Final results

Phys. Rev. C **87,** 034607/1 – 8 (2013)

A. Del Popolo, F. Pace, S.P. Maydanyuk, J.A.S. Lima, J.F. Jesus

Shear and rotation in Chaplygin cosmology

Phys. Rev. D **87,** 043527/1 – 9 (2013)

J.P. Blocki, A.G. Magner, P. Ping, O.O. Vlasenko

Nuclear asymmetry energy and isovector stiffness within the effective surface approximation

Phys. Rev. C **87,** 044304/1 – 10 (2013)

M. Zadro, P. Figuera, A. Di Pietro, M. Fisichella,

M. Lattuada, T. Lönnroth, M. Milin, V. Ostashko, M. G. Pellegriti, V. Scuderi, D. Stanko, E. Strano, and D. Torresi

Quasielastic backscattering and barrier distributions for the ^{6,7}Li+^{64}Zn systems

Phys. Rev. C **87,** 054606/1 – 10 (2013)

A. Di Pietro, P. Figuera, E. Strano, M. Fisichella, O. Goryunov, M. Lattuada, C. Maiolino, C. Marchetta, M. Milin, A. Musumarra, V. Ostashko, M.G. Pellegriti, V. Privitera, G. Randisi, L. Romano, D. Santonocito, V. Scuderi, D. Torresi, and M. Zadro

Heavy residue excitation functions for the collisions ^{6,7}Li+^{64}Zn near the Coulomb barrier

Phys. Rev. C **87,** 064614/1 – 10 (2013)

A.I. Levon, G. Graw, R. Hertenberger, S. Pascu, P.G. Thirolf, H.-F. Wirth, P. Alexa

0^+ states and collective bands in ^{228}Th studied by the (p, t) reaction

Phys. Rev. C **88,** 014310/1 – 21 (2013)

V.M. Kolomietz, A.I. Sanzhur

Gibbs-Tolman approach to the curved interface effects in asymmetric nuclei

Phys. Rev. C **88,** 044316/1 – 10 (2013)

V.Yu. Denisov

Multidimensional model of cluster radioactivity

Phys. Rev. C **88,** 044608/1 – 11 (2013)

R. Aaij, V. Iakovenko, O. Okhrimenko, V. Pugatch, et al (the LHCb collaboration)

Analysis of the resonant components in $B^{-0}\to J/\psi\pi^+\pi^-$

Phys. Rev. D **87,** 052001 (2013)

R. Aaij, V. Iakovenko, O. Okhrimenko, V. Pugatch, et al (the LHCb collaboration)

Search for the decay $B^0s\to D^{*\mp}\pi^\pm$

Phys. Rev. D **87,** 071101 (2013)

R. Aaij, V. Iakovenko, O. Okhrimenko, V. Pugatch, et al (the LHCb collaboration)

Observation of the decay $B^+c\to\psi(2S)\pi^+$

Phys. Rev. D **87,** 071103 (2013)

R. Aaij, V. Iakovenko, O. Okhrimenko, V. Pugatch, et al (the LHCb collaboration)

Amplitude analysis and the branching fraction measurement of $B^{-0}s\to J/\psi K^+K^-$

Phys. Rev. D **87,** 072004 (2013)

R. Aaij, V. Iakovenko, O. Okhrimenko, V. Pugatch, et al (the LHCb collaboration)

Study of $B^0\to D^{*-}\pi^+\pi^-\pi^+$ and $B^0\to D^{*-}K^+\pi^-\pi^+$ decays

Phys. Rev. D **87,** 092001 (2013)

R. Aaij, V. Iakovenko, O. Okhrimenko, V. Pugatch, et al (the LHCb collaboration)

First observations of $B^{-0}s\to D^+D^-$, D^+sD^- and D^0D^{-0} decays

Phys. Rev. D **87,** 092007 (2013)

R. Aaij, V. Iakovenko, O. Okhrimenko, V. Pugatch, et al (the LHCb collaboration)

Measurement of the branching fractions of the decays $B^0s\to D^{-0}K^-\pi^+$ and $B^0\to D^{-0}K^+\pi^-$

Phys. Rev. D **87,** 112009 (2013)

R. Aaij, V. Iakovenko, O. Okhrimenko, V. Pugatch, et al (the LHCb collaboration)

Measurement of CP violation and the B0s meson decay width difference with $B^0s\to J/\psi K^+K^-$ and $B^0s\to J/\psi\pi^+\pi^-$ decays

Phys. Rev. D **87,** 112010 (2013)

R. Aaij, V. Iakovenko, O. Okhrimenko, V. Pugatch, et al (the LHCb collaboration)

Observation of $B_c^+\to J/\psi D_s^+$ and $B_c^+\to J/\psi D_s^{*+}$ decays

Phys. Rev. D **87,** 112012 (2013)

R. Aaij, V. Iakovenko, O. Okhrimenko, V. Pugatch, et al (the LHCb collaboration)

Measurement of the polarization amplitudes in $B^0\to J/\psi K^*(892)^0$ decays

Phys. Rev. D **88,** 052002 (2013)

R. Aaij, V. Iakovenko, O. Okhrimenko, V. Pugatch, et al (the LHCb collaboration)

Studies of the decays $B^+\to p\bar{p}h^+$ and observation of $B^+\to\bar{\Lambda}(1520)p$

Phys. Rev. D **88,** 052015 (2013)

R. Aaij, V. Iakovenko, O. Okhrimenko, V. Pugatch, et al (the LHCb collaboration)

First observation of $\bar{B}^0\to J/\psi K^+K^-$ and search for $\bar{B}^0\to J/\psi\phi$ decays

Phys. Rev. D **88,** 072005 (2013)

G. Bellini, J. Benziger, D. Bick, G. Bonfini, D. Bravo, M. Buizza-Avanzini, B. Caccianiga, L. Cadonati, F. Calaprice, P. Cavalcante, A. Chavarria, A. Chepurnov, D. D'Angelo, S. Davini, A. Derbin, I. Drachnev, A. Empl, A. Etenko, K. Fomenko, D. Franco, C. Galbiati, S. Gazzana, C. Ghiano, M. Giammarchi, M. Goger-Neff, A. Goretti, L. Grandi, C. Hagner, E. Hungerford, Aldo Ianni, Andrea Ianni, V. Kobychev,

D. Korablev, G. Korga, D. Kryn, M. Laubenstein, T. Lewke, E. Litvinovich, B. Loer, F. Lombardi, P. Lombardi, L. Ludhova, G. Lukyanchenko, I. Machulin, S. Manecki, W. Maneschg, G. Manuzio, Q. Meindl, E. Meroni, L. Miramonti, M. Misiaszek, P. Mosteiro, V. Muratova, L. Oberauer, M. Obolensky, F. Ortica, K. Otis, M. Pallavicini, L. Papp, L. Perasso, S. Perasso, A. Pocar, G. Ranucci, A. Razeto, A. Re, A. Romani, N. Rossi, R. Saldanha, C. Salvo, S. Schonert, H. Simgen, M. Skorokhvatov, O. Smirnov, A. Sotnikov, S. Sukhotin, Y. Suvorov, R. Tartaglia, G. Testera, D. Vignaud, R.B. Vogelaar, F. von Feilitzsch, J. Winter, M. Wojcik, A. Wright, M. Wurm, J. Xu, O. Zaimidoroga, S. Zavatarelli, G. Zuzel

New limits on heavy sterile neutrino mixing in ^{8}B decay obtained with the Borexino detector

Phys. Rev. D **88,** 072010/1 – 7 (2013)

A.G. Magner, O.O. Vlasenko, K. Arita

Semiclassical trace formula for the two-dimensional radial potentials

Phys. Rev. E **87,** 062916/1 – 17 (2013)

R. Aaij, V. Iakovenko, O. Okhrimenko, V. Pugatch, et al (the LHCb collaboration)

First Evidence for the Decay $B^0s \to \mu^+\mu^-$

Phys. Rev. Lett. **110,** 021801/1 – 9 (2013)

R. Aaij, V. Iakovenko, O. Okhrimenko, V. Pugatch, et al (the LHCb collaboration)

Measurement of the CP asymmetry in $B^0 \to K^{*0}\mu^+\mu^-$ decays

Phys. Rev. Lett. **110,** 031801/1 – 8 (2013)

R. Aaij, V. Iakovenko, O. Okhrimenko, V. Pugatch, et al (the LHCb collaboration)

Observation of D^0–D^{-0} oscillations

Phys. Rev. Lett. **110,** 101802/1 – 9 (2013)

R. Aaij, V. Iakovenko, O. Okhrimenko, V. Pugatch, et al (the LHCb collaboration)

First observation of the $B^*s2(5840)^0 \to B^{*+}K^-$ and studies of excited B0s mesons

Phys. Rev. Lett. **110,** 151803/1 – 9 (2013)

R. Aaij, V. Iakovenko, O. Okhrimenko, V. Pugatch, et al (the LHCb collaboration)

Measurement of the Λ0b, Ξ–b and Ω–b baryon masses

Phys. Rev. Lett. **110,** 182001/1 – 8 (2013)

R. Aaij, V. Iakovenko, O. Okhrimenko, V. Pugatch, et al (the LHCb collaboration)

Search for rare $B^0(s) \to \mu^+\mu^-\mu^+\mu^-$ decays

Phys. Rev. Lett. **110,** 211801/1 – 8 (2013)

R. Aaij, V. Iakovenko, O. Okhrimenko, V. Pugatch, et al (the LHCb collaboration)

First observation of CP violation in the decays of B_s^0 mesons

Phys. Rev. Lett. **110,** 221601/1 – 9 (2013)

R. Aaij, V. Iakovenko, O. Okhrimenko, V. Pugatch, et al (the LHCb collaboration)

Determination of the X(3872) meson quantum numbers

Phys. Rev. Lett. **110,** 222001/1 – 8 (2013)

R. Aaij, V. Iakovenko, O. Okhrimenko, V. Pugatch, et al (the LHCb collaboration)

First measurement of the CP-violating phase in $B^0s \to \phi\phi$ decays

Phys. Rev. Lett. **110,** 241802/1 – 8 (2013)

R. Aaij, V. Iakovenko, O. Okhrimenko, V. Pugatch, et al (the LHCb collaboration)

Measurement of CP violation in the phase space of $B^\pm \to K^\pm\pi^+\pi^-$ and $B^\pm \to K^\pm K^+K^-$ decays

Phys. Rev. Lett. **111,** 101801/1 – 9 (2013)

R. Aaij, V. Iakovenko, O. Okhrimenko, V. Pugatch, et al (the LHCb collaboration)

Measurement of the $B_s^0 \to \mu^+\mu^-$ branching fraction and search for $B^0 \to \mu^+\mu^-$ decays at the LHCb experiment

Phys. Rev. Lett. **111,** 101805/1 – 9 (2013)

R. Aaij, V. Iakovenko, O. Okhrimenko, V. Pugatch, et al (the LHCb collaboration)

Precision measurement of the Λ_b^0 baryon lifetime

Phys. Rev. Lett. **111,** 102003/1 – 8 (2013)

R. Aaij, V. Iakovenko, O. Okhrimenko, V. Pugatch, et al (the LHCb collaboration)

Observation of a resonance in $B^+ \to K^+\mu^+\mu^-$ decays at low recoil

Phys. Rev. Lett. **111,** 112003/1 – 8 (2013)

R. Aaij, V. Iakovenko, O. Okhrimenko, V. Pugatch, et al (the LHCb collaboration)

Search for the lepton-flavor violating decays $B_s^0 \to e^\pm\mu^\mp$ and $B^0 \to e^\pm\mu^\mp$

Phys. Rev. Lett. **111,** 141801/1 – 9 (2013)

R. Aaij, V. Iakovenko, O. Okhrimenko, V. Pugatch, et al (the LHCb collaboration)

Measurement of the CP asymmetry in $B^+ \to K^+\mu^+\mu^-$ decays

Phys. Rev. Lett. **111,** 151801/1 - 9 (2013)

R. Aaij, V. Iakovenko, O. Okhrimenko, V. Pugatch, et al (the LHCb collaboration)
Observation of the decay $B_c^+ \to B_s^0 \pi^+$
Phys. Rev. Lett. **111,** 181801/1 – 9 (2013)

R. Aaij, V. Iakovenko, O. Okhrimenko, V. Pugatch, et al (the LHCb collaboration)
Measurement of form-factor independent observables in the decay $B^0 \to K^{*0} \mu^+ \mu^-$
Phys. Rev. Lett. **111,** 191801/1 – 8 (2013)

R. Aaij, V. Iakovenko, O. Okhrimenko, V. Pugatch, et al (the LHCb collaboration)
Measurement of the $D^\pm$ production asymmetry in 7 TeV pp collisions
Phys. Lett. B **718,** 902 – 909 (2013)

R. Aaij, V. Iakovenko, O. Okhrimenko, V. Pugatch, et al (the LHCb collaboration)
Measurement of the B0--B¯0 oscillation frequency Δmd with the decays $B^0 \to D^- \pi^+$ and $B^0 \to J\psi K^{*0}$
Phys. Lett. B **719,** 318 – 325 (2013)

R. Aaij, V. Iakovenko, O. Okhrimenko, V. Pugatch, et al (the LHCb collaboration)
Measurement of the time-dependent CP asymmetry in $B^0 \to J/\psi K^0 S$ decays
Phys. Lett. B **721,** 24 – 31 (2013)

G. Bellini, J. Benziger, D. Bick, G. Bonfini, D. Bravo, M. Buizza-Avanzini, B. Caccianiga, L. Cadonati, F. Calaprice, P. Cavalcante, A. Chavarria, A. Chepurnov, D. D'Angelo, S. Davini, A. Derbin, A. Empl, A. Etenko, G. Fiorentini, K. Fomenko, D. Franco, C. Galbiati, S. Gazzana, C. Ghiano, M. Giammarchi, M. Goeger-Neff, A. Goretti, L. Grandi, C. Hagner, E. Hungerford, Aldo Ianni, Andrea Ianni, V.V. Kobychev, D. Korablev, G. Korga, Y. Koshio, D. Kryn, M. Laubenstein, T. Lewke, E. Litvinovich, B. Loer, P. Lombardi, F. Lombardi, L. Ludhova, G. Lukyanchenko, I. Machulin, S. Manecki, W. Maneschg, F. Mantovani, G. Manuzio, Q. Meindl, E. Meroni, L. Miramonti, M. Misiaszek, P. Mosteiro, V. Muratova, L. Oberauer, M. Obolensky, F. Ortica, K. Otis, M. Pallavicini, L. Papp, L. Perasso, S. Perasso, A. Pocar, G. Ranucci, A. Razeto, A. Re, B. Ricci, A. Romani, N. Rossi, A. Sabelnikov, R. Saldanha, C. Salvo, S. Schonert, H. Simgen, M. Skorokhvatov, O. Smirnov, A. Sotnikov, S. Sukhotin, Y. Suvorov, R. Tartaglia, G. Testera, D. Vignaud, R.B. Vogelaar, F. von Feilitzsch, J. Winter, M. Wojcik, A. Wright, M. Wurm, J. Xu, O. Zaimidoroga, S. Zavatarelli, G. Zuzel
Measurement of geo-neutrinos from 1353 days of Borexino
Phys. Lett. B **722,** 295 – 300 (2013)

R. Aaij, V. Iakovenko, O. Okhrimenko, V. Pugatch, et al (the LHCb collaboration)
Search for direct CP violation in $D^0 \to h^- h^+$ modes using semileptonic B decays
Phys. Lett. B **723,** 33 – 43 (2013)

R. Aaij, V. Iakovenko, O. Okhrimenko, V. Pugatch, et al (the LHCb collaboration)
Observation of the suppressed ADS modes $B^\pm \to [\pi^\pm K^\mp \pi^+ \pi^-]D K^\pm$ and $B^\pm \to [\pi^\pm K^\mp \pi^+ \pi^-]D \pi^\pm$
Phys. Lett. B **723,** 44 – 53 (2013)

R. Aaij, V. Iakovenko, O. Okhrimenko, V. Pugatch, et al (the LHCb collaboration)
Measurements of the $\Lambda^0 b \to J/\psi \Lambda$ decay amplitudes and the Λ0b polarisation in pp collisions at $\sqrt{s}$=7 TeV
Phys. Lett. B **724,** 27 – 35 (2013)

R. Aaij, V. Iakovenko, O. Okhrimenko, V. Pugatch, et al (the LHCb collaboration)
Searches for violation of lepton flavour and baryon number in tau lepton decays at LHCb
Phys. Lett. B **724,** 36 – 45 (2013)

R. Aaij, V. Iakovenko, O. Okhrimenko, V. Pugatch, et al (the LHCb collaboration)
Search for $D^+_{(s)} \to \pi^+ \mu^+ \mu^-$ and $D^+(s) \to \pi^- \mu^+ \mu^+$ decays
Phys. Lett. B **724,** 203 – 212 (2013)

R. Aaij, V. Iakovenko, O. Okhrimenko, V. Pugatch, et al (the LHCb collaboration)
Search for the rare decay $D^0 \to \mu^+ \mu^-$
Phys. Lett. B **725,** 15–24 (2013)

R. Aaij, V. Iakovenko, O. Okhrimenko, V. Pugatch, et al (the LHCb collaboration)
Measurement of the CKM angle γ from a combination of $B^\pm \to Dh^\pm$ analyses
Phys. Lett. B **726,** 151–163 (2013)

R. Aaij, V. Iakovenko, O. Okhrimenko, V. Pugatch, et al (the LHCb collaboration)
Model-independent search for CP violation in $D^0 \to K^- K^+ \pi^- \pi^+$ and $D^0 \to \pi^- \pi^+ \pi^+ \pi^-$ decays
Phys. Lett. B **726,** 623 – 633 (2013)

R. Aaij, V. Iakovenko, O. Okhrimenko, V. Pugatch, et al (the LHCb collaboration)
Branching fraction and CP asymmetry of the decays $B^+ \to K_S^0 \pi^+$ and $B^+ \to K_S^0 K^+$

Phys. Lett. B **726,** 646 – 655 (2013)

R. Aaij, V. Iakovenko, O. Okhrimenko, V. Pugatch, et al (the LHCb collaboration)

Measurement of the differential branching fraction of the decay $\Lambda_b^0 \to \Lambda\mu^+\mu^-$

Phys. Lett. B **725,** 25–35 (2013)

V.I Soroka, S.O. Lebed, M.G. Tolmachov, O.G. Kukharenko, O.O. Veselov

Nuclear microanalysis study of surface nanolayers in gold-silicon structures

Ukr. J. Phys. **58,** 311 – 317 (2013)

T.V. Obikhod

Matter from Toric Geometry and its Search at the LHC

Universal Journal of Physics and Application **1,** 93 – 97 (2013)

Atomic energy:

И. Вишневский, В. Слисенко, В. Боднар, И. Большинский, Дж. Дьюес, Н. Мазина, В. Макаровский

Конверсия высокообогащенного топлива исследовательского реактора в рамках международной инициативы

Вопросы атомной науки и техники **5(87),** 63 – 68 (2013)

С.І. Азаров, В.Л. Сидоренко

Економічна оцінка відверненого екологічного ризику (соціального збитку) для населення, що проживає на техногенно-небезпечних територіях

Екологічні науки **3,** 69 – 73 (2013)

Ю.В. Литвинов, С.І. Азаров, В.Л. Сидоренко

Оцінка радіаційного впливу при гасінні пожеж на об'єкті "Укриття"

Збірник наукових праць СНУЯЕ та П **2(46),** Севастополь, 125 – 133 (2013)

С.І. Азаров, Ю.В. Литвинов, В.І. Паламарчук, В.Л. Сидоренко

Забезпечення життєдіяльності населення у складних радіологічних умовах

Збірник наукових праць Інституту державного управління у сфері цивільного захисту **1,** 98 – 101 (2013)

С.І. Азаров, В.М. Євланов

Кількісний аналіз полів іонізуючого випромінювання працюючого прискорювача заряджених частинок

Ядерна та радіаційна безпека **3(59),** 38 – 41 (2013)

В.Л. Демехин, В.В. Илькович, В.Н. Буканов

Верификация и валидация: процесс vs процедура

Ядерна фізика та енергетика**14,** 50–153 (2013)

В.В. Гальченко, В.Л. Дємьохін

Розрахункова залежність концентрації 137Cs у відпрацьованому паливі та її використання для обробки експериментальних даних

Ядерна фізика та енергетика**14,** 142–149 (2013)

Radiation physics and radiation material science:

А.П. Долголенко

Электронные уровни конфигураций дивакансии в кремнии

Вопросы атомной науки и техники **5(87),** 37 – 42 (2013)

О. Майборода, О. Шкапяк

Оцінювання точності та достовірності при побудові дозових залежностей зсувів критичної температури крихкості згідно з методикою VERLIFE на основі даних досліджень зразків-свідків АЕС України

Вісник Тернопільського національного університету **3(71),** 244 – 252 (2013)

В. Ревка, О. Тригубенко, Ю. Чайковський, Л. Чирко

Зміна характеристик міцності корпусної сталі при довготривалому опроміненні

Вісник Тернопільського національного університету **3(71),** 252 – 258 (2013)

А.Н. Гонтарук, А.В. Коваленко, О.В. Конорева, Е.В. Малый, И.В. Петренко, М.Б. Пинковская, В.П. Тартачник

Электролюминисценция серийных светодиодов GaP в зеленой области спектра

Прикладная спектроскопия **80,** 859 – 864 (2013)

В.М. Ревка, О.В. Тригубенко, Ю.В. Чайковський, Л.І. Чирко

Особливості окрихчення металу корпусу реактора ЗАЕС-2

Проблемы прочности **4,** 119 – 124 (2013)

A.Ya. Dzyublik

Nuclear excitation by electron transition
Український фізичний журнал **58,** 619-628 (2013)

А.А. Гроза, П.Г. Литовченко, Л.О. Матвєєва, П.Л. Нелюба, М.Б. Пінковська, М.І. Старчик
Вплив нейтронного опромінення та термообробки на виникнення ефекту самоорганізації, Франца-Келдиша та квантово-розмірного ефектів у монокристалічному кремнії
Фізика і хімія тв. тіла **14,** 40 – 45 (2013)

I.Yu. Goliney, V.I. Sugakov, G.V. Vertsimakha
Gold nanoshell effect on light-harvesting in LH2 complexes from photosynthetic bacteria
Хімія, фізика та технологія поверхні **4,** 157-164 (2013)

A.Ya. Dzyublik
Triggering of $^{178}Hf^{m2}$ by photoinduced electronic transition
Ядерна фізика та енергетика **14,** 13-17 (2013)

V.M. Revka, L.I. Chyrko, Yu.V. Chaikovskiy, O.V. Trygubenko
Different approaches to estimation of reactor pressure vessel material embrittlement
Ядерна фізика та енергетика **14,** 38 – 41 (2013)

О.В. Конорева, П.Г. Литовченко, Є.В. Малий, І.В. Петренко, М.Б. Пінковська, В.П. Тартачник, В.В. Шлапацька
Поверхневий розподіл інтенсивності свічення фосфід-галієвих детекторів
Ядерна фізика та енергетика **14,** 158 – 162 (2013)

А.П. Долголенко
Конфигурационные переходы дивакансий в кремнии и германии
Ядерна фізика та енергетика **14,** 163 – 171 (2013)

A.Ya. Dzyublik, V.Yu. Spivak, A.V. Chaus
Emission of conductivity electrons from metals, produced by ions
Ядерна фізика та енергетика **14,** 265-270 (2013)

A.Ya. Dzyublik, A. Gosselin, V. Méot, P. Morel
Role of screening in Coulomb excitation of nuclei by electrons in hot plasma
Eur. Phys. Lett. **102**, 62001 (2013)

P. Selyshchev, V. Sugakov
Competing influence of vacancies and interstitial atoms on temperature dependence of creep under irradiation
FFEMS **36,** 1123 – 1129 (2013)

A.Ya. Dzyublik, E.K. Sadykov, G.I. Petrov, V.V. Arinin, F.G. Vagizov, V.Yu. Spivak
Transmission of Mössbauer rays through ferromagnets in radio-frequency magnetic field
Hyperfine Interact **222,** P. 23 – 36 (2013)

O.I. Dmytruk, V.I. Sugakov
Amplification and passing through the barrier of the exciton condensed phase pulse in double quantum wells
Physica B: Condensed Matter **436,** 80 – 87 (2013)

I.I. Fishchuk, A. Kadashchuk, J. Genoe, S.T. Hoffmann, S. Athanasopoulos, H. Bässler, A.A. Köhler
A unified description for hopping transport in organic semiconductors including both energetic disorder and polaronic contributions
Phys. Rev. B **88,** 125202/1 – 11 (2013)

A.Ya. Dzyublik
General theory of nuclear excitation by electron transition
Phys. Rev. C **88,** 054616/1 – 8 (2013)

V. Mykhaylovskyy, V. Sugakov, G. Vertsimakha
Degradation of quantum dots under nuclear irradiation and its influence on exciton spectra in semimagnetic semiconductors
Physica Status Solidi (b) **250,** 108 – 114 (2013)

I. I. Fishchuk and A. Kadashchuk,
Small Organic Molecules on Surfaces
H. Sitter et al. (eds.), Springer Series in Materials Science **173**, Springer-Verlag Berlin Heidelberg, – 2013.– P. 171–201.

I.I. Fishchuk, A. Kadashchuk, X. Li and J. Genoe
Hopping Model of Charge-Carrier Transport in Organic Nanoparticle System
O. Fesenko et al. (eds.), Nanoaterials Imaging Techniques, Surface Studies and Applications, Springer Proceedings in Physics 146, Springer Science+Business Media New York. – 2013 – P. 205–242.

Plasma physics:

В.В. Юхименко, И.И. Федирчик, В.Я. Черняк, Е.В. Мартыш, Т.Е. Лиситченко, Н.В.Беленок, О.А. Федорович
Получение и исследование свойств плазменных образований при импульсном разряде в водном аэрозоле
Вопросы атомной науки и техники **1(83),** 180 –

182 (2013)

О.А. Федорович

О просветлении неидеальной водородно-кислородной плазмы при концентрации электронов $N_e \leq 3\ 10^{19}$ см$^{-3}$

Вопросы атомной науки и техники **1(83),** 198 – 200 (2013)

О.А. Федорович, Л.М. Войтенко

О влиянии степени неидеальности плазмы на коэффициенты распада

Вопросы атомной науки и техники **1(83),** 201 – 203 (2013)

P.V. Porytskyy

On the influence of metal impurities on the transport properties of multicomponent arc plasma

Вопросы атомной науки и техники **1(83)**, 222 – 224 (2013)

A. Goncharov, A. Dobrovolskiy, I. Litovko, V. Gushenets, E. Oks, A. Bugaev

Plasma lens for manipulating large area hogh current electron beams

Вопросы атомной науки и техники **4(86),** 44 – 47 (2013)

V.F. Semenyuk, V.F. Virko, I.V. Korotash, L.S. Osipov, D.Yu. Polotsky, E.M. Rudenko, V.M. Slobodyan, K.P. Shamrai

Controlling parameters determining technological properties of a helicon discharge system

Вопросы атомной науки и техники **4(86),** 179 – 182 (2013)

О.А. Федорович, Л.М. Войтенко

О распаде плотной плазмы в диапазоне концентраций электронов 10^{17}см$^{-3} \leq N_e \leq 10^{22}$см$^{-3}$

Вопросы атомной науки и техники **4(86),** 217 – 222 (2013)

О.А. Федорович

Эмпирическая формула зависимости величины «оптической щели» от концентрации электронов в диапазоне 10^{17}см$^{-3} \leq N_e \leq 10^{22}$см$^{-3}$

Вопросы атомной науки и техники **4(86),** 223 – 228 (2013)

A.M. Dobrovolskiy, A.A. Goncharov, E.G. Kostin, E.K. Frolova

Gas magnetron deposition of structured TiO_2 nanofilms

Вопросы атомной науки и техники **4(86),** 311 – 314 (2013)

В.И. Гушенец, А.А. Гончаров, А.Н. Добровольский, И.В. Литовко, Е.М. Окс, А.С. Бугарев

Фокусировка и транспортировка інтенсивного пучка электронов в устройстве на основе конфигурации плазменной линзы

Известия ВУЗов, Серия Физика **56**, 27 – 30 (2013)

Л.С. Максименко, О.Н. Мищук, И.Е. Матяш, Б.К. Сердега, Е.Г. Костин, Б.П. Полозов, Г.К. Савинков, О.А. Федорович

Модуляционная поляриметрия полного внутреннего отражения, нарушенного алмазоподобными пленками

Технология и конструирование в электронной аппаратуре **1,** 3 – 8 (2013)

А.Г. Борисенко

Источник бескапельных плазменных потоков для наноэлектроники

Технология и конструирование в электронной аппаратуре **4,** 37 – 42 (2013)

V.I. Gushenets, A.A. Goncharov, A.M. Dobrovolskiy, S.P. Dunets, I.V. Litovko, E.M. Oks, A.S. Bugaev

Electrostatic Plasma Lens Focusing of an Intense Electron Beam in an Electron Source with a Vacuum Arc Plasma Cathode

IEEE Trans.Plasma Sci. **41,** 1408-1411 (2013)

Yu. K. Moskvitina, A. O. Moskvitin, O. A. Shyshkin, V. O. Yavorskij, K. Schoepf

The Effect of Externally Applied Resonant Magnetic Perturbations on Fusion Product Dynamics in Toroidal Plasmas: Numerical Simulation

Journal of Fusion Energy **32,** 247 – 253 (2013)

V. Chernyak, O. Nedybaliuk, S. Sidoruk, V. Yukhymenko, Eu. Martysh, Ol. Solomenko, Yu. Veremij, D. Levko, A. Tsimbaliuk, L. Simonchik, A. Kirilov, O. Fedorovich, A. Liptuga, V. Demchina, S. Dragnev

Hydrogen Conversion in DC and Impulse Plasma-Liquid Systems

Liquid, Gaseous and Solid Biofuels Conversion Techniques, **13,** 401 – 429 (2013)

S.E. Sharapov, B. Alper, H.L. Berk, D.N. Borba, B.N. Breizman, C.D. Challis, I.G.J. Classen, E.M. Edlund, J. Eriksson, A. Fasoli, E.D. Fredrickson, G.Y. Fu, M. Garcia-Munoz, T. Gassner, K. Ghantous, V. Goloborodko, N.N. Gorelenkov, M.P. Gryaznevich, S. Hacquin, W.W. Heidbrink,

C. Hellesen, V.G. Kiptily, G.J. Kramer, P. Lauber, M.K. Lilley, M. Lisak, F. Nabais, R. Nazikian, R. Nyqvist, M. Osakabe, C. Perez von Thun, S.D. Pinches, M. Podesta, M. Porkolab, K. Shinohara, K. Schoepf, Y. Todo, K. Toi, M.A. Van Zeeland, I. Voitsekhovich, R.B. White, V. Yavorskij, ITPA EP TG, and JET-EFDA contributors

Energetic Particle Instabilities in Fusion Plasmas

Nucl. Fusion **53,** 104022 (2013)

P. Porytsky, I. Krivtsun, V. Demchenko, et al.

Transport properties of multicomponent thermal plasmas

Phys. Plasmas **20,** 023504 (2013)

V.N. Pavlenko and V.G. Panchenko

Radiation processes in turbulent plasma with ion temperature anisotropy

Physica Scripta **87,** 055503 (2013)

V.G. Kiptily, S.E. Sharapov, T.Gassner, C. Perez von Thun, S.D. Pinches, B. Alper, E. Cecil, D.Darrow, V. Goloborod'ko, C. Hellesen, J. Mailloux, W. Morris, V. Yavorskij and JET-EFDA Contributors

Study of Interaction between Fast ion and MHD Instabilities by Fusion Product Measurements in Joint European Torus

Plasma and Fusion Research **8,** 2502071/1 – 8 (2013)

V.S. Marchenko and O.S. Baschenko,

Suppression of the Alfvén cascades during electron cyclotron resonance heating

Plasma Phys. Control. Fusion **55,** 052002 (2013)

Ya.I. Kolesnichenko, Yu.V. Yakovenko

Can stochasticity of field lines be responsible for sawtooth crashes?

Plasma Phys. Control. Fusion **55,** 115006 (2013).

Ya.I. Kolesnichenko, B.S. Lepyavko, V.V. Lutsenko

Geodesic acoustic mode in tokamaks: local consideration and eigenvalue analysis

Plasma Phys. Control. Fusion **55,** 125007 (2013).

S. Shinohara, T. Tanikawa, T. Hada, I. Funaki, H. Nishida, T. Matsuoka, F. Otsuka, K. P. Shamrai, T. S. Rudenko, T. Nakamura, A. Mishio, H. Ishii, N. Teshigahara, H. Fujitsuka, S. Waseda

High-Density Helicon Plasma Sources: Basics and Application to Electrodeless Electric Propulsion

Trans. Fusion Sci. Technol. **63** 164 – 167 (2013)

Radioecology and radiobiology:

М.Д. Бондарьков, Ю.И. Иванов, Е.К. Гаргер, Н.Н. Талерко Н.П. Дикий, И.П. Дрозд, М.В. Желтоножская, А.И. Липская, В.Т. Маслюк, О.Н. Парлаг

Радиоэкологический и радиобиологический мониторинг с целью реконструкции и прогнозирования последствий радиационной аварии

Винахідник і раціоналізатор. Наука і техніка, **3**, 18 — 33, 2013 р.

Н.Н. Жданова, В.А. Захарченко, А.И. Василевская, А.Т. Школьный, Н.Д. Кучма, Л.В. Артышкова, Ю.С. Садовников, В.В. Вембер, Л.Т. Наконечная, И.Н. Купченко, Е.В. Соколова, А.А. Орлов, Т.И. Редчиц, В.А. Желтоножский, Л.В. Садовников, Т.Н. Лашко, М.В. Желтоножская, А.А. Гродзинская, С.А. Сырчин, С.П. Вассер, Ю.В. Карпенко, А.К. Павличенко, С.В. Олишевская, Т.И. Тугай

Микобиота Украинского Полесья: последствия Чернобыльской катастрофы

Інститут мікробіології і вірусології ім.Д.К.Заболотного, Київ. Наукова думка (2013).- 384

Т.И. Тугай, А.В. Тугай, М.В. Желтоножская, Л.В. Садовников

Влияние низких доз облучения на рост Aspergillus versicolor Paecilomyces lilacinus

Мікробіологічний журнал **75,** 33 – 40 (2013)

О.Л. Зарубін, В.А. Костюк, І.А. Малюк

^{137}Cs у біотичних компонентах екосистеми водойми-охолоджувача ЧАЕС до початку її трансформації

Надзвичайна ситуація **2(183),** 48 – 49 (2013)

О.Л. Зарубін, Д.І. Гудков, О.М. Волкова, В.В. Бєляєв, О.Є. Каглян, В.А. Костюк, І.А. Малюк, О.Б. Назаров, А.С. Білоконь, О.М. Маренкою

Радіоактивність риб України через 26 років після аварії на ЧАЕС (Дані досліджень фахівців з водної радіаційної екології. «Ловись краще маленька…»)

Надзвичайна ситуація **5(186),** 40 – 43 (2013)

О.Л. Зарубін, В.А. Костюк, І.А. Малюк

^{137}Cs у біотичних компонентах екосистеми водойми-охолоджувача ЧАЕС до початку її трансформації

Надзвичайна ситуація **2(183),** 48 – 49(2013)

О.Л. Зарубін, Д.І. Гудков, О.М. Волкова, та ін.

Радіоактивність риб України через 26 років після аварії на ЧАЕС
Надзвичайна ситуація **5 (186),** 40 – 43 (2013)

Н.Є. Зарубіна
Радіаційне забруднення їстівних грибів на території Київської області
Надзвичайна ситуація **6 (187),** 50 – 52 (2013)

А.І. Липська, В.О. Желтоножський, В.І. Ніколаєв, В.А. Шитюк, Н.В. Куліч
Особливості міграції техногенних радионуклідів в грунтово-рослинних комплексах ближньої зони відчуження ЧАЕС
Техногенна безпека **198,** 40 – 45 (2013)

Л.В. Тарасенко, Л.К. Бездробна, Т.В. Циганок, Ю.О. Носач, Т.В. Мельник
Спонтанні рівні аберацій хромосом у жителів міста Києва у віддалений період після Чорнобильської аварії
Техногенна безпека **198,** 120 – 123 (2013)

І.П. Дрозд, О.А. Сова, В.А. Шитюк
Дозоутворення у лабораторних щурів за перорального надходження ^{131}I з блокуванням та без блокування щитоподібної залози стабільним йодом
Техногенна безпека **210,** 23 – 30 (2013)

І.П. Дрозд
Хронічний вплив іонізуючої радіації на організм тварин і людини
Ядерна фізика та енергетика **14,** 42 – 50 (2013)

Ю.П. Гриневич, І.П. Дрозд, А.І. Липська, С.В. Телецька, Л.І. Маковецька
Пероксидазна активність крові щурів за тривалого надходження ^{137}Cs
Ядерна фізика та енергетика **14,** 64 – 68 (2013)

О.О. Бурдо, А.І. Липська, В.І. Ніколаєв, В.А. Шитюк, Н.В. Куліч
Вплив радіаційних умов на цитогенетичні показники мишоподібних гризунів із зони відчуження ЧАЕС
Ядерна фізика та енергетика **14,** 69 – 74 (2013)

Л.В. Тарасенко, Т.В Циганок, Л.К. Бездробна, Ю.О. Носач, О.Ф. Сенюк
Біологічні індикація впливу виробничих умов на персонал ДСП по поводженню з радіоактивними відходами і дезактивації «Комплекс» у зоні відчуження ЧАЕС
Ядерна фізика та енергетика **14,** 75 – 80 (2013)

А.Н. Берлизов, И.А. Малюк, А.Д. Саженюк, В.В. Тришин
Особенности технологии получения образцов для определения активности радионуклидов в материале топливных канальных труб реакторов РБМК
Ядерна фізика та енергетика **14,**. 165 – 170 (2013)

О.Л. Зарубин, Н.Е. Зарубина, Д.И. Гудков, Е.Н. Волкова, В.В. Беляев, А.Е. Каглян, В.А. Костюк, И.А. Малюк, А.Б. Назаров, А.С. Белоконь, О.Н. Маренков
^{137}Cs у рыб Украины через 25 лет после аварии на ЧАЭС
Ядерна фізика та енергетика **14,** 177 – 182 (2013)

Yu.N. Lobach, G. Toth
Design for the WWR-M reactor vessel removal
Nuclear engineering and design **258,** 184 – 188 (2013)

Yu.N. Lobach
Development of the decommissioning planning system for the WWR-M reactor
IAEA-TECDOC-1702, Vienna, 215 – 241 (2013)

The talks at the international conferences

Nuclear physics:

F.A. Danevich

Radiopurity of $ZnMoO_4$ crystals with natural and enriched materials

LUMINEU meeting, Orsay, France, February 4, 2013

D.M. Chernyak

Suppression of random coincidences in $ZnMoO_4$ bolometers with pulse shape discrimination

LUMINEU meeting, Orsay, France, February 4, 2013

V.V. Kobychev

AMoRE background evaluation with GEANT4 simulation

Int. Worksop on Nucl, Part. And Astrophys., HIGH1 resort, Gangwon-do, Korea, February 13 – 16, 2013

V.A. Plujko

Average Description of Dipole Gamma-Transitions in Hot Atomic Nuclei

International Conference on Nuclear Data for Science and Technology (ND2013), NY, USA, March 4 – 8, 2013

В.А. Желтоножский, А.П. Лашко, Т.Н. Лашко, А.Н. Саврасов

Внутриядерная конверсия К-запрещенных Е1-переходов в деформированных ядрах

XI конференция по физике высоких энергий, ядерной физике и ускорителям, Харьков, Украина, 11 – 15 марта 2013 г.

В.И. Гранцев

Энергетические распределения протонов в D(d, p) реакциях

XI конференция по физике высоких энергий, ядерной физике и ускорителям, Харьков, Украина, 11 – 15 марта 2013 г.

Т.В. Обиход

Сечение образования нейтрального бозона Хиггса MCCM-модели в реакциях слияния глюонов и b-кварков с NNLO QCD-расчетами

XI конференция по физике высоких энергий, ядерной физике и ускорителям, Харьков, Украина, 11 – 15 марта 2013 г.

Ю.М. Павленко

Механізми формування кінцевого стану реакції $^{7}Li(d, \alpha\alpha)n$ при низьких енергіях дейтронів

XI конференция по физике высоких энергий, ядерной физике и ускорителям, Харьков, Украина, 11 – 15 марта 2013 г.

Ю.М. Павленко

Особливості розпаду першого збудженого стану ядра ^{8}Be в реакції $^{11}b(p, \alpha\alpha)\alpha$ при низьких енергіях протонів

XI конференция по физике высоких энергий, ядерной физике и ускорителям, Харьков, Украина, 11 – 15 марта 2013 г.

D.M. Chernyak

Development of cryogenic low background detectors based on enriched $ZnMoO_4$ crystal scintillators to search for neutrinoless double beta decay of ^{100}Mo

Journées Des Doctorants 2013, Orsay, France, March 27 – 28, 2013

Т.В. Ковалінська

Пастеризация пищевых продуктов на радиационной установке

Международный семинар «Электронная стерилизация пищевых продуктов и изделий медицинского назначения», Астана, Казахстан, 3 – 5 апреля 2013 г.

S.P. Maydanyuk

Overview of nuclear bremsstrahlung and proposal of proton/nucleus-nucleus experiments at IMP

International Conference on Nuclear Physics, Shenzhen, China, May 2 – 5, 2013

V.V. Kobychev

AMoRE: expected backgrounds and how to reduce them

Korea Research Institute of Standards and Science, Daejeon, Korea, May 18, 2013

В.М. Мокіна

Розробка сцинтиляційних кристалів $PbWO_4$ з археологічного свинцю для експериментів з пошуку подвійного бета-розпаду і темної матерії

Int. Conference of young scientists and post-graduates, Uzhgorod, Ukraine, May 20 – 23, 2013

В.М. Яковенко

Фізика важких мезонів на Великому Адронному Колайдері. Радіаційні розпади $B^0 \to K^*\gamma$ та $B^0_s \to \phi\gamma$ в експерименті LHCb

Міжнародна конференція молодих вчених та аспірантів, Ужгород, Україна, 20 – 23 травня, 2013 р.

O. Okhrimenko

Performance of the metal Radiation Monitoring System

LAL−Ukraine workshop on HEP instrumentation, Orsay, France, May 20 – 24, 2013

V. Pugatch

Position Sensitive Metal and Hybrid Microdetectors in HEP and Nuclear Physics experiments

LAL−Ukraine workshop on HEP instrumentation, Orsay, France, May 20−24, 2013

I. Panasenko

Characterization Studies of the Detector Modules for Silicon Tracking System

LAL−Ukraine workshop on HEP instrumentation, Orsay, France, 20−24 May 2013

O. Kovalchuk

Metal Microstrip Detectors

LAL−Ukraine workshop on HEP instrumentation, Orsay, France, 20−24 May 2013

D.M. Chernyak

Scintillating bolometers – rejection of background due to standard two-neutrino double beta decay

Le Groupe de Recherche Neutrino meeting, Paris, France, May 21 – 23, 2013

Yu.N. Pavlenko.

The detector setup for the Coulomb impact studies on the observed properties of two-fragment resonances

Joint LAL – INR NASU Workshop on HEP Instrumentation, Orsay, France, May 22 – 24, 2013

T.V. Obikhod

Matter from Toric Geometry and its Search at the LHC

Міжнародна конференція "Геометрия в Одессе — 2013", Одеса, Україна 25 травня – 1 червня 2013 р.

В.М. Яковенко

Metal Micro-detectors for Radiation Therapy

XIII Міжнародна наукова школа «Проблеми фундаментальної та прикладної радіобіології», Обнінск, Росія, 27 – 31 травня, 2013 р.

V.A. Plujko, O.M. Gorbachenko, E.P. Rovenskykh, V.A. Zheltonozhskii

Test of closed-form gamma-strength functions

4-th Workshop on Level Density and Gamma Strength, Oslo, Norway, May 27 – 31, 2013

В.М. Мокіна

Оптимізація умов збору світла у низькотемпературних сцинтиляційних детекторах темної матерії та подвійного бета-розпаду

Международная школа молодых ученых по ядерной физике и энергетике, Алушта, Украина, 3 – 7 июня, 2013 г.

F.A. Danevich

R&D of crystal scintillators from enriched isotopes for high sensitivity double β decay experiments

Int. Conf. MEDEX'2013, Prague, Czech Republic, June 11 – 14, 2013

V.I. Tretyak

Search for rare nuclear decays with HPGe detectors at LNGS STELLA facility

Int. Conf. MEDEX'2013, Prague, Czech Republic, June 11 – 14, 2013

F.A. Danevich

$ZnMoO_4$ purification and crystallization in Novosibirsk

ISOTTA meeting, Orsay, France, June 24, 2013

F.A. Danevich

Requirements and prospects for production of radiopure $CaMoO_4$ crystal scintillators

AMoRE collaboration meeting, Heidelberg, Germany, July 25 – 26, 2013

V.V. Kobychev

Background simulation of AmoRE

AMoRE collaboration meeting, Heidelberg, Germany, July 25 – 26, 2013

V.V. Kobychev

Solar axion search

CUNPA kick-off meeting, Daejeon, Korea, August 22 – 23, 2013

V.V. Kobychev

Background simulation for materials

CUNPA kick-off meeting, Daejeon, Korea, August 22 – 23, 2013

V.I. Tretyak

First results of the experiment to search for double beta decay of ^{106}Cd with $^{106}CdWO_4$ crystal scintillator in coincidence with four crystals HPGe detector

Int. Workshop on Radiopure Scint. PScint'2013, Kyiv, Ukraine, September 17 – 20, 2013

D.V. Poda

Search for 2β decay of ^{116}Cd with the help of enriched $^{116}CdWO_4$ crystal scintillators

Int. Workshop on Radiopure Scint. PScint'2013, Kyiv, Ukraine, September 17 – 20, 2013

V.V. Kobychev

Expected backgrounds in AMoRE experiment

Int. Workshop on Radiopure Scint. PScint'2013, Kyiv, Ukraine, September 17 – 20, 2013

V.I. Tretyak

Semi-empirical calculation of quenching factors for scintillators: new results

Int. Workshop on Radiopure Scint. PScint'2013, Kyiv, Ukraine, September 17 – 20, 2013

Т.В. Ковалінська

Электрофизические технологии – инновации в сфере соленой рыбопродукции

IX Міжнародна науково-практична конференція «Производство рыбной продукции: проблемы, новые технологии, качество», Світлогорськ, 17 – 20 вересня, 2013 р

A.I. Sanzhur

Symmetry energy: from nuclear matter to finite nuclei

The 1-st International conference "Isospin, structure, reactions and energy of symmetry", Častá-Papiernička, Slovak Republic, September 23 – 27, 2013

V.M. Pugatch

LHCb Overview (on behalf of the LHCb Collaboration)

International Conference „New Trends In High-Energy Physics", Alushta (Crimea), Ukraine, September 23 – 29, 2013

В.М. Яковенко

Development and Application of New Detector Systems for Dosimetry in Radiation Therapy

Міжнародна конференція «The future of radiation oncology: imaging, dosimetry, biology & therapy», Berder island, Франція, 25 – 28 вересня, 2013 р.

F.A. Ivanyuk

The shell effects in the scission point configuration of fissioning nuclei

20-th Nuclear Physics Workshop "Maria and Pierre Curie", Structure and Dynamics of Atomic Nuclei, Kazimierz Dolny, Poland, September 25 – 29, 2013

A.G. Magner

Nuclear asymmetry and isovector dipole resonance structure in the effective surface approximation

20-th Nuclear Physics Workshop "Maria and Pierre Curie", Structure and Dynamics of Atomic Nuclei, Kazimierz Dolny, Poland, September 25 – 29, 2013

S.P. Maydanyuk

Quarks study via photon bremsstrahlung emission during proton nucleus collisions at low energies

International Symposium on Physics of Photons, ISPP-13, Lanzhou, China, September 27 – 29, 2013

S.P. Maydanyuk

Method of determination of parameters of scattering proton-nucleus potential from the experimental bremsstrahlung data

International Symposium on Physics of Photons, ISPP-13, Lanzhou, China, September 27 – 29, 2013

M.S Borysova.

Tubular initial conditions and ridge formation in HKM

Ecole Joliot Curie School 2013 "A colourful journey: from Hadrons to Quark-Gluon Plasma", Fréjus, France, September 29 – October 4, 2013

V.I. Tretyak

Possible other physics measurements with NEMO-3/SuperNEMO

NEMO-3/SuperNEMO Collaboration Meeting, Bratislava, Slovakia, October 1 – 4, 2013

V.I.Abrosimov

Pairing collective modes in superfluid nuclei: a semi-classical approach.

LXIII International Conference "Nucleus 2013", Moscow, Russia, 8 – 12 October, 2013

V.Yu. Denisov

Isotopic and neutron excess effects of both the nucleus-nucleus interaction and the fusion cross sections

63 international conference of nuclear physics "Nucleus 2013", Moscow, Russia, October 8 – 12, 2013

V.Yu. Denisov

The multi-dimensional model of cluster decay ^{242}Cm-›^{208}Pb + ^{34}Si

63 international conference of nuclear physics "Nucleus 2013", Moscow, Russia, October 8 – 12, 2013

A.M . Savrasov

Penetration effects in the E1 and E2-forbidden transitions in the ^{120}Sn

63 international conference of nuclear physics "Nucleus 2013", Moscow, Russia, October 8 – 12, 2013

A.M . Savrasov

Investigation of high-spin isomeric states in ^{196,198}Au nuclei in (p,n) reactions

63 international conference of nuclear physics "Nucleus 2013", Moscow, Russia, October 8 – 12, 2013

A.M . Savrasov

Measurements of isomeric yields ratios at 235U photofission

63 international conference of nuclear physics "Nucleus 2013", Moscow, Russia, October 8 – 12, 2013

A.M. Savrasov

Neutron emission by positron annihilation in ^{9}Be

63 international conference of nuclear physics "Nucleus 2013", Moscow, Russia, October 8 – 12, 2013

V.T. Kupryashkin

Exit of the near-zero energy electrons from the target surface at low energies of alpha-particles

Международное совещание по ядерной спектроскопии и структуре атомного ядра "Nucleus 2013", Москва, Россия, 8 – 12 октября 2013 г.

A.P. Lashko

The gamma-ray intensities from the ^{175}Hf decay

LXIII international conference "Nucleus 2013". «Fundamental problems of nuclear physics and atomic power engineering» (LXIII meeting of nuclear spectroscopy and nuclear structure), Moscow, Russia, October 8 – 12, 2013

A.P. Lashko

Internal conversion electrons of the 362 keV gamma-transition for K- and L-shells of ^{165}Ho

«Fundamental problems of nuclear physics and atomic power engineering» (LXIII meeting of nuclear spectroscopy and nuclear structure), Moscow, Russia, October 8 – 12, 2013

A.P. Lashko

The study of the low-energy range of the ^{177m}Lu gamma-spectrum

«Fundamental problems of nuclear physics and atomic power engineering» (LXIII meeting of nuclear spectroscopy and nuclear structure), Moscow, Russia, October 8 – 12, 2013

В.М. Пугач

Позиційно-чутливий кремнієвий детектор для рентгенівської дифрактометрії швидкоплинних процесів

V Науково-практична конференція НАН України «Новітні розробки наукового обладнання провідних приладобудівних компаній. Розвиток центрів колективного користування в НАН України», VI Міжнародний форум «Комплексне забезпечення лабораторій», Київ , Україна, 15 – 16 жовтня 2013 р.

Ж.И. Писанко

Опыт сотрудничества Украинского Центра ИНИС с ИНИС Секцией МАГАТЕ (1973 – 2013гг.)

Международное совещание "Роль международной системы ядерной информации (ИНИС) в информационной поддержке ядерного образования и организации ядерной индустрии", Москва, Россия, 22 – 24 октября, 2013 г.

V.S. Olkhovsky

About the similarity of particle and photon tunneling and multiple internal reflections in 1-dimensional, 2-dimensional and 3-dimensional photon tunneling

Materialy IX mezinarodni vedecko-prakticka conference "Zpravy vedecke ideje – 2013", Praha, Czech Republic, 27 října – 05 listopadu 2013 roku

V.V. Kobychev

AMoRE experiment to search for neutrinoless double beta decay of molybdenum-100 with scintillating bolometers

IEEE Nucl. Sci. Symposium, Seoul, Korea, October 27 – November 2, 2013

Atomic energy:

Н.В. Белошицкий

Мобильная лабораторія комплексной оценки и прогнозирования чрезвычайных ситуаций

Международная научно-практическая конференция «Предупреждение. Спасение. Помощь», Химки, Россия, 28 марта 2013 г.

O.O. Gritzay

Ukrainian Nuclear Data Centre Progress Report, 2012/13

Технічна нарада МАГАТЕ «Technical Meeting on International Network of Nuclear Reaction Data Centres (NRDC)», Відень, Австрія, 21 – 27 квітня 2013 р.

С.І. Азаров

Особливості побудови й експлуатації системи моніторингу навколишнього середовища за допомогою мобільної лабораторії

Міжнародний екологічний форум "Довкілля для України", Київ, Україна, 23 – 25 квітня 2013 р.

Ю.В. Литвинов

Оцінка радіаційного ризику для населення від пожеж в лісах, забруднених радіонуклідами Чорнобильського походження

Науково-практична конференція в рамках міжнародного форуму «довкілля України», «Радіоекологія-2013. Чорнобиль-Фукусіма. Наслідки», Київ, Україна, 26 – 27 квітня, 2013 р.

С.І. Азаров

Комплексний екологічний моніторинг навколишнього середовища в регіоні за допомогою мобільної лабораторії

XV Міжнародна науково-практична конференція "Ідеї академіка В.І. Вернадського та проблеми сталого розвитку регіонів ", Кременчук, 07 – 08 червня 2013 р.

O.O. Gritzay

Analysis for filtered neutron transmission

Технічна нарада МАГАТЕ «EXFOR Compilation Workshop», Відень, Австрія, 25 – 31 серпня 2013 р.

O. Gritzay

UKRNDC Activity on Nuclear Data Support to Meet the Requirements Connected with Fundamental Science and Applications

XII-а Міжнародна школа-семінар "The Actual Problems of Microworld Physics», Гомель, Білорусія, 22 липня – 2 серпня 2013 р.

O. Diakov

Implementation of research reactor ageing management programme at KINR WWR-M reactor

Joint IGORR 2013 & IAEA Technical Meeting, Daejeon, Korea, 13 – 18 October 2013

А.В. Гаврилюк-Буракова

Становление культуры физической ядерной безопасности в Украине

Трехсторонний семинар по учету и контролю ядерных материалов: Результаты и планы развития Российской государственной системы учета и контроля ядерного материала, г. Обнинск, Калужская обл., Россия, 12 – 15 ноября, 2013 г.

Radiation physics and radiation material science:

V. Revka

Radiation embrittlement of WWER-1000 RPV welds at high neutron fluence: surveillance test experience

17-th meeting of the IGRDM (International Group on Radiation Damage Mechanisms) – Embiez Island, France, 19 – 24 May 2013

Л.І. Чирко

Охрупчивание материалов КР ВВЭР-1000 при запроектных флюенса нейтронов

8-я МНТК "Обеспечение безопасности АЭС с ВВЭР", Подольск, Россия, 21 – 24 мая 2013 г.

Л.І. Чирко

Радиационное охрупчивание основного металла корпуса реактора энергоблока №2 Запорожской АЭС

8-я МНТК "Обеспечение безопасности АЭС с ВВЭР", Подольск, Россия, 21 – 24 мая 2013 г.

V.I. Sugakov

Control of the exciton condensed phase movement in double quantum wells

International research and practice conference "Nanotechnology and nanomaterials", Bukovel, Ukraine, August 29 to September 1, 2013

V.V. Tomylko

Exciton density pattern formation in laser irradiated quantum wells under electrodes of various shapes

International research and practice conference "Nanotechnology and nanomaterials", Bukovel, Ukraine, August 29 – September 1, 2013

I. Fishchuk

Analytic Model of Hopping Transport in Organic Semiconductors Including Both Energetic Disorder and Polaronic Contributions

15-th International Conference on Transport in Interacting Disordered Systems, Sant Feliu de Guíxols, Barcelona, Spain, September 15, 2013

R. Frankov

Program modernization of container assembly with the specimen VVER-1000

The Regional IAEA Workshop on Degradation of Primary Components of Pressurized Water Cooled Nuclear Power Plants, Vienna, Austria, November 4, 2013

O.Trygubenko

Evaluation of mechanical properties for heat affected zone in WWER-1000 RPVs based on surveillance test data

TM on "Degradation of primary system components of water cooled nuclear power plants current issue and future challenges", Vienna, Austria, November 5 – 8, 2013

В.В. Михайловский

Изменение спектра экситонов в низкоразмерных системах в полумагнитных полупроводниках под действием ядерного облучения

IV Международная научная конференция Наноразмерные системы: Строение, Свойства, Технологии" Київ, 19 – 22 листопада 2013 р.

E. Anokhin

Silicon Planar structures as Detectors for Microbeam Radiation Therapy

9-th IEEE Nuclear Science Symposium and Medical Imaging Conference, Seoul, Korea, October 27 – November 2, 2013

Plasma physics:

Ya. Kolesnichenko

Geodesic acoustic mode and the structure of Alfvén continuum in high-β plasmas with energetic ions

6-th IAEA TM "Theory of plasma instabilities", Vienna, May 27 – 29, 2013

О.А. Федорович

Системы мониторинга профиля и положения пучков ионизирующего излучения на базе ММД

14 международная научно-практическая конференция «СИЭТ», Одесса, Украина, 27 – 31 мая 2013 г.

I. Litovko

Plasma lens for focusing intense negative charged particle beams

International Conference on Phenomena in Ionized Gases ICPIG2013, Granada, Spain, July 14 – 19, 2013

О.А. Федорович

О влиянии эффекта нереализации уровней атомов в плотной плазме импульсных разрядов в воде на коэффициенты распада

XVI международная научная конференция «ФИРКС», Николаев, Украина, 19 – 22 августа 2013 г.

О.А. Федорович

О влиянии параметра неидеальности на коэффициенты распада плотной плазмы

XVI международная научная конференция «ФИРКС», Николаев, Украина, 19 – 22 августа 2013 г.

П.Д Старчик

Развитие турбулентного перемешивания в инициируемых взрывающимися проволочками импульсных разрядах в жидких средах

Международная научная конференция «Физика импульсных разрядов в конденсированных средах - XVI», Николаев, Украина, 19 – 21 августа 2013 г.

I. Litovko

Plasma lens for manipulating large area high-current electron beams

XII International Workshop "Plasma Electronics and New Acceleration Methods", Kharkiv, Ukraine, August 26 – 30, 2013

S. Shinohara, T. Tanikawa, T. Hada, I. Funaki, H. Nishida, F. Otsuka, D. Kuwahara, K.P. Shamrai

Characterization of High-Density Helicon Plasma Sources and Application to Electrodeless Plasma Thrusters

2013 Asia Pacific Radio Science Conf. (AP-RASC2013), Taipei, China, September 3 – 7, 2013

Yu.V. Yakovenko

Effect of magnetic islands on the energetic ion transport in tokamaks with magnetic shear reversal

13-th IAEA Technical Meeting on Energetic Particles in Magnetic Confinement Systems, , Beijing, China 17–20 September 2013

V. M. Lashkin

Soliton and zonal flow generation in drift wave turbulence

9-th Int.Conf. "Electronics and Applied Physics", Kiev, Ukraine, October 14 – 18, 2013

Ya. Kolesnichenko

Selected results of collaboration between Kyiv Institute for Nuclear Research (KINR) and Max-Planck-Institut für Plasmaphysik (IPP)".

Agreement for Co-operation between the European Atomic Energy Community (Euratom) and the Cabinet of Ministers of Ukraine in the field of Controlled Nuclear Fusion. 2nd meeting of the Coordinating Committee (CC-2), Brussels, Belgium, 19 November 2013

Ya. Kolesnichenko

Selected results of collaboration between Kyiv Institute for Nuclear Research (KINR) and US institutions

Agreement for Co-operation between the European Atomic Energy Community (Euratom) and the Cabinet of Ministers of Ukraine in the field of Controlled Nuclear Fusion. 2nd meeting of the Coordinating Committee (CC-2), Brussels, Belgium, November 19, 2013

О.А. Федорович

О влиянии на коэффициенты распада плотной плазмы ионизации, фото-, и тройной рекомбинации на основное состояние атома

Научно-координационная Сессия "Исследования неидеальной плазмы", Москва, Россия, 3 – 4 декабря 2013 г.

Radioecology and radiobiology:

O. Gaidar

Development of a Nuclear Forensics Library in Ukraine

International conference on Nuclear Security: Enhancing Global Efforts, Vienna, Austria, 1 – 5 July 2013

Yu. Lobach

Training on practical aspects of nuclear forensics expertise

ITWG-18, Sankt-Petersburg, Russia, October 8 – 10, 2013

І.П. Дрозд

Розробка й апробація методики оцінки індивідуальної радіорезистентності людини

Науково-практична конференція в рамках міжнародного форуму "Довкілля України", Радіоекологія-2013. Чорнобиль-Фукусіма. Наслідки, Київ, Україна, 25 – 27 квітня 2013 р.

А.І. Липська

Техногенні радіонукліди в грунтово-рослинних комплексах ближньої зони відчуження ЧАЕС на сучасному етапі

IX Міжнародна науково-практична конференція "Екологічна безпека: проблеми і шляхи вирішення, Алушта, Україна, 9 – 13 вересня 2013 р.

Н.В.Кулич

Метод одновременного измерения активности ^{90}Sr и ^{137}Cs в объектах окружающей среды

IX Міжнародна науково-практична конференція "Екологічна безпека: проблеми і шляхи вирішення, Алушта, Україна, 9 – 13 вересня 2013 р.

І.П.Дрозд

Сталий розвиток і техногенний вплив на довкілля

VII міжнародна науково-практична конференція «Проблеми природокористування, сталого розвитку та техногенної безпеки регіонів», Дніпропетровськ, Україна, 08 – 11 жовтня 2013 р.

І.П.Дрозд

Дозоутворення у лабораторних щурів за перорального надходження ^{131}I з блокуванням та без блокування щитоподібної залози стабільним йодом

Міжнародна науково-практична конференція "Радіаційна і техногенно-екологічна безпека людини і довкілля: стан, шляхи і заходи покращення ", Ялта, Україна, 5 – 9 червня 2013 р.

А.І. Липська

Особливості міграції техногенних радионуклідів в грунтово-раслинних комплексах ближньої зони відчуження ЧАЕС

Міжнародна науково-практична конференція "Радіаційна і техногенно-екологічна безпека людини і довкілля: стан, шляхи і заходи покращення ", Ялта, Україна, 5 – 9 червня 2013 р.

Е.А. Сова

Оценка доз облучения форменных элементов крови человека in vivo при внутреннем одноразовом поступлении радионуклидов

Международная научная конференция «Радиация, экология и техносфера», Беларусь, Гомель, 26 – 27 сентября 2013 г.

Н.В. Кулич

Исследование вертикальной миграции радионуклидов на загрязненных территориях

Международная научная конференция «Радиация, экология и техносфера», Беларусь, Гомель, 26 – 27 сентября 2013 г.

М.В. Желтоножская

Метод одновременной спектроскопии ^{137}Cs і ^{90}Sr

Международная научная конференция «Радиация, экология и техносфера», Беларусь, Гомель, 26 – 27 сентября 2013 г.

М.В. Желтоножская

Исследование концентрации радионуклидов во фрагментах ЛТСМ из 4-го энергоблока ЧАЭС

Международная научная конференция «Радиация, экология и техносфера», Беларусь, Гомель, 26 – 27 сентября 2013 г.

M.V. Zheltonozhskaya

New methods of measuring Sr-90 without radiochemical investigation in environmental samples

LXII international conference «Nucleus 2013», Moscow, Russia, October 8 – 12, 2013

И.П. Дрозд

Разработка методологии профотбора персонала по критерию индивидуальной радиочувствительности

VI международная научно-практическая конференция “Медицинские и экологические эффекты ионизирующего излучения”, Российская Федерация, Северск-Томск, 11 – 13 марта 2013 г.

The conferences and workshops, organized by the institute in 2013

The 3rd International Workshop on Radiopure Scintillators, September 17 - 20, 2013 Dedicated to the 70th anniversary of Prof. Yuri Zdesenko (1943-2004)

The 3rd International Workshop on Radiopure Scintillators was held from September 17 to September 20 in Kyiv, Ukraine at the Institute for Nuclear Research. This meeting was dedicated to 70th anniversary of Prof. Yuri Zdesenko (1943-2004). The idea of workshop was to bring together physicists, chemists, scintillator experts and producers to discuss different aspects of radiopure scintillator developments, measurements and applications.

The workshop program included the following topics:

-radiopure scintillators in nuclear and astroparticle physics;

-requirements of low-count rate experiments regarding radiopurity and scintillation properties;

-radioactive contamination of scintillation materials;

-selection and screening of input materials;

-instruments and methods to test radioactive contamination of materials and scintillators;

-purification of materials and preparation of raw compounds;

-crystal growing, annealing and handling;

-test of scintillators including scintillation, optical, luminescence, low-background and low-temperature measurements;

-search for and development of new scintillating materials.

During the workshop the 22 plenary reports and 9 poster reports were presented. The detailed information on the workshop is available on the webpage http://lpd.kinr.kiev.ua/rps13/ .

Plenary reports:

R. Bernabei. Crystal scintillators for low background measurements.

H.J. Kim et al. $CaMoO_4$ crystal scintillator based 0νββ experiment: AMoRE .

P. Belli et al. Search for rare processes with $ZnWO_4$ crystal scintillators .

V. Lozza et al. Neutrinoless double beta decay search with SNO+

V.I. Tretyak et al. First results of the experiment to search for double beta decay of ^{106}Cd with $^{106}CdWO_4$ crystal scintillator in coincidence with four crystals HPGe detector

D.V. Poda et al. Search for 2β decay of ^{116}Cd with the help of enriched $^{116}CdWO_4$ crystal scintillators

V.V. Kobychev et al. Expected backgrounds in AMoRE experiment

D.A. Spassky et al. Influence of traps on the luminescent and scintillation properties of molybdates

N. Coron et al. Response of parylene-coated NaI(Tl) scintillators at low temperature

O.A. Busanov et al. Low-background setup for measurement of the intrinsic background of $CaMoO_4$ scintillation crystals

V. Mikhailik et al. Monte-Carlo simulation of light collection efficiency of scintillation detectors using ZEMAX

M. Uffinger et al. Temperature dependent light output of scintillating crystals

V.I. Tretyak. Semi-empirical calculation of quenching factors for scintillators: new results

L. Pattavina. Lithium-containing scintillating bolometers for low background physics

I. Dafinei et al. Search for scintillating crystals for rare events physics application

R. Belhoucif et al. Growth and spectroscopic properties of ^{6}Li- and ^{10}B-enriched crystals for heat-scintillation cryogenic bolometers used in the rare events searches

V.N. Shlegel et al. Purification of molybdenum oxide and growth of medium size zinc molybdate crystals for the LUMINEU program

V. Kornoukhov et al. Production and deep purification of isotopically- enriched materials for $^{40}Ca^{100}MoO_4$ crystal growing

S. Galkin. Synthesis of ZnSe charge and growing methods of ZnSe single crystals

M. von Sivers et al. Scintillating $CaWO_4$ single crystals for CRESST-II and EURECA

O.A. Busanov et al. Background radioactivity of construction raw materials, raw substance and ready-made $CaMoO_4$ crystals

I. Tupitsyna et al. $Zn_xMg_{1-x}WO_4$ - A new crystal scintillator

Ukrainian conference on plasma physics and controlled fusion, September 24 – 25, 2013.

Ukrainian conference on plasma physics and controlled fusion was held from September 24 to September 25 in Kyiv, Ukraine at the Institute for Nuclear Research with the support Bogolyubov Institute of theoretical physics of NASU (BITP). The purpose of this conference is to summarize the results of studies in Ukraine in plasma physics and controlled fusion per year, as well as coordination of research. The conference was extended series of conferences initiated in Kyiv [Institute for Nuclear Research (KINR), 1992], and continued in Kharkiv, Kyiv and Alushta on the base of NSC «Kharkiv Institute of Physics and Technology» (KIPT) and KINR with the support of BITP. Programming committee and local organizing committee was headed by Prof. Ya.I. Kolesnichenko.

At the conference 83 reports were presented. At four sections 25 oral presentations were delivered. The remaining 58 report were presented at the poster session. The complete information on the conference is available at the webpage

http://www.kinr.kiev.ua/UCPPCF/2013.html .

Plenary reports:

1 Yu. V. Yakovenko. Physics of thermonuclear plasma (on the base of IAEA conference, Beijin, Chine, September17-20 2013.)
2 A.A. Kasilov. Characteristics of periferal plasma in torsatron URAGAN-3M
3 Ya.I. Kolesnichenko. Can stochastisity of field lines be responsible for sawtooth crashes in tokamaks?
4 O.V. Lozin. HF-heating with three-halfturn antenna in URAGAN-3M
5 V.O. Yavorskij. Convective and diffusive of fast ions from toroidal plasma
6 I.M. Pankratov. Analysis of synchroton radiation of escaping electrons in tokamaks
7 I.M. Onischenko. Perspectives to design colliders based on the novel methods of acceleration for high energy physics
8 A.G. Zagorodny Kinetic description of dusty plasmas and effective grain potentials
9 M.O. Azarenkov. Eigenmodes in tube coaxial plasma-metal wave structures with azimuthal magnetic field
10 S.V. Ivko. Energetic characteristics of electromagnetic wave in layered plasma structure
11 M.I. Grishanov .Mechanisms of wave absorption in laboratory collisionless magnetospheric plasma
12 V.V. Kulish. Cerenkov radiation of
13 electromagnetic wave by charged paritcles in magnetized plasma
14 Yu.V. Kovtun. Study of oscillation along the magnetic field in the pulsed reflex discharge
15 I.Ye. Garkusha. Annual 2013 results from stellarators URAGAN.
16 D.G. Solyakov. Generation of power plasma flows in quasistationary plasmadynamical system
17 16.V.O. Makhlaj. Drop-grain mechanism of tungsten disruption under plasma influence condition simulating ITER ELM
18 V.F. Virko. Inductive discharge created by linear wire array
19 V.A. Zhovtyansky. Peculiarities of solution of energy balance equation for electric arc
20 V.Ya. Chernyak. Discharge between two solid electrodes in mixture of inert gas with liquid spray
21 O.I. Kelnyk. Kinetics of electrons in microplasma discharge in dielectric PDP cell with additional electron source
22 R.Yu. Chaplyskyi. Space distribution of radiative intesity of continuum for plasma of capacitive HF-discharge at atmospheric pressure
23 O.V. Alexeenko. Designing of HF ion sources in the Institute of applied physics of NASU
24 A.G. Borysenko. Nonself-sustained vacuum arc discharge as a sourse of non-drop plasma flows
25 A.M. Veklych. Physical properties of thermal multicomponent plasma with metal vapors
26 I.O. Misruk. Plasma nitriding of medical implants

The reports by the members of INR NASU:

V.S. Marchenko. Dumping of Alfvén cascades under heating by electron cyclotron resonance

Yu. V. Yakovenko. Effect of magnetic islands on the energetic ion transport in tokamaks

M. H. Tyshchenko. Investigation of stochastization of fast ion motion by high-frequency plasma instabilities and spatial energy channelling in the ITER reactor

B.S. Lepyavko. Equations for heodesic acustic mode in tokamaks with high plasma pressure and energetic ions

O.S. Burdo. Investigation of stochastization of particle motion in tokamaks with screw excitation of magnetic field
V.Ya. Goloborod'ko. Influence of ion injected distribution function on the behaviour TAE modes in tokamak-reactors
O.P. Fesenyuk. Influence of ellipticity of plasma cross section on the frequency of both geodesic acoustic mode and Alfvén acoustic mode
A.V. Tykhyy. Stochastic diffusion of energetic ions in configurations liked Wendelstein
V.M. Pavlenko. Radiative processes in magnetized plasma with ion temperature anizotropy
V.M. Pavlenko. Transformation of Langmuir waves in turbulent plasma in the presence of upper – hybrid pump
V.B. Taranov. Physical results due to the symmetry of non-relativistic and partialy non-relativistic plasma
M.A. Beloshenko. Non-linear mechanisms of acceleration of helicon plasma in rotating fields
V.M. Slobodyan. The control of characteristics of helicon discharge in system with planar antenna by potentials of metal electrodes
V.M. Slobodyan .The study of characteristics of helicon discharge in the medium of methane and it's mixtures with hydrogen
P.V. Porytsky. Turbulent transport processes in plasma of pulse discharge in water
P.V. Porytsky. Transport properties of air and vapor plasma with electrode material admixtures
I.V. Litovko. Plasma lens for large area electron beams manipulating
V.V. Gladkovskiy. About the influence of HF-discharge characteristics on heating temperature of the substrate at synthesis of diamond-like films
L.M. Voitenko. Peculiarities of characteristics of dense plasma of pulse discharge under relaxation stage

11th Ukrainian Conference on physical protection, control and accounting of nuclear material, Netishyn, September 10–12 2013

The 11th Ukrainian Conference on physical protection, control and accounting of nuclear material, was held on September 10–12, 2013, in Netishyn, Ukraine at the Khmelnitska Nuclear Power Plant. The conference was organized by the George Kuzmycz Training Center on physical protection, control and accounting of nuclear materials (GKTC) of Insitute for Nuclear Research and the management and experts of Khmelnitska NPP with the sponsor's support of the European Commission and Swedish Radiation Safety Authority, and with the support of the Ministry of Power and Coal Industry of Ukraine and NAEC "Energoatom".

The objective of the 11th Ukrainian MPC&A Conference was to promote the experience exchange between specialists in the MPC&A field.< The conference covered the following topics:

- Matching of the activity in MPC&A field with the requirements of normative-legislative acts
- Problems of the vulnerability assessment taking for Ukrainian nuclear facilities
- Problems of the advanced training of MPC&A specialists
- Ensuring of the interaction of PP and MC&A systems
- -Experience of the application of nuclear security culture at the facilities
- Programs and techniques of the NM measurement system and improvement of NM accounting
- -Taking of functional tests for the engineering-technical means of PP systems

Complete information about the conference is available on the webpage

http://www.mpca.kiev.ua/confer.htm

The 49 experts from Belarus, Sweden, Ukraine, EU and IAEA took part in the conference. At the conference 27 plenary reports were presented:

A.V. Boyko. Experience, establishment, improvement and retooling of system of physical protection at Khmelnitska NPP

O.M. Onishchenko. Status and Prospects of physical protection in Ukraine

S.D. Lopatin. Compliance with regulatory and legal acts and accounting control of nuclear materials
V.A. Kiriyachenko. System of training in physical protection, accounting and control of nuclear materials in SNUNEP for atomic energetics in Ukraine

V.A. Kiriyachenko, A.N. Frolova. System of training for students in SNUNEP
A.R. Fatakhov. Requirements of normative documents physical protection, accounting and control of nuclear materials in training for SSP ChNPP
V.I. Kirischuk. On professional control and accounting nuclear materials in Ukraine
A.S. Tekhova. State of training of specialists on accounting and control of nuclear materials in OP ZNPP: Problems and implementation
V.I. Gavryliuk, A.V. Gavryliuk-Burakova, S.S Drapey, O.O. Levina, V.V. Parkhomenko, D.V. Pro-

skurin, O.P. Romanova. Training ground engineering and technical facilities of the system of physical protection

O.V. Makarenko, O.M. Korobenko. Vulnerability assessment, technical re-equipment SPT, counteraction to nuclear terroristic acts

I.O. Artukh. Problems of vulnerability assessment of nuclear plant in Ukraine

A.V. Artushkin. Problems of vulnerability assessment of nuclear plants in Ukraine

R.I. Zaporozhets. Experience OP KhNPP on the interplant transportation of fresh nuclear fuel in 2012

N.G. Kuznetsov. Personnel training on detection of radioactive (nuclear) materials at the state border of Ukraine.

G.O. Shatokhin. Practical experience of the interaction of subdivision physical protection of KhNPP with subdivision of sequrity of m/d 3043 while ensuring physical protection KhNPP

I.V. Omelyanov. Execution of IAEA warranties in Rivne NPP

D.A. Rusetskiy, A.A. Povorotnyi. Modernization of physical protection of nuclear objects in the Institute

V.I. Gavryliuk, A.V. Gavryliuk-Burakova, S.S Drapey, O.O. Levina, V.V. Parkhomenko, D.V. Proskurin, O.P. Romanova .A culture of security of nuclear plant in Ukraine

V.P. Paschenko. Creating of information system for monitoring of physical protection of nuclear materials and the sources of ionizing radiation under transportation and on the objects

Yu.P. Soltis. Formation and maintenance of security culture on nuclear plant

P.V. Tsykalchuk. Experience of establishing and implementing of nuclear security culture at Khmelnitska NPP

V.V. Solovyov. Approach to nuclear materials control and accounting at Chernobyl NPP

D.V. Stukalov. Nuclear fuel as accounting unit of nuclear materials

I.O. Polyakova, Ye.G. Borovik. Accounting and control system of nuclear materials in nuclear fuel production plant. Prospects and Problems

S.A. Koblitskiy. Functional inspections of technical means of physical protection system, which are putted into operation to subdivisions of internal forces of the MIA of Ukraine

M.I. Vershinin. Functional inspections of technical means of physical protection systems

A.V. Gaevskiy. Integrated solutions on the radiation safety

A.I. Tkachuk. Experience of JSV «Yugo-Zapad» in the construction systems of extended perimeter

A.N. Krivoshey Control system and access control “FORTNET”. The challenge of ensuring of physical protection on the strategic objects with the systems based on the integrated complex «INTELLECT - FORTNET».

T. Tsytulya. Radiative control in TM «ECOTEST»

S.V. Baranovskiy, A.Yu. Polyakov. Interactive control system of physical protection on the object

The annual scientific conference of INR NASU, January 27 -31, 2014.

The annual scientific conferences of INR NASU was organized in order to summarize the scientific results obtained during last year. The conference was held on January 27-31, 2014. The reports at the conference presented the main achievements of the Institute on:

Nuclear physics.

Atomic energy.

Radiation physics and radiation material science .

Theory of nuclear fusion and plasma physics.

Radioecology and radiobiology.

In the conference took part the participants from other scientific institutions of Ukraine.

At the conference there was a plenary session with 30 min. report and parallel sessions with the original message (10-15 min.). In addition, some research papers were presented at the poster session. Complete information on the conference is available at the webpage

http://www.kinr.kiev.ua/kinr-2014

The talks at plenary session:

V.M. Kolomiets Metastable state and boiling of liquid ^{3}He.

I.M.Vyshnevskyi, V.I. Slisenko Research nuclear reactor WWR-M. Current status and prospects

Ya.I. Kolesnichenko. European Roadmap to thermonuclear energetics and cooperation between Ukraine - EU

I. Yu. Goliney. Localized plasmons and amplification of kinetic processes in condensed media.

INTERNATIONAL SCIENTIFIC COLLABORATION

Within the year 2013 the Institute for Nuclear Research maintained the scientific cooperation with a number of nuclear scientific centers abroad, namely, with the :

- National Institute for Nuclear Physics (INFN), Italy;
- Gran-Sasso National Laboratory, Italy;
- University of Florence, Italy;
- Milano University, Italy;
- Henryk Niewodniczanski Institute for Nuclear Physics, Krakow, Poland;
- Andrzej Zoltan Institute for Nuclear Studies, Warsaw, Poland;
- Deutsche Synchrotron (DESY), Hamburg, FR Germany
- European Organization for Nuclear Research (CERN), Geneva, Switzerland;
- International Atomic Energy Agency, (IAEA), Vienna, Austria;
- Culham Center for Fusion Energy Abingdon, United Kingdom;
- Innsbruck University, Innsbruck, Austria;
- Gesellschaft für Schwerionen Forschung (GSI), Darmstadt, FR Germany;
- National University of Seoul, South Korea;
- US Ministry of Energy;
- Institute for Reference Materials and Measurements of the Joint Research Centre of the European Commission, Geel, Belgium;
- Joint Institute for Nuclear Research, Dubna, Russia;
- Institute of Nuclear Physics of Uzbekistan, Tashkent, Uzbekistan;
- Institute of Power Plant Engineering, Obninsk, Russia;
- National Nuclear Center of Republic Kazakhstan, Alma-Ata, Kazakhstan;
- Institute for Nuclear Research of Russian Academy of Sciences, Moscow, Russia.

Within this year the lepton physics department continued the successful international collaboration.

1. Within the collaboration with the group DAMA, Universities La Sapience and Tor Vergata, Rome, and the corresponding section of National Institute for Nuclear Physics, National Laboratory Gran-Sasso, Italy, the investigations of double beta-decay, rare alpha- and beta-decays, the search for hypothetical processes and particles, the development of low background detectors for studies of the rare nuclear processes were carried out, see also http://people.roma2.infn.it/~dama/web/members.html.

2. Within the SuperNEMO project (France, Great Britain, USA, Russia, Spain, Japan, Czech Republic, Finland, Ukraine, Poland, Slovakia) http://nemo.in2p3.fr/collaboration/) in 2013 the large scale experiment to search for neutrino-less double beta-decay of ^{82}Se with the sensitivity to the neutrino mass on the level of 0.05–0.1 eV was in preparation.

In particular, the detector BiPo for the high sensitivity analysis of radioactive Selenium foils and the calorimeter for future experiment has been developed.

3. The scientists of the department are active participators of the AMORE collaboration (Korean Republic, Russia, Ukraine, China, FR Germany), http://q2c.snu.ac.kr/DBD/), aimed to prepare a large-scale experiment to search for neutrino-less double beta-decay of ^{100}Mo with the help of cryogenic scintillating bolometers based on calcium molybdate crystal scintillators.

4. Within the collaboration EURECA (Great Britain, FR Germany, France, Switzerland, Russia, Ukraine, Spain), http://www.eureca.ox.ac.uk/, the scientists of the department investigate the possibility of using in the experiment the scintillator crystals. In particular, in 2013 the final design of low-background, multy-cristal, low-temperature detector was developed and accepted.

5. Investigations of solar and geo-neutrino were carried out in the frame of the Borexino collaboration by using a large scale liquid scintillation detector operated in the Gran-Sasso National Laboratory (Italy). A new neutrino oscillation experiment SOX (Short distance neutrino Oscillations with BoreXino) was proposed in 2013 by the Borexino collaboration.

6. Beginning from 2012 the department participate in the LUMINEU project (Expérience souterraine avec détecteurs luminescents de molybdate de zinc pour l'étude de la masse et la nature des neutrinos) supported by the Agence Nationale de la Recherche of France. The aim of the project is research and development of cryogenic scintillating bolometers based on zinc molybdate crystal scintillators to search for neutrinoless double beta decay on ambiguous level of sensitivity to the effective Majorana neutrino mass corresponding to the normal hierarchy of the neutrino mass (~ 0.02 eV).

In 2013 the department of high energy physics continued the international collaboration within the Memorandum between the Institute for Nuclear Re-

search, Kiev, and collaboration LHCb (CERN, Geneva, Switzerland) on mutual understanding concerning technical maintenance and exploitation of detector LHCb. From the analysis of the data obtained in the proton-proton collisions at energy 7 and 8 TeV in LHCb experiment (LHC, CERN) the frequencies of oscillations of B-mesons with different quark structure were obtained. These frequencies characterize the unique physical phenomenon of mixing of particles and anti-particles, due to their mass difference by the evolution of matter and antimatter. In particular, it was found that in the decays of B-mesons with light quarks the mixing frequency Δm_d is equal to $\Delta m_d = 0.5156 \pm 0.0051 \pm 0.0033$ ps^{-1}, and in decays of B-mesons with heavier strange quarks the mixing frequency is 34 times larger, $\Delta m_s = 17.768 \pm 0.023 \pm 0.006$ ps^{-1}

The scientists of the department carried out the modernization of the system of radiational monitoring of internal tracker in experiment LHCb. They have developed the prototype of detector module for the monitoring of neutron fluxes with using micropixel detector TimePix (in collaboration with MEDIPIX, CERN).

During this year within the agreement on scientific collaboration between GSI, Darmstadt, FRG and INR NASU on the physics of elementary particles and experimental technique the development of elements of the Silicon tracking system for the experiment CBM (FAIR, GSI, Darmstadt) was continued. The prototype of the cooling system for the detector module of micro-strip detectors was created.

It was found out that the measured transitional, strip-to-strip and total capacities of the double-sided Silicon sensors and their response to the relativistic charged particles in test experiments are in agreement with the modeled technical characteristics.

In 2013 the nuclear theory department continued collaboration with the:

- Cyclotron Laboratory of McMaster and Texas University, College Station, Texas, USA;
- National Institute for Nuclear Physics, University of Florence, Italy;
- Oxford University, Oxford, Great Britain,
- Uniwersytet Marii Curie-Sklodowskiej, Lublin, Poland;
- Institute for Nuclear Studies, Warsaw, Poland;
- Tokyo Institute of Technology, Tokyo, Japan.

In the result of common work with the Institute for Nuclear Studies (Swierk, Poland) and Technical Munich University (Munich, FRG) the analytical expression for the constant of the surface symmetry energy of heavy atomic nuclei in leptodermous approximation were derived. The known experimentally structural effects of the strength function of isovector dipole resonances were explained within the Landau Fermi-liquid model.

In collaboration with K. Pomorski (Uniwersytet Marii Curie-Sklodowskiej, Lublin, Poland) and N. Carjan (Bordeaux University, Bordeaux, France). The formal definition of the scission point – the maximal elongation at which the nucleus brakes into two pieses – was given. Within the macroscopic-microscopic model the shape and the deformation enerhy of nucleus ^{236}U at the scission point were calculated. Three minima in the deformation energy corresponding to standard, super-short and super-long fission modes were found.

In the year 2013 the nuclear reactions department continued successful collaboration with Flerow Laboratory for Nuclear Reactions, JINR, Russia. Within this collaboration the investigations of the properties of light nuclei with neutron or proton excess in reactions with the secondary radioactive beams were carried out on the mass-separator COMBAS. The investigation of the fragmentation process of ions ^{20}Ne and ^{40}Ar for the production of secondary beams of radioactive nuclei ^{18}Ne and ^{38}Cl were continued.

The nuclear reaction department has started the collaboration with the Kurchatov Atomic Energy Institute, Moscow, Russia. The common investigations of elastic and inelastic rainbow scattering of alpha-particles on ^{9}Be and deuterons on ^{12}C aiming at the studies of peculiarities of rainbow effects in the excitation of weekly bound and unbound states of nuclei were initiated.

The heavy ions physics department continued the collaboration with the Kurchatov Atomic Energy Institute, Moscow, Russia and JINR Dubna, Russia. A number of experiments were carried out also e Cyclotron laboratory of A. Zoltan Institute for Nuclear Studies, Swierk, together with co-workers of the Heavy ion laboratory of Warsaw University, Poland. The common experiments and the analysis of experimental data on the nuclear reactions were also carried out at H. Niewodniczanski Institute for Nuclear Physics, Cracow, Poland.

The scientists of department of theoretical physics collaborate with the Lebedev Institute of Physics, Moscow, Russia, Pretoria University, South Africa, Bayreuth University, Germany, Johannes Kepler University, Linz, Austria, CEA/DAM ile de France, Bruay la Shatel, France, Center for Medical Radiation Physics, Wollongong University, Australia.

In the year 2013 the investigations on the common project by the State foundation of the fundamental investigations of Ukraine and the Russian foundation of the fundamental investigations “Collective phenomena and the space self-organization in the system of di-polar excitons in quasi-two-

dimensional Silicon-Germanium getero-structures were continued".

In collaboration with P. Selishchev (Pretoria University, South Africa) the calculations of the metal creep and the auto-vibrations of temperature due to nuclear irradiation were carried out.

Together with the scientists of Center for Medical Radiation Physics (Wollongong University) the modeling of the properties of various Silicone detectors were investigated for the application in radiation medicine.

Together with the Institute of Semiconductors, Institute of Solid State Physics (Linz University, Austria) the theoretical and experimental investigation of the jump transport in non-ordered organic semiconductors at arbitrary concentration of the charge carrier was continued (H. Sitter, I.I. Fishchuk). Together with the co-workers of CEA/DAM ile de France (Bruay la Shatel) A. Ya. Dzyublik has continued the investigations on the Coulomb excitations of nuclei by electrons in hot plasma.

The fusion theory department continued in 2013 the scientific collaboration with Innsbruck University, Austria, (Profs. K. Schoepf, M. Khan, T. Hassner) and Kalem Center of Thermonuclear Synthesis (JET Great Britain). The investigations on the problem of maintaining of charged particles of nuclear synthesis in tokamaks were carried out together with the scientists from the Colorado Mountain School, Colorado, USA.

The department of research reactor successfully continued the collaboration with the National Nuclear Safety Administration (United States Department of Energy) aimed at the improvement of the safety of nuclear research reactors and developing of new type of reactors. During 2013 nine experts on the nuclear security from USA and IAEA visited KINR NASU. The department took part in the organization of technical meeting on the program of returning of used Russian nuclear fuel from the research reactors, Sevastopol, June 12 – 14, 2013.

The radiobiology and radioecology department has established the collaboration with Institute of Biophysics of the Academy of Sciences of Russian Federation (Siberian branch). Within this collaboration the project "Estimation of the migration properties of transuranium elements in hydro ecological systems of rivers Enisej and Pripiat (Chernobyl zone, Ukraine)" was prepared and submitted for the common concurs of projects on fundamental researches of Siberian branch of Academy of Sciences of Russian Federation and National Academy of Sciences of Ukraine.

The Center for Ecological Problems of Atomic Energy (CEPAE) carries out a number of research projects together with the nuclear centers of other countries and international organizations.

In collaboration with the Institute of Applied Physics NASU, Institute of Geophysics of Environment NASU, Kharkov Physical-Technical Institute NASU, Livermore National Laboratory (USA) the attributive features of uranium-containing materials of different origin are investigated for the improvement of technical abilities of Ukrainian specialists in the field of nuclear criminality. In this activity participated also the partners from Georgia, Azerbaijan and Moldova.

In collaboration with Russia, Moldova, Georgia, Kazakhstan, Institute of Transuranium Elements (European Commission) the CEPAE implements effective efforts to prevent illegal displacement of nuclear and radioactive materials in Ukraine. In 2013 the CEPAE got the mobile expertise laboratory equipped by the modern radio-metric, dose-metric, alpha- and gamma- dosimetric equipment, automatic system of the air pumping for the determination of the contamination of the air by radioactive aerosols, systems of analysis of water and soil. The laboratory is completely autonomic what allows carrying out radiologic measurements in the fields conditions.

The CEPAE plans different seminars and the training courses for the organizations dealing with counteracting to illegal displacement of the radioactive materials in Ukraine and the states of former Soviet Union.

The George Kuzmycz Training Center (GKTC) for Physical Protection, Control and Accounting of Nuclear Material, http://www.mpca.kiev.ua/, continued its activity according to agreement for development of Ukraine's national nuclear material control, accounting and physical protection system aimed to promote the prevention of proliferation of nuclear weapons from Ukraine signed on 18 December 1993 by the State Committee of Ukraine for Nuclear Radiation Safety and the US Department of Defense.

In 2013 Training Center for Physical Protection, Control and Accounting of Nuclear Material kept implementing the tasks set to the Center by decision-making authorities of Ukraine. Thus in accordance with the President's Decree dated Feb 02, 2013, № 73/2013 "On National Plan of realization of decisions of the Seoul Summit for Nuclear Security for 2013 – 2014" Training Center has developed 2 normative documents on security culture, namely:

"Procedure for Forming and Development of Security Culture at Nuclear Facilities and Objects Associated with Radioactive Waste Handling, Other Sources of Ionizing Radiation", registered in the Ministry of Justice of Ukraine, dated September 6, 2013, № 1543/24075;

"Instruction on Conducting Assessment of Security Culture Level of Nuclear Facilities, Objects Associated with Handling of Radioactive Waste, Other Sources of Ionizing Radiation", registered in the Ministry of Justice of Ukraine, dated September 6, 2013, № 1543/24076.

Training Center continues working at Training Complex for Engineering and Technical means of Physical Protection System, which has been established in accordance with the President's Decree dated November 15, 2010, № 1035/2010 "On National Plan of realization of decisions of the Washington Summit for Nuclear Security for 2010 – 2012". The Training Complex is equipped with modern engineering and technical means of physical protection system. During this year the Site of Training Complex has been widely used for practical training on physical protection and for drills of special sub-units of response forces.

In addition to that Training Center has developed training programs and training materials and conducted training courses on the following topics:

"Nuclear Security Culture Training Course for Top-Level Managers" (the Course was conducted on May 21 – 22, 2013);

Nuclear Security Culture Training Course for Heads of Guard Units" (the Course was conducted on June, 10 – 12, 2013);

Nuclear Security Culture Training Course for Mid-Level Managers" (the Course was conducted on August 12 – 16, 2013);

Nuclear Security Culture Training Course for Nuclear Security Culture Coordinators" (the Course was conducted on September 2 – 6, 2013);

In 2013 The GKTC organized 11th Ukrainian Conference on Control and Accounting of Nuclear Material (MPC&A), September 10-12, Neteshin (Khmelnytska NPP). The 11th Ukrainian MPC&A Conference was dedicated to the questions of interaction of physical protection systems and MC&A systems at the nuclear facilities of Ukraine. The objective of the MPC&A Conference was to promote the experience exchange between specialists in the MPC&A field

Under the aegis of the IAEA George Kuzmycz Training Center has conducted Technical Meeting on the issues of cooperation with the IAEA for the future years and two National Training Courses:

1) On Coordination of MEST/FLO (experts/first line officers) work with Sources of Ionizing Radiation, August 12 -16 2013;
2) Real-time exercise of illicit trafficking incidents prevention, December 10 -13, 2013.

In the year 2013 the Ukrainian center of International Nuclear Information System (INIS) continued its activity. The INIS accumulate the information on the research in nuclear physics published more that in 13 000 scientific journals all over the world. The information on 1945 research works related to nuclear physics (nuclear theory and experiments, the physics of elementary particles, plasma physics, material science, nuclear reactors, ecology, influence of radiation on humans, animals and biologic materials) which were published in Ukraine in 2013 was sent to IAEA for the incorporation into the database of INIS. On the request of co-workers of KINR NASU and other institutions the various information was subtracted from the database of INIS. On the request of scientists from many countries the Ukrainian center of INIS supplied them by the full text of publications of Ukrainian scientists.

The KINR NASU maintains the exchange by information with the Physics Section, Division of Physical and Chemical Sciences of IAEA. Within this exchange the Ukrainian Nuclear Data Center has compiled in format EXFOR the experimental data on the interaction of atomic nuclei with neutrons, charged particles and photons obtained by Ukrainian scientists and published in Ukrainian and international journals for incorporation in the international
data base of experimental results CSISRS/EXFOR.

On September 17 – 20 the 3rd International workshop on Radiopure Scintillators was held in Kyiv, Ukraine at the Institute for Nuclear Research. This meeting was dedicated to 70th anniversary of Prof. Yuri Zdesenko (1943-2004). The idea of workshop was to bring together physicists, chemists, scintillator experts and producers to discuss different aspects of radiopure scintillator developments, measurements and applications.

In 2013 the INR NASU was in contact with IAEA on current problems. Besides, experts from IAEA visited institute regularly for current inspection of the research reactor WWR-M, for inspection of condition of keeping the used nuclear fuel, for providing the informational help on safe exploitation of the research reactor. In 2013 four official delegations from IAEA (experts and inspectors) visited INR NASU.

In 2013 53 scientists from the counties of former Soviet Union visited INR NASU for taking part in seminars and workshops. The co-workers of the institute have undertaken 116 visits abroad, 52 for common scientific work, 22 for the work on probation, 41 for the participation in international conferences, symposia, workshops.

70th anniversary of Prof. Yuri Zdesenko

Yuri Georgievich Zdesenko was born on October 6, 1943 in Dmytrivka of Chernigov region of Ukraine. In 1970 he was graduated from Department of Physics of the Kyiv State University. He obtained degrees of Philosophy Doctor in 1981 (INR, Moscow, Russia), Doctor of Science in 1990 (INR, Kyiv, Ukraine) and status of Full Professor in 2000 (INR, Kyiv, Ukraine). Because of high scientific achievements, he was elected a Corresponding Member of the National Academy of Sciences of Ukraine in 2003. He started researches in the Laboratory of Nuclear Physics of the Kyiv State University (1970-1971) and in the Institute of Geochemistry and Physics of Minerals (1971-1980) where he dealt with neutron activation analysis of minerals and built up the low background set up for radiocarbon measurements. In the following he created in the Institute for Nuclear Research (Kyiv) the Laboratory for Low Background Measurements (1980-1986), where, in particular, low background installations with plastic scintillators to study 2β decays of ^{130}Te, ^{100}Mo and ^{96}Zr were developed. The Laboratory was transformed in further to the Lepton Physics Department of the INR (1986). From 1983 the huge work has been fulfilled by Yuri Zdesenko and his group to build up the Solotvina Underground Laboratory of the INR which is situated in Solotvina, small town on the west of Ukraine, in a salt mine on the depth of 430 m underground (1000 m of water equivalent). Starting from 1984, series of experiments were performed in this Laboratory devoted to search for rare α and β nuclear decays and for rare or forbidden in the Standard Model effects, mainly for neutrinoless 2β decay of atomic nuclei. As the most successful, we can mention:

(1) the most stringent limits on 0ν2β decay of ^{116}Cd with $CdWO_4$ crystal scintillators enriched in ^{116}Cd at 83% - in fact, one of the best world limits for this process;

(2) first observation of ^{116}Cd 2ν2β decay;

(3) first observation of one of the rarest α decays (^{180}W);

(4) investigation of rare ^{113}Cd β decay;

(5) search for 0ν2β decay of ^{160}Gd and ^{186}W.

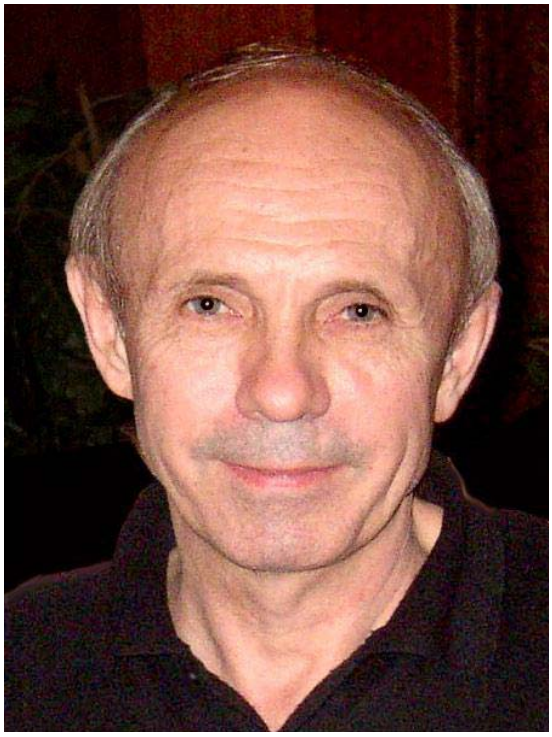

Among others, there were searches for cluster nuclear decays, nuclear transitions to super-dense state, decays of nucleons into invisible channels, decays of electron with non-conservation of the electric charge, charge-non-conserving β decays. In many cases, investigations were fulfilled in collaboration with colleagues abroad. He was author or co-author of above 300 scientific publications for which there are near 2000 references in papers of other scientists.

Yuri was very clever, initiative and persistent person. He had a good habit: doing something, to do it on the highest level. In addition to great scientific achievements, he was Master of Sports in pentathlon. He achieved to hook fishes of the same size as he was. Yuri suddenly died on September 1, 2004 during operation on stomach because of the heart's halt. His death was very unexpected and shocking event for everyone who knew this lively man. It was significant loss not only for Ukrainian but also for world science in which he actively participated during many years. Everybody, for whom he was a teacher, and all who knew him, will miss his intense interest and enthusiasm in the science and his energy in life.

Авторський покажчик / Author index

Scientific publication

Annual report - 2013

Technical redactor L.M. Troyan
Computer aided makeup F.O. Ivanyuk, O.D. Grygorenko

Підп. до друку 03.04.2014. Формат 60×84/8. Ум. друк. арк. 19,53.
Тираж 150 пр. Зам. № 3.

Інститут ядерних досліджень НАН України,
просп. Науки, 47, м. Київ, 03680, тел. 525-14-56
Свідоцтво суб'єкта видавничої справи ДК № 4051 від 18 квітня 2011 р.

Надруковано у ЦСТРІ м. Києва, філія № 7 «КОПІ ЦЕНТР»,
просп. Перемоги, 37, м. Київ, 03056, тел.: 277-88-93, 277-37-49
Свідоцтво суб'єкта видавничої справи ДК № 37096928 від 15 березня 2005 р.